Monitoring and Analysis of Mn/DOT Precast Composite Slab Span System (PCSSS)

A Thesis
Submitted to the Faculty of the Graduate School
of the University of Minnesota
By

Matthew Jacob Smith

In Partial Fulfillment of the Requirements
for the Degree of
Master of Science

Catherine French, Carol Shield

January 2010

Acknowledgements

The work chronicled within this thesis was largely a team effort. I would like to especially thank my advisors, Cathy French and Carol Shield, for their help and guidance. I would also like to thank Charles M. Bell for his efforts during the design of the system and the instrumentation of the Center City Bridge. I would also like to thank Paul Bergson, Charlie DeVore, Whitney Eriksson, Bulent Erkmen, Katie Johnson, and Roberto Piccinin for their ongoing help throughout the research effort. The following people are also greatly appreciated for the assistance they provided during the construction, instrumentation, and testing of the laboratory specimen: Andrew Atkins, Beth Brueggen, Gary Hahn, Benton Johnson, Bulent Mercan, Jake Reneson, Ryan Rohne, Brian Runzel, Mike Stevens, and Vanessa Storlie.

I would also like to thank the Minnesota Department of Transportation (Mn/DOT) and County Materials for their contributions during this project. Mn/DOT provided all of the funding for this project, in addition to much engineering guidance.

Abstract

The Mn/DOT Precast Composite Slab Span System (PCSSS) was initially designed by Mn/DOT with input from the University of Minnesota (U of MN) researchers and local fabricators. The bridge system consisted of a series of precast prestressed concrete inverted tee bridge elements which also served as stay-in-place formwork for the cast-in-place (CIP) portion of the deck placed in the field. One of the Mn/DOT implementations, located in Center City, MN, was instrumented, and subsequently, monitored for 24 months to investigate reflective cracking and continuity over the piers since the deck was cast. The data obtained from the field study indicated that cracking had initiated in the bridge at the locations of some of the transverse gages in the CIP just above the longitudinal flange joint at midspan and some of the longitudinal gages near the support. The cracking was associated with the restraint of environmental effects and shrinkage rather than due to vehicular loads. Transverse load distribution was evaluated with a static truck test. In addition, a two-span laboratory specimen was constructed and load tested to investigate effects of variations in flange thickness, bursting reinforcement, horizontal shear reinforcement, and flange surface treatment. The positive restraint moment that developed at the pier was also monitored for the first 250 days after continuity was made. The data from the laboratory and field tests was analyzed with respect to reflective cracking, transverse load distribution, pier continuity, bursting, and restraint moment, and design recommendations were made.

Table of Contents

List of Tables

List of Figures

Chapter 1: Introduction

1.1 Motivation for Study

The main motive for this study was to develop a robust system for short to moderate span bridges (20-50ft. range) that could accelerate construction and reduce impact on the traveling public. Systems incorporating precast concrete elements offer advantages including reduced impact on the environment, improved quality control and safety, as well as accelerated construction compared to cast-in-place (CIP) slab span systems. A team of engineers who participated in a 2004 FHWA International Scanning Tour of Prefabricated Bridge Elements and Systems utilized for accelerated construction identified a number of systems to be considered for implementation in the United States. A variation of one of these systems, the precast Poutre Dalle slab span system originally developed in France, has been implemented by the Minnesota Department of Transportation (Mn/DOT). This system, termed the Mn/DOT Precast Composite Slab Span System (PCSSS), was initially designed by Mn/DOT with input from the University of Minnesota (U of MN) researchers and local fabricators. The concept consists of a series of shallow precast prestressed concrete inverted tee elements which preempt the need for any formwork for the cast-in-place (CIP) portion poured in the field. The objectives of this research were to better understand the performance of the system through a combination of laboratory testing and field monitoring, improve design guidelines, and improve standard details for future projects.

1.2 Background

Implementation of the Mn/DOT PCSSS began in 2005 with the design and construction of two bridges. A typical cross section is shown in Figure 1.1. The first bridge was a three span superstructure replacement in Beltrami County, MN, where the precast section was 16 in. deep, and the CIP concrete topping brought the total depth to 22 in. Each of the three spans was 45 ft. long. The second implementation was located in Center City, MN, where the precast section was 12 in. deep, and the total section depth was 18 in. The Center City Bridge had spans of 22, 27, and 22 ft. The Center City Bridge was instrumented with 96 Vibrating Wire (VW) strain gages to facilitate monitoring the bridge performance

over the first two years of service. The development of the system and instrumentation of the Center City Bridge was outlined in *Mn/DOT Report 2006-37 Application of Precast Decks and Other Elements to Bridge Structures* (Bell 2006). The final, nominal cross section for the Center City Bridge precast sections is given in Figure 1.2. In Figure 1.2, the bar diameters (in metric) are denoted by the first two numbers in the reinforcement label.

1.3 Research Objectives

The objective of this research was to evaluate the performance of the Mn/DOT PCSSS. This included both comparing the measured performance to the design expectations and identifying and investigating areas for improvement. The research was largely divided into two parts, a field study of the Center City Bridge and a laboratory study for a more controlled investigation and an opportunity to investigate design modifications.

The field study of the Center City Bridge included both monitoring the instrumentation for the first two years of service and performing a live load truck test. The primary considered behaviors of this study were the tendency for reflective cracking to develop at the flange joint and/or web corners, the effectiveness of the reinforcement used to control reflective cracking at the flange joint, the distribution of live load, and the degree of continuity provided over the pier supports. Reflective cracking at the flange joints was evaluated for both environmental and repeated vehicular loading effects during the monitoring period and for static vehicular loading during the truck test in which wheel loads were placed directly above the flange joints to maximize transverse stresses. Live load distribution and continuity over the pier supports were investigated during the truck test by utilizing the instrumentation on the longitudinal reinforcement to compare the measured results to the assumptions made during the Mn/DOT design.

To augment the field investigation of the Mn/DOT PCSSS, a laboratory study was performed. Based on the constraints of the Structures Laboratory, a two span laboratory specimen was chosen with the same 22 ft span length as the outer spans of the Center City Bridge. Each of the spans had two precast sections. Modifications to the original design were made to improve the system's performance and economy. Behaviors investigated included restraint moment, load distribution, and prestress losses. In addition, as part of a

larger NCHRP 10-71 project, *Cast-in-Place Concrete Connections for Precast Deck Systems*, the effects of fatigue loading, composite action, and bursting were investigated.

The laboratory study provided an opportunity to vary details among the sections and to instrument within the precast sections, whereas all of the Center City Bridge instrumentation was located in the CIP. The laboratory study also afforded the opportunity to apply larger loads than at the Center City Bridge to provide more conclusive results as many of the measured strains associated with the live load truck test were small (i.e. on the order of 10 με).

1.4 Organization

Chapter 2 of this report presents a summary of the literature related to restraint moment development in composite precast bridge systems. Chapter 3 covers the two year monitoring of the Center City Bridge. Chapter 4 presents a description of the live load truck tests conducted on the Center City Bridge and the corresponding results. Chapter 5 outlines the modifications made to the design of the Center City Bridge that were implemented in the design of the laboratory specimen to study and improve upon the system performance. Chapter 6 describes laboratory specimen instrumentation. Chapter 7 outlines the monitoring, testing, and analysis of the laboratory specimen. Summaries, conclusions, and recommendations are given in Chapter 8. The Appendices include precast section design calculations, material testing, data acquisition set up, analysis programs, and instrumentation designation and measured locations.

Chapter 2: Literature Review

The design, implementation, and analysis of the restraint moment investigation in the laboratory study were performed after consideration of previously published research. This included the paper which Mn/DOT used as a design guideline (Freyermuth 1969), and a paper presenting an alternative design method (Peterman and Ramirez 1998).

2.1 Restraint Moments in Continuous Composite Bridges

When precast prestressed bridges are made continuous with a CIP deck, end rotations caused by creep and shrinkage that would occur in a simply-supported span are restrained by the continuity diaphragm leading to the development of restraint moments at the continuous piers. Due to the increased use of continuous composite bridges in the 1960's to eliminate the maintenance associated with the joints of simply-supported, multiple span bridges, a report was published to introduce bridge designers to the concept of restraint moments and to provide a method to predict restraint moments for design purposes (Freyermuth 1969). This report included the required equations to calculate the restraint moment as well as charts to predict the creep and shrinkage values needed in these equations. Equations 2.1-2.3 are the basis of the restraint moment calculation.

$$M_R = \left(C_u \times M_p + C_p \times M_D\right) \times \left(1 - e^{-f}\right) - C_u \times M_s \times \left(\frac{1 - e^{-f}}{f}\right) \tag{2.1}$$

$$M_p = P_e \times d_1 \tag{2.2}$$

$$M_s = e_s \times E_d \times A_d \times d_2 \tag{2.3}$$

where M_R is the calculated restraint moment, M_p and M_s are the uniform moments due to prestress and shrinkage, respectively, M_D is the midspan moment due to dead load, C_u and C_p are the moment coefficients for uniform and parabolic moment diagrams, respectively, φ is the creep coefficient, P_e is the prestress force after losses, d_1 and d_2 are the distances between the center of gravity of the composite section and the center of gravity of the prestress force and CIP concrete, respectively, ε_s is the differential shrinkage between the CIP and precast, and E_d and A_d are the elastic modulus and cross-sectional area of the CIP concrete, respectively. The moment coefficients, C_u and C_p, are calculated by distributing the effects of the prestress, dead load, and shrinkage moments. The moments are applied to the linear,

continuous model of the bridge, and a method such as moment distribution or slope-deflection is utilized to reach equilibrium and uphold the given boundary conditions. These coefficients will be different for the prestress and shrinkage moments which are assumed to be uniformly applied to the spans compared to those for the dead load moments which are assumed to be parabolic. These coefficients will also differ for bridges with different numbers of spans and span lengths. For example, a three span bridge of any, but equal span lengths will have moment coefficients of 1.2 and 0.8 for uniform and parabolic moments, respectively.

A complete design example for a four span continuous prestressed I-girder bridge with a CIP deck was also presented in the Freyermuth report (Freyermuth, 1969). The design procedure in the report is generally referred to as the PCA method and was used by Mn/DOT in the design of the first two applications of the Mn/DOT Precast Composite Slab Span System (PCSSS), which were the Beltrami County and Center City Bridges.

Research at Construction Technology Laboratories (CTL) was performed in the 1980's to improve the predicted behavior of continuous composite bridge systems (Oesterle 1989) compared to the PCA method. This research included creep and shrinkage studies which found that the models given in ACI 209 (1982) gave reasonable predictions. An analytic evaluation of the PCA method was done using the fiber element model PBEAM. For the example given, it was found that the PCA method and PBEAM predicted similar restraint moments when continuity was established at a precast section age of 17 days, but when the age was extended to 67 days, the two predictions diverged with the PCA method predicting a positive restraint moment and PBEAM predicting a negative restraint moment. This divergence seen in the model was attributed to PBEAM accounting for the role of the steel reinforcement in reducing shrinkage, which was not accounted for in the PCA method. It was expected that PBEAM's fiber model set up was capable of handling the complex time dependent analysis required to calculate restraint moments, but it was decided that the program was too difficult to use and computationally expensive. Therefore, another program, BRIDGERM, was developed to calculate restraint moments for design. BRIDGERM is often referred to as the CTL method in literature. This program used the same relationship between creep and shrinkage effects and restraint moment as the PCA

method, but provided a time step method using ACI 209 (1982) to calculate creep and shrinkage rather than charts as in the PCA method. The CTL method also accounted for the effect of losses over time to calculate M_p. There was also a factor introduced to account for the restraint of CIP shrinkage provided by the precast sections that considered the relative axial stiffness of the precast and CIP elements.

Restraint moments were investigated in precast panel bridges made continuous with a CIP deck (Peterman and Ramirez 1998) to determine the applicability of existing restraint moment models, including the PCA method, on shallow bridge sections. The experimental program consisted of two continuous bridge specimens each with equal 20 ft. spans where the restraint moment that developed at the center support was determined by measuring the change in the end reactions over time using load cells. The cross section consisted of two 6 in. deep precast, prestressed panels side by side that were made composite with a 6 in. CIP deck. When the results were compared to the models, it was found that the PCA method greatly overestimated the negative restraint moment that developed over the first 50 days after the continuity pour. The CTL method, which accounted for the restraint of shrinkage provided by the precast section, better predicted the restraint moment than the PCA method, but slightly under-predicted the negative restraint moment before transverse cracking was observed over the center support. However, the CTL method over-predicted the negative restraint moment after diaphragm cracking was observed. Neither the CTL nor PCA method considered the effects of loss of stiffness due to diaphragm cracking in their respective models. On average between the two specimens, the CTL and PCA methods predicted negative restraint moments after cracking larger than those measured by factors of 2.4 and 4.8, respectively. To better match the measured results, the P-method was created including a provision to reduce the stiffness of the diaphragm once the cracking moment was reached. Thus less additional restraint moment was predicted at the pier due to the reduced stiffness after cracking. The P-method used the same basic equations as the PCA and CTL methods for relating creep and shrinkage values to restraint moments, and like the CTL method, the P-method was calculated in time steps and accounted for the shrinkage restraint provided by the precast section, but unlike the CTL method, the P-method also accounted for the shrinkage

restraint provided by the longitudinal deck steel as shown in the reduction factor given in Equation 2.4.

$$RF = \left(\frac{1}{1 + \frac{E_{pc} \times A_{pc}}{E_d \times A_d}} \right) \left(\frac{1}{1 + \frac{E_s \times A_s}{E_d \times A_d}} \right) \tag{2.4}$$

where E_{pc}, E_d, and E_s are Young's moduli of the precast section, CIP deck and deck steel, respectively, and A_{pc}, A_d, and A_s are the cross-sectional areas of the precast section, CIP deck and deck steel, respectively. On average between the two specimens, the P-method over-predicted the measured negative restraint moment after cracking by a factor of 1.4. Peterman and Ramirez (1998) also included a design example using the P-method.

The AASHTO LRFD Specifications (2004) provided only one provision with respect to positive restraint moment design. This was that the bottom fiber stress at the pier was required to be compressive under the combination of restraint moments and 50% of the live load moment in order to consider the connection fully continuous. This must be met for all times in service, but since the positive restraint moment will continue to increase as the precast section creeps due to prestress, the critical time is generally the end of service when the ultimate creep is assumed to be reached.

In 2004, a state-of-the-art report was published on prestressed bridges made continuous with CIP decks (Miller 2004). The focus of this report was on the positive restraint moments that develop in continuous I-girder bridges, and included an experimental program. This report also published recommended revisions to the AASHTO LRFD Specifications (2004) to provide more complete design guidelines. The existing provision that required the bottom fiber stress at the pier to be compressive under the combination of restraint moments and 50% of the live load moment was recommended to remain in the provisions as it seemed reasonable to maintain the effectiveness of the continuity over the pier, but the origin of this provision could not be found. It was also proposed to add a recommendation to the commentary that the positive restraint moment be limited to 1.2 times the cracking moment of the diaphragm as analytical studies (Mirmiran et al. 2001a, b) had found that providing additional reinforcement was not effective and the design of the section or age of the precast sections at which continuity is to be established should be reconsidered

if the predicted positive restraint moment exceeds this value. From the experimental portion of Miller's research, it was found that designing the positive moment capacity for 1.2 times the cracking moment maintained continuity over the pier until the positive moment connection was near its ultimate moment and positive moment cracks extended into the deck.

Positive moment connections of 0.6 and 1.2 times the cracking moment were both tested in Miller's study. It was found that the cracking moment under positive moments at the pier would likely be lower than predicted due to lack of bond at the interface between the end face of the precast section and the CIP in the diaphragm.

Chapter 3: Monitoring of Field Bridge

3.1 Objectives and Methodology of Bridge Monitoring

There were two primary objectives of the monitoring program for the Center City Bridge. The first was to observe the effects of environmental and repeated vehicular loading on the bridge for the first 24 months after continuity was made by pouring the CIP deck. The second was to measure the bridge response when loaded with trucks of known weights and locations as described in Chapter 4. The main concern during the monitoring period was the development of reflective cracking in the CIP deck between adjacent precast sections. However, all of the instrumentation was monitored to look for any unexpected behaviors, such as a positive moment crack that developed at the east pier.

A photograph of the Center City Bridge is provided in Figure 3.1, and a general layout of the bridge instrumentation is given in Figure 3.2. The instrumentation and data acquisition system are described in detail in the Mn/DOT Report 2006-37 (Bell 2006). The instrumentation consisted of 96 vibrating wire (VW) strain gages. There were 15 concrete embedment and seven spot-weldable strain gages oriented in the transverse direction in each of three instrumented joints at midspan of the center span. The 30 remaining gages were VW spot-weldable strain gages on the longitudinal reinforcement distributed along the east and center span. The measured location and naming convention of the Center City Bridge instrumentation is given in Appendix F.

The strain gages were zeroed at 10:00am on October 1, 2005 when the lowest thermal gradient was observed through the depth of the cross section on the first day the readings were automatically taken at two hour intervals. For all of the strain values presented, mechanical strains are given that were obtained by subtracting the thermal strains from the total strains. The thermal strains were calculated using the measured temperatures from the gages and the experimentally determined coefficient of thermal expansion of the CIP concrete (α_c = 5.67 $\mu\varepsilon/^oF$), which is described in Appendix H. For all of the Center City Bridge measurements presented, positive strains are tensile and negative strains are compressive. Plotted results for all 96 VW strain gages are given in Appendix G. The measurement of the strain gage locations was made to the nearest ¼ in.

3.2 Reflective Cracking

Results from monitoring the bridge for 24 months showed satisfactory behavior. Strain fluctuations were such that significant reflective cracking between the adjacent precast sections that were monitored was not observed. However, two of the three monitored joints had daily changes in the VW concrete embedment strain readings that indicated that cracking had initiated. The strain gages were monitored at two hour intervals to observe the daily trends. Daily strain fluctuations of 165 and 260 με in the transverse direction at midspan of the middle span in Joints 1 and 3, respectively, were observed, as compared to only 70 με in Joint 2. These strain fluctuations can also be compared to the those from before cracking was believed to initiate when maximum daily fluctuations of 66, 63, and 55 με were observed in Joints 1, 2, and 3, respectively. The VW spot-weldable strain gage readings from the adjacent mild reinforcement fluctuated similarly, indicating that the reinforcement was effectively spanning the crack. Stresses in the mild steel reduced along the reinforcement away from maximum over the joint between the precast sections indicating that the crack was centered on the joint.

Because VW strain gages are not dynamic, the strain fluctuations were not believed to have resulted from vehicular traffic that would not remain on bridge long enough to be read. Also, the daily fluctuation peaked in the early afternoon when the solar radiation was the highest, and the strains gradually increased and decreased between the daily maximum and minimum. Thus these strain fluctuations and the associated presumed cracking were attributed to the daily thermal changes due to solar radiation. The strain gages immediately over the joint in Joints 1 and 3 first indicated increased strains on April 25, 2006 as shown in Figure 3.3 which shows the strain readings for the VW concrete embedment gage located immediately over the Joint 1 longitudinal joint at midspan of the center span. Because the data was sampled at a two hour interval, the exact daily maximums were not known, but the readings taken indicated that this day had the largest daily change in thermal gradient to which the bridge had been exposed since construction. The thermal gradients were obtained by calculating the slope of the best fit line using the method of least squares through the measured temperatures from the three gages (at heights of 8 ¾, 12, and 15 in. from the bottom of the 18 in. composite section) in a vertical line at midspan of the center span in

Joint 1. The daily change in thermal gradient is plotted in Figure 3.4 from March 16 to May 15, 2006. The value obtained April 25, 2006 was slightly higher than those measured April 17, 2006 and April 23, 2006. Readings in Joint 2 provided similar results. The cracking was most likely due to a combination of shrinkage and temperature effects that produced tensile stresses.

The absence of similar behavior in the embedment gages above the web corners indicated that the crack had not propagated to that level, although there were visible longitudinal cracks on the deck that ran the entire length of the bridge discussed in Section 4.3. There was some divergence of two of the gages near Joint 1 and one of the gages near Joint 3 starting at the end of April 2006, but these three concrete embedment gages were at the far ends of the line of gages centered 8 in. from the web corner. It is highly unlikely that these gages were measuring a phenomenon that originated at the web corner as none of the gages closer to the web corner showed a similar divergence. The complete data for the gages above the web corners is given in Appendix G.

Similar, respective strain fluctuations continued in Joints 1, 2, and 3 for the remainder of the 24 month monitoring period as shown in Figures 3.5-3.7 in which the measured strains for the VW concrete embedment gages located immediately above each of the joints at midspan of the center span were plotted for the entire monitoring period. The spiking of gage CJ2-51-2 from December 16, 2005 to January 5, 2006 was believed to be due to a problem with the gages and not actual strain increases in the bridge.

3.3 Cracking Attributed to Positive Restraint Moment

At the east pier, longitudinal strain readings on the reinforcement at mid-depth of the section indicated a crack due to positive restraint moment. Daily strain changes of greater than 700 με were recorded compared to a maximum daily strain change of 45 με prior to cracking. A plot of the strains over the monitoring period is given in Figure 3.8. The relative position of the gages can be seen in the inset. The inset also shows that the positive moment reinforcement was only provided over the flange regions and not evenly distributed across the width of the bridge. The strains for gage SJ1-C3-2 ended June 21, 2007 when the gage began to malfunction. The 700 με fluctuation corresponded to a stress in the positive

moment steel of 20 ksi, which was near the cyclic stress limit of 23.4 ksi from AASHTO LRFD Specifications (2004) 5.5.3.2, but this is a high cycle fatigue limit generally applied to stresses due to vehicular loads, and the environmental loads are applied less frequently. As with the transverse cracking, there was no unusual activity observed in the instrumentation directly above the strain gage exhibiting the large daily changes, indicating that cracking had not propagated to the top of the CIP. This was the only location in which the reinforcement was instrumented over the pier, as positive moment cracking over the pier was not considered during the design of the instrumentation. The significance of the positive moment crack on bridge performance under live load is discussed in Section 4.5.

The development of the positive moment crack at the pier could not have been caused by vehicular traffic, which would have caused negative moments at the pier. Again, it was expected that the behavior was driven by thermal gradients in the bridge superstructure where the solar radiation heated the top of the bridge. This caused the individual spans of the bridge to camber which generated positive restraint moments. Positive restraint moments are also generated by creep of the precast sections due to their prestress, but this would result in a steady increase in strain over time, not the daily fluctuation observed before the initiation of cracking. The strain fluctuations began April 23, 2006, two days before the large strain fluctuations were observed in the transverse strain gages immediately above the longitudinal joint at midspan. The maximum strain increased over the summer of 2006, remained constant over the following winter, and increased again over the summer of 2007. Also, it appeared that the daily strain fluctuation was somewhat constant, but the overall strain values increased over both the summer of 2006 and the summer of 2007. This would indicate that the positive moment connection might not be able to prevent crack growth. Future monitoring of the Center City Bridge may provide additional information about the adequacy of the positive moment connection. However, at the end of the monitoring period, the strain readings from the mid-depth gage indicated the positive moment crack was causing strains in the VW gage nearing its bound. It was expected that continued monitoring might not be possible if the strain would increase beyond this bound, at which point only the two VW spot-weldable gages directly above could be used to monitor the performance of the positive moment connection. Also, if future applications of the Mn/DOT PCSSS would be built with

the reduced flange thickness as proposed in Section 3.2.1, the positive moment reinforcement would be lower in the cross section and better able to control such cracking.

3.4 Seasonal Trends from Thermal Effects

As can be seen in the plots of the transverse gages immediately above the flange joint given in Figures 3.5 and 3.7, strain fluctuations due to seasonal changes were relatively small compared to daily fluctuations in Joints 1 and 3 where cracking was believed to have occurred as discussed in Section 3.2. For transverse strain gages not measuring the large strain fluctuations immediately above Joints 1 and 3, and for all of the transverse strain gages immediately above Joint 2 shown in Figure 3.6, the seasonal strain fluctuations observed by these gages were likely the results of restraint of thermal expansion of seasonal temperature trends. The strains measured during the summer became more compressive which was attributed to the restrained thermal expansion of the entire bridge superstructure, rather than the thermal gradients that were believed to cause the cracking discussed in Sections 3.2 and 3.3.

Except for the longitudinal pier cracking discussed in Section 3.3, there was little activity in the longitudinal spot-weldable VW gages as these gages were installed to investigate load distribution during the truck test described in Chapter 4. The trends and magnitudes of the longitudinal strains were similar at the various gage locations. The strains from three vertical elevations for which the gages were nominally located at midspan of the center span in Joint 1 are given in Figure 3.9. Two of the four lines plotted come from strain gages placed on the longitudinal deck reinforcement (i.e. at the same elevation). Similarly to the transverse gages, the seasonal strain fluctuations observed by the longitudinal gages were likely the results of restraint of thermal expansion of seasonal temperature trends. Complete plots for the 24 month monitoring period are given in Appendix G for all 96 VW gages. Some of the longitudinal gages located near the east pier (i.e., those shown in Figure G.18) indicated a change at the end of April 2006, but these gages were located too close to the bearing support to infer the cause of these changes.

Chapter 4: Live Load Truck Test of Field Bridge

4.1 Design and Execution of the Live Load Truck Test

The objectives of the live load truck test at the Center City Bridge were to evaluate the design assumptions made with respect to the transverse load distribution and continuity over the pier and to observe the effects of static vehicular live loads on transverse strains above the longitudinal flange joints. The truck test consisted of seven single truck and five paired truck configurations. The locations of the center of the load for each test are shown in Figures 4.1 and 4.2 for the single and paired truck positions, respectively. The nominal coordinates of the truck(s) for the twelve configurations performed and a diagram outlining the dimensions used in this table is given in Figure 4.3. Because it was unknown whether there would be enough time during the truck test to perform all of the configurations, the primary configurations were given numbers and the secondary configurations were given letters.

Configurations 1, 2, 3, 4, A, and B consisted of a single truck with the rear tandem centered on midspan of the center span at various lateral positions. These configurations were designed to provide curvature profiles across the width of the bridge to evaluate distribution factors and continuity over the pier. In addition, transverse strains above the longitudinal joint were measured to investigate the potential for reflective cracking. Wheel loads were centered over the instrumentation in many of the loading configurations to maximize transverse strain readings. Both the truck axle and precast panels were 6 ft. wide, so in Configurations 1, 3, and B, the wheel loads were centered over longitudinal joints, and in Configurations 2, 4, and A, the wheel loads were centered over the webs of the precast sections. Configuration 6 consisted of a single truck with the rear tandem centered on midspan of the outer span to evaluate continuity over the pier.

Originally proposed single truck Configurations 5, C, and D (not shown) were not performed. Configuration 5 involved a single truck 36 in. further from the parapet than Configuration 4 and could not be performed because it interfered with traffic access during the test set up. Configurations C and D involved single trucks at the quarter span of the center spans and were not performed as they were not expected to yield measureable strains.

Configurations 8, 9, 10, and 11 involved paired trucks (stationed side by side as closely as feasible) centered over Joint 1 where most of the longitudinal instrumentation was located. These tests were designed to evaluate continuity over the pier. The final configuration, Configuration E, consisted of two trucks with the rear tandems centered at midspan of the center span, but spaced 12 ft. on center laterally to observe the effects on transverse strains. In this configuration, all three instrumented longitudinal joints would be loaded on each side to evaluate the portion of the transverse strains that was due to global plate bending rather than the stress concentrations when the joint was directly below the load. Originally proposed Configuration 7 (not shown), involving paired trucks 72 in. further from the parapet than Configuration 10, could not be performed because it interfered with traffic access during the test set up.

The live load truck test began on April 18, 2007 at 7:00pm and concluded the following morning at 1:30am. Two tandem dump trucks were filled with sand and had gross vehicle weights of 52.0 and 51.7 kips as measured at a weigh station by the contractor. The rear axle weights were calculated by multiplying the ratio of the axle weight to total truck weight (determined at the field site using drive-on scales) to the gross truck weights (measured at the weigh station). This was done because the total truck weights measured by the scales in the field were not consistent and fluctuated somewhat during reading because the scales required the individual wheel loads being measured to be elevated with respect to the other wheel loads. The measured truck axle weights are given in Table 4.1. The average rear axle weight of the trucks was estimated to be 18.6 kips (scaling the field scale weights to the weigh station weights). Truck dimensions and a photograph of the trucks during the test are given in Figures 4.4 and 4.5, respectively.

The truck locations for each configuration were marked on the pavement before testing began. Measurements were taken to verify the positions of the trucks during testing. The measurements were made to the nearest 0.1 ft. The bridge was cleared of all traffic except the truck(s) employed in the test for four minutes during each test position to ensure that there would be three sets of replicate strain readings recorded at one minute intervals. Start and end times for each test were recorded by two individuals whose watches were synchronized to the data acquisition system to ensure the correct readings would be attributed

to each test. A log of test times and measured truck locations is given in Table 4.2 which shows the number of repeats for each test position. Complete tabulated strain measurements from the live load truck test are given in Appendix I. As discussed in Chapter 2, all of the strain values presented are mechanical strains that were obtained by subtracting the thermal strains from the total strains. These strain values were also corrected for the thermal restraint effects that occurred over the truck test time as the thermal gradient in the bridge superstructure decreased. This was accomplished by zeroing all of the data to a piecewise linear base line of strain readings when the bridge was known to be unloaded. The measured locations and naming convention of the instrumentation is given in Appendix F.

4.2 Reflective Cracking

When wheel loads were placed directly above the three instrumented joints at midspan of the center span, increases in transverse strains of approximately 19 and 32 με in the concrete embedment gages immediately above Joints 1 and 3, respectively, were measured, compared to 7 με in Joint 2. Measurements of the increases in transverse strains in Joint 1 were obtained from the two repeats of Configuration 3 which both indicated 19 με. Measurements of the transverse strains in Joint 2 were averaged from the two repeats each of Configurations 1 and 3 which indicated 6 and 8 με, respectively. Measurements of the increases in transverse strains in Joint 3 were averaged from the two repeats of Configuration 1 which indicated 30 and 31 με and the single test of Configuration B which indicated 34 με. For all of the joints, the maximum increase in transverse strain was experienced by the middle gage of the five concrete embedment gages that was located directly above the transverse joint. Strain increases for the other four gages were lesser and can be seen in Appendix I. The transverse strain results are summarized in Table 4.3. The transverse instrumentation of these three joints is shown in Figure 3.2. Instrumentation designation and measured gage locations are given in Appendix F.

In these configurations when wheel loads were directly above the instrumented longitudinal joints, the loads were trying to open the joint. The resulting transverse strains were expected to be the same in all three joints unless different cracks pre-existed above the joints in the CIP concrete. Because Joints 1 and 3 experienced significantly larger transverse

strains, it was concluded that Joints 1 and 3 had reduced stiffness. This was corroborated by the 24 month monitoring results where it was also concluded that Joints 1 and 3 had experienced some cracking above the longitudinal joint as discussed in Section 3.2. These small strain readings also indicate how negligible the effects of vehicular loads were compared to environmental loads where Joints 1 and 3 experienced daily strain fluctuations of 165 and 260 με, respectively, as discussed in Section 3.2. Assuming the bridge behavior was linear-elastic, a truck would require an axle weight of more than 60 tons to generate the same transverse mechanical strains that thermal effects caused over the course of a day.

Strains measured by the spot-weldable gages on the transverse hooks were slightly smaller than those measured in the adjacent concrete embedment gages, even though the embedment gages were 1 ¼ in. further up from the top of the flange than the spot-weldable gages. This was likely to have been caused by slip between the transverse hook and the CIP concrete due to the large #6 bar diameter, epoxy coating, and perhaps locally due to the prevention of bond by the strain gage cover. It can also be seen in Figure 4.6 that the strain in the transverse hooks dissipated as the distance from the flange joint increased regardless of hook orientation as a similar decrease in strain was seen from the center of the joint to the hooked and embedded ends of the transverse reinforcement. This indicated that the concrete away from the crack was still bonded to the transverse hook and sharing the load. Reflective cracking over the web corners was also a concern for the system, but none of the truck configurations caused tensile stresses in the embedment gages over the web corners over any of the three monitored joints. This can be seen in the complete truck test mechanical strain results presented in Appendix I.

4.3 Surface Cracking

At the end of the live load truck test, surface cracks on the bridge deck were investigated. The lighting was not adequate to clearly see all of the cracks. Those that were observed are identified on the plan view in Figure 4.7. The full length longitudinal cracks appeared to be spaced at 24 to 36 in. throughout the area investigated. All of these cracks appeared to be located over the beam webs with the exception of one crack that appeared to be located over a web corner. This indicated that these were likely shrinkage cracks which

occurred over the webs because the CIP deck was restrained by the precast beam webs. The lone crack over the web corner was over the transverse instrumentation, so if it had propagated down to the web corner it would have been captured by the instrumentation. Because the instrumentation did not pick up this crack, this crack was likely caused by surface shrinkage. There were also smaller full length longitudinal cracks that were spaced at approximately 6 in. There were likely more shrinkage cracks than observed; however, the transversely raked surface treatment of the deck in conjunction with the poor lighting made the cracks difficult to discern.

4.4 Transverse Load Distribution

The truck test was also used to evaluate the load distribution factor used by Mn/DOT to design the Center City Bridge. Because none of the categories in AASHTO LRFD (2004) 4.6.6.2 directly addressed the Mn/DOT Precast Composite Slab Span System (PCSSS), the equation for effective width of a monolithic concrete slab type bridge given in AASHTO LRFD (2004) 4.6.2.3 was used for design. Due to the lack of continuity between the flange faces of the adjacent precast sections, a reduction in transverse stiffness may cause the effective width to be smaller than that of a monolithic system. Load distribution was evaluated by loading the center span at midspan with a single truck at six locations across the width of the bridge. The six locations used were Configurations 1, 2, 3, 4, A, and B. Midspan curvatures were calculated using gages welded to the longitudinal reinforcement in Joints 1 and 2 shown in Figure 4.8. Figure 4.9 shows the typical layout of the rear axles. The transverse distance from the center of the load to the instrumentation in Joints 1 and 2 varied for the six configurations. For these midspan configurations, the truck faced west (left in the Center City Bridge figures), and the front axle load was neglected because it was 6.2 ft past the west pier in the outer span and would have little effect on midspan curvatures in the center span.

Curvatures were calculated by fitting a line through the strains from gages nominally located 9, 12½, and 15½ in. from the bottom of the 18 in. thick composite section. Measured depths of the gages (given in Appendix F) were used for the curvature calculations. Results for the six truck configurations are shown in Figure 4.10 along with the results of a finite

element model of an isotropic flat plate with a smeared stiffness calculated by combining the stiffnesses of the precast sections, CIP deck, and mild deck reinforcement and assuming no cracking. The modulus of elasticity for the concrete components was estimated using AASHTO LRFD (2004) equation C5.4.2.4-1 where the measured 28-day concrete strengths were obtained for the bridge components from Mn/DOT and had values of 9.9 ksi for the precast sections and 4.0 ksi for the CIP deck. The parapets were included in the model, but only had an effect on the results close to the parapet which allowed for superposition of the data for the six tests onto a single plot. In the model, the boundary conditions at the piers were assumed to be single rollers at the center of the piers, resulting in modeled spans of 264, 324, and 264 in. The midspan curvature of the center span corresponding to the same load assumed to be carried over the effective width from the AASHTO equation is also given. For the simply-supported model, the center span was modeled alone with rollers at the center of bearing of the two piers resulting in a span of 306 in , as the distance between the centers of bearing of the adjacent precast sections on a pier was 18 in.

The results generally followed the trend of the isotropic model, from which it can be observed that a design equation for a monolithic slab system is a valid assumption for this system. It can be assumed that longer spans would behave similarly because they would have a deeper overall section, and the height of the gap at the flange tips would be unchanged, so longer span bridges should behave more like monolithic systems than shorter ones.

The isotropic model was also used to predict strains near the pier in the middle span when the bridge was loaded at midspan where another series of gages was located as shown in Figure 4.8. Because the gages were within one depth of the bearing, the assumption of beam theory was not valid, but the strains in the deck steel were compared to those predicted in the isotropic model at the same depths as the gages. Predicted and measured strains for both the positive and negative moment reinforcement are given in Figure 4.11. The model predicted negligible strain for the positive moment steel because it was located at mid-depth of the 18 in. composite section (i.e., neutral axis in the model). Again, the results generally followed the trend of the isotropic model, except that the plot of the strains across the width of the bridge appeared to be slightly more pinched, but the assumption of a monolithic

system appeared to be reasonable. It can also be seen that the strains in the positive moment reinforcement at mid-depth were compressive, which corroborates the existence of positive moment cracking at the pier discussed in Section 3.3 as the concrete below mid-depth must have had a reduced stiffness. The same analysis was performed for Configuration 10 where two trucks were centered at midspan of the center span. In these models, the gap between the trucks was ignored and the inner wheel loads of the two trucks were combined in a single 10 in. by 20 in. patch load to simplify the models. The design assumption also had to be modified because the trucks were spaced closer than the AASHTO effective width. Thus the effective width used in the two truck analysis was equal to the average of the center to center truck spacing plus one half of the AASHTO effective width to the outer side of each truck. The results from these analyses are given in Figures 4.12 and 4.13, respectively for the results at midspan and near the pier.

4.5 Continuity over Piers

Continuity over the piers was evaluated by analyzing the truck test data obtained from instrumentation in Joint 1. The instrumentation used is highlighted in Figure 4.8. When the center span was loaded at midspan, the midspan deck steel strain in the adjacent span due to negative bending was 1.2 με for a single truck and 1.5 με for two trucks, compared to 1.9 and 3.7 με predicted by the isotropic model. The loads in these tests were centered on the Joint 1 instrumentation to maximize the results. The discrepancies were most likely due to moment transferred into the substructure at the piers and abutments of the bridge where perfect rollers were assumed in the model. Because the midspan curvatures from the truck test were smaller than those predicted by the isotropic model, the assumption of full continuity appeared to be conservative. The midspan curvature of the center span for the case without continuity at the pier (i.e., simply-supported case) is also plotted in Figures 4.10 and 4.12 to confirm that the continuity assumption was valid.

There was also concern that the positive moment cracking that had been observed at the east pier would reduce the effectiveness of the negative moment continuity. The positive moment crack due to the effects solar radiation would have to close due to the negative bending or only the positive moment reinforcement would be in compression. As previously

mentioned, the strains measured at midspan of the loaded span were smaller than predicted by the continuous model, so the positive moment crack did not appear to reduce the continuity over the pier. However, the truck test was performed at night in when there would not be an effect of solar radiation, such that the crack may have been closed. If the test was performed on a sunny afternoon in summer when solar radiation effects would be most significant, the crack would be expected to be at its widest, and there may be a reduction in live load continuity in this case.

The neutral axis depth of the specimen was investigated to determine the effects, if any, of transverse shrinkage cracking of the CIP concrete. These cracks would reduce the stiffness of the composite section and lower the neutral axis. This was not expected as the measured longitudinal strains and curvatures were well predicted by the finite element model which assumed no reduction in stiffness of the CIP concrete. Only the data with the largest strains were considered to minimize the error due to gage placement and accuracy. At midspan of the center span when the two trucks were side by side in Configuration 10, the strain readings in Joint 1 and 2 resulted in neutral axis heights of 8.1 and 8.7 in., respectively. These heights average to the predicted neutral axis height for the Center City Bridge of 8.4 in. using transformed sections. However, when the outer span was loaded at midspan with both trucks in Configuration 8, the strain readings in Joint 1 at midspan of the outer span resulted in a neutral axis depth of 7.7 in. This 0.4 in. difference was not considered particularly significant as the gage depths used to obtain the measured neutral axis depth were only taken to the nearest ¼ in., and thus it was determined that any shrinkage cracking did not significantly reduce the effective stiffness of the CIP deck in the Center City Bridge.

Chapter 5: Design Modifications

5.1 Introduction to Design Modifications

To augment the field study of the Mn/DOT Precast Composite Slab Span System (PCSSS), a laboratory study was performed. This afforded the possibility to study behaviors such as bursting, composite action, and prestress losses that required instrumentation of the precast sections which was not possible for the Center City Bridge. The laboratory study also allowed for the primary behaviors of interest (reflective cracking, transverse load distribution, and continuity) to be investigated in a more controlled setting. In addition, the laboratory study provided an opportunity to investigate a variety of modifications to improve the performance and economy of the Mn/DOT PCSSS. The modified parameters were identified through discussion with design engineers, fabricators, and contractors and through investigation into the original Mn/DOT design. A parameter study was performed to finalize the configuration selected for the laboratory specimen.

The size of the laboratory specimen was dictated by the space in the Structures Laboratory and span length of the Center City Bridge. The space in the Structures Laboratory was not long enough to accommodate two spans equal to the 27 ft. center span of the Center City Bridge, so 22 ft. was chosen as the span length which was equal to the outer span lengths of the Center City Bridge. The laboratory specimen was chosen to be two panels wide as the space available could not accommodate an 18 ft. wide specimen. It was also decided to terminate the CIP deck at the web corner of the outer side of the precast sections. This was done to ease the fabrication of the formwork so that the depth of the form could be 6 in. rather than 15 in. Also, in this manner, the side deck forms were bolted to the sides of the precast sections and did not require external bracing which would have been required if the CIP had been carried to the outer flanges.

The boundary condition at the continuous middle support was chosen to match the piers at the Center City Bridge as closely as possible. The top surface of the center support was the same size as that of the Center City Bridge piers and had protruding dowels of the same size and spacing as those in the Center City Bridge. The only difference between the center support of the laboratory specimen and piers of the Center City Bridge was that the

center support was tensioned to the floor with threaded rod which prohibited rotation while the Center City Bridge piers were supported on piles which would allow some rotation. It was decided to model the non-continuous ends in the laboratory as simply supported, which also enabled investigation of restraint moment development at the center pier though monitoring the reactions at the simple supports. The ends of the precast sections were placed on 12 in. wide bearing pads to create the simple support conditions.

5.1.1 Description and Methodology used to design the Original Mn/DOT PCSSS

As mentioned in Sections 1.1 and 1.2, the Mn/DOT PCSSS, based on the French Poutre Dalle System, was originally used in two bridges, a bridge in Beltrami County, MN with three 45 ft spans and a bridge in Center City, MN with spans of 22, 27, and 22 ft. The final cross section of the Center City Bridge precast sections is shown in Figure 1.2.

The flange thickness of 5 ¼ in. was chosen so that the flange could fit an 180^{o} hook around flange mild longitudinal reinforcement vertically spaced at the same 2 in. grid as the prestressing tendons. In the as-built sections, the mild reinforcement was replaced with prestressing tendons nominally stressed to 5 kips each for ease of fabrication. The 6 in. depth of the CIP deck over the webs of the precast section was chosen as the minimum to provide adequate cover for the deck reinforcement. Another critical consideration for the original design was the spacing of the transverse hooks that crossed the longitudinal joint between the flanges of adjacent precast sections. Both the transverse hooks and the hoops around the longitudinal reinforcement in the trough area over the flanges were designed at a 12 in. spacing which was scaled from drawings of the Poutre Dalle system and shown to be a conservative implementation of the AASHTO LRFD (2004) transverse distribution reinforcement requirements, which are further discussed in Section 5.2.3. The same 12 in. spacing was used in both of the initial Mn/DOT PCSSS bridge implementations because the choice was somewhat arbitrary and conservative with respect to the AASHTO requirements. The bursting reinforcement used at the ends of the sections in both bridges was based on a maximum span length of 50 ft. to minimize variations in fabrication.

5.1.2 Objectives of Design Modifications and Parameter Study

The objective in the design of the laboratory sections was to create a system that would allow for investigation of the original design in comparison to the data collected from the field, as well as investigation of design alternatives in comparison to the original design. The laboratory specimen was divided into eight regions to reduce the number of variables considered in any given comparison. Each of the two spans (i.e., 1 and 2) had a north and a south precast section, and each precast section had an east and a west end as shown in Figure 5.1. This approach allowed for comparisons between spans, between side by side precast sections in the same span, and between ends of the precast sections as dictated by the parameter being considered.

Primary considerations in selecting the modifications to be implemented in the laboratory specimen were improving system performance and easing fabrication to reduce labor cost and fabrication time. Once potential modifications were identified and designed, a parameter study was performed to determine how to lay out the test specimen to facilitate comparison between the original and proposed designs. The eleven proposed modifications originally considered are summarized in Table 5.1 which also indicates the effects which might be impacted by the proposed modification, as well as the potential sections considered for modification. Descriptive images of the proposed modifications are given in Table 5.2 which shows a comparison of the proposed versus the original details. The final parameters chosen for study are summarized in Figure 5.1. The as-built cross sections and layouts of the laboratory precast sections are given in Figures 5.2-5.13, and notes are included where the as-built sections deviated from the design. As a control, the west end of Beam 2S of the laboratory specimen was identical to the precast sections in the Center City Bridge.

The following sections each address a performance concern (e.g., reflective cracking) that was investigated as listed in Table 5.1. The subsections then address the expected influence of the associated proposed modifications (e.g., reduced flange thickness) on that aspect of performance. Restraint moment was added as a performance concern as it had a considerable effect on the original design, and there was interest in investigating the effects of varying the age of the precast sections when the continuity pour was made.

5.2 Reflective Cracking

Reflective cracking is a primary concern for all systems that incorporate precast panels covered by CIP concrete. These cracks are of particular concern in states with cold weather climates such as Minnesota where deicing chemicals can seep into cracks and corrode the reinforcement. In addition to corrosion, significant reflective cracking could lead to separation of the panels from each other resulting in differential deflections between the panels and a decrease in transverse load distribution. Reflective cracking modes of concern for the Mn/DOT PCSSS are shown in Figure 5.14. Initiation of reflective cracking was thought to be influenced by loading, relative thickness and stiffness of the layers, and bond between the layers. In the case of precast panels topped with CIP concrete, the adjacent precast panel flanges that form the longitudinal joint simulate a crack along the joint. A potential stress concentration located above the flange joint caused concern for reflective cracking in the CIP. There was also concern for a stress concentration in the CIP at the web corners of the precast concrete that could propagate a crack from the web corner to the top of the CIP.

The original Mn/DOT PCSSS design was an improved detail compared to panel type bridges where the longitudinal flange joint would be the full depth of the precast section, but a reduction in flange thickness was investigated to further decrease the likelihood of reflective cracking. In addition, it was thought that the use of bond breakers and a smooth surface on the top of the precast flange may reduce the likelihood of reflective cracking by reducing the abrupt stress concentration at the joint. However, there was concern that the reduced bond would also reduce the longitudinal stiffness of the composite section. The alignment and spacing of the transverse hooks that cross the longitudinal flange joint were investigated as the purpose of this reinforcement was to control reflective cracks. Lastly, the size of the chamfers at the web corners of the precast sections was investigated to reduce the stress concentration that would lead to reflective cracking.

5.2.1 Reduced Flange Thickness

Reducing the flange thickness was thought to decrease the transverse tensile stresses in the CIP deck directly above the flange joint. As the thickness of the flange is reduced, the transverse stiffness of the CIP deck increases greatly because the moment of inertia is

proportional to depth cubed. As a result, it was expected that this modification would serve to both decrease the stress concentration at the flange joint and enhance the ability of the CIP above the joint to manage the stress concentration without cracking. There was also the added benefit of being able to place transverse reinforcement lower in the section to transfer load between adjacent panels.

Discussions among Mn/DOT bridge engineers, U of MN researchers, precast fabricators, and bridge contractors were held to arrive at a consensus of a minimum flange thickness that would be required for fabrication, transportation, placement, and construction loads. All agreed that 3 in. was a reasonable minimum thickness for fabrication and transportation purposes, and more than adequate for construction. The capacity of the flange was calculated by representing the flange as a cantilever and finding the distributed load that would cause the flange to reach the cracking moment at the web-flange interface. The 3 in. flange assuming 6 ksi concrete was estimated to be able to withstand 1450 psf without cracking, which was much more than the 188 psf required to support the CIP concrete during construction. Use of a 3 in. thick flange reduced the ratio of the depth of the discontinuity to section depth from 29% with the original 5.25 in flange to 16%.

As can be seen in the drawing of the original section (Figure 5.12), the change in flange thickness required redesign of the reinforcement in the flange. The transverse bars with 180^{o} hooks that extended into the flange, labeled S1301E in Figure 5.12, were reduced to a single #4 bar that was spaced at 12 in. to meet shrinkage and temperature requirements. The rebar labeling system used was from the Mn/DOT plans for the Center City Bridge which were included in the *Mn/DOT Report 2006-37 Application of Precast Decks and Other Elements to Bridge Structures* (Bell 2006), the first two numbers give the bar diameter in mm., the next two numbers are the label for the reinforcement shape, and the "E" signifies that the bar is epoxy coated. The #4 bar was placed as shown in Figure 5.2 and spaced shown in Figure 5.4. The top two prestressing strands in each flange were eliminated. These strands were not taken into account in the original calculations and no other considerations needed to be made for their exclusion as they were only stressed to 5 kips as a replacement for mild steel.

The reduced flange thickness also affected the placement of the #6 transverse hooks that extended out of the sides of the webs. These bars were used to control cracking over the joint and to prevent such cracks from propagating to the roadway surface; therefore, they should be located as close to the flange surface as possible. However, the transverse hooks could not be lowered as close to the flange as desired due to the raised permanent side edge of the form and the location of the prestressing strand anchorage template at ends of the precasting bed where the sections were fabricated. Although not used in the reduced flange precast sections, the top two prestressing strands used in the precast sections with the 5 ¼ in. flange were present on the precasting bed as all four of the laboratory specimen precast sections were cast at the same time.

As a result, even though the flange was reduced by 2¼ in. to 3 in., the transverse hooks could only be lowered by ¾ in. The position for the transverse hook is shown in Figure 5.2 for the reduced flange section. This was expected to negate to some degree the benefits of flange thickness reduction on reflective cracking; however, it was felt that the overall change in behavior would still be beneficial. If the reduced flange thickness is used in the future, this constraint could be eliminated by making new side forms for the flanges so that the transverse hooks can sit as close to the flange surface as possible. In the laboratory specimen, Span 1 had the reduced flange thickness, and Span 2 had the original flange thickness.

The reduction in flange thickness also necessitated a change in the vertical dimension of the cage placed in the trough over the precast flanges. The out-to-out cage dimension for the 5.25 in. flange was 5.5 in. by 20 in., as in the field bridge. Whereas for the 3 in flange, the out-to-out cage dimension was increased to 8.5 in. by 20 in., with this design change, the cage intentionally protruded above the top of the precast webs to enhance composite action.

5.2.2 Smooth Flange Surface

It was thought that reducing the bond between the CIP concrete and the top precast flange surface would decrease the stress concentration in the CIP directly above the abutting flanges, and consequently reduce the likelihood of developing reflective cracking. The top surface of the flange was altered such that it no longer had a ¼ in. roughened contact surface as in the original design. The alteration also eased fabrication as it was difficult to remove

the form from the top of the flange out from under the transverse hooks, especially with the roughened surface. This change was not expected to have a significant negative impact on the longitudinal behavior of the specimen because the interface was below the neutral axis of the section in positive bending. The effects of this change were expected to be somewhat negated as the flange surface was still slightly roughened due to unintentional small, shallow surface voids as shown in Figure 5.15. These voids were caused by air bubbles trapped under the flange top forms. In the laboratory specimen, Span 1 had "smooth" flanges and Span 2 had flanges with an intentionally roughed surface.

5.2.3 Alignment and Spacing of Transverse Hooks

In addition to reducing the stress concentrations that would initiate reflective cracking, the amount and distribution of transverse reinforcement that would intersect such cracks were also investigated. In the original design, the transverse hooks were slightly staggered such that the hooks from adjacent precast sections would line up next to each other but not interfere with each other during placement. The original design was somewhat arbitrary, and loosely scaled from what was used in the French Poutre Dalle bridges and conservative compared to the requirements in AASHTO LRFD (2004) 5.14.4.1 for transverse distribution reinforcement. This resulted in #6 bars protruding from adjacent precast sections placed right next to each other crossing the flange joint every 12 in. The AASHTO LRFD (2004) 5.14.4.1 transverse distribution requirement for the Center City Bridge was only 0.09 $in.^2/ft.$ compared to the 0.44 $in.^2/ft.$ from the #6 bars. For the modified design, it was thought that there may be some advantage to staggering the transverse hooks. It was expected that the combined anchorage of the hook and rebar cage would provide adequate development such that a single hook from one web would be sufficient for controlling cracking over the flange joint without being lapped by another hook from the opposite web. An additional advantage of staggering the transverse hooks was that the increased space around the bars should enable better development than the case where the loop of the rebar cage (identified in Figure 1.1) and both transverse hooks were located adjacent to each other.

Changing the overall spacing of the transverse hooks in the modified sections was also considered as the 12 in. spacing in the original design was somewhat arbitrary. There was not a strong consensus in the literature (Bice and Frosch 2006, Broms 1965, and Gilbert

2005) on how to calculate the amount of reinforcement for crack control, nor was there a clear way to determine the transverse tensile stresses that would develop over the flange discontinuity.

Due to the limited number of precast sections in the laboratory study, neither alignment nor spacing of the transverse hooks were selected for investigation as these parameters were thought to potentially obscure the results of other selected modifications (e.g., reduced flange thickness) that could affect reflective cracking.

Further investigation into the transverse connection between the precast sections including the spacing and alignment of the transverse hooks may be performed in NCHRP 10-71 *Cast-in-Place Concrete Connections for Precast Deck System*.

5.2.4 Increased Chamfer of Web Corners

There was also concern that reflective cracking could occur over the corners of the beam web as shown in Figure 5.14. A right angle in the precast section was a potential source of stress concentration in the CIP concrete. To reduce this stress concentration, the original sections were designed with a ¾ in. chamfer. It was not known whether or not this chamfer would be sufficient, so it was proposed to increase the original chamfer to 1½ in. to ease this transition in the modified sections. After fabrication it was observed that the chamfer was roughly 1 in. by ½ in. as shown in Figure 5.16 compared to the designed ¾ in. by ¾ in., and the fabricator did not attempt the higher 1 ½ in. chamfer on one side as they simply used the edger they had on hand. For comparison, the web corners of the north beams were ground to roughly 1 in. by 1 in. as shown in Figure 5.17 to see if the aspect ratio of the chamfer would be important or if the original method of fabrication was adequate.

5.3 Transverse Load Distribution

As discussed in Section 4.4, none of the bridge types described in the distribution factor section of the AASHTO LRFD Specification (2004) had criteria completely met by the Mn/DOT PCSSS. During the initial design, the system was assumed to be closest to a slab span bridge (AASHTO LRFD (2004) 4.6.2.3), even though the system was not monolithic. The equation that was used to calculate the distribution factors was simple, and because it assumed a monolithic deck, the depth of the discontinuity was not considered even though it

was expected to have a significant effect on transverse load distribution. Therefore, one of the objectives of the laboratory study was to investigate the validity of this aspect of the design and make further recommendations if needed.

However, unlike the Center City Bridge, the precast sections of the laboratory specimen were cast with two different flange thicknesses. In addition to improving reflective cracking performance, the reduction in flange thickness from 5 ¼ in. in Span 2 to 3 in. in Span 1 was expected to improve transverse load distribution because of the increased transverse stiffness of the CIP over the flange joint.

5.3.1 Reduced Flange Thickness

The reduction in flange thickness was expected to improve transverse load distribution. The distribution of load depended on the relative stiffnesses in the longitudinal and transverse directions as well as on the span length and bridge width. The stiffness in the transverse direction is proportional to the depth of the CIP over the flange cubed, so it was expected that the transverse load distribution would be sensitive to the thickness of the flange. Having two spans, one of 3 in. and one of 5 ¼ in. flange thickness, allowed for the investigation of this change on transverse load distribution.

5.4 Longitudinal Flexural Behavior

In the design of the Mn/DOT PCSSS, it was assumed that the CIP portion of the deck would provide full negative moment continuity over the piers. Because the continuity diaphragm over the pier was provided for the full depth of the section, this was expected to be a valid assumption, and one objective of this project was to verify this assumption. This allowed for reduced positive live load moments at midspan and a more economical design. There was also concern that positive moments at the piers due to restraint of creep, shrinkage, and thermal gradients could cause cracks at the pier that would have to close before the connection at the pier could effectively transfer negative moment. Because the bond between the ends of the precast sections and the 4 in. of concrete cast between the precast section ends over the pier was not expected to be effective in resisting positive moment and the reinforcement at the bottom of the cross section at the pier was sparse (four #8 bars over the flanges of each precast section, located 9 in from the top of the pier),

cracking was expected to readily occur if subjected to positive moments at the pier. No design changes where considered to improve the continuity over the pier. The only change related to continuity over the piers was a reduction in longitudinal deck steel to reduce conservatism in the original design.

5.4.1 Reduced Longitudinal Deck Steel

The amount of longitudinal reinforcement required to provide continuity over the piers for the Center City Bridge was much less than that provided due to conservatism in the negative restraint moment design as will be discussed in Section 5.7. The deck steel was reduced from two #7's and one #8 per 12 in. to #6 bars at 6 in., as shown in Figure 5.18. The clear cover of 3 in. from the original Mn/DOT design was maintained, resulting in an effective depth of 14.5 in. for the #8 bars which was also used for the other bars to simplify analysis. The reduced deck steel satisfied the same live load moment as the Mn/DOT design, but with a reduced assumed negative restraint moment (i.e., the value tabulated in Table 5.4). This modification reduced the reinforcement ratio from 1.14% to 0.51%. The reduction in deck steel was not expected to have an adverse impact on the continuity because of the conservatism in the original design, but it was decided to provide the original design on one side of the bridge and the proposed design on the other. This allowed for investigation of the 4% reduction in the longitudinal stiffness on deflections and transverse load distribution. The reduced deck steel design was implemented on the North side of the laboratory specimen and the original deck steel design was implemented on the South side, as shown in Figure 5.1.

5.5 Composite Action

For the Center City Bridge, the shear strength of the concrete was such that no transverse reinforcement was required for vertical shear. Thus the only requirement for transverse reinforcement was for horizontal shear transfer between the precast sections and the CIP deck. There were two areas needing improvement in the transverse reinforcement design. First, as will be discussed in Section 5.8, the stirrup placement was time consuming during fabrication, so any increase in stirrup spacing would be an economical improvement.

Second, it was noted that the stirrup returns were too close to the top surface of the precast section to provide much benefit to composite action.

5.5.1 Increased Stirrup Spacing

The original design of the horizontal shear reinforcement according to Section 5.8.4.1 of the AASHTO LRFD Specification (2004) gave a maximum spacing of 15 in. near the ends of the span where shears were larger and 24 in. for the rest, which was conservatively rounded to 12 in. for the entire span. To investigate increasing the stirrup spacing, horizontal shear calculations were done using both the AASHTO LRFD (2004) and ACI 318-02 codes as these provisions gave different values and may not have been developed considering a slab type element. These calculations are included in Appendix A. The factored shear force at the critical section of the inner span of the Center City Bridge was 68.5 k, compared to the design strength from the AASHTO LRFD (2004) of 78.3 k. ACI 318-02 has different provisions for horizontal shear than AASHTO, so the design strength predicted by ACI 318-02 was also investigated and found to require minimum reinforcement to satisfy the strength requirement. Assuming minimum reinforcement requirements are met (e.g., #5 bars at 12in.), results in a calculated design strength of 128 k. A recent study by Naito and Deschenes (2006) conducted at Lehigh University indicated that current design requirements are excessively conservative with respect to horizontal shear reinforcement. As a consequence, the proposed horizontal shear reinforcement (i.e., #5 stirrups at 24 in.) met the strength requirements of AASHTO LRFD (2004), although it exceeded the minimum reinforcement requirements. All of Span 1 had the proposed spacing, and all of Span 2 had the original reinforcement spacing as shown in Figure 5.1.

It was considered that the portion of the side face of the web above the neutral axis would also contribute to composite action, but this might not be conservative because if the precast section were to undergo flexural cracking, the neutral axis would move up in the section. There was also a consideration to remove all horizontal shear reinforcement as it was expected that the laboratory specimen would still maintain full composite action to failure at ultimate, but it seemed that one test would not be sufficient to ignore the AASHTO maximum horizontal shear reinforcement spacing. Therefore the proposed reduction represented an improvement in economy that would be more readily adopted in practice.

5.5.2 Increased Clear Spacing under Stirrup Returns (Hooks)

During the construction of the Center City Bridge, it was observed that the returns for the horizontal shear transfer reinforcement had insufficient clearance relative to the top of the section and could block concrete from getting under the hook, creating a void. The lack of clear distance under the hooks for the Center City Bridge is shown in Figure 5.19 for one of the precast sections. Looking at the specified size of these stirrups from the original design, there was a nominal ¼ in. gap between the bottom of the bar and the top of the precast section. In the design modifications, the gap was increased to 1-3/8 in. to facilitate concrete placement and development of the reinforcement. To increase the gap, the hooks were placed at the same level as the transverse deck steel for shrinkage and temperature. This was the largest clear spacing that could be achieved without having to thread the longitudinal deck steel under the hooks, which is what would be required to meet the AASHTO LRFD Specifications (2004) anchorage requirement for horizontal shear transfer reinforcement to be fully developed at the precast and CIP interface (5.8.4.1), but it would be impractical due to the increase in cost to construct the bridge. The increased clear spacing under the hooks was used in Span 1, and the original clear spacing was used in Span 2 as shown in Figure 5.1.

5.6 Bursting

In the bursting design for the Mn/DOT PCSSS, a single detail for bursting was created for bridges with spans up to 50 ft. and including 1,000 kips of prestress force. This design was implemented in the Center City Bridge. The AASHTO code provision was particularly restrictive for the slab span system because of the high prestress force and the short beam height. This required a large amount of reinforcement placed over a short distance which increased the difficulty and cost of fabrication. The provision was intended to control the formation of horizontal cracks in the web of precast beams due to vertical tension forces. Research at the Portland Cement Association (PCA) Laboratory (Marshall and Mattock 1962) found that the tensile stress carried by this reinforcement was proportional to the beam height as well as the prestress force, and it was believed that this report was the basis of the AASHTO LRFD Specification (2004) provision 5.10.10.1, which was simplified for design purposes. For a precast I-section with a height of 48 in. reinforced

with ½ in. strands, both the AASHTO provision and the PCA report called for 4% of the prestressing force to be resisted by vertical bursting reinforcement. However, for shallow precast sections such as those in the Mn/DOT PCSSS, the AASHTO provision would still call for 4% of the prestress forces to be resisted by the vertical bursting reinforcement while the PCA report would call for only 1%. Thus it can be inferred that the AASHTO bursting provision was simplified to ease the design of I-girders and other deeper precast sections and not for a slab type section. Application of a rational approach that includes section depth in the bursting design, such as that given in the PCA report, seemed reasonable for the shallow inverted "T' sections. This topic was further investigated as part of the NCHRP 10-71 *Cast-in-Place Concrete Connections for Precast Deck System* project.

5.6.1 Reduced Bursting Reinforcement

Because of the perceived conservatism in the AASHTO bursting provisions for these shallow sections, each of the four beam ends with a given flange thickness had a different bursting configuration to investigate the stresses in the vertical bursting reinforcement and surrounding concrete in the precast sections during prestress release at the precast plant. Similar bursting reinforcement details were implemented in the sections with different flange thicknesses to investigate any potential effect that the 8% reduction in cross-sectional area from the decrease in flange thickness might have on the distribution of stresses due to the prestress force. In each span, the SW precast section end had the bursting steel used in the Center City Bridge, which was conservatively based on the requirements for a longer span (i.e., 4% of 1,000 kips of prestress force) and consisted of three sets of double #5 stirrups at a 2 in. spacing. The SE precast section end bursting steel detail was designed using the actual prestress force (i.e., 496 kips) using the same AASHTO 4% requirement and consisted of two sets of single #5 stirrups at a 2 in. spacing. The north precast section ends of each span had the height proportional design resulting from the PCA research where 1% of the 496 kips of prestress force was resisted by the bursting reinforcement. Two different configurations were used to meet the required steel area, Configuration I which used two #3 stirrups spaced at 2 in. and Configuration II which used a single #4 stirrup. Section and reinforcement layouts are given in Figures 5.2-5.13. The bursting calculations are given in Appendix A.

5.7 Restraint Moment

When bridge systems are made continuous by a CIP deck, restraint moments at the bridge piers need to be considered due to the variation in time-dependent effects from differential shrinkage and creep in the precast sections relative to the CIP concrete. These moments can be positive or negative, but the development of positive restraint moments is of greater concern. Positive restraint moments develop at the supports when CIP concrete is cast on relatively young precast concrete sections, and they negate to some degree the benefit gained by making the bridge continuous. The effects of age of the precast sections at the time of continuity on restraint moment are shown in Figure 5.20. The positive restraint moment was predicted by the P-method (Peterman and Ramirez 1998) for the Center City Bridge assuming continuity when the precast sections were 7, 14, 21, 45, and 90 days old. The expected magnitude of the restraint moments were predicted using both the original design methodology based on the PCA method (Freyermuth 1969) and by applying the P-method as found in the literature. Design considerations from *NCHRP 519* (Miller 2004) proposed to supplement the limited guidelines that currently exist in the AASHTO LRFD Specifications (2004) were also investigated.

5.7.1 Restraint Moment Analysis

Two methods for determining restraint moments were considered: one developed by the PCA and the P-method. There are three primary differences between the PCA method and the P-method: span modeling assumptions, shrinkage constraint, and creep and shrinkage models.

Using the PCA method, the diaphragm was modeled as a single point, whereas the P-method considered the diaphragm as its own span with a finite length. The difference can be seen for the Center City Bridge in Figures 5.21 and 5.22. This modeling difference affected the contribution of the prestress, shrinkage, and dead load moments (i.e., M_p, M_s, and M_d) to the restraint moments as the moment coefficients introduced in Section 2.1 depend on the number of spans and the span length. As shown in the figures, both the PCA and P-methods use the modeling assumption that the supports at the pier and abutments act as rollers, which was also the assumption used when Mn/DOT designed the original PCSSS bridges. Both the

pier and abutments were expected to provide some rotational stiffness, but neglecting these effects greatly simplified the model and was conservative. It should also be noted that in design of the Center City Bridge, Mn/DOT used the simplifying assumption that the maximum moment due to dead load in the shorter outer spans was the same as that of the longer center span to obtain the applicable moment coefficients. This resulted in higher apparent dead load creep, reduced the predicted positive restraint moment, and increased the predicted negative restraint moment.

Due to these modeling differences, the PCA method had smaller moment coefficients than the P-method for the Center City Bridge. For the PCA method, the uniform moments, M_p and M_s, had a moment coefficient of 1.18 and the parabolic moment, M_d, had a moment coefficient of 0.67. The restraint moment coefficients for the PCA method are graphically shown in Figure 5.23. For the P-method, different restraint moments were obtained for the inner and outer spans because the P-method included an extra span for the diaphragms resulting in a five span linear, continuous model. Each diaphragm had a length of 18 in., which was the length between the centers of bearings of the adjacent beams. For the outer spans, M_p and M_s had a moment coefficient of 1.37 and M_d had a moment coefficient of 0.63. For the inner span, M_p and M_s had a moment coefficient of 0.94 and M_d had a moment coefficient of 0.63. The restraint moment coefficients for the P-method are graphically shown in Figure 5.24. These values took into consideration that the shorter spans would have a smaller midspan dead load moment. Thus the moment coefficient for M_p and M_s were predicted to be 14% less using the PCA method than the larger value from the P-method for the Center City Bridge. However, the longer inner span of the Center City Bridge had a larger positive dead load moment at midspan than the outer spans; therefore, the positive restraint moment contribution to the controlling midspan positive moment for design was smaller for the P-method than the PCA method. The moment coefficients for the Center City Bridge are summarized in Table 5.3.

The same analysis was applied to the Beltrami County Bridge, which had three equal spans of 45 ft. and the same diaphragm length of 18 in. For the PCA method, the uniform moments, M_p and M_s, had a moment coefficient of 1.2 and the parabolic moment, M_d, had a moment coefficient of 0.8. Using the P-method for the outer spans, M_p and M_s had a moment

coefficient of 1.43 and M_d had a moment coefficient of 0.96. Using the P-method for the inner span, M_p and M_s had a moment coefficient of 0.96 and M_d had a moment coefficient of 0.64. The moment coefficient for M_p and M_s was predicted to be 16% less using the PCA method rather than the P-method for the outer span of the Beltrami County Bridge. Similarly, the moment coefficient for M_d was predicted to be 17% less using the PCA method rather than the P-method for the Beltrami County Bridge. The moment coefficients for the Beltrami County Bridge are also summarized in Table 5.3.

The second primary difference between the PCA method and the P-method was that the PCA method neglected restraint of the deck shrinkage by the precast section and deck steel. The assumed free shrinkage cannot occur because both the deck steel and the precast section take on compressive load as the deck shrinks longitudinally, reducing the amount of relative shortening that occurs. As mentioned in Section 2.1, the CTL method included a reduction factor to account for the shrinkage restraint provided by the precast beam, and the P-method accounted for the shrinkage restraint provided by both the precast beam and longitudinal deck steel. This was consistent with the findings in *NCHRP 519* which reported that models generally over predict the negative restraint moments due to differential shrinkage which leads to larger than expected positive restraint moments and suggested this problem as an area requiring further research.

The third primary difference between the PCA method and P-method was the values of creep and shrinkage that were used to compute the restraint moments. The paper outlining the PCA method (Freyermuth 1969) included charts for computing creep and shrinkage. The P-method, on the other hand, did not provide creep and shrinkage values, so the method in the AASHTO LRFD Specifications (2004), which was a slight modification from the method presented in ACI 209, were used for the P-method calculations. For the Center City Bridge, the PCA method charts resulted in creep predictions higher than those calculated using the AASHTO equations. The ultimate creep coefficient using the method from the PCA method charts was 3.58, while the AASHTO equations gave a value of 1.92. Twenty years was assumed as the time to reach the ultimate creep for both methods. The differences obtained for the ultimate creep coefficients were similar for the Beltrami County Bridge with the PCA method charts and the AASHTO equations giving values of 3.43 and 1.83, respectively.

Thus, use of the creep coefficients from the PCA method charts resulted in larger ultimate positive restraint moments compared to those using the AASHTO equations.

The overall comparison between the design values for the restraint moments for the PCA method using the Freyermuth paper charts for creep and the P-method using the AASHTO LRFD Specifications (2004) for creep showed that the PCA method predicted a much larger maximum negative restraint moment and a lesser positive restraint moment compared to the P-method. Table 5.4 compares the maximum positive and negative restraint moments, and times after continuity at which they are observed to occur, over the course of a 20 year period calculated using the PCA method and the P-method assuming times of continuity at either 14 or 90 days for both the Center City and Beltrami County Bridges. The 20 year period was assumed as the time after which time dependent effects plateaued.

5.7.2 Restraint Moment Design

As mentioned in Section 2.1, *NCHRP 519* discussed two design considerations for positive restraint moments. The first was limiting φM_n to $1.2M_{cr}$ of the continuity diaphragm, effectively limiting the amount of positive moment reinforcement. The second limit, taken from AASHTO LRFD (2004) 5.14.1.2.7c, restricted the allowable positive restraint moment to be no larger than the sum of the moments at the support due to sustained loads (i.e., superimposed dead loads) and 50% of the live load.

Although *NCHRP 519* recommendations had not yet been incorporated into the AASHTO LRFD (2004) at the time the bridges were designed, the application of the *NCHRP 519* criteria for both the Center City and Beltrami County Bridges is shown in Table 5.5, where $RM_{14d,max}$ and $RM_{28d,max}$ are the predicted maximum positive restraint moments for continuity made at 14 and 28 days, respectively, using the P-method. These two times were used for this comparison because 14 days was considered the youngest, likely precast girder age and 28 days was considered a typical precast girder age. The allowable positive restraint moment is taken as the lesser of $0.5M_{LL}+ M_{SDL}$ and $1.2\ M_{cr}$. For the Center City Bridge, this allowable positive restraint moment was exceeded for continuity made at either 14 or 28 days. Because of the small live load moment at the pier due to the short span length, the allowable positive restraint moment in this case was only $0.46M_{cr}$. The predicted restraint moment in the 14-day case using the P-method was $0.69M_{cr}$. It seemed reasonable to

consider these fractions of M_{cr} as acceptable, and thus consider the bridges to behave as continuous. This was not an issue addressed in *NCHRP 519* as the design examples for the I-girder and box girder that were presented were controlled by $1.2M_{cr}$ rather than the AASHTO continuity requirement. However, there was commentary that cracking at smaller moments than predicted by assuming a monolithic cross section was likely due to the cold joint between the CIP diaphragm and the end of the precast beam. Therefore, a minimum value of the allowable positive restraint moment could be established as a percentage of the cracking moment, as the research in *NRCHP 519* found that positive moment cracking did not affect continuity over the pier until the positive moment connection was near failure.

Comparing the positive moment connections of the Mn/DOT PCSSS bridges to the $1.2M_{cr}$ *NCHRP 519* recommendation showed that these connections were fairly well designed, but could have had a slightly higher design strength. For the Center City Bridge the design strength (φM_n) was $0.89M_{cr}$ for the 5 ¼ in. original flange thickness, and the design strength increased to $1.10M_{cr}$ when the flange was reduced to 3 in. for the proposed design because the same four #8 bars would be lower in the section. This calculation was made assuming the bars could be lowered the full 2 ¼ in. flange thickness, which was not the case for the laboratory specimen as discussed in Section 5.2.1. For the Beltrami County Bridge the positive moment design strength was $0.84M_{cr}$. The positive moment connection calculations for ϕM_n and M_{cr} are given in Appendix A.

5.8 Fabrication and Construction Economy

Many of the design changes were focused on making the precast sections easier and more economical to fabricate, and often these changes originated due to concerns expressed by the fabricators. The most overwhelming concern was the congestion of reinforcement. Due to the shape of the transverse reinforcement and the constraints of the precasting bed, the strands had to be strung through each stirrup prior to stressing. The congestion is evident in Figure 5.25. This method of fabrication was time consuming, and if a strand was found to miss just one stirrup, it would have to be released and restrung.

Two steps were taken to modify the reinforcement to ease fabrication. First, the design changes discussed above reduced the amount of transverse reinforcement required for

both horizontal shear transfer and bursting. Second, the stirrups were altered such that they could be placed after the strands were stressed. The returns at the top of the bursting stirrups were removed because they did not provide anchorage during release when bursting stresses were of concern, and horizontal shear transfer was not required for these stirrups as they were located within one half spacing of the end of the precast section for the horizontal shear requirement. The horizontal shear reinforcement was modified by separating the "U" shape into two "C" shapes. The width of the precast sections provided sufficient room for adequate development of the horizontal shear reinforcement without requiring the stirrups to be continuous as shown in the calculations of Appendix A.4. A closed loop was still provided through the combination of the straight #4 bar (S13AE), the two "C" shaped stirrups (S16HE), and the upside down "U" shaped #4 (S1307E) as seen in Figure 5.2.

Another fabrication concern was the difficulty of removing the panel that formed the top of the flange due to the tight constraint of the #6 hooks that protruded from the side of the web. Because of the intentionally roughened surface, these forms had to be lifted from the surface before they could be slid out. The modification of the forms to provide the proposed smooth surface alleviated this concern as the forms were able to be slid out more easily.

Chapter 6: Instrumentation of Laboratory Bridge Specimen

6.1 Instrumentation Objectives and Specimen Design

The instrumentation plan for the laboratory bridge specimen was developed to meet several objectives. The first objective was to facilitate the comparison of behaviors between the Center City Bridge and the laboratory bridge specimen. To achieve this objective, the laboratory specimen instrumentation was placed in similar locations to that of the bridge in the field in equal or greater quantity. The second objective was to investigate differences in the responses of the four precast sections which each addressed particular design modifications as shown in Figure 5.1.

The number of gages and the types of instruments used was restricted by the data acquisition systems available. In total, 30 vibrating wire (VW), 344 resistive strain gages, and 16 linear variable differential transformers (LVDT's) were used. A general layout of the laboratory specimen strain gage instrumentation is given in Figure 6.1. At the precast facility, the 8 VW gages embedded in the precast were monitored with the Geokon 403 Readout Box, and 77 of the resistive gages were monitored with two Campbell CR10X's. In the structures laboratory during each test, the 32 VW gages were monitored with one CR10X, 80 of the 120Ω resistive gages were monitored with the National Instruments (NI) data acquisition system, 64 of the 350Ω resistive gages were monitored with the Campbell CR9000, and the 16 LVDT's were monitored with the NI system. The following sections describe the particular behaviors investigated and the associated instrumentation used to monitor the performance of the laboratory bridge specimen with respect to each behavior.

6.2 Reflective Cracking

6.2.1 Reflective Cracking over Flange Joints

Whereas the reflective cracking was only monitored at midspan of the center span at the Center City Bridge where it was expected to initiate, the laboratory specimen was instrumented such that the development and propagation of a reflective crack could be observed at the ends, quarter-span, and midspan of both spans. Nominally, these locations were 20, 78½, 137, 195½, and 256 in. from the center of the pier for each span. At each

location, there were five concrete embedment gages that overlapped to ensure that if a reflective crack developed, it could be detected. The overlapping gages were spaced at 4 in. in the transverse direction centered at the longitudinal joint between the precast sections. Overlapping the gages (as was done in the field) enabled pinpointing the location of the cracks within half of one gage length of the instruments. The more expensive VW gages used in the Center City Bridge were replaced with more economical resistive gages, but to ensure correlation between the VW and resistive gages, one set of five VW concrete embedment gages identical to the Center City Bridge instrumentation was placed at midspan of Span 2 adjacent to the resistive set. The long term accuracy of the VW gages over time was not required for this aspect of the laboratory study because it was assumed that the reflective cracking would likely initiate during load testing. Resistive gages may drift over time, but are accurate during short term load testing and more economical. In Figure 6.1, the five resistive gage sets are represented by a single line, and the five VW gage set is represented by an open rectangle of the same length. These gage sets were preassembled by using a rectangular frame made of tied rebar to ensure proper spacing and alignment of the instruments as shown in Figure 6.2. A cross section cut along the longitudinal flange joint is shown in Figure 6.3 which shows the transverse instruments in elevation. Measured locations of the as-placed instrumentation are given in Appendix E.

6.2.2 Reflective Cracking over Web Corners

Similar to the gages over the flange joints, the instrumentation over the web corners consisted of assemblies of overlapping resistive concrete embedment gages as shown in Figure 6.4. The laboratory specimen was instrumented such that the development and propagation of reflective cracks from the web corners could be observed at the ends and midspan of both spans. Because the distance monitored was twice as long as over the flange joints, ten overlapping gages spaced at 4 in. were used which extended across the flange joint to a distance of 10½ in. beyond the web corners. These gages enabled monitoring of reflective cracks initiating at the web corners. In addition, these gages provided an opportunity to investigate whether cracks initiating at the flange joint would propagate up to this level of the cross section. In Figure 6.1, the ten resistive gage sets are represented by a

longer line than the five gage assemblies. Measured locations of the as-placed instrumentation are given in Appendix E.

6.2.3 Effectiveness of Transverse Hooks

The transverse hooks that protruded from the sides of the webs of the precast sections were intended to help with the transverse distribution of load as well as control reflective cracking. Because the design spacing of these hooks was somewhat arbitrary, one of the objectives of the instrumentation was to monitor the stresses in these bars. A single spot-weldable VW gage was placed over the flange joint on one of the transverse hooks at the quarter-spans, midspan, and pier end of both spans as shown in Figure 6.1. The capacity of the data acquisition system limited the amount of instruments that could be added to the transverse hooks as it was not feasible to mimic the rows of seven spot-weldable VW gages used in the Center City Bridge. Measured locations of the as-placed instrumentation are given in Appendix E.

6.2.4 Opening of the Flange Joint

The gap between the flange joints was expected to increase when the section was subjected to positive bending. The magnitude of the opening was expected to correlate with the transverse stresses in the CIP concrete above the flange joint up to cracking, and to the stresses in the steel across the joint after cracking. The opening of the flange joint could also be used with the transverse concrete stress measurements to determine the effectiveness of the changes to the flange. Because the thickness of the flange was decreased, the increased depth of the CIP above the flange joint made the system stiffer in the transverse direction which was expected to reduce the gap opening. Because the roughened surface was removed when the flange thickness was reduced, it was possible that the flange could act independently of the CIP deck which would reduce the stresses leading to reflective cracking. In this case, the deflection could be the same or higher than the section with the original flange, but the transverse stresses in the CIP concrete would be reduced.

Linear variable differential transformers were utilized to measure the gap opening. The LVDT's were placed across the longitudinal joint between adjacent precast panels as shown in Figure 6.5. The LVDT's were placed at the same locations as the five resistive

gage crack monitoring assemblies, with the exception that the LVDT's were not placed at the location closest to the pier in either span due to instrumentation limitations and the assumption that the large block of CIP concrete at the pier would inhibit opening of the flange joint at that location. Thus there were four such LVDT's in each span. Measured locations of the as-placed instrumentation are given in Appendix E.

6.3 Transverse Load Distribution

6.3.1 Curvature across Laboratory Specimen

Longitudinal curvature measurements to investigate transverse load distribution and continuity over the pier were taken at eight points across the width at the continuous end of each span and at six points across the width at midspan and at the quarter spans as shown in Figure 6.1 to investigate the transverse load distribution. This grid of curvature measurements allowed for analysis of the effectiveness of the joint between the slabs to see if the system performed as a monolithic slab span. At each location, strain was measured at three depths through the cross section so that curvature could be determined with an extra gage for redundancy. The redundancy provided both confirmation that the instruments were functioning properly and that plane sections remained plane during the load test. Instrumentation consisted of resistive strain gages on the prestressing strand, longitudinal reinforcement in the joint area, and longitudinal reinforcement in the deck to measure curvatures at the locations over a flange. Instrumentation consisted of resistive strain gages on the prestressing strand, longitudinal reinforcement at the top of the precast sections, and longitudinal reinforcement in the deck to measure curvatures in the web region. Instrumentation layouts within the cross sections are given in Figures 6.6-6.8, and the designations are given for the different resistive gage types. The strain gage types are described in Appendix E. Measured locations of the as-placed instrumentation are given in Appendix E.

6.3.2 Transverse Curvature

The resistive concrete embedment gages used for monitoring the initiation and propagation of reflective cracks were also intended to be used to investigate the transverse

curvature across the joint. Because there were only gages at two depths, there was no redundancy, but there were multiple gages at each location to provide assurance that the gages were functioning properly. However, any error in the location of the gages in the section depth would have created errors in the results. If there was cracking at the flange joint, these gages could no longer have been used for this purpose because the strains in these gages would have been dominated by the local crack and would no longer provide information about the general plate bending behavior of the system. Location of these instruments is given in Sections 6.2.1 and 6.2.2.

6.4 Continuity over Piers

6.4.1 Curvature along Laboratory Specimen

The same longitudinal curvature instrumentation used to calculate transverse load distributions was utilized to investigate continuity provided by the CIP connection over the pier. The instrumentation was laid out such that curvatures along the loaded and unloaded span could be measured to allow for comparisons with idealized continuous connections. To ensure that the measured results were valid, a good deal of redundancy was provided. Because all of the curvature locations for transverse load distribution were used, and the curvatures should be constant across the width of the section when loaded evenly across the width (which was one of the load cases used), there were at least six locations across the width of the section that should have provided the same result. There was additional redundancy in each curvature measurement by measuring strains at three depths at each location.

6.5 Composite Action

6.5.1 Section Compatibility

During the ultimate load test to be performed as part of the NCHRP 10-71 *Cast-in-Place Concrete Connections for Precast Deck Systems*, longitudinal curvature instrumentation was to be used at midspan of the loaded span to investigate section compatibility between the precast and CIP components of the cross section. At the four

central curvature locations across the width, four resistive strain gages were installed rather than the usual three, and resistive surface gages could be added so that the curvature in the precast and CIP components could be independently calculated. The instrumentation at midspan is shown in Figure 6.7.

6.6 Bursting

6.6.1 Effectiveness of Bursting Reinforcement

If the bursting tensile stresses caused horizontal cracking, the vertical reinforcement would carry the tensile load across the horizontal bursting cracks. One resistive gage was placed at mid depth of each of the stirrups used in the bursting zone to measure the contribution of the reinforcement in resisting the vertical tensile forces. Therefore, the number of gages at each location was dependent on the bursting detailing for that end of the precast section. Measured locations of the as-placed instrumentation are given in Appendix E.

6.6.2 Stresses on Concrete Surface

Instrumentation was also provided to investigate vertical stresses in the concrete to determine the effectiveness of the bursting reinforcement by providing context to the rebar strain gage readings. Rosettes consisting of three resistive gages were installed on one side of the web on each end of the precast sections. Surface gages were chosen over embedment gages because of ease of placement and reduced potential for misalignment. It was expected that the vertical tensile stresses would not vary much over the width of the precast section due to the prestressing strands being well distributed, so the vertical stress on the surface of the precast section was assumed to be representative of vertical stresses at that depth across the width of the precast section. Measured locations of the as-placed instrumentation are given in Appendix E.

6.7 Restraint Moment

6.7.1 Restraint Moment of Laboratory Bridge Specimen

To generate large positive restraint moments at the pier support of the laboratory specimen, the CIP concrete had to be cast when the precast sections were at a young age. In the design of the positive restraint moment study, it was decided that seven days was the earliest age at which the continuity pour could be made to allow for construction and instrumentation of the laboratory specimen. It was also decided to allow the laboratory bridge specimen to be monitored for 150 days to investigate the development of positive restraint moments prior to live load testing. After 150 days, a positive restraint moment of 670 in-kips was predicted by the P-method (Peterman and Ramirez, 1998). The MATLAB m-file used to calculate the P-method predictions is given in Appendix D. Similarly, the PCA method (Freyermuth 1969) predicted a positive restraint moment of 900 in-kips after 100 days. It would not have been possible to reliably measure the development of positive restraint moments using strain gages as the peak strain after 150 days would only be 50 με. Two 25-kip load cells at each simply-supported end were used to indirectly determine the restraint moment. The drawback of using load cells with sufficient resolution was that the 25-kip load cells did not have the capacity for load testing the specimen. Thus the load cells had to be removed prior to load testing and replaced with steel plates. An elevation and cross section of the simply-supported end reaction with embedded load cells is given in Figure 6.9, and the same figure is repeated in Figure 6.10 but with the load cells replaced with spacer plates as required for live load testing of the laboratory specimen. A photograph showing the cross section of the end reaction is given in Figure 6.11.

6.8 Prestress Losses

Prestress losses were investigated to ensure that code equations for losses would be adequate for the Mn/DOT Precast Composite Slab Span System (PCSSS). The measurement of prestress losses was also used in the analysis of the positive restraint moments discussed in Section 6.7 as the creep and shrinkage of the precast sections, along with the shrinkage of the CIP concrete, caused the rotations that resulted in the restraint moments.

6.8.1 Prestress Force at Jacking

The prestress force after jacking was measured using resistive strain gages attached to each strand at both the live and dead ends of the prestressing bed. The strain gages located near the live end are shown in Figure 6.12. The location of these gages was chosen such that they would be in the same line as the longitudinal curvature strain gages near the pier end of Beams 1N and 2N to maximize the number of gages that could serve a dual purpose of prestress force and curvature measurements. Measured locations of the as-placed instrumentation are given in Appendix E.

6.8.2 Losses at Transfer

The same instrumentation used for the measurement of the jacking prestress force was monitored during transfer to determine the immediate losses due to the elastic shortening of the precast section. In addition, vibrating wire concrete embedment gages were installed at the center of gravity of the strands in the center of the web as well as in one of the flanges at midspan of each of the precast sections. These gages provided a redundant measurement of the prestress losses at transfer due to the compatibility of strains between the concrete and the prestressing strands at the same location. Measured locations of the as-placed instrumentation are given in Appendix E.

6.8.3 Time Dependent Losses

Prestress losses over time due to creep and shrinkage were measured by the same vibrating wire concrete embedment gages used at transfer. Prestress losses due to relaxation of the prestressing strands could not be measured by these gages because it is a loss of stress without an associated loss of strain; therefore, this loss was estimated using the method presented in the AASHTO LRFD (2004).

6.9 Instrumentation and Construction of the Laboratory Specimen

The reinforcement inside the precast sections was instrumented at County Materials in Roberts, WI on August 22-24, 2006. The sections were cast on September 6, 2006, and the concrete surface gages were added just prior to the transfer of prestress on September 7, 2006. Transfer occurred 24 hours after casting (16 days after tensioning). The precast

sections were delivered to the Structures Laboratory on September 8, 2006, and the formwork construction, rebar tying, and instrumentation placement was performed September 8-12, 2006. The CIP deck was cast on September 13, 2006, and thus the precast beams were seven days old at the time of continuity. The CIP deck was sprayed with a curing compound and then moist-cured for eight days under a poly-coated burlap blanket that was kept continuously moist. The measured global locations of the gages used in the laboratory study are given in Appendix E, as are the measured locations of the gages used for stressing and transfer. The instrumentation designation is given in Appendix E.

Chapter 7: Monitoring, Testing, and Analysis of Laboratory Specimen

7.1 Objectives and Description of the Laboratory Bridge Study

The objective of the laboratory study was to load the Mn/DOT Precast Composite Slab Span System (PCSSS) in a controlled environment to enable more conclusive analysis of the behaviors of interest than was possible with the field study. The specific behaviors investigated in the laboratory study included reflective cracking, transverse load distribution, continuity over the piers, composite action (part of NCHRP 10-71 study), bursting, restraint moment and prestress losses, which are summarized in Sections 7.2 through 7.8. The instrumentation used to investigate the behaviors was summarized in the corresponding sections in Chapter 6. This section summarizes the tests performed to investigate the behaviors.

The laboratory study included monitoring the end reactions with load cells to indirectly determine restraint moments as described in Sections 6.7 and 7.7. The load cells in the end reactions for the restraint moment study had to be removed and replaced with spacer plates prior to load testing, and this procedure is described in Section 7.1.2. A companion creep and shrinkage study was performed on cylinders in association with the restraint moment study. The laboratory study also included a series of load tests with various configurations of eight potential static load test positions on the bridge specimen, four at midspan of each span.

Measured, nominal, and calculated properties for the laboratory specimen are given in Table 7.1, and elevation and plan layouts of the laboratory specimen are given in Figures 7.1 and 7.2 which details the pier connection and span lengths. The material testing done to provide the measured quantities for Table 7.1 is described in Appendix B.

7.1.1 Overview of Laboratory Bridge Specimen Load Testing

Several constraints influenced the design of the laboratory testing. First, the data acquisition systems in the laboratory could not read all of the instruments in the specimen at the same time, so the most critical gages were read during each test. All of the longitudinal and transverse gages of the loaded span were read, and only the longitudinal midspan gages were read in the other span. Thus a total of 144 resistive gages, 30 vibrating wire gages, and

18 LVDT's were monitored during each test. Another critical constraint was the patch load limit of 35 kips which was the load determined for the fatigue testing of the laboratory specimen for a companion NCHRP 10-71 project. The load was expected to cause the same transverse tensile stresses in the laboratory specimen as would be seen in a 31 ft. continuous span bridge loaded with the AASHTO LRFD Specification (2004) design tandem multiplied by a dynamic load factor of 1.33. The three span, 31 ft. continuous bridge was chosen for comparison because it was the longest span that could be practically achieved with the same cross section (i.e., 12 in. deep precast section with 6 in. CIP deck). This concentrated patch load was not surpassed during the Mn/DOT laboratory investigation to maintain the condition of the transverse joint until after the cyclic testing could be completed. The limiting load was only surpassed with the application of the spreader beam which was intended to act as a uniform line load across the width of the laboratory specimen. The object of the spreader beam loading was to obtain larger longitudinal strains to better analyze the continuity over the pier. This loading was not expected to cause large transverse strains in the joint region. With the spreader beam, the specimen was loaded to 140 kips, which was just below the calculated longitudinal tensile stress limit at midspan assuming the nominal design strength which considered continuity of the Mn/DOT PCSSS at the center support. A layout of the test positions is given in Figure 7.3, where the test position notation consists of the number of the span being loaded, and then either the letter(s) "N" for the center of the north beam, "S" for the center of the south beam, "C" for the joint between the two beams, or "spr" for the spreader beam loading.

7.1.2 Removal of Load Cells

Prior to load testing the laboratory bridge specimen, the load cells that were embedded in the end reactions for the measurement of restraint moment, as shown in Figures 6.9-6.11 had to be removed. The two load cells in each end support had a combined capacity of 50 kips, and the dead weight of the specimen already placed approximately 30 kips on the load cells. The load cells were removed one end at a time using hydraulic jacks to raise the specimen off the load cells. Two jacks were placed as close to the end reaction as possible with the jacks centered under each of the precast sections as shown in Figure 7.4. The jacks had a common pressure source to ensure even loading. The load in the jacks and in the load

cells were monitored during jacking as an increase in total force would provide an indication of the stress imposed on the specimen. The positive moment at the pier due to jacking was equal to the increase in force at the end reaction times the length of the span. A calculated maximum force of 7.7 kips beyond the weight of the specimen was expected to generate the cracking moment at the pier, assuming *EI* for the span of 330 x 10^6 k-in^2. This corresponded to a jacked deflection of 0.44 in. Due to the weakness of the bond between the end face of the precast sections and the CIP concrete at the pier, it was expected the cracking might occur at a lower load.

The west span was jacked on September 25, 2007, and the west load cells were removed. The measured force in the jacks was 34.3 kips, whereas the load cells measured a loss of 29.4 kips. The difference of 4.9 kips was only 64% of the cracking moment of the CIP concrete over the pier, and the 0.25 in. measured deflection was slightly less than theory predicted would crack the pier. However, cracking was observed at the center of the pier during jacking and is sketched in Figure 7.5. It did not appear that the cracks extended to the top of the section. After the load cells were replaced with plates, the final position of the west reaction was 0.12 in. higher than before. The cracking of the CIP diaphragm over the pier at a load below the cracking moment of the CIP concrete was likely due to the lack of bond between the ends of the precast sections and the CIP diaphragm. A crack could have initiated at this surface and reduced the stiffness of the pier as was seen by the jacks causing larger than expected displacements given the loads. Two side-by-side longitudinal vibrating wire gages located 2¾ in. above the top surface of the pier at the center of the pier measured a large change in strain (greater than 1000 με) during jacking, but an exact value was not known as the strain exceeded the bounds of the gages. The jacking damaged these VW gages so that they could not be used in the jacking of the east load cells or any of the load tests. All of the other west span instrumentation was monitored during the process of jacking the west span to remove the west load cells, and none of the other gages indicated that any damage was done to the specimen during jacking elsewhere in the span.

Load testing of the west span was performed prior to the removal of the east load cells so that they would provide additional information about the continuity of the pier during loading of the west span. The east span was jacked on November 1, 2007, and the east load

cells were removed. This time, the measured force in the jacks was 36.6 kips, whereas the load cells measured a loss of 30.2 kips, and the measured jacked displacement was 0.34in. After the load cells were replaced with plates, the final position of the west reaction was 0.22 in. higher than before. It was unknown why there was a 0.10 in. difference between the east and west supports after plate replacement. The cracks at the pier were somewhat wider than during the first jacking as seen in Figure 7.6, but it again appeared that the positive moment cracks did not propagate to the surface of the diaphragm. Also, the east span strain gages did not show any indication of damage caused by jacking of the east span. The implications of the crack with regard to transverse load distribution and continuity over the pier are discussed in Sections 7.3 and 7.4, respectively.

7.1.3 Load Testing of the Laboratory Specimen

The single actuator test centered on the south beam in the west span (Beam 1S) was the first live load test and was performed October 16, 2007. A similar test, centered on Beam 1N, was also performed on October 16, 2007. The west span was loaded with the spreader beam on October 26, 2007, and the west span patch test over the longitudinal joint was performed October 29, 2007. Each static test was repeated three times to verify the consistency of the response to loading, and during each test the load was held for six minutes to observe the variations in the strain readings and to allow the CR10X to read the vibrating wire gages three times. A photograph of the specimen during the spreader beam test of the west span (i.e., Span 1) is given in Figure 7.7.

Because of a limitation with the number of functioning channels on the CR9000 data acquisition system, each of the tests had to be repeated nine times for the east span tests to get three repeats for all of the gages. The strain gages read on the CR9000 were divided into three sets (CR9000a, b, and c) and were swapped such that all of the sets were each read three times. There was overlap between gages read on the CR9000 to ensure consistency between the loadings. All of the instrumentation on the CR10X and National Instruments data acquisition systems was read during all nine loadings of each test to ensure consistency. Because the specimen was assumed to remain elastic during the tests, the data from the three sets of CR9000 gages was superimposed to obtain one complete set of data for each load position. The first set of tests of both single actuator patch loads centered on the Beams 2N

and 2S, respectively, was performed on November 19, 2007, and both sets of tests were repeated the next day. The first two sets for both the spreader beam test and the patch load over the longitudinal joint were performed on November 21, 2007. The third set of tests for all three single actuator positions was performed on November 27, 2007, and the third set of tests for the spreader beam test was performed the next day. A summary of all of the tests performed is given in Table 7.2.

After testing, it was decided to lower the end supports by replacing the existing plates (totaling 2 in. thick) with thinner ones in an attempt to close the positive moment cracks at the pier that were caused when the load cells (totaling approximately 1-15/16 in. thick, including buttons) were replaced with the slightly thicker spacer plates. The spacer plates can be seen in Figures 6.9 and 6.10 as they were immediately after replacing the load cells with spacer plates and added spacer plates to the center of the end reaction. The thinner plates were used due to a concern that the positive moment crack would reduce the effective continuity of the pier under live load. To reduce the height of the plates, top 1 in. plates at the ends of the support was replaced with a series of plates that totaled 15/16 in. thickness. The top spacer plates of the two middle plate sets were removed entirely as these plates were not used when the CIP was cast nor during the restraint moment monitoring period. This was done to allow the HSS spreader beam in the end reaction to deflect as it was when the CIP was cast. Then once the end of the specimen was set down, the gap between the two remaining 1 in. plates and the bottom of the HSS section was filled with ¾ in. plates and shim plates as needed so that when the large actuator loads were applied the HSS section would not have to span the entire length of the end reaction.

The spacer plate replacements were performed on January 10, 2008. The east end plates were replaced first, and the measured final position of the adjacent LVDT measuring vertical displacement was 0.16 in. lower in elevation, resulting in a net displacement of 0.06 in. higher than before the load cell was removed. The west end plates were replaced next, and the measured position recorded by the adjacent LVDT was 0.08 in. lower in elevation, resulting in a net displacement at the west end of 0.04 in. higher than before the load cell was removed. The crack was still visible at both sides of the pier. All of the transverse gages and the longitudinal gages nearest the pier were monitored during jacking to monitor potential

damage to the precast sections or CIP concrete, but no significant strain changes were measured. After the plates were replaced, the spreader beam test was repeated, and the strains of all of the gages were within 10 με of the previous test, which was within the assumed accuracy of the gages.

7.2 Reflective Cracking

The reflective cracking instrumentation near the pier, at midspan, and at both quarter spans was monitored for the span which was loaded at the time (i.e., the Span 1 transverse instrumentation was monitored when test positions 1N, 1C, 1S, and 1spr were performed). As expected, neither of the patch tests centered on the beams nor the spreader beam test generated significant transverse strains. The transverse instrumentation was monitored during these tests largely to ensure that no reflective cracking occurred prior to the cyclic testing that was to be performed under NCHRP 10-71. The remainder of this section focuses on the patch test on each span that was centered over the longitudinal joint.

7.2.1 Reflective Cracking over the Flange Joints

During the patch load test over the longitudinal joint, small but measureable tensile strains were observed in the CIP concrete immediately over the flange joint. As expected, the largest strains were at midspan which was both under the load and the location of the largest moment. Near midspan of Span 1 which had the 3 in. flange thickness, the concrete embedment VW and resistive strain gages gave maximum transverse tensile stresses of 11 and 15 με, respectively, during Test 1C. The small difference may be due to the fact that the VW gage was 16 in. from the center of the load, but the resistive gage was only 7 in. from the center of the load. Near midspan of Span 2 which had the 5¼ in. flange thickness, the concrete embedment VW and resistive strain gages measured maximum transverse tensile strains of 25 and 20 με, respectively, during Test 2C. In this case, the VW gage was ¼ in. closer to the flange-CIP interface than the resistive gage, and the VW gage was 5 in. from the center of the load whereas the resistive gage was 6 in. from the center of the load. The strains from the resistive gages appeared to increase linearly with the load, but it was difficult to quantify the linearity due to the noise in the readings. Under constant load, the standard deviation of the transverse resistive gages at midspan was 5 με for both Span 1 and 2 which

included changes between the successive test repeats of up to 15 με. The VW gages were read at two minute intervals when the loading was at a pause and were not synchronized to the load during load ramps to analyze the linearity of the strains.

Considering the larger of the strain values for each span, the midspan transverse tensile strains for Span 1 with the 3 in. flange thickness and Span 2 with the 5¼ in. flange thickness were 15 and 25 με, respectively. However, comparing these results is difficult because the strain gage in Span 1 was lower in the overall thickness than in Span 2 by 1 in., but also was higher above the flange thickness by 1 ¼ in. Because the load patch was 10 in. wide, and the gages were towards the middle of the section depth, it was not expected that the difference in longitudinal placement from the center of the load of 5 in. versus 7 in. would significantly affect these results.

Even with the limited results, it was expected the reduction in flange thickness would improve the behavior of the Mn/DOT PCSSS by reducing the transverse tensile strains that could lead to reflective cracking. The results of this analysis also showed that loading directly over the flange joint generated small transverse tensile strains in the CIP concrete which were smaller than what would be predicted to cause cracking, although an unknown quantity of the available transverse tensile strain was expected to be taken up by the restraint of CIP shrinkage. The future cyclic testing as part of the NCHRP 10-71 project will give a better indication of the robustness of the Mn/DOT PCSSS with respect to reflective cracking, as the occurrence of reflective cracking in the longitudinal joint under a certain load and number of cycles in one span compared to the other would alleviate many of the difficulties in measuring and comparing the transverse stresses.

7.2.2 Reflective Cracking over Web Corners

Transverse tensile strains were not observed to develop over the web corners under any load condition. In fact, the strains in these gages were generally small and compressive, as would be expected in positive bending above the neutral axis. There was no difference between the strains over the north and south web corners, so it did not appear that the increase in the chamfer from the original ½ in. by 1 in. to the modified 1 in. by 1 in. had an impact under these load levels. Therefore, it appeared that the original chamfer design of ¾ in. by ¾ in. did not have to be increased, and the exact measurement of the chamfer need not

be closely enforced. The future cyclic testing will better indicate the likelihood of reflective cracking over the web corners.

7.2.3 Effectiveness of Transverse Hooks

Due to the small transverse tensile strains, it was difficult to assess the effectiveness of the transverse hooks as their performance would be much more important if reflective cracking had occurred in the longitudinal joint between adjacent precast sections. As it was, the strains measured from the VW spot weldable strain gages installed on the transverse hooks were slightly smaller than those measured by the concrete embedment gages. At midspan of Span 1, the measured strain was 9 με in the transverse hook compared to 15 με in the concrete embedment gage during Test 1C. At midspan of Span 2, the measured strain was 19 με in the transverse hook compared to 25 με in the concrete embedment gage, during Test 2C. The spot weldable strain gage at midspan of Span 1 was ¼ in. lower in the section than the adjacent concrete embedment gage, and spot weldable and concrete embedment gages were measured to be at the same depth in Span 2. The difference between the strains in the transverse hooks and the surrounding concrete was likely due to imperfect bond between the hook and concrete. The bond could be affected by the large size of the #6 transverse hooks, the epoxy coating of the hook, and/or the close spacing of the transverse hooks with the #5 stirrups of the drop-in reinforcement cage. As in the concrete embedment gages, the spot-weldable VW gages were read at two minute intervals during load pauses and were not synchronized to the load during load ramps to analyze the linearity of the strains.

7.2.4 Opening of the Flange Joint

Given the small magnitude of the transverse strains, as expected, the transverse LVDT's between the adjacent precast sections measured no separation between the two precast sections. At midspan of Spans 1 and 2, only signal noise of +/- 0.008 and 0.004 in., respectively, was observed and the readings appeared independent of the applied load during Tests 1C and 2C, respectively.

7.3 Transverse Load Distribution

The longitudinal instrumentation was monitored near the pier, at midspan, and at both quarter spans of the span being loaded, and the midspan instrumentation was monitored in the span without the actuator load. However, the focus of the transverse load distribution analysis was the strains at midspan and at the quarter span on the pier side of the loaded span. At each location, there were sets of three gages in a vertical line located transversely 3, 21, and 45 in. from the center of the specimen in each direction. A least squares regression was used to calculate the curvature using the three strains which corresponded to the moment on the section at that location. The measured curvatures across the width of the specimen at midspan and at the inner quarter span of Span 1 under the three patch load tests on Span 1 are given in Figures 7.8 and 7.9, respectively. The same plots for Span 2 for the three patch load tests on Span 2 are given in Figures 7.10 and 7.11, respectively. Of the 24 total curvature locations from midspan and quarter span of each span, four were not used at all as two of the three gages were non-functional. Seven had one non-functional gage so curvatures could be calculated, but without redundancy. Thirteen had three or four gages in a vertical line where the average R^2 value for the least squares regression was 0.96 with a coefficient of variation of 4.9%. These errors were expected to be caused by the +/- 1/8 in. accuracy of the gage depth measurements and the accuracy of the gages.

It can be seen in the curvature plots at both midspan and at the inner quarter span of Span 1 that there was a bias for higher curvatures on the north side than the south side. This was especially evident at the inner quarter span where there were higher curvatures on the north side even when the patch load was at the center of the web on the south precast section. It can also be seen at midspan where the curvatures were higher on the north side when the specimen was loaded at the center and where the slope of the curvature plot across the width was higher when the north precast section was loaded than the south precast section. One possible explanation for this behavior was the positive moment crack at the pier caused by replacing the load cells with slightly thicker plates. If the crack was not uniform across the width, it could close under lower loads in some locations resulting in varied stiffness across the width of pier. However, it was expected that the positive moment crack would equally

affect both spans, and it is unknown why the same curvature bias was not observed in Span 2.

In comparing the results of Span 1 and Span 2, it can be seen that under the load at midspan, the curvature across the width of the specimen was more uniformly distributed in Span 1 than in Span 2 except for the case of the north beam patch load in which the results were similar between the two spans. It was expected that the curvature would be more uniformly distributed in Span 1 than in Span 2 because the reduced 3 in. flange thickness was used in Span 1 compared to the original 5 ¼ in. used in Span 2. Thus the transverse stiffnesses at the joint of Span 1 would be greater than that of Span 2 with the difference proportional to the difference in the depth of the CIP at the flange joint cubed. The effects of the stiffness difference were expected to be more noticeable between the load and the pier as the curvatures would become more uniform than they where under the load. At the inner quarter span of Span 1, it can be seen that there was virtually no difference between curvatures across the width of the specimen regardless of the load position. However, in Span 2, the curvatures were higher to the side where the load was located. These results indicated that the change in flange thickness resulted in a measureable improvement in transverse load distribution.

7.4 Continuity over Piers

As mentioned above, the longitudinal resistive gages used to calculate curvatures were monitored near the pier, at midspan, and at both quarter spans of the span being loaded, and the midspan instrumentation was monitored in the other span. The 140 kip spreader beam load was large enough to generate measurable strains (i.e., greater than 100με at the top and bottom of the section near midspan) at both quarter spans of the loaded span and at midspan of the opposite span. The strain gages near the pier in both spans indicated significant variation across the width, and as the gages were nominally 11 in. from the center of bearing, it was expected that this was due to the gages being located within the disturbed region. Thus these gages were not considered in the continuity analysis. At each quarter and midspan location, there were sets of three gages in a vertical line located transversely 3, 21, and 45 in. from the center of the specimen in each direction. A least squares regression was

used to calculated the curvature using the three strains at each location. Also, a vertical LVDT was placed under the center of each precast section at midspan and near the pier.

The strains and deflections measured in Span 1 during the Span 1 tests were larger than those predicted using a linear, continuous model, and the midspan strains in the loaded span were even larger than those predicted by the simply supported model. The calculated stiffness of the transformed section used in this calculation, and all other laboratory specimen transformed section calculations took the average of the deck steel from the North and South sides and assumed the section had a uniform stiffness across its width. This was done to simplify the analysis, and it was assumed reasonable, as there was only a 7% difference in the predicted stiffnesses of the two sides. There was concern that the positive moment crack at the pier effectively eliminated the continuity and the pier was behaving as a simple support which would increase strains and deflections in the loaded span. However, continuity created negative bending of the opposite span which generated an upward midspan deflection that was 40% of what was expected from the continuous model. The continuous model consisted of two 265 in. spans supported at the ends and center by a simple support, and the model stiffness was calculated using transformed sections (which averaged the longitudinal deck reinforcement from the two sides) and measured modulus of elasticity values. During each of the three loadings, the bottom surfaces of the precast sections were examined to find any flexural cracks, but none were observed.

After further analysis, it was found that the measured neutral axis using the strain gage data averaged 7.1 in. above the bottom of the precast section whereas the transformed section predicted 8.0 in. in the 18 in. cross section. This large of an error was not expected as the neutral axis depth was predicted using measured elastic moduli from cylinder tests. However, the sides of the CIP deck were investigated and vertical cracks were found at a spacing of approximately 12 in. along the entire length. The cracks initiated at the top of the CIP concrete and propagated down toward the top of the precast sections. Some of the cracks propagated all the way to the top of the precast sections. A photograph of some of the cracks which have been marked is given in Figure 7.12. It was suspected that these cracks were caused by shrinkage. The neutral axis depth from the Center City Bridge is discussed in Section 4.5, where a variation in the neutral axis depth from the transformed sections

calculation was not observed. It was expected that the cracks would reduce the effective stiffness of the deck. This was taken into account by multiplying the elastic modulus of the CIP by a reduction coefficient until the neutral axis in the transformed section calculation reflected the 7.1 in. determined from the strain gages. This coefficient was found to be 0.49 which reduced the elastic modulus of the CIP from 3540 ksi to 1740 ksi.

The deflections measured while Span 1 was loaded are shown in Figure 7.13. Calculated deflections assuming continuous and simple support assumptions at the pier, each using the full and reduced stiffness of the CIP, are also given. The continuous, linear model with the reduced stiffness best matched the measured deflections at midspan of the loaded span. The reduced stiffness assumption was also validated by the measurements taken while jacking the load cells. Using linear, continuous beam theory, the force-deflection ratio at the jacked end should be constant and predictable. At the west end, the jacked displacement was 0.25 in., and the measured jacking force over the existing dead load was 4.9 kips. Using the full stiffness of the CIP, the predicted force was 6.6 kips, but with the reduced stiffness it was 4.8 kips.

During the loading of Span 2, flexure cracks were observed under the specimen. As the 140 kip load was chosen based on keeping the section uncracked assuming the full stiffness of the CIP, this was not surprising. Using the reduced stiffness of the CIP concrete, the calculated total bottom fiber stress under live load at midspan was 725 psi for Span 2, which was higher than $6\sqrt{f'_c}$ (680 psi) but lower than $7.5\sqrt{f'_c}$ (850 psi). It was somewhat surprising then that the same cracking was not observed in Span 1 because the calculated bottom fiber stress of 703 psi also fell between the two cracking stress limits. The unknown crack depth made it impossible to perform the same procedure to calculate the effective stiffness of the CIP in Span 2, as the crack would greatly affect the neutral axis depth. Therefore, the same 0.49 reduction coefficient for the elastic modulus of the CIP was assumed. This was validated by the load cell jacking which was performed before the precast section was cracked under live load. At the east end, the jacked displacement was 0.34 in., and the measured jacking force over the existing dead load was 6.4 kips. Using the full stiffness of the CIP, the predicted force was 9.0 kips, but with the reduced stiffness it was 6.5 kips. In addition to the shrinkage cracks in the CIP, the flexure cracks reduced the

stiffness of the specimen in Span 2. This was taken into account using the effective moment of inertia as defined by Equations 4.8.3 and 4.8.4 of the PCI Design Handbook (1999) as shown in Equations 7.1 and 7.2.

$$I_e = \left(\frac{M_{cr}}{M_a}\right)^3 \times I_g + \left[1 - \left(\frac{M_{cr}}{M_a}\right)^3\right] \times I_{cr} \tag{7.1}$$

$$\frac{M_{cr}}{M_a} = 1 - \frac{f_{tl} - f_r}{f_l} \tag{7.2}$$

where M_{cr} and M_a are the cracking and applied moments, respectively, I_e, I_g, and I_{cr} are the effective, gross, and cracked moments of inertia, respectively, and f_{tl}, f_r, and f_l are the calculated total stress, the modulus of rupture, and the live load stress, respectively. The modulus of rupture was assumed as $6\sqrt{f'_c}$, because the applied stress was lower than the predicted cracking stress of $7.5\sqrt{f'_c}$. This assumption was somewhat arbitrary as the modulus of rupture measured from the concrete samples was 8.7% higher than $7.5\sqrt{f'_c}$ as discussed in Appendix B. This was used to reduce the transformed stiffness of the span by 7% regardless of whether the reduction in deck stiffness was considered. The deflections measured while Span 2 was loaded are shown in Figure 7.14 for both continuous and simple support assumptions at the pier, each using the full and reduced stiffness of the CIP. Here the continuous model with reduced stiffness underestimated the measured deflections, but this was most likely due to the effect of the flexural cracking being underestimated.

The results for the measured curvatures at midspan and both quarter spans for the loaded span and for midspan of the other span are given in Figures 7.15 and 7.16 for loading in Span 1 and 2, respectively. Both the continuous and simply supported models were calculated using linear beam theory and the reduced stiffness of the CIP for both spans, and the flexural cracking stiffness reduction was used for both models in Span 2. In Span 1, the results were well predicted by the continuous model, but in Span 2, the continuous model under predicted the midspan curvatures. The variation in curvatures at each location seen in Figures 7.15 and 7.16 represent the change in curvature across the width of the laboratory specimen as the assumption of the spreader beam test uniformly loading the specimen was not well realized.

Because the assumed reduced stiffness of the CIP was well supported by the neutral axis depth from the measured strains and the jacking forces, the assumption of full continuity appeared valid for both the measured curvatures and deflections in Span 1. For Span 2, the continuous model with reduced CIP stiffness was somewhat unconservative, but it was expected that this was most likely due to the effect of the flexural cracking being underestimated by the PCI equation given in Equations 7.1 and 7.2. The measured deflections in the span with actuator load due to negative bending were 40% of what was expected from the fully continuous model for loading in both spans; this was also consistent with the negative bending in the span without external load during the live load truck test discussed in Section 7.5. The reduced deflection was likely due to the rotational stiffness of the center pier that was assumed to be a roller in the continuous model. If the positive moment crack had reduced the stiffness of the section over the pier, a similar opposite span deflection of some fraction of the continuous, linear model would be expected; however, then the strains and deflections in the loaded span would be higher than expected, which was not the case as shown in Figures 7.13 and 7.15. Therefore it appeared that even with the positive moment crack imposed by the replacement of the load cells with slightly thicker plates, the laboratory specimen exhibited fully continuous behavior under live load.

Also, the reduction in deck steel on the north half of the laboratory specimen did not appear to influence the negative moment continuity over the pier, but this was expected as the pier did not undergo negative moment cracking.

7.5 Composite Action

Composite action will be evaluated during the ultimate load tests performed as part of the NRCHP 10-71 investigation. It was out of the scope of this study.

7.6 Bursting

Strains from the resistive gages on the bursting reinforcement and concrete surface near the precast section ends were monitored at a one minute interval during the transfer of prestress when the girders were fabricated using the Campbell Scientific CR10X data acquisition system described in Appendix C. No measureable change in strain in the

concrete or reinforcement was observed upon release. During the transfer of prestress, no cracking was observed in the end regions of the precast sections that would indicate a bursting problem. Thus it appeared that no bursting reinforcement would be required. However, it would be reasonable to provide reinforcement consisting of one #4 stirrup or two #3 stirrups , even though they only provide 40 and 44 percent of what was required by AASHTO LRFD (2004) 5.10.10.1, respectively, as this amount of reinforcement was determined by a rational process described in Section 5.6.

7.7 Restraint Moment

After continuity between the precast sections and the CIP deck was established, the restraint moment was monitored by evaluating the changes in the load cell readings which provided the reactions at the simply-supported exterior supports. The changes in end reactions were monitored for the first 250 days after establishing continuity. The results from the end reactions were zeroed by subtracting the calculated dead weight that would be supported at that reaction. The weights were calculated using the measured density of the concrete cylinders and an assumed density of 490 pcf for the steel reinforcement. The boundary conditions of the laboratory specimen are shown in elevation and plan in Figures 7.1 and 7.2. Figure 7.17 compares the measured results to the calculated restraint moments for the P-method and PCA method using measured material and geometrical parameters for each span of the laboratory specimen. The MATLAB m-file used to calculate the P-method predictions is given in Appendix D.

For the PCA method, the charts from the publication describing the method (Freyermuth 1969) were used to obtain the creep and shrinkage values. For the P-method, creep and shrinkage values were calculated using AASHTO LRFD Specifications (2004). Restraint moments based on the two models were calculated using both the volume/surface (V/S) ratio of the individual components as if the precast and CIP were separate, as was done by Mn/DOT, and the V/S ratio of the precast and CIP components not considering the shared surface. It was believed that the V/S ratio not considering the shared surface would more accurately predict the creep and shrinkage of the laboratory specimen. The predictions

obtained from the PCA method were piecewise linear due to the limited data points for creep over time; whereas the P-method results were obtained using a daily time step.

A line at $0.6M_{cr}$, half the recommended limit for maximum positive restraint moment from *NCHRP 519*, is shown in Figure 7.17 for scale. The P-method predicted different restraint moments for the two spans that reflect the design changes in the specimen (e.g., reduction in precast concrete area due to reduced flange thickness). There was not a difference in restraint moment for the two spans with the PCA method because the model assumed a single roller support at the pier resulting in a single value for the restraint moment at the pier that combined the effects of the two spans.

The data from the west span is missing in Figure 7.17 from the 14th to the 161st day due to an error in monitoring setup. The daily fluctuations in the data resulted from temperature changes which became more pronounced towards the end of the monitoring period when work related to other projects began requiring the exterior loading dock doors to the Structures Laboratory to be open causing temperature changes ranging from 50 to 86 ^{o}F. The measured data were expected to be less than the predictions because the models assumed roller supports at the pier where in reality the pier support should have behaved as a rotational spring as can be seen in the pier connection in Figure 7.1. The negative restraint moment that developed over the first several days was likely due to the cooling of the CIP deck after casting, which was not considered by either of the models.

Considering the high degree of uncertainty due to the variability of material properties and imperfect modeling assumptions, both the PCA and P-methods provided reasonable estimates of the positive restraint moment that developed over the first 250 days. But this was somewhat of a coincidence as competing differences within the models canceled out. If continuity had been made when the precast sections were older, the difference in the positive moment prediction between the models would increase as shown in Table 7.3. As age of the precast sections at continuity is increased, the differential shrinkage between the precast and CIP elements would increase, and because the PCA method does not account for shrinkage restraint, the negative shrinkage moment cancels out a larger portion of the positive moment due to creep than if shrinkage restraint was accounted for as in the P-method. Specifying an older precast section at continuity is one of the only options a design

engineer has to mitigate possible positive restraint moment problems, and thus the choice of which model to use can greatly influence the allowable age at continuity as well as the positive and negative moment designs at the pier.

Although the PCA method appeared to provide a better estimate of the positive restraint moment, the creep and shrinkage results from the center of gravity of the strands (cgs) in the laboratory specimen shown in Figure 7.18 show that the PCA method over predicted the strains that drove the positive restraint moment development (lines iii and v compared to lines i and ii, respectively). In contrast, the AASHTO LRFD Specifications (2004) creep and shrinkage models used in the P-method had a closer relation to the measured data in Figures 7.18 (lines vii and ix compared to lines i and ii, respectively). However, both the AASHHTO (2004) creep and shrinkage models and the P-method incorporating those models over-predicted the respective measured data in Figures 7.18 (at later ages ~100 days) and 7.17, respectively. The change in V/S ratio and restraint in the laboratory bridge specimen were the only changes that should have affected the creep and shrinkage strains, and the shrinkage restraint should have similarly affected the accuracy of both the AASHTO and PCA models.

As described in Appendix B, coefficients were fitted to the AASHTO and PCA shrinkage and creep models using least squares regression with the data from the shrinkage and creep study performed with samples taken when the components of the laboratory bridge specimen were cast. When using the models with the fitted coefficients, the AASHTO model better predicted the measured strains at the cgs than the PCA method.

The creep and shrinkage coefficients from the fitted models were also used to revise the restraint moment prediction. Figure 7.19 shows a comparison of the laboratory results to the PCA method and P-method predictions using both fitted and unfitted creep and shrinkage models. All of the predicted models in this plot were calculated using the higher V/S ratio from not using the shared surface. When the fitted coefficients were used, the P-method predictions were much closer to the measured results, but the PCA method prediction moved much further from the results. The PCA prediction went from reasonably predicting the positive restraint moment measured to predicting a relatively large negative restraint moment. From this it can be inferred that the mechanism by which the creep and shrinkage

strains contribute to the restraint moment was better modeled by the P-method than the PCA method. This was likely due to the shrinkage restraint factor and creep and shrinkage models assumed for the P-method providing a better model of the behavior than the PCA method. Without the large creep coefficient used by the PCA method, there would not have been enough positive restraint moment from prestress creep to counter the large negative restraint moment due to the assumption of unrestrained shrinkage.

Figure 7.20 shows the two models carried out to 20 years, at which point it is reasonable for design purposes to assume that creep and shrinkage have reached their ultimate values. It is unknown whether the positive restraint moment would have reached 100 ft-kips as predicted by the P-method as it appeared to have tapered off closer to 40 ft-kips in the laboratory specimen as shown in Figure 7.17. This was consistent with the readings of the strain gages at the center of gravity of the strand shown in Figure 7.18 where the creep and shrinkage strains in the precast sections that drove positive moment development leveled off faster than the models predicted. This was also consistent with the creep strains from the concrete creep samples that leveled off faster than the creep and shrinkage models predicted as discussed in Appendix B.

It should also be noted that the effects of concrete creep due to tensile loads were neglected by both the PCA and P-method in this research. These effects are further discussed in *Vertical Tensile Stresses in End Regions of Precast Composite Slab-Span Systems and Restraint Moments* (Eriksson, 2008).

7.8 Prestress Loss

7.8.1 Prestress Force at Jacking

To calculate the prestress force at jacking, the change in strain of the strands was monitored at a one minute interval using the Campbell Scientific CR10X data acquisition program described in Appendix C. Because the gages were aligned along the individual wires (not along the axis of the overall 7-wire strand), material testing was performed on similarly gaged 7-wire strand samples taken from the same prestressing strand stock used in the precast sections of the laboratory bridge specimen to obtain an effective modulus of elasticity. This effective modulus of 30,100 ksi was used to relate measured strains to the

force in the strand. This test is outlined in Appendix B. The average measured strain in the prestressing strands after jacking was 6833 με with a coefficient of variation of 2.5%. This excluded the results of three of the 32 strain gages for which the strains were sufficiently low (e.g. 2000 με below the average) which indicated that the gages may not have been properly bonded to the strand. The stress in the strand, calculated with the experimentally obtained effective modulus, was 206 ksi, which was 1.6% higher than the design jacking stress of 202.5ksi. Thus, the total prestress force at jacking was 503 k, which was 1.4% higher than the design of 496 k.

7.8.2 Losses at Transfer

The instantaneous losses at transfer due to elastic shortening of the precast section were monitored at a one minute interval with the same data acquisition system used for the jacking force measurement. However, the gages were only approximately 20 in. from the end of the precast sections whereas the transfer length was expected to be approximately 25 in., so about half of the gages indicated some degree of strand slip as the strands were cut. This was evident through stepped drops in strain exhibited by the gages in the minutes following the strands being cut. The remaining eight gages in Beam 1N indicated an average loss of 8.5 ksi with a coefficient of variation of 14%, and the remaining seven gages in Beam 2N indicated an average loss of 7.4 ksi with a coefficient of variation of 10%. This trend was consistent with what was expected; that is, the losses were expected to be higher in the Span 1 precast sections than in the Span 2 precast sections due to the decreased precast area. The vibrating wire gages at the center of gravity of the strands were manually read with the Geokon GK-403 readout box before and after the prestress force was transferred. The average of the two gages in each of the Span 1 and Span 2 precast sections were 7.3 and 6.9 ksi, respectively, after correcting for the effects of self weight moment at midspan. Thus the strand gages measured instantaneous elastic shortening losses that were higher than those measured by the vibrating wire gages by 16% for Span 1 and 7% for Span 2. The losses measured by the vibrating wire gages were expected to be more reliable because they were located at the midspan of the precast section while the strand gages were near the end of the precast section and could have experienced some slip. Thus, the losses measured with the vibrating wire gages were used for comparison in the following analyses.

Losses at transfer were predicted with the Zia (AASHTO LRFD (2004) 5.9.5.2.3a), PCI Committee (PCI Committee on Prestress Losses 1975), and AASHTO alternative (AASHTO LRFD (2004) C5.9.5.2.3a) methods. Losses due to relaxation were predicted using AASHTO LRFD (2004) Equation 5.9.5.4.4b-2 for low relaxation strands as given in Equation 7.3.

$$\Delta f_{pR1} = \frac{\log(24.0t)}{40.0} \times \left[\frac{f_{pj}}{f_{py}} - 0.55 \right] f_{pj}, \tag{7.3}$$

where Δf_{pR1}, was the loss due to relaxation, t was the time since stressing (in days), and f_{pj} and f_{py} were the jacking and yield stresses of the prestressing tendons, respectively, (i.e., 206 and 243 ksi, respectively). Strand area and modulus of elasticity were taken as 0.153 in^2 and 28500 ksi, respectively, which were averages from the manufacturer's given values for the spools of strand used. The modulus of elasticity of the precast section concrete was computed using experimentally measured unit weight and compressive strength in AASHTO LRFD (2004) equation 5.4.2.4-1 as shown in Equation 7.4.

$$E_c = 33{,}000 w_c^{1.5} \sqrt{f'_c}, \tag{7.4}$$

where E_c is the elastic modulus of concrete, w_c is the unit weight of concrete (in kcf), and f'_c is the strength of concrete (ksi). Measured values were used for both the compressive strength at transfer and the unit weight of the precast. The values for elastic shortening at transfer predicted by the three methods were similar as seen in Table 7.4. For both the Zia and PCI methods, the predictions were recalculated including the extra prestress force due to the strands in the flange area which were nominally stressed to 5 kips. This increased the elastic shortening predictions by about 3% for the thinner flange sections and 6% for the original flange sections (note, the thicker flange sections had 2 layers of strand in the flange tips compared to a single layer in the thinner flange sections). Overall, the predictions were unconservative by 23-32%, likely due to the modulus of elasticity being lower than calculated. If the stiffness was calculated using the design initial compressive strength of 4.5 ksi versus the measured one day strength of 7.2 ksi, the models would yield conservative results.

7.8.3 Time Dependent Losses

The change in strain at the cgs in the web of each of the four precast sections in the laboratory specimen was monitored since the beams were cast. The strains were read manually immediately before and after transfer, and when the precast sections were 2, 16, 19, and 21 days old. After 22 days, the strains were read at two hour intervals until the load cells were removed. The data showed better agreement with the combined creep and shrinkage predicted by the models in AASHTO LRFD Specifications (2004) than the charts associated with the PCA method as shown in Figure 7.18 although both methods greatly overestimated the measured results. When the coefficients that fit the creep and shrinkage models to the measured cylinder data as discussed in Section B.5 were used, both the PCA and AASHTO models gave better predictions of the change in strain at the cgs. The PCA models still gave a fairly conservative prediction, but the AASHTO models became somewhat unconservative. It was also observed that the general trend of the AASHTO prediction was different from that of the measured strains which was unexpected as the trend was well predicted in the creep and shrinkage measurements from the precast and CIP samples as shown in Section B.5. The cause of this difference was not known, but it was still expected that the AASHTO models better predicted the time dependent losses than the PCA method. Parameters required for creep and shrinkage calculations that were not outlined in Table 7.1 included the age at prestress transfer (1 day), the cure time for the precast beams (1 day) and CIP deck (8 days).

Chapter 8: Summary, Conclusions, and Recommendations

8.1 Summary and Conclusions

The Mn/DOT Precast Composite Slab Span System (PCSSS) was designed as a faster construction alternative to cast-in-place slab span systems. The original design was implemented in two bridges, one in Beltrami County, MN and the other in Center City, MN. The Center City Bridge was instrumented by University of Minnesota researchers (Bell 2006).

The Center City Bridge instrumentation was monitored for the 24 months following construction to observe the effects of environmental and vehicular loading. Strains indicating reflective cracking were observed over two of the three instrumented flange joints in the transverse direction and at the east pier in the longitudinal direction. Maximum daily transverse normal strain fluctuations of 160 and 265 με were observed at midspan of the center span in Joints 1 and 3, respectively, while Joint 2 only experienced a maximum daily fluctuation of 70 με over the course of the monitoring period. The maximum longitudinal normal strain fluctuation over the pier was 700 με. The measured transverse strains in Joints 1 and 3 and longitudinal strains over the pier were high enough such that it was assumed that cracking had occurred as it was expected that cracking would initiate at approximately 130 με. The large transverse strain fluctuations at midspan of Joints 1 and 3 were likely due to solar radiation causing temperature gradients in the bridge superstructure. It was believed that the reflective cracking initiated due to the restraint of the combined effects of shrinkage and thermal gradients. The same source of cracking was assumed for the positive moment crack observed at the east pier. The crack at the east pier was suspected to continue to grow with time as observed with the continued strain increases. As a consequence, it was unknown whether the positive moment connection was adequate to control the positive moment cracking over the pier. The live load truck test was performed April 18, 2007 at the Center City Bridge. Seven single truck and five paired truck configurations were used. The trucks were filled with sand and had tandem rear axles for which each rear axle averaged 18.7 kips. When the wheel loads were placed directly over the longitudinal joints at midspan of the center span, transverse normal strains of 19, 7, and 32 με were observed in Joints 1, 2,

and 3, respectively. The transverse load distributions determined from strain measurements compared well to simple finite element models of the bridge assuming continuous supports at the piers, as well as, to the simplified method used by Mn/DOT for design.

Design modifications to the original Mn/DOT PCSSS design were identified to improve system performance and economy. Such modifications included reducing the flange thickness of the precast sections and increasing the spacing of the transverse reinforcement for horizontal shear transfer. The design modifications were applied to a two-span laboratory bridge specimen utilizing a parametric study to maximize the comparisons that could be made. Of the four precast sections that comprised the laboratory bridge specimen, one was similar to the sections used in the Center City Bridge. The two precast sections in Span 1 were fabricated with a thinner flange (i.e., 3 in. rather than 5¼ in.). The bursting reinforcement in the precast sections and the longitudinal deck reinforcement were also varied in the laboratory bridge specimen. The primary behaviors investigated with the laboratory bridge specimen included reflective cracking, transverse load distribution, continuity over the pier, composite action, bursting, restraint moment, and prestress losses.

The laboratory specimen was instrumented with 30 vibrating wire (VW) strain gages, 344 resistive strain gages, and 16 linear variable differential transformers (LVDT's). This included the 80 resistive strain gages in the precast sections that were read at the precast fabrication plant. Load cells were embedded in the end supports of the laboratory specimen to monitor restraint moments by measuring the change in the end reactions over time.

During fabrication of the precast sections, no significant strains were measured by the strain gages on the bursting reinforcement or on the concrete surface in that region during prestress release. These results indicated that the reduced bursting reinforcement provided in the ends of the specimen was sufficient.

The CIP concrete was poured when the precast sections were seven days old, the youngest age that was deemed feasible for construction. The restraint moment was monitored for 250 days following the continuity pour using the end reactions measured by load cells placed at the simply-supported ends of the continuous two-span laboratory bridge specimen. The results were compared to two models from the literature, the PCA method (Freyermuth 1969) and the P-method (Peterman and Ramirez 1998). The PCA method was

used by Mn/DOT in the designs of the PCSSS bridges in the field. Both the PCA and P-methods overestimated the positive restraint moment measured in the laboratory specimen. However, when the creep and shrinkage models used in these methods were corrected using the measured creep and shrinkage strains from concrete samples, the P-method provided a good estimate of the positive restraint moment while the PCA method predicted a large, negative restraint moment. This indicated that the assumption of CIP shrinkage restraint assumed by the P-method (neglected by the PCA method) was valid as the unrestrained CIP shrinkage resulted in the predicted negative restraint moment. Also, the strains from the creep cylinders showed that the creep charts from the PCA method over-predicted the creep strains by 294% compared to 185% for the equations in the AASHTO LRFD Specifications (2004).

After the monitoring period was over, the load cells were removed to allow for larger loads to be placed on the laboratory specimen during actuator loading. During the removal of the load cells, positive moment cracks were observed at the pier at the end faces of the precast sections. These cracks remained open at the pier because the plates used to replace the load cells were found to be slightly thicker (i.e., 1/16 in.) than the load cells. After the first round of testing, the plates were replaced with 1/16 in. thinner plates to attempt to close these cracks, but they remained open, and no significant changes were observed to the strain measurements when the tests were repeated after the placement of the thinner plates

Both spans were tested at midspan with four loads. Three patch loads of 35.5 kips were used, one at the center of each of the two precast sections (not simultaneously) and one over the longitudinal flange joint. The fourth load was applied with two actuators and a spreader beam to give a line load across the width of the specimen with a load of 140 kips.

In the laboratory specimen, loading of the longitudinal joint with the patch load resulted in midspan transverse strains of only 15 and 25 με in Spans 1 and 2, respectively. However, it was difficult to draw a conclusion on this result due to the varied depth of the gages. Loading directly over the longitudinal flange joint did not result in large transverse strains for either Span 1 with the 3 in. thick flange or Span 2 with the 5 ¼ in. thick flange. The transverse strain of only 7 με directly under the wheel load in Joint 2 during the truck test at the Center City Bridge was consistent with the results of the laboratory study that

showed that vehicular patch loads did not cause large transverse strains in the concrete over the longitudinal joint so long as the joint had not previously been cracked by the restraint of environmental effects.

As no tensile stresses were observed over the web corners during the truck test or in the laboratory study with either chamfer condition, reflective cracking from the web corners did not appear to be a concern for the Mn/DOT PCSSS.

Curvatures across the width of the laboratory specimen during the patch load tests were more uniform in Span 1 with the 3 in. flange thickness than in Span 2 with the 5 ¼ in. flange thickness, indicating that the reduced flange thickness improved system performance with respect to transverse load distribution. However, the transverse curvature distribution measured from the truck test at the Center City Bridge, where all precast sections had the original 5 ¼ in. flange thickness, fit well with the simple isotropic plate model, indicating that the assumption of a monolithic slab superstructure used to obtain distribution factors for the original design was valid. Both the field and laboratory study found that the distribution factor used by Mn/DOT in the original design was conservative and that a wider effective width participated in carrying the loads to the supports. This included the case at the Center City Bridge when the two trucks were side by side at midspan of the center span where the Mn/DOT design assumption was both conservative and reasonable.

Flexural cracking was observed in Span 2 under the 140 kip live load, but not in Span 1 under the same load. This was in agreement with the stress calculations that predicted a smaller tensile strain at the bottom of the precast section under live load for Span 1, but was not expected without the consideration of shrinkage cracking in the CIP.

The measured curvatures from the laboratory study fit well with the fully continuous model when a 51% reduction in CIP stiffness was assumed to account for observed transverse shrinkage cracking. The reduction appeared to be valid as it was supported by both the measured neutral axis height and the measured jacking force versus displacement stiffness relationship associated with removing the load cells. The average measured neutral axis height from the Center City Bridge truck test results was similar to that predicted by calculations assuming transformed sections., It was unknown why shrinkage cracking had such a large effect on the laboratory bridge specimen but not the full field bridge, given that

the laboratory bridge could slide at the abutments and the age differential between the precast and cip deck in the laboratory bridge was smaller than that of the field bridge, which should have resulted in less differential shrinkage. The Center City Bridge was constructed in two phases, seven and six panels wide, respectively, while the laboratory bridge specimen was only two panels wide. Consequently, the aspect ratio of the two structures was different, which may have also had an affect. Longitudinal shrinkage cracks were observed in the field bridge (tining of the field deck obscured any ability to observe transverse cracks, however, the neutral axis depth in the field bridge did not indicate the presence of transverse cracks), whereas in the laboratory bridge, only transverse shrinkage cracks were observed. The results from the laboratory study indicated that the pier connection provided full continuity despite the positive moment crack induced by removing the load cells.

The ongoing research performed on the laboratory specimen may further explain the condition of continuity at the pier. Also, the reduction in deck steel on the north half of the laboratory specimen did not appear to influence the negative moment continuity over the pier, but this was expected as the pier did not undergo negative moment cracking. Similarly at the Center City Bridge, the midspan curvatures from the truck test were smaller than those predicted by the continuous isotropic model; therefore, if the benefit of the moment connections at the abutments and piers is ignored, the assumption of full continuity appears to be conservative. Both the laboratory and field studies found that the assumption of full continuity at the piers was valid despite observed positive moment cracking in both cases.

8.2 Recommendations

Although the Center City Bridge and Span 2 of the laboratory specimen with the original 5 ¼ in. flange performed well, the test results indicated that the reduction in flange thickness to 3 in. improved transverse load distribution. Also, there was no indication that the reduced flange was not durable enough for transportation and construction. Therefore it is recommended to use the 3 in. flange in future implementations of the Mn/DOT PCSSS.

It was difficult to determine the effects of the smooth flange surface on reflective cracking, considering that the reduction in flange thickness would have a larger effect. Also, the smooth flange surface did allow for easier removal of the forms during fabrication, as

expected. However, the effect of the smooth flange surface on composite action as the bridge is loaded to ultimate should be considered when that research is concluded at which point a recommendation can be made.

As transverse tensile strains over the web corners were not observed under any conditions, it is recommended to not change the original chamfer that was specified at ¾ in. by ¾ in. and as built at 1 in. by ½ in.

The equation used to obtain distribution factors for the original design from the AASHTO LRFD Specification (2004) 4.6.2.6 was reasonable and conservative and it is recommended that its use be continued.

The decrease in longitudinal deck steel was calculated as adequate for ultimate load, but as that test has yet to be performed, no recommendation can be made at this time.

The original design assumptions of full continuity over the pier and of a monolithic slab superstructure for load distribution appeared to be valid, and it is recommended that their use be continued.

Use of the reduced bursting reinforcement details did not result in any cracking during transfer, and it was believed that the AASHTO LRFD Specifications (2004) were unreasonably conservative for precast sections similar to the Mn/DOT PCSSS. Therefore, it is recommended that bursting stresses be estimated by a procedure that includes the height of the precast section such as the one described in Section 5.6.

The P-method better predicted positive restraint moments in the laboratory specimen than the PCA method, so it is recommended that the P-method replace the PCA method in future designs or that the PCA method be modified such that CIP shrinkage restraint is considered and another method for creep and shrinkage prediction, such as AASHTO LRFD Specifications (2004) 5.4.2.3, replaces the charts in the PCA method paper (Freyermuth 1969).

In all, the results of the field and laboratory study confirmed the durability of the Mn/DOT PCSSS, which has been shown to be a practical, economical accelerated construction alternative to cast-in-place slab construction.

References

American Assoc. of State Highway and Transportation Officials. 2004. *AASHTO LRFD Bridge Design Specifications, Third Edition.* Washington, D.C.: American Assoc. of State Highway and Transportation Officials.

ACI Committee 209. 1992. *Prediction of Creep, Shrinkage, and Temperature Effects in Concrete Structures*. Farmington Hills, MI: American Concrete Institute.

ACI Committee 318. 2002. *Building Code Requirements for Structural Concrete (ACI 318-02) and Commentary (ACI 318R-02)*. Farmington Hills, MI: American Concrete Institute.

ACI Committee 363. 1998. *Guide to Quality Control and Testing of High-Strength Concrete*. Farmington Hills, MI: American Concrete Institute.

Bell, Charles II, Shield, Carol K., French, Catherine. 2006. *Application of Precast Decks and Other Elements to Bridge Structures*. Mn/DOT Report 2006-37. St. Paul, MN: Minnesota Department of Transportation.

Bice, J., Erickson, J., Frosch, R., J. 2006. Evaluation of Design Methods for Control of Restrained Shrinkage Cracking in Concrete Bridge Decks. *Proceedings, National Concrete Bridge Conference, HPC: Build Fast, Build to Last*. Reno, NV.

Broms, B., B. 1965. Crack Width and Crack Spacing in Reinforced Concrete Members. *ACI Structural Journal* 62(10), 1237-1256.

Eriksson, Whitney. 2008. *Vertical Tensile Stresses in End Regions of Precast Composite Slab-Span Systems and Restraint Moments*. Unpublished master's thesis. University of Minnesota – Twin Cities.

Freyermuth, C.L. 1969. Design of Continuous Highway Bridges with Precast, Prestressed Concrete Girders. *Journal of the Prestressed Concrete Institute* 14(2), 14-39.

Gilbert, R., I. 2005. Time-Dependent Cracking and Crack Control in Reinforced Concrete Structures. *American Concrete Institute (ACI) Structural Journal, Special Publication SP 225-15*, Vol. 225, 223-244.

Marshall, W. T., & Mattock, A. H. 1962. Control of horizontal cracking in ends of pretensioned prestressed concrete girders. *Journal of the Prestressed Concrete Institute* 7(5), 56-74.

Miller, R.A., Castrodale, R., Mirmiran, A and Hastak, M. 2004. *Connection of Simple-Span Precast Concrete Girders for Continuity*. NCHRP Report 519. Washington, D.C.: Transportation Research Board, National Research Council.

Mirmiran, A., Kulkarni, S., Castrodale, R., and Hastak, M. 2001. Nonlinear Analysis of Precast, Prestressed Concrete Girders with Cast-in-Place Decks and Diaphragms. *PCI Journal* 46(5), 60-80.

Mirmiran, A., Kulkarni, S., Hastak, M., Sharhrooz, B., and Castrodale, R.C. 2001. *Positive Moment Cracking in Diaphragms of Simple Span Prestressed Girders Made Continuous*. ACI SP 204. Farmington Hills, MI: American Concrete Institute.

Naito, C., Deschenes, D. 2006. Horizontal Shear Capacity of Composite Concrete Beams without Ties. *Proceedings, Prestressed/Precast Concrete Institute (PCI) National Bridge Conference*, Grapevine, TX.

Neville, A. M. 1981. *Properties of Concrete, Third Edition*. New York: John Wiley and Sons.

Oesterle, R. G., Gilkin, J. D., and Larson, S. C. 1989. *Design of Precast Prestressed Bridge Girders Made Continuous*. NCHRP Report 322. Washington D.C.: Transportation Research Board, National Research Council.

PCI Industry Handbook Committee. 1999. *PCI Design Handbook: Precast and Prestressed Concrete, Fifth Edition*. Chicago, IL: Precast/Prestressed Concrete Institute.

PCI Committee on Prestress Losses. 1975. Recommendations for Estimating Prestress Losses. *Journal of the Prestressed Concrete Institute* 20(4), 43-75.

Peterman, R.J., and Ramirez, J.A. 1998. Restraint Moments in Bridges with Full-Span Prestressed Concrete Form Panels. *PCI Journal* 43(1), 54–73.

Tables

Table 4.1: Measured truck axle weights for live load truck test

	Truck A	
	Weigh Station (kips)	Field Scales (kips)
Front	--	16.2
Front Tandem	--	20.1
Rear Tandem	--	19.3
Total	52.0	55.6

	Truck B	
	Weigh Station (kips)	Field Scales (kips)
Front	--	14.4
Front Tandem	--	19.3
Rear Tandem	--	19.0
Total	51.7	52.7

Table 4.2: Measured times and coordinates for live load truck test positions

Test	Start Time	End Time	Y_F (ft)	Y_{R2} (ft)	X_{R2} (ft)	ΔY_F (ft)	ΔY_{R2} (ft)
1.1	20:30:30	20:34:06	9.8	9.7	33.7	X	X
1.2	21:09:45	21:14:10	10.0	10.0	33.7	X	X
2.1	20:35:25	20:40:10	12.8	12.7	33.6	X	X
2.2	21:15:18	21:20:49	12.9	12.8	33.5	X	X
3.1	20:43:34	20:48:37	15.8	15.5	33.7	X	X
3.2	21:21:54	21:27:09	15.8	15.9	33.8	X	X
4.1	20:50:20	20:56:12	18.7	18.3	33.3	X	X
4.2	21:28:22	21:34:07	18.8	18.5	33.8	X	X
6.1	21:01:27	21:05:44	18.0	18.2	14.7	X	X
6.2	21:50:15	21:54:31	18.0	18.2	15.4	X	X
A.1	22:59:44	23:04:21	13.7	13.7	14.5	1.2	1.5
B.1	23:26:25	23:31:24	13.1	13.2	14.2	1.3	1.6
8.1	24:10:51	24:14:55	13.6	13.6	14.9	0.8	1.5
8.2	22:38:48	22:43:46	14.3	14.2	27.1	1.5	1.5
8.3	23:06:25	23:11:16	13.7	13.6	26.4	1.7	2.2
9.1	23:34:35	23:38:17	14.1	14.0	27.6	2.1	2.3
9.2	22:45:15	22:49:37	14.1	14.3	33.3	1.7	2.3
9.3	23:12:28	23:17:09	13.7	13.7	33.7	1.7	2.3
10.1	23:39:49	23:43:16	14.1	14.0	33.9	2.2	2.4
10.2	22:54:51	22:59:07	13.5	13.7	45.6	1.2	1.8
10.3	23:21:42	23:25:50	12.9	13.2	46.6	1.4	1.8
11.1	24:05:07	24:09:32	13.3	13.3	45.5	1.5	2.1
11.2	21:36:28	21:40:30	6.9	6.8	33.4	X	X
11.3	21:41:57	21:47:00	3.6	3.6	33.3	X	X
E.1	23:45:40	23:49:57	7.6	7.6	33.6	1.9	2.3
E.2	23:52:04	23:55:37	5.9	5.8	33.6	4.9	5.2
E.3	23:57:31	24:01:12	3.9	3.7	33.7	8.8	9.2

The terms are defined in Figure 4.3

Table 4.3: Increases in transverse strains immediately over longitudinal flange joint when loaded directly above with wheel load

	Truck Configuration	Strain Value(s) (με)
Joint 1	3	19, 19
Joint 2	1	6, 6
Joint 2	3	8, 8
Joint 3	1	30, 31
Joint 3	B	34

Table 5.1: Proposed modifications to the laboratory bridge specimen

			Effects						Locations	
			Reflective Cracking	Transverse Load Distribution	Longitudinal Flexural Behavior	Composite Action	Bursting	Constructability/ Economy	Potential	Recommended
Parameter	A	Smooth Flange Surface	+	?	-	- -		+ +	1 vs. 2 or 1W vs. 1E	1 vs. 2
	B	Increased Stirrup Spacing			-	- -		+ +	1 vs. 2 or 1 and 2N vs. 2S	1 vs. 2
	C	Decreased Flange Thickness	+ +	+ +	+	+			1 vs. 2	1 vs. 2
	D	Increased Clear Spacing Under Hooks			+	+ +			1 vs. 2 or 1 and 2N vs. 2S	1 vs. 2
	E	Staggering Hooks over Flanges	?	?					1 vs 2	None
	F	Separating Reinforcement into Two Pieces						+ +	1 vs. 2 or All	1 vs. 2
	G	Decreased Bursting Reinforcement					-	+	Each End	Each Beam
	H	Decreased Longitudinal Deck Steel			?			+	N vs. S	N vs. S
	I	Decreased Transverse Deck Steel	?	?				+	1 vs. 2	1 vs. 2
	J	Increased Chamfer	+	?					N vs. S	N vs. S

Expected Change in Performance			
+ +	Greatly improve performance	- -	Greatly impair performance
+	Improve performance	-	Impair performance
?	Unknown change in performance	(blank)	No expected change

Table 5.2: Descriptive images of proposed modifications

		Proposed	Original			Proposed	Original
A	Smooth Flange Surface	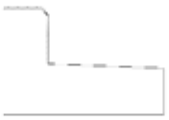		F	Separating Web Reinforcement into Two Pieces		
B	Increased Stirrup Spacing	24 in.	12 in.	G	Decreased Bursting Reinforcement	#4 Stirrups @ 2 in. or #3 Stirrups @ 2 and 4 in.	2 #5 Stirrups @ 2, 4, and 6 in.
C	Decreased Flange Thickness	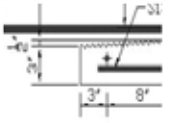	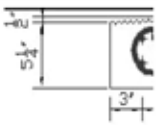	H	Decreased Longitudinal Deck Steel	#6 @ 6 in.	#7,#7,#8 @ 12 in.
D	Increased Clear Spacing Under Hooks		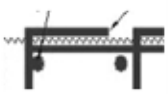	I	Decreased Transverse Deck Steel	#4 @ 12 in.	#5 @ 12 in.
E	Staggering Transverse Hooks over Flanges	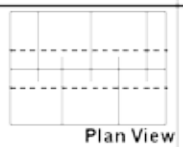 Plan View	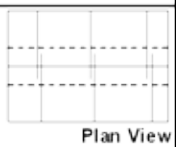 Plan View	J	Increased Chamfer @ Web Corner	1-1/2 in.	3/4 in.

Table 5.3: Summary of Moment Coefficients for Center City and Beltrami County Bridges

	Center City Bridge		
	PCA method	P-method inner span	P-method outer span
C_u	1.18	0.94	1.37
C_p	0.67	0.63	0.63

	Beltrami County Bridge		
	PCA method	P-method inner span	P-method outer span
C_u	1.20	0.96	1.43
C_p	0.80	0.64	0.96

Table 5.4: Predicted restraint moments for Center City and Beltrami County Bridges

Center City Bridge					
Max Positive			Max Negative		
	PCA method	P-method		PCA method	P-method
$t_{continuity}$	14 days	14 days	$t_{continuity}$	90 days	90 days
t_{after}	20 yrs	20 yrs	t_{after}	100 days	85 days
RM (ft*k)	**78.5**	**106**	**RM (ft*k)**	**-198**	**-48.4**
	% Difference	26%		% Difference	-309%

Beltrami County Bridge					
Max Positive			Max Negative		
	PCA method	P-method		PCA method	P-method
$t_{continuity}$	14 days	14 days	$t_{continuity}$	90 days	90 days
t_{after}	20 yrs	20 yrs	t_{after}	100 days	98 days
RM (ft*k)	**141.8**	**149**	**RM (ft*k)**	**-266**	**-101**
	% Difference	5%		% Difference	-163%

Table 5.5: Application of AASHTO LRFD (2004) Specification provision 5.14.1.2.7c for the Center City and Beltrami County Bridges for maximum allowable positive restraint moment

	Center City	**Beltrami County**
	ft-k	ft-k
M_{LL}	-119	-262
M_{SDL}	-11	-50
$0.5M_{LL}+M_{SDL}$	-71	-181
M_{cr}	154	230
$1.2M_{cr}$	184	276
$RM_{pos,allowed}$	71	181
$RM_{14d,max}$	106	149
$RM_{28d,max}$	74	104
$\varphi M_{n,provided}$	137	194

Table 7.1: Measured, nominal and calculated properties of the laboratory bridge specimen

	Property	Symbol	Unit	Span 1	Span 2	Comments
Measured	Initial precast concrete compr. strength (1 day)	f'_{ci_pc}	ksi	7.4	7.4	
	28 day precast concrete compr. strength	f'_{c_pc}	ksi	12.9	12.9	
	Elastic modulus of precast concrete (413 days)	E_c	ksi	6160	6160	
	28 day CIP comp. strength	f'_{c_CIP}	ksi	4.16	4.59	
	Elastic Modulus of CIP (427 days)	E_c	ksi	3540	3780	
	Unit weight of precast	w_{pc}	kcf	154	154	
	Unit weight of CIP	w_{CIP}	kcf	136	139	
	Average laboratory RH	RH	%	41	41	
	Age at prestress transfer	t_i	day	1	1	
	Cure time for precast	t_{d_pc}	day	1	1	
	Age of prestress at time of continuity	t_c	day	7	7	
	Moist cure time for CIP	t_{d_CIP}	day	8	8	
Nominal	Prestress strand area (excludes flange strands)	A_{ps}	in^2	2.44	2.44	From strand manufacturer
	Elastic modulus of strands	E_{ps}	ksi	28500	28500	From strand manufacturer
Calculated	Prestress force after transfer (excludes flange strands)	P_i	kips	481	482	Using measured jacking strain and transfer loss (elastic shortening) and predicted initial relaxation loss
	Prestress force after transfer (includes flange strands)	P_i	kips	497	515	same as above
	Initial elastic modulus of precast concrete	E_{pci}	ksi	5350	5350	Using measured unit weight and initial strength in AASHTO LRFD (2004) C5.4.2.4-1

Table 7.2: Summary of laboratory bridge specimen tests

Date	Test	CR9000 set	Load (kips)	Repeats
10/16/2007	1S	all	35.5	3
10/16/2007	1N	all	35.5	3
10/26/2007	1spr	all	140	3
10/29/2007	1C	all	35.5	3
11/19/2007	2N	a	35.5	3
11/19/2007	2S	a	35.5	3
11/20/2007	2N	b	35.5	3
11/20/2007	2S	b	35.5	3
11/21/2007	2spr	b	140	3
11/21/2007	2spr	a	140	3
11/21/2007	2C	a	35.5	3
11/21/2007	2C	b	35.5	3
11/27/2007	2C	c	35.5	3
11/27/2007	2N	c	35.5	3
11/27/2007	2S	c	35.5	3
11/28/2007	2spr	c	140	3

- Test configurations shown in Figure 7.3
- CR9000 set indicates which set of 350Ω gages were monitored

Table 7.3: Predicted positive restraint moments for Center City Bridge after 20 years for differing age of precast sections at continuity

	Restraint Moment (ft-k)		
Age at Continuity	P-Method	PCA Method	Difference (%)
7 days	128	107	16%
14 days	106	79	25%
28 days	74	43	42%
45 days	45	--	100%
90 days	--	--	--

Table 7.4: Predicted and measured losses due to elastic shortening (ksi)

	Outer Strands Considered?	Span 1	Span 2
		Δf_{pES} (ksi)	Δf_{pES} (ksi)
Measured from strand gages	--	8.5	7.4
Measured from concrete embedment gages	--	7.3	6.9
Zia (EQ 5.9.5.2.3a-1)	No	5.4	4.9
	Yes	5.6	5.3
PCI Committee	No	5.2	4.7
	Yes	5.4	5.1
AASHTO Alt. Eq (EQ C5.9.5.2.3a-1)	No	5.2	4.7

Figures

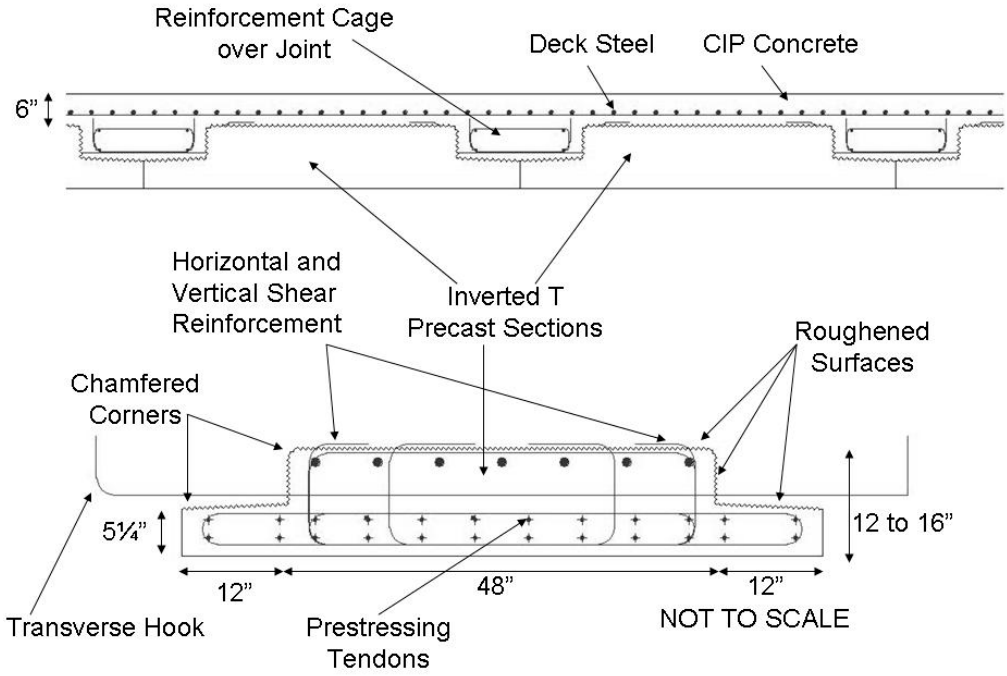

Figure 1.1: Conceptual cross section of Mn/DOT Precast Composite Slab Span System (PCSSS)

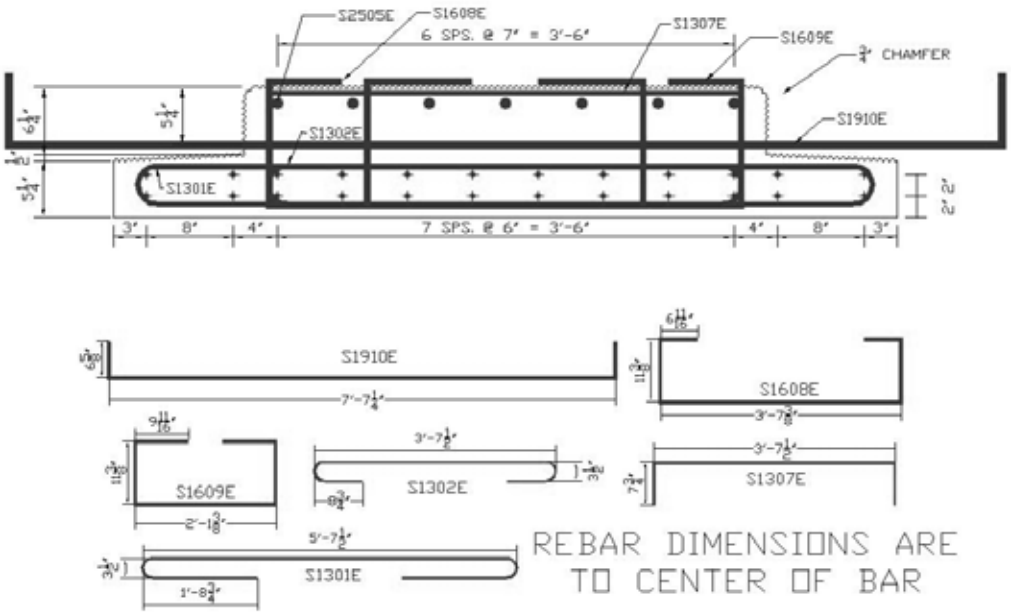

Figure 1.2: Final, nominal cross section for Center City Bridge precast sections

Figure 3.1: Photograph of the Center City Bridge

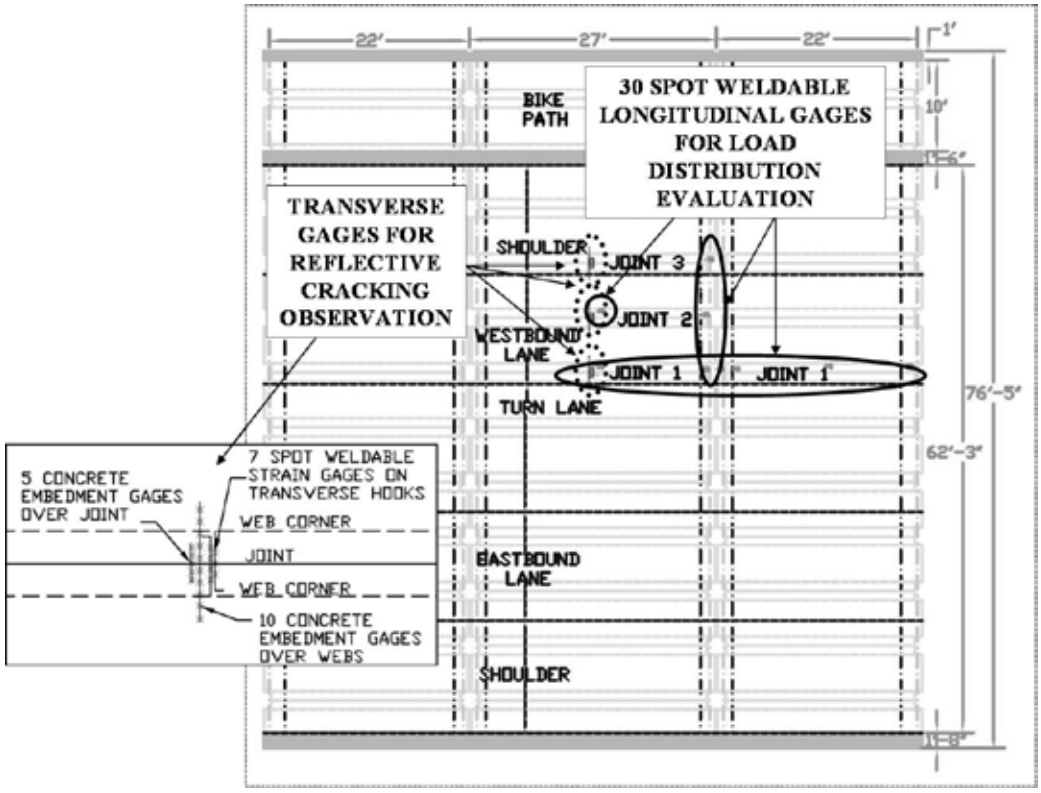

Figure 3.2: General layout of Center City Bridge instrumentation

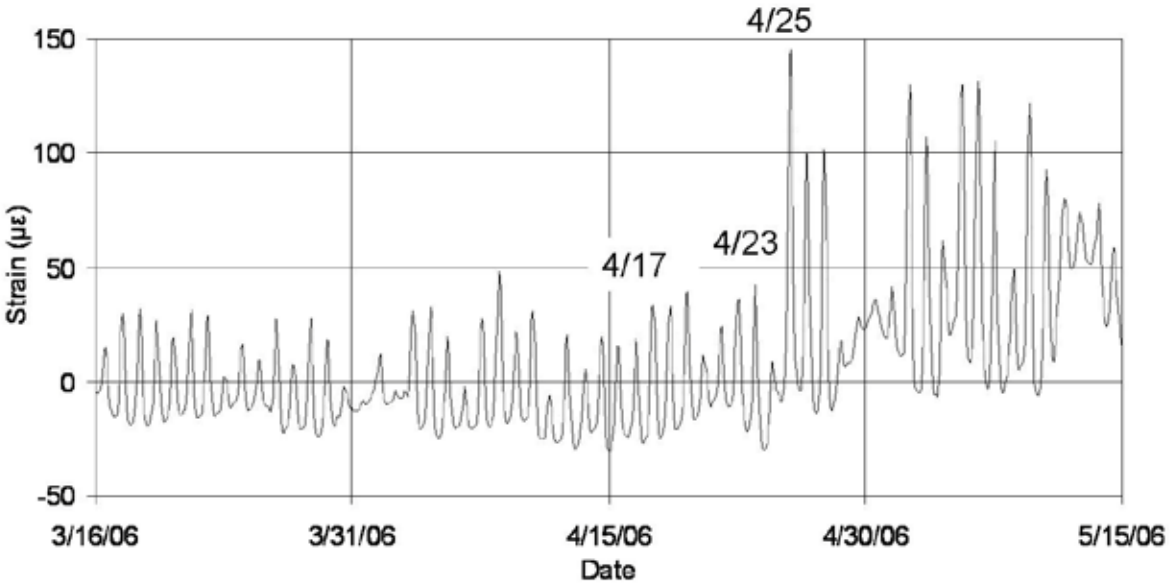

Figure 3.3: Transverse strains immediately over Joint 1 at midspan of the center span of the Center City Bridge

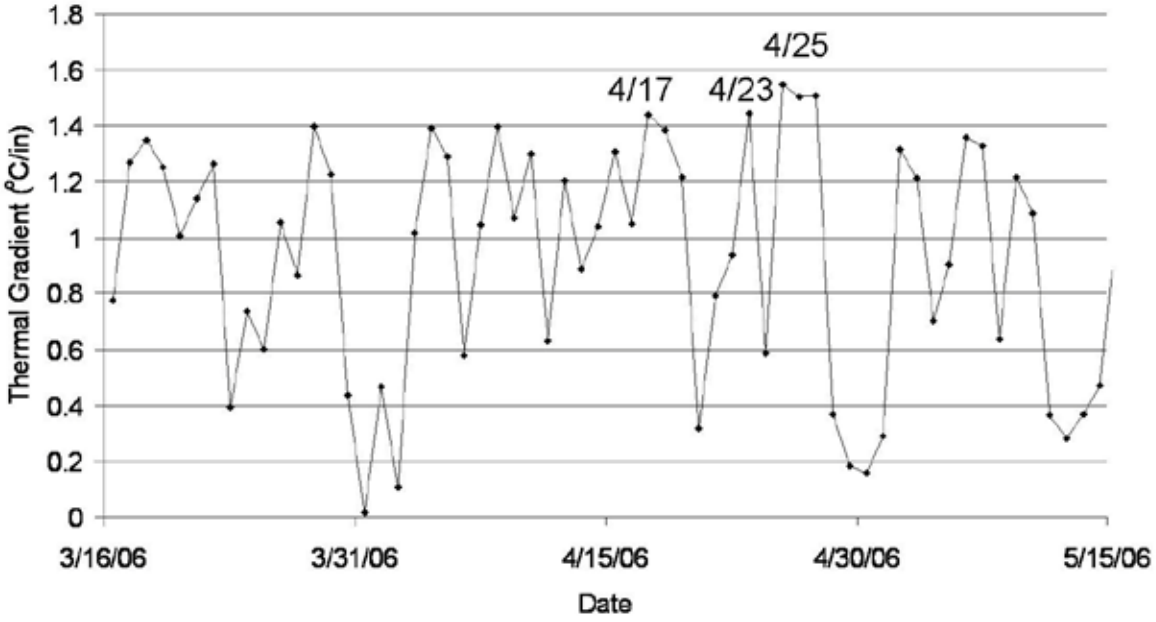

Figure 3.4: Daily fluctuations in thermal gradients at midspan of the center span of the Center City Bridge

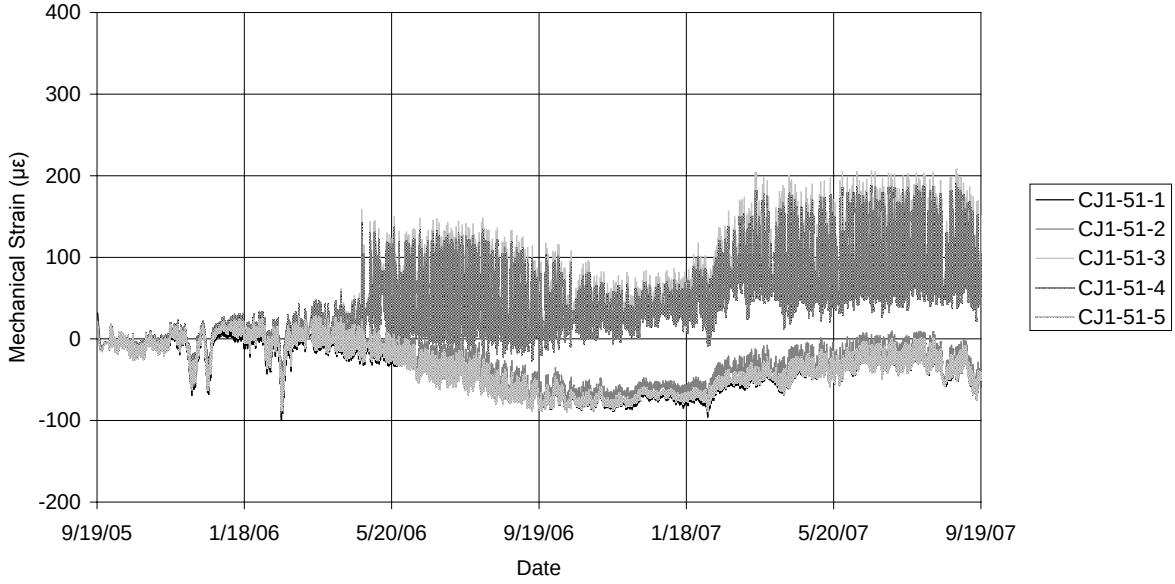

Figure 3.5: Transverse strains immediately over Joint 1 at midspan of the center span of the Center City Bridge over 24 month monitoring period

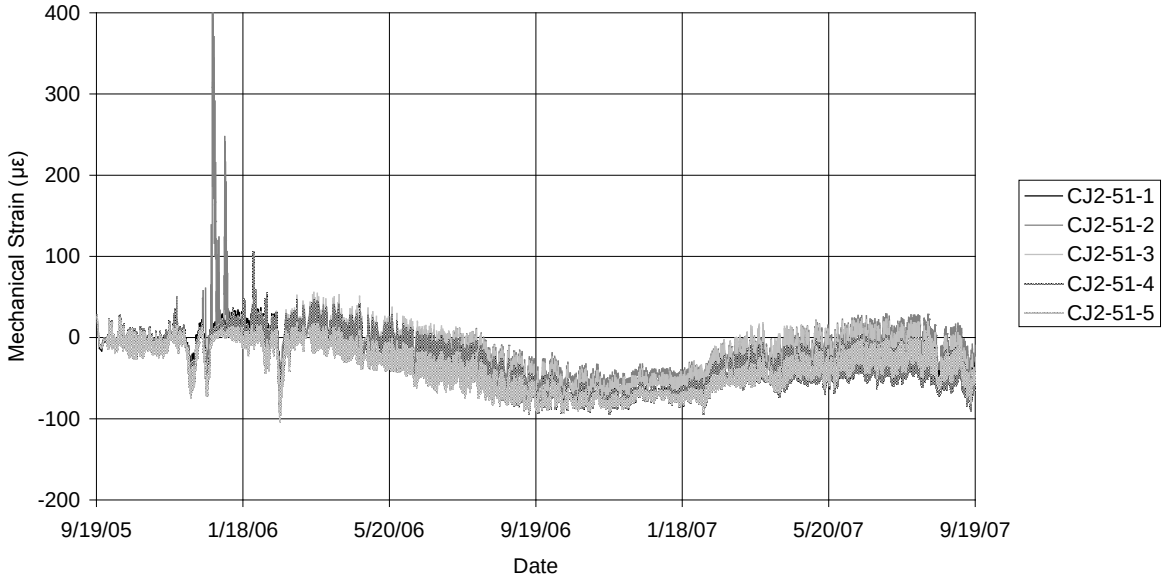

Figure 3.6: Transverse strains immediately over Joint 2 at midspan of the center span of the Center City Bridge over 24 month monitoring period

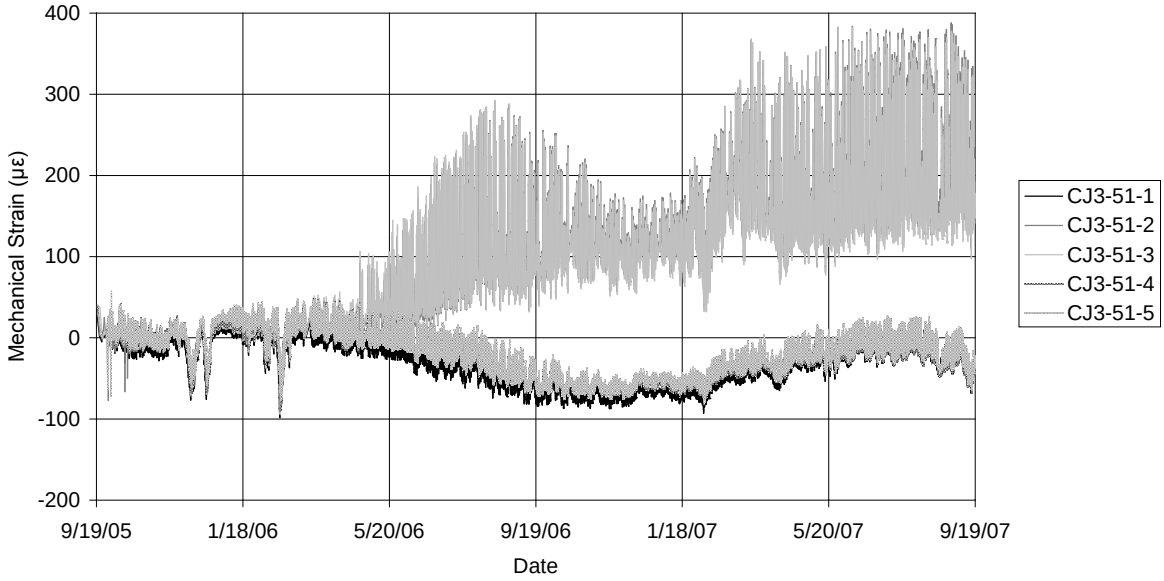

Figure 3.7: Transverse strains immediately over Joint 3 at midspan of the center span of the Center City Bridge over 24 month monitoring period

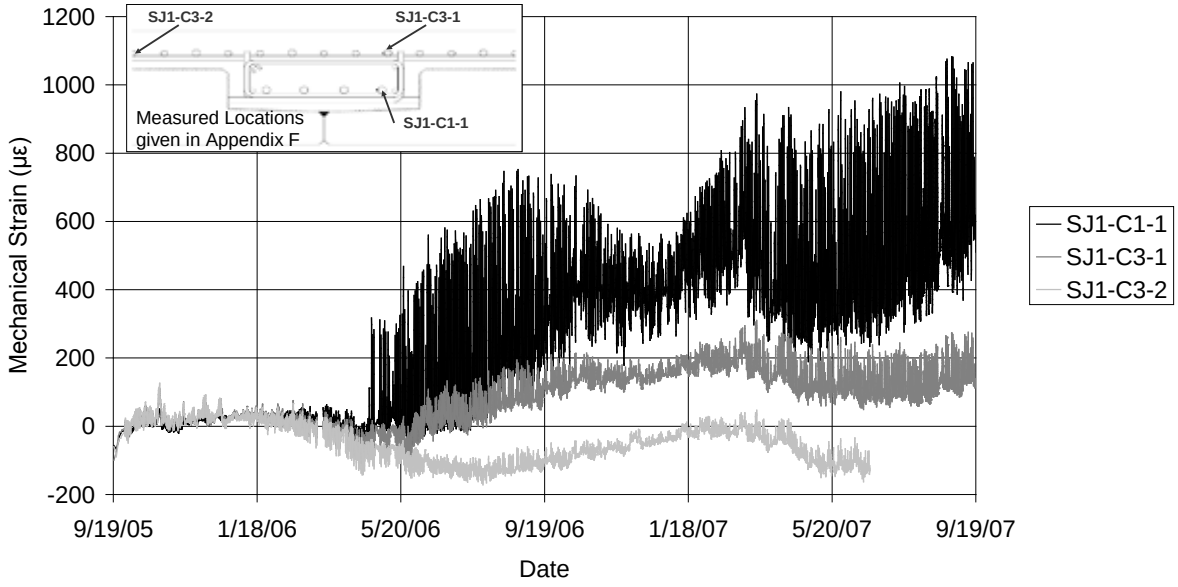

Figure 3.8: Strains in the positive and negative moment reinforcement at the center line of the east pier

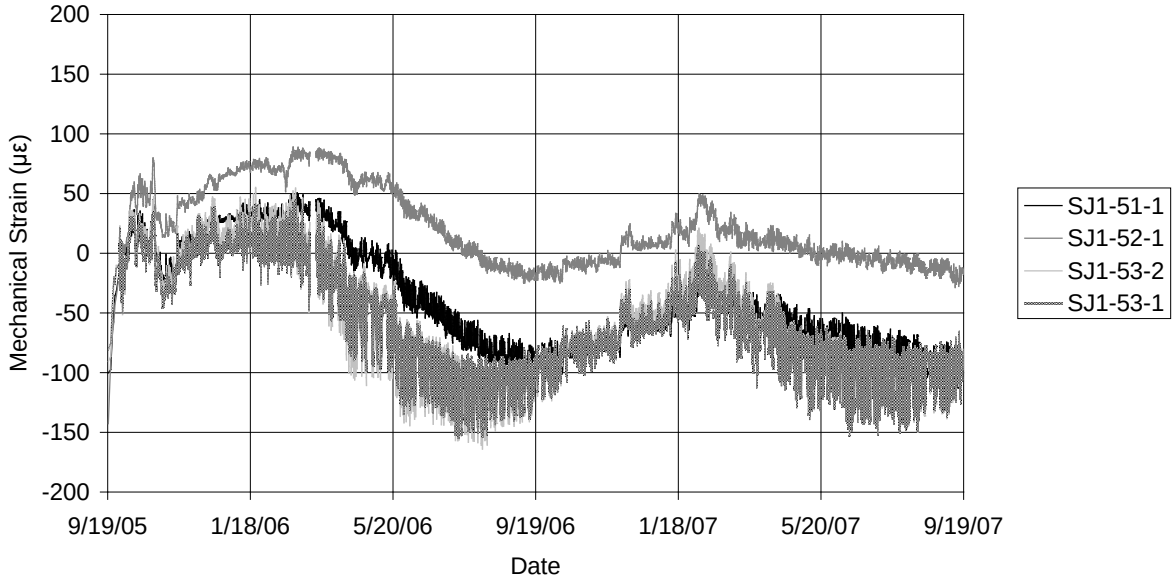

Figure 3.9: Seasonal trends of typical longitudinal gages (spot-weldable gages located at midspan of the center span)

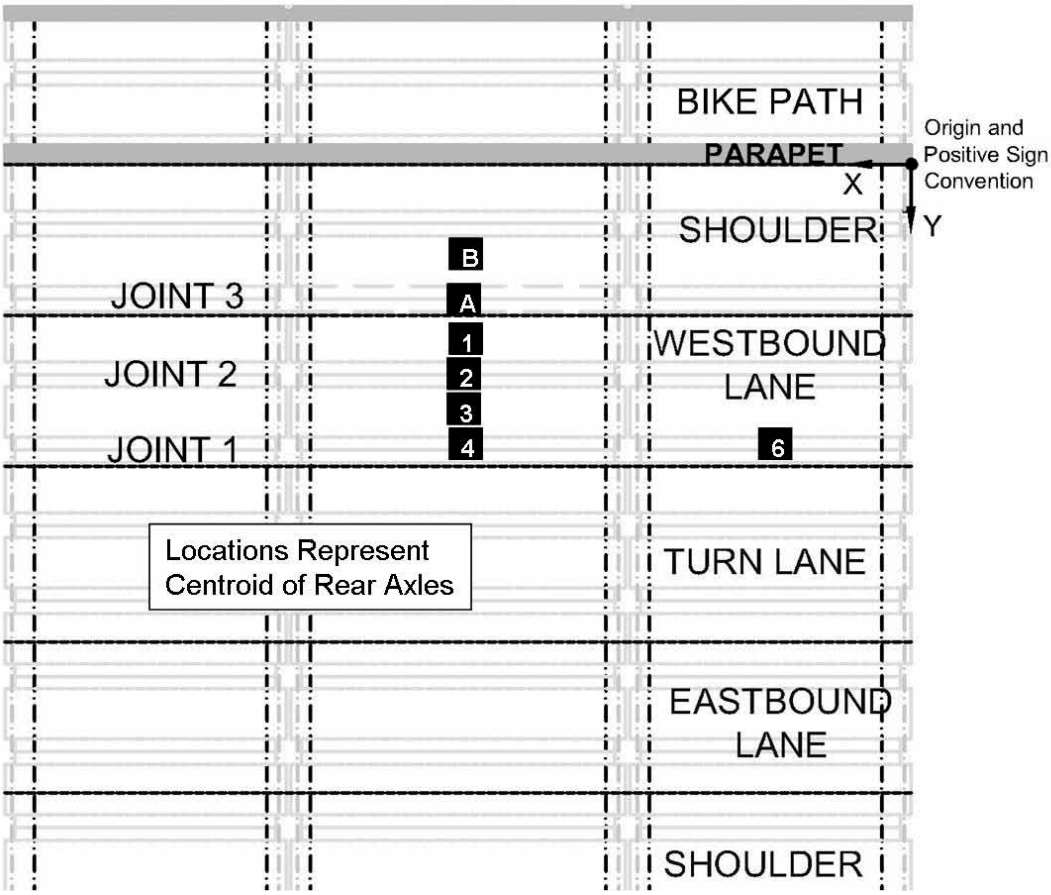

Figure 4.1: Single truck positions for live load truck test

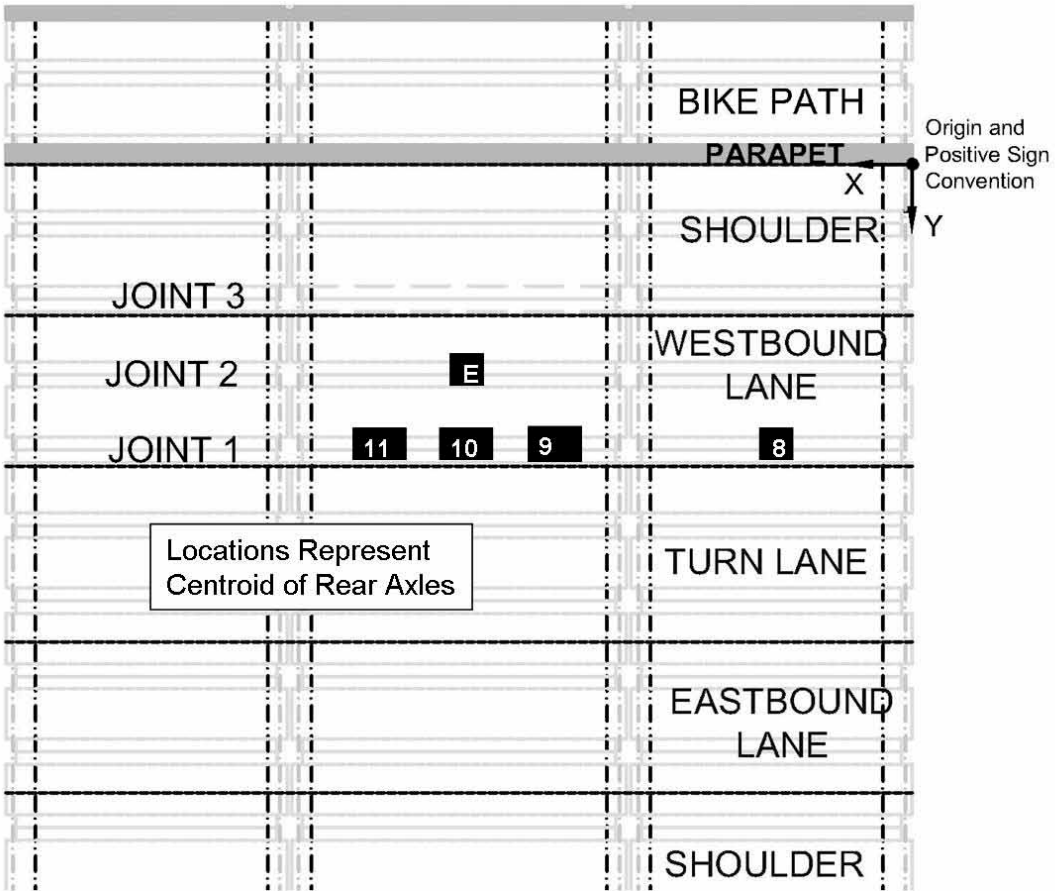

Figure 4.2: Paired truck positions for live load truck test

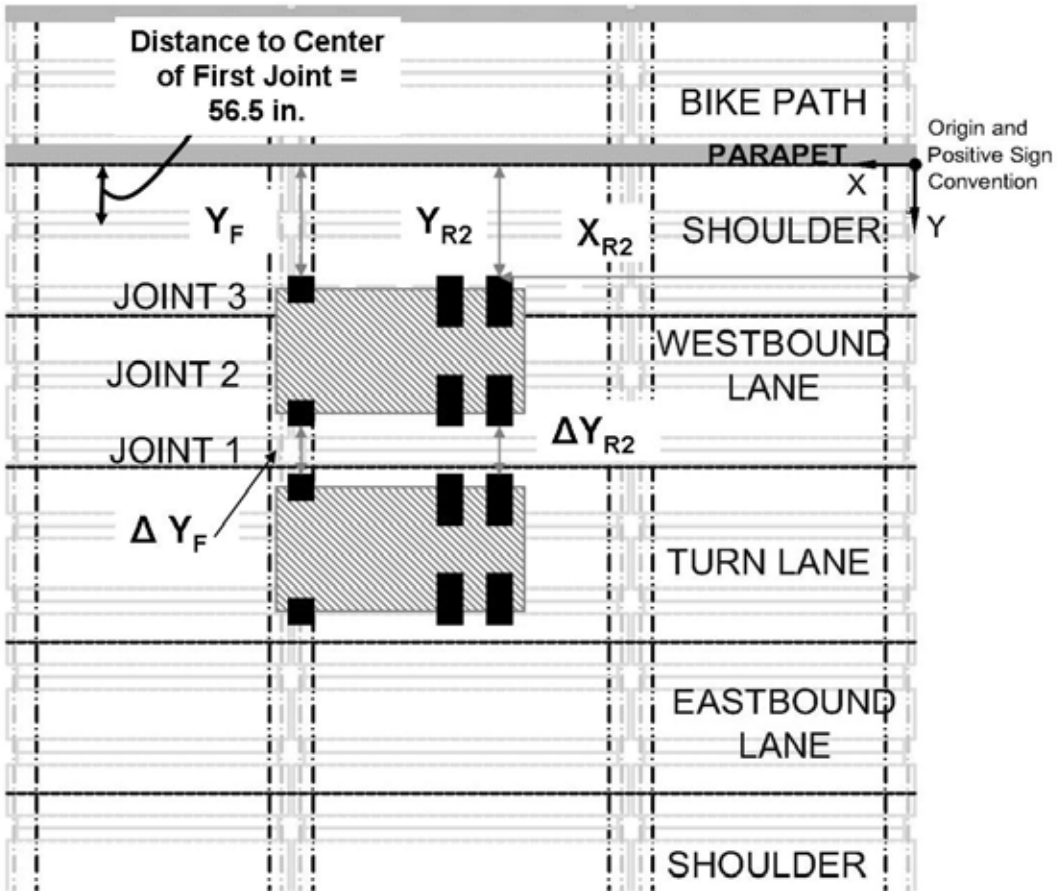

Single Truck Tests

Truck A	Test	Y_F	Y_{R2}	X_{R2}
	1	9.7	9.7	33.8
	2	12.7	12.7	33.8
	3	15.7	15.7	33.8
	4	18.7	18.7	33.8
	6	18.7	18.7	13.5
	A	6.7	6.7	33.8
	B	3.7	3.7	33.8

Paired Truck Tests

North: Truck A South: Truck B	Test	Y_F	Y_{R2}	X_{R2}	ΔY_F	ΔY_{R2}
	8	13.9	13.9	13.5	1.5	1.5
	9	13.9	13.9	27.5	1.5	1.5
	10	13.9	13.9	33.8	1.5	1.5
	11	13.9	13.9	44.7	1.5	1.5
	E	13.9	13.9	33.8	4.0	4.0

X measured from east end of the bridge in ft.
Y measured from south side of parapet that separates bike path in ft.

Figure 4.3: Diagram of measurements and nominal location of truck test positions

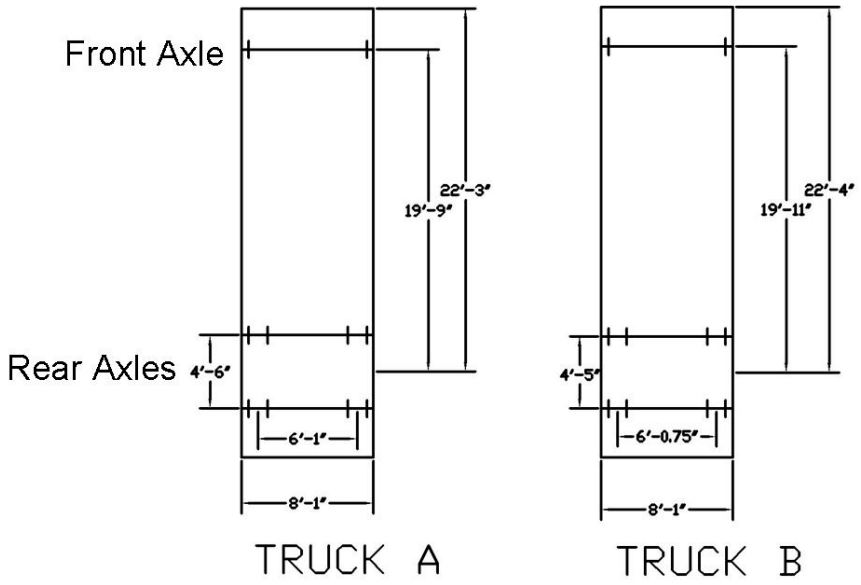

Figure 4.4: Dimensions of trucks used in live load test

Figure 4.5: Photograph of the trucks during a paired position of the live load test

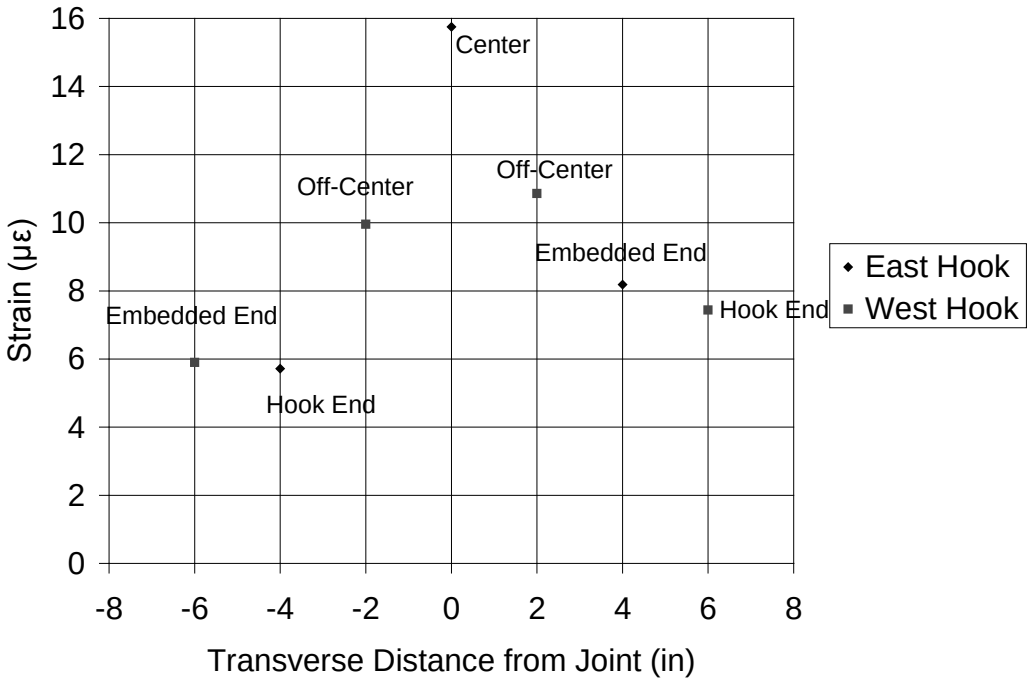

Figure 4.6: Increases in tensile strains in transverse hooks at Joint 1 immediately under wheel load

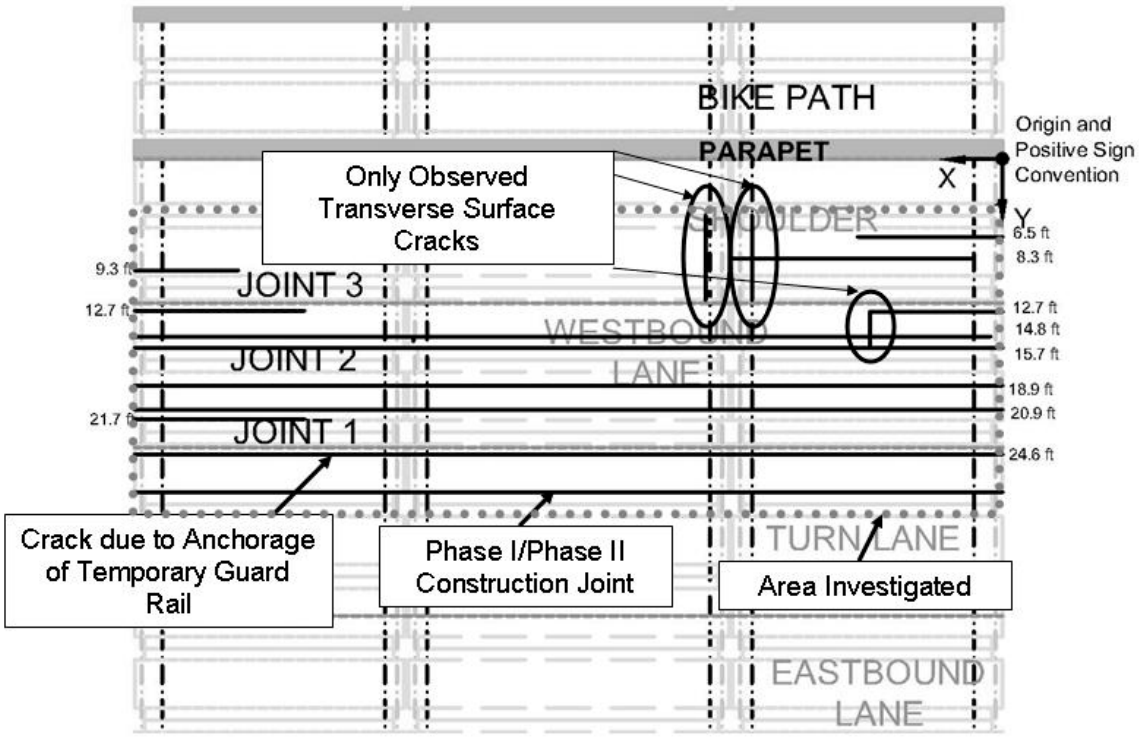

Figure 4.7: Observed surface cracking layout at Center City Bridge

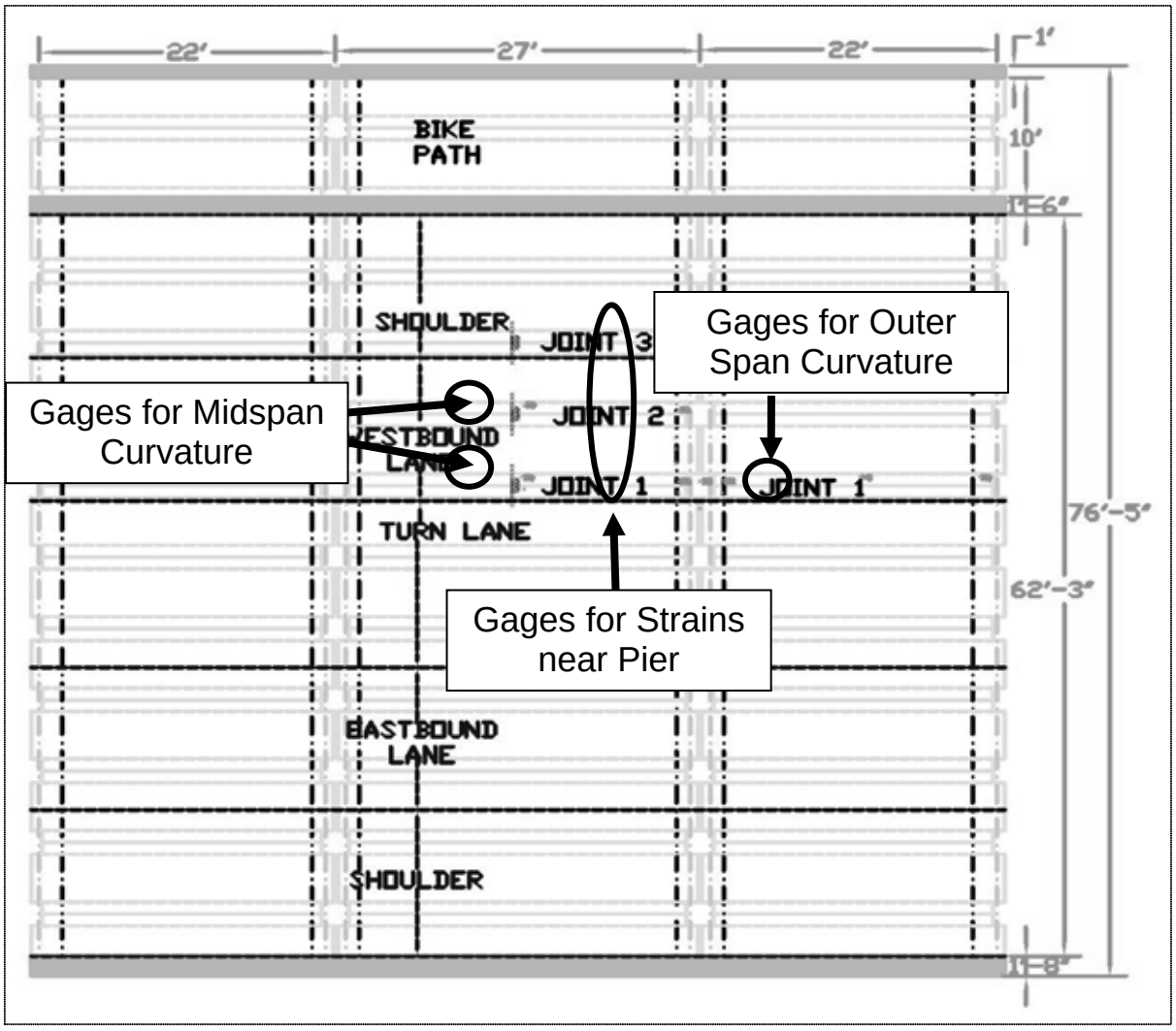

Figure 4.8: Locations of spot-weldable strain gages on longitudinal reinforcement of Center City Bridge

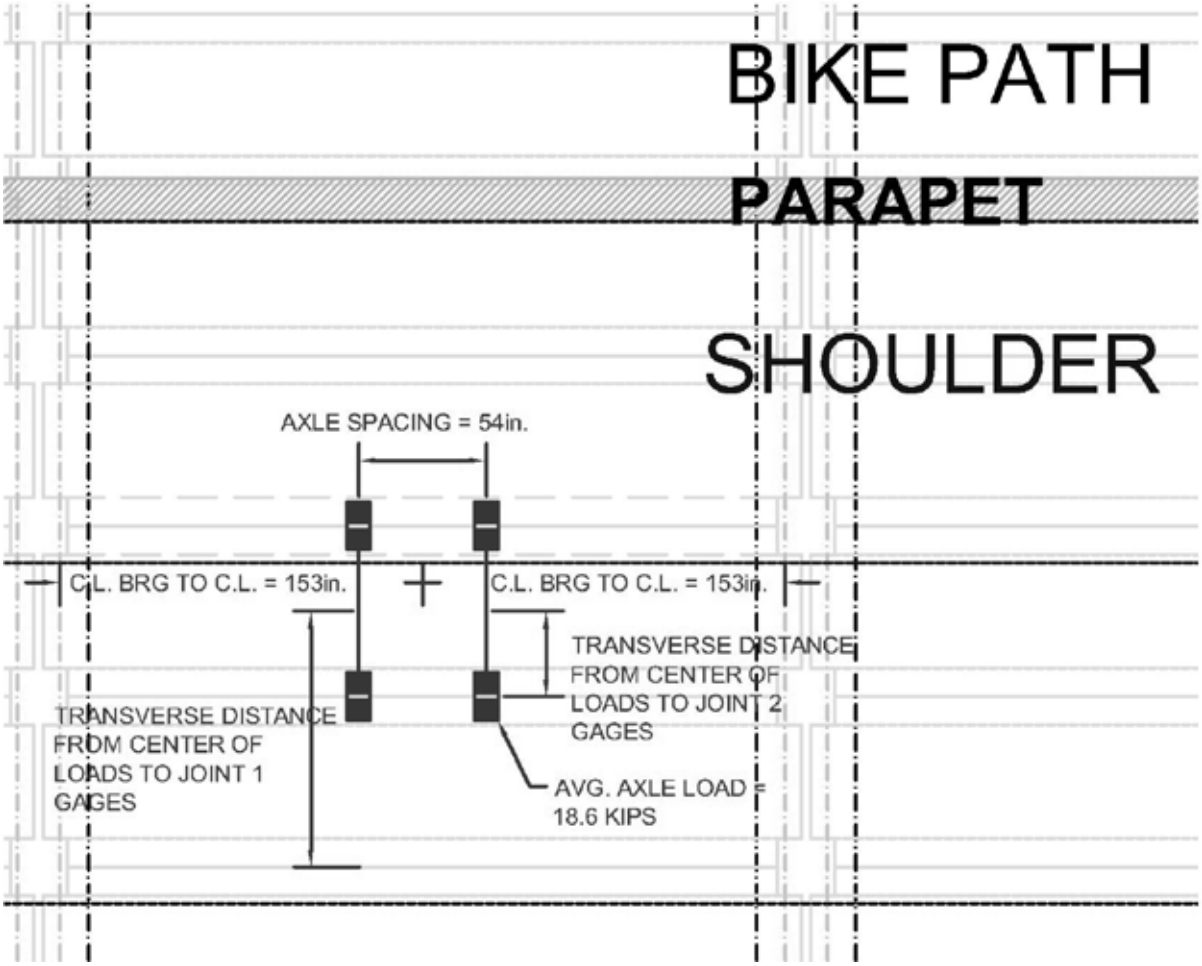

Figure 4.9: Truck position layout example for transverse load distribution

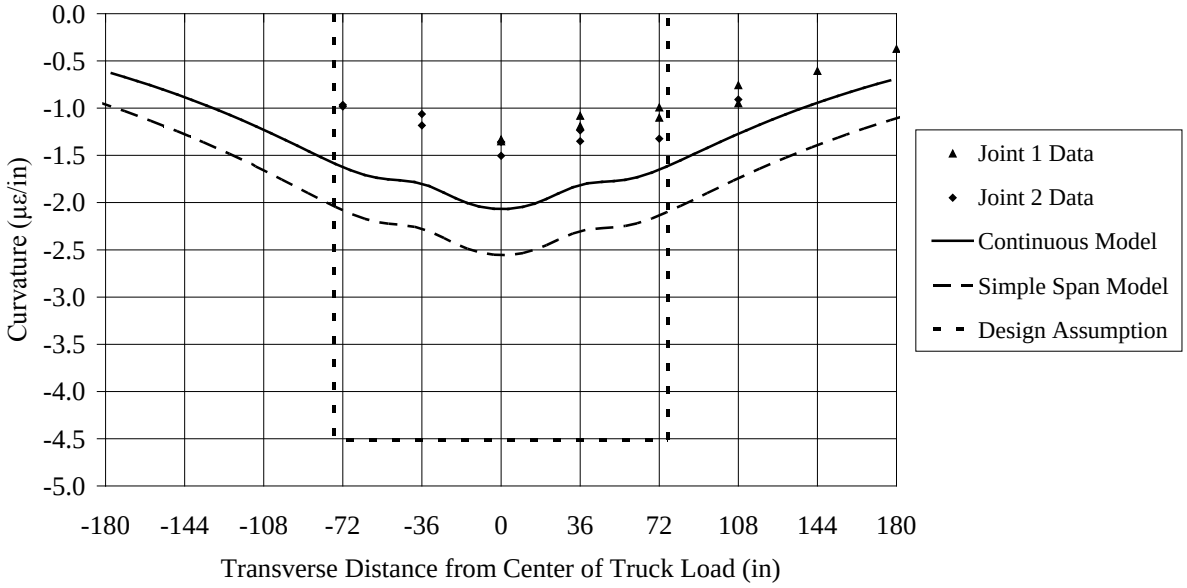

Figure 4.10: Curvatures at midspan due to a single truck at midspan of the center span

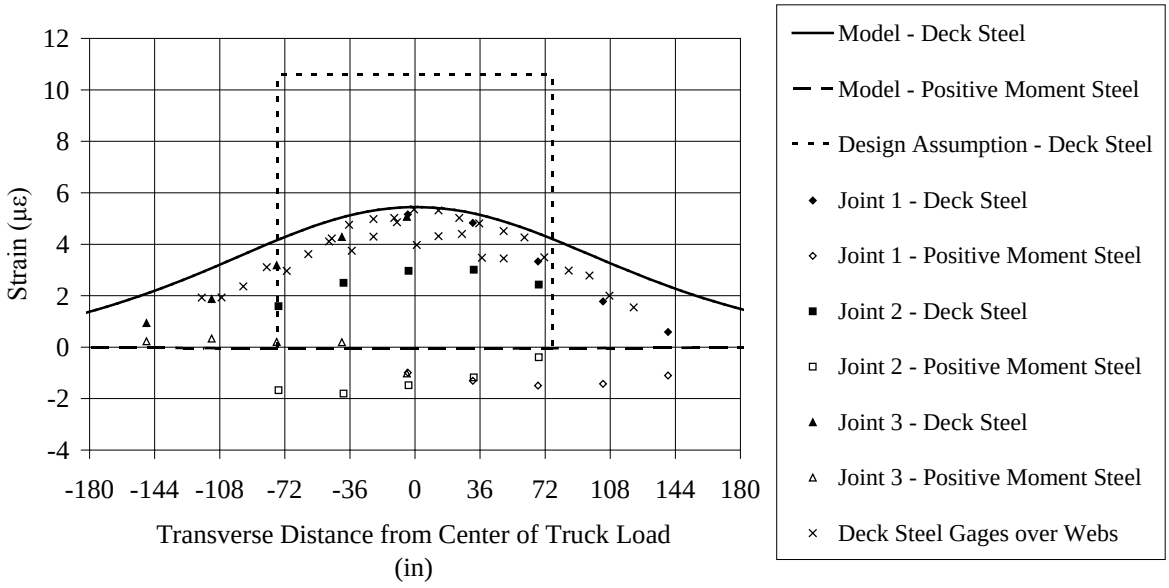

Figure 4.11: Strains near pier due to a single truck at midspan of the center span

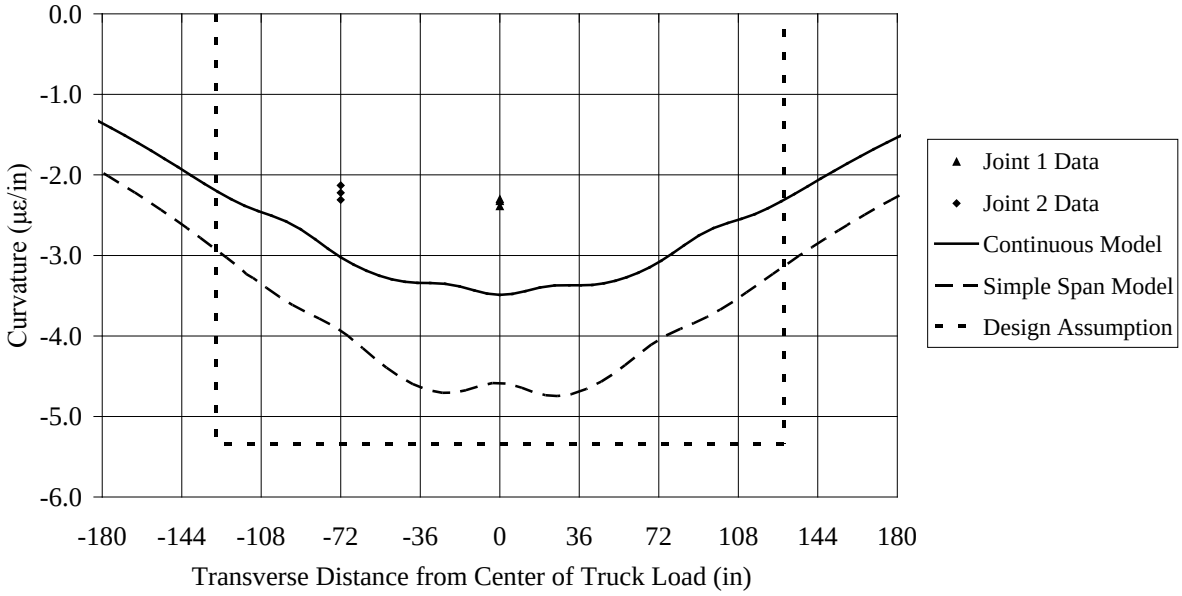

Figure 4.12: Curvatures at midspan due to two trucks at midspan of the center span

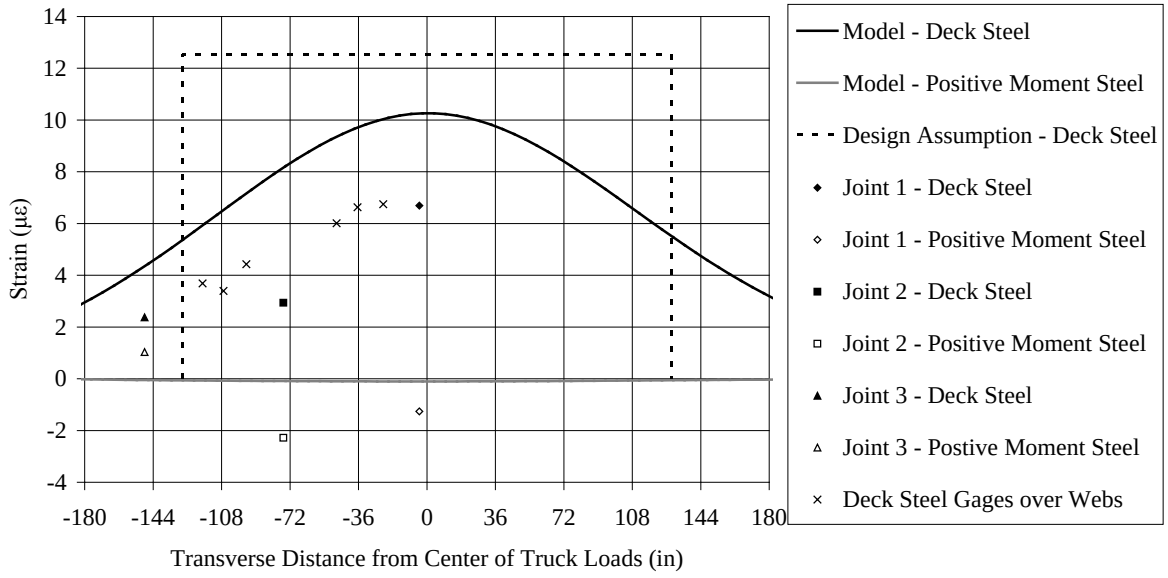

Figure 4.13: Strains near pier due to two trucks at midspan of the center span

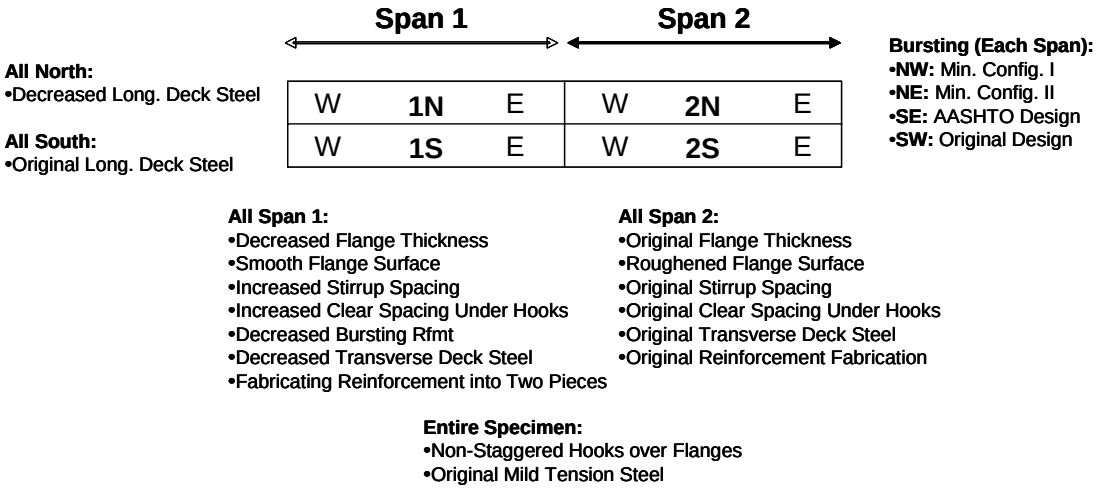

Figure 5.1: Conceptual layout of laboratory bridge specimen

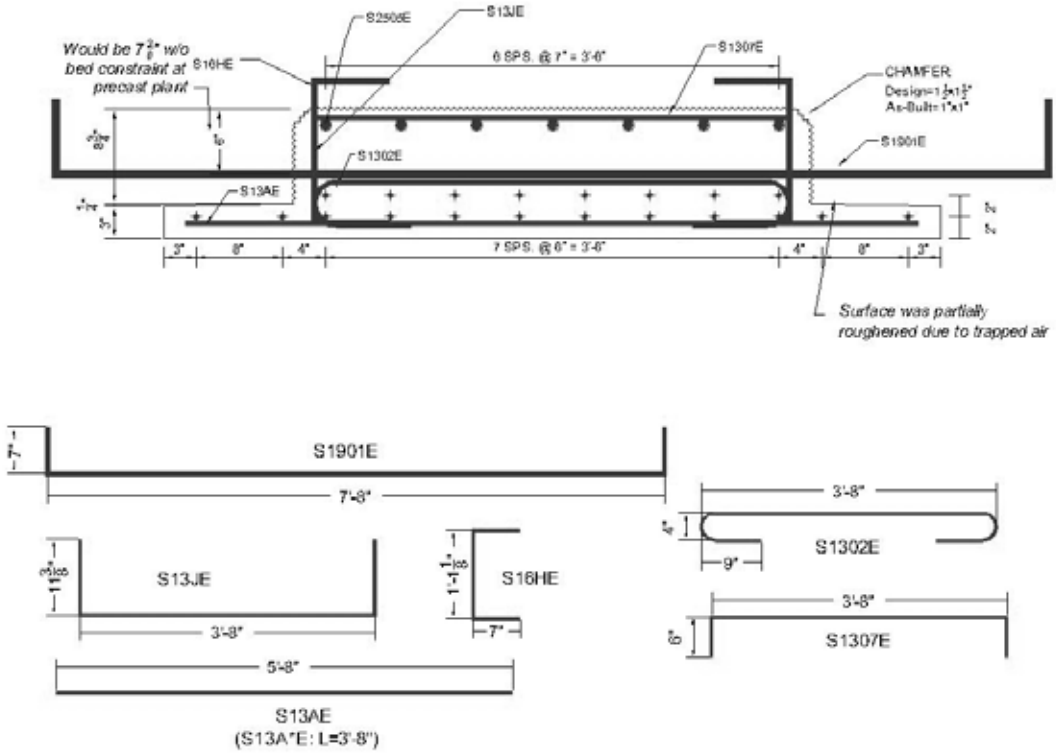

Figure 5.2: As-built cross section and reinforcement details for the east end of Beam 1N

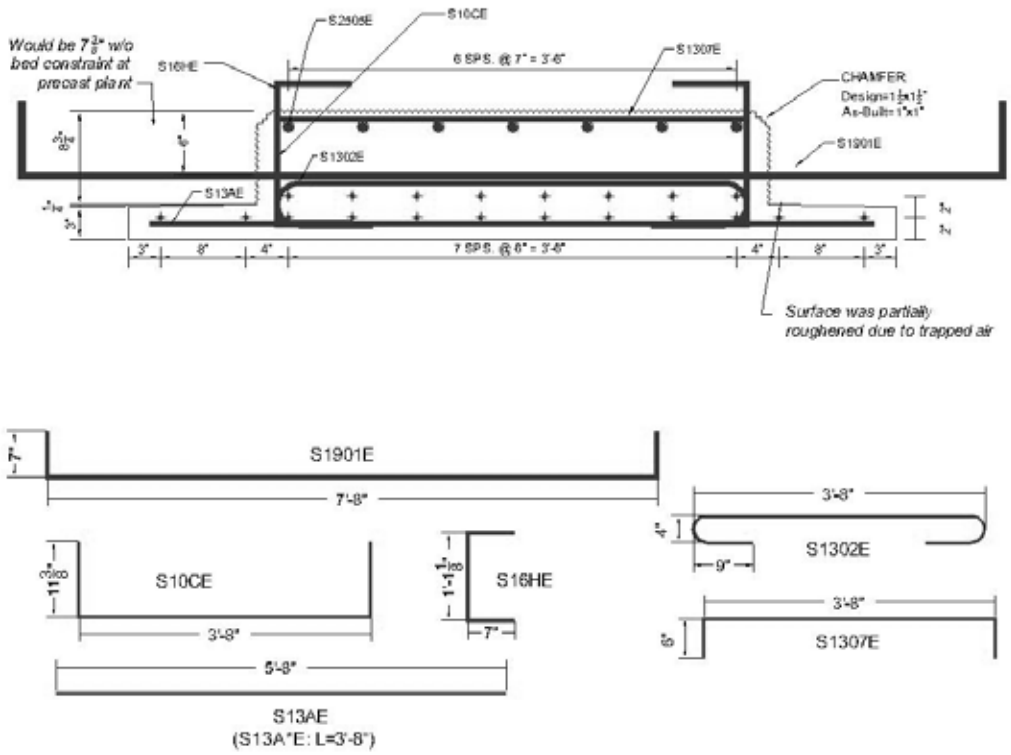

Figure 5.3: As-built cross section and reinforcement details for the west end of Beam 1N

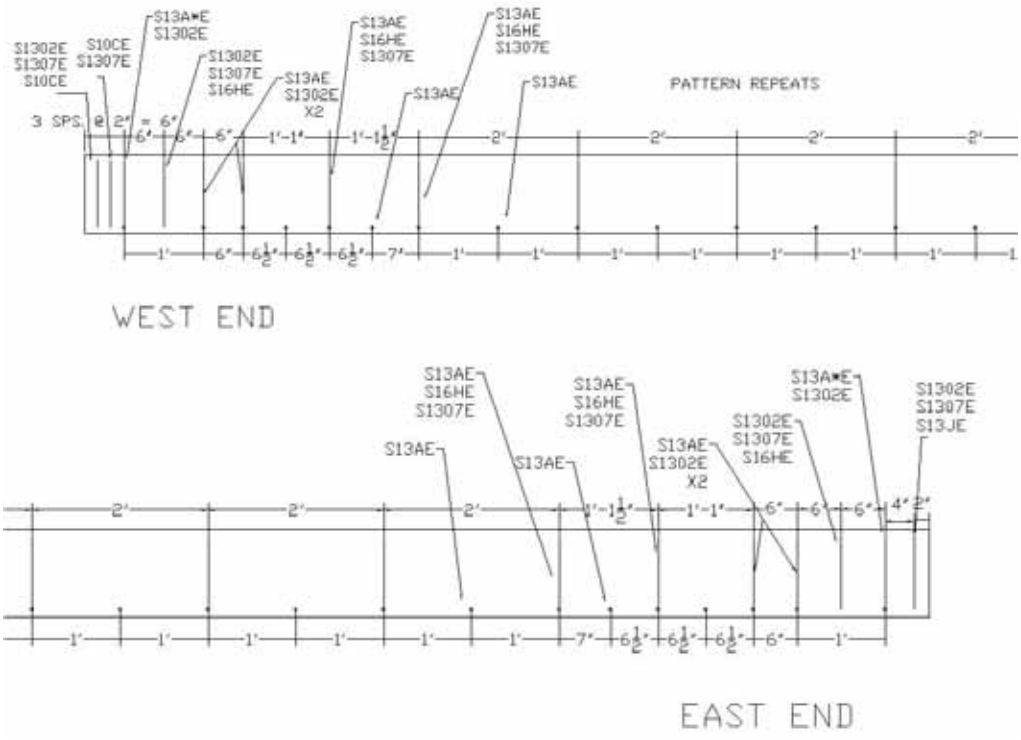

Figure 5.4: As-built reinforcement layout for Beam 1N (elevation view)

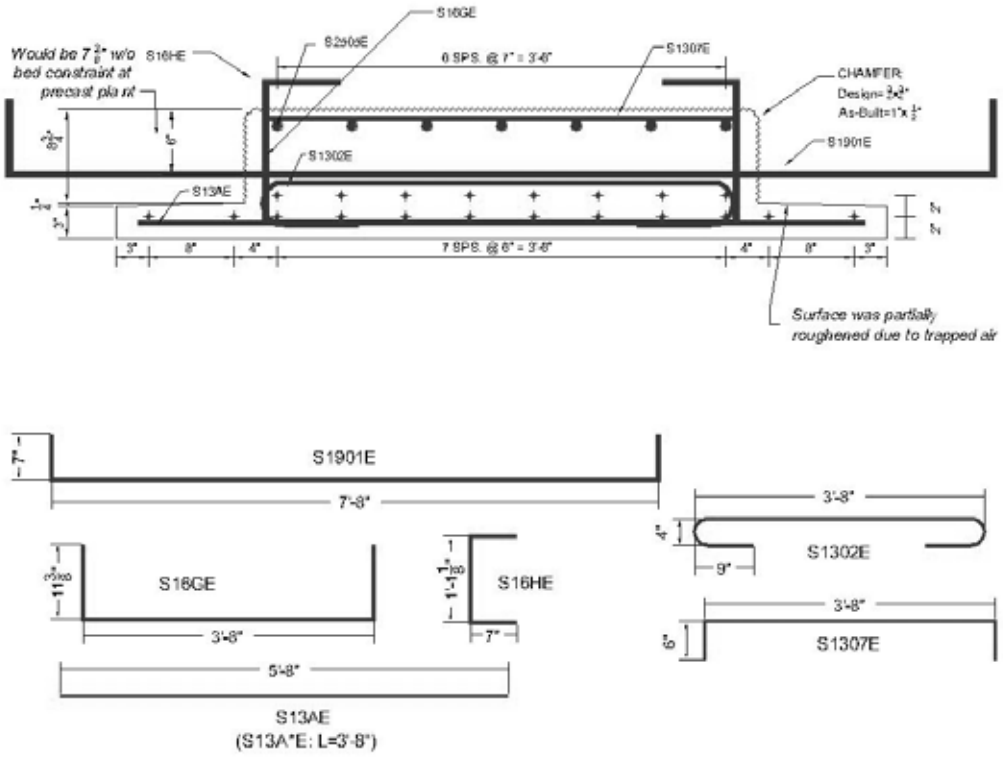

Figure 5.5: As-built cross section and reinforcement details for the east end of Beam 1S

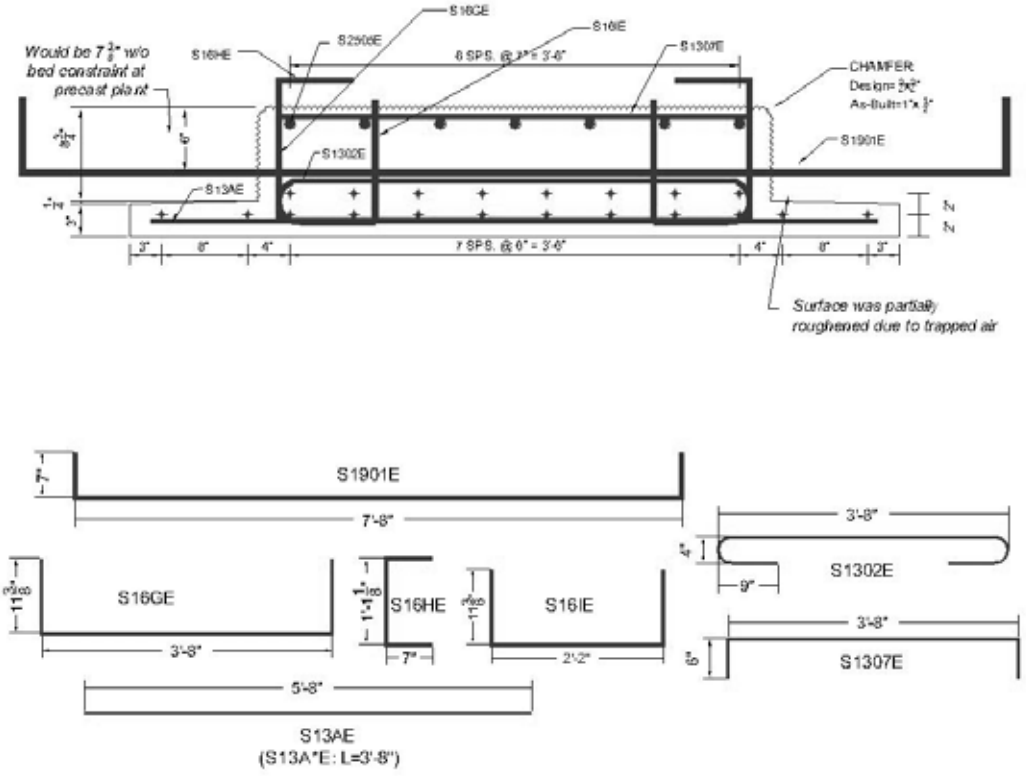

Figure 5.6: As-built cross section and reinforcement details of the west end Beam 1S

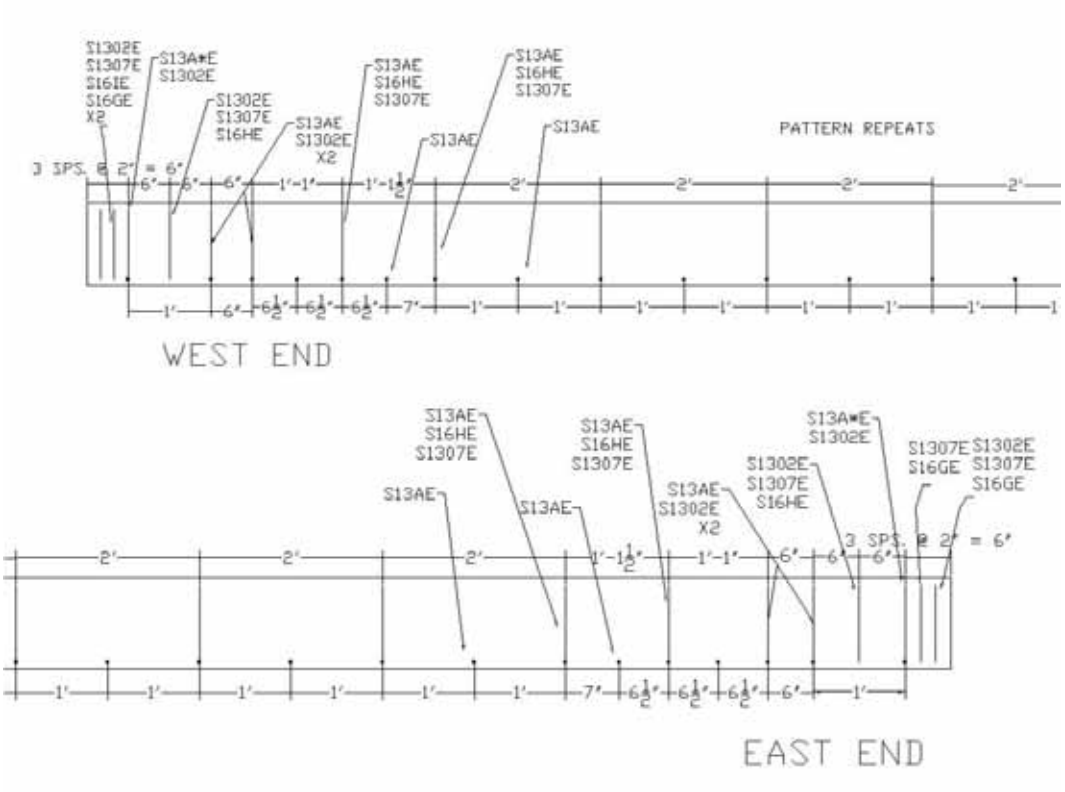

Figure 5.7: As-built reinforcement layout of Beam 1S (elevation view)

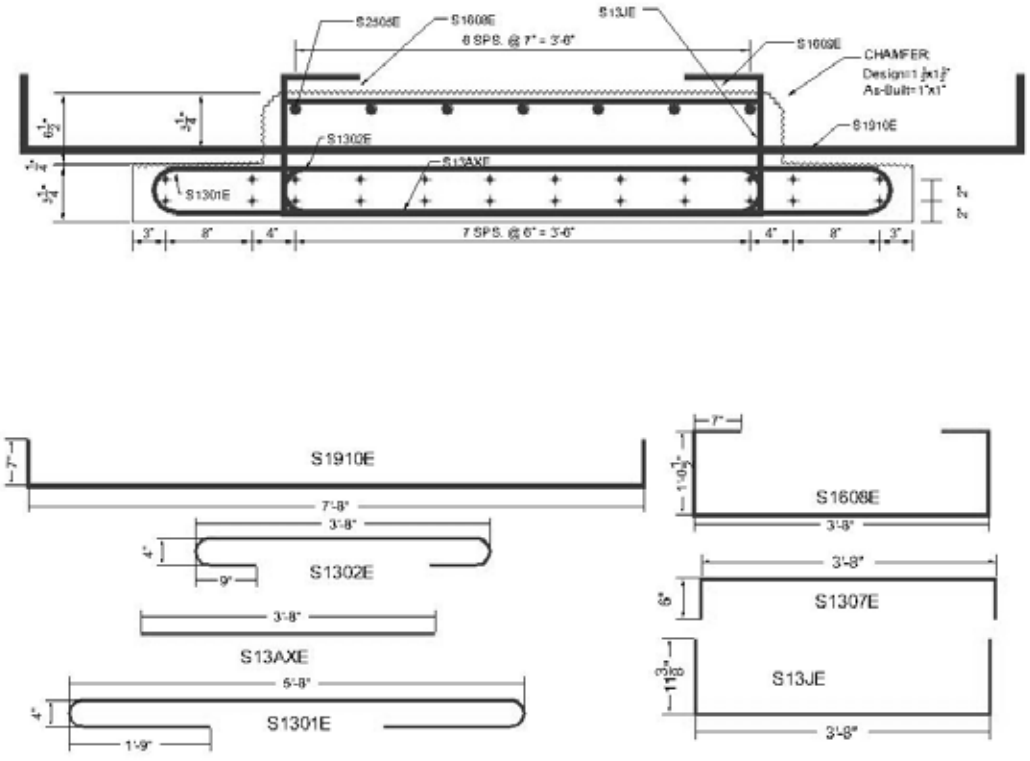

Figure 5.8: As-built cross section and reinforcement details for the east end of Beam 2N

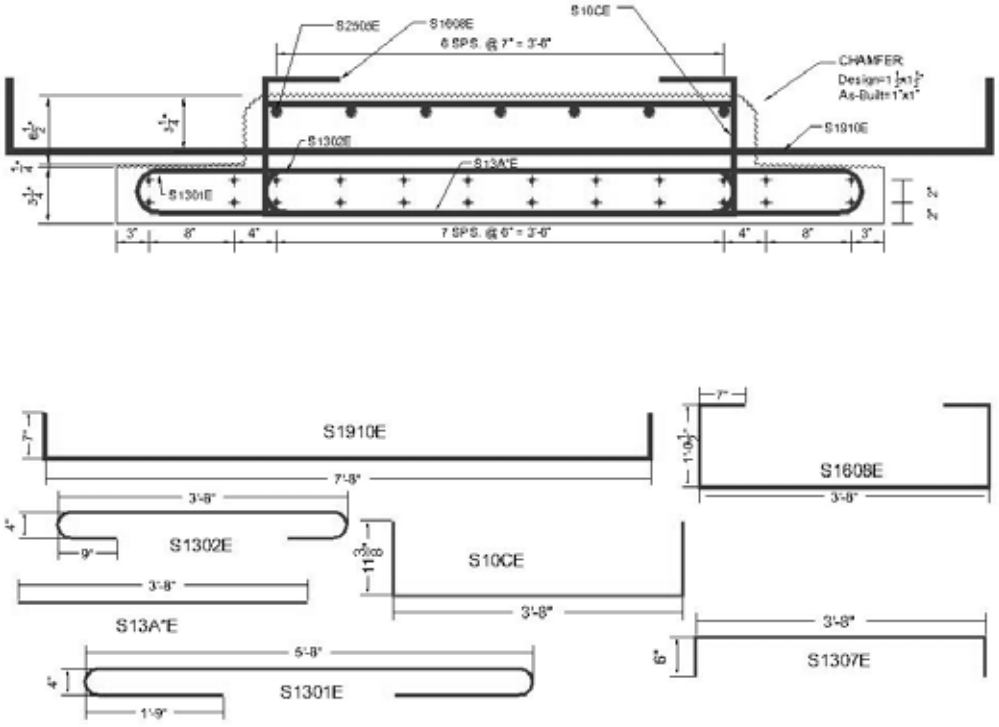

Figure 5.9: As-built cross section and reinforcement details for the west end of Beam 2N

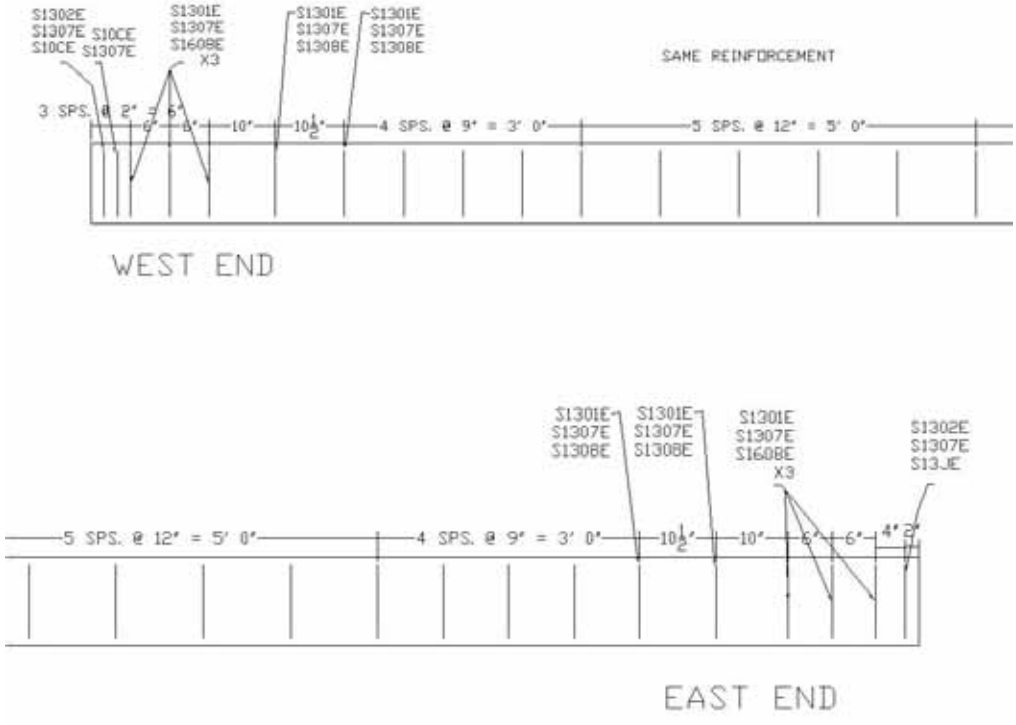

Figure 5.10: As-built reinforcement layout for Beam 2N (elevation view)

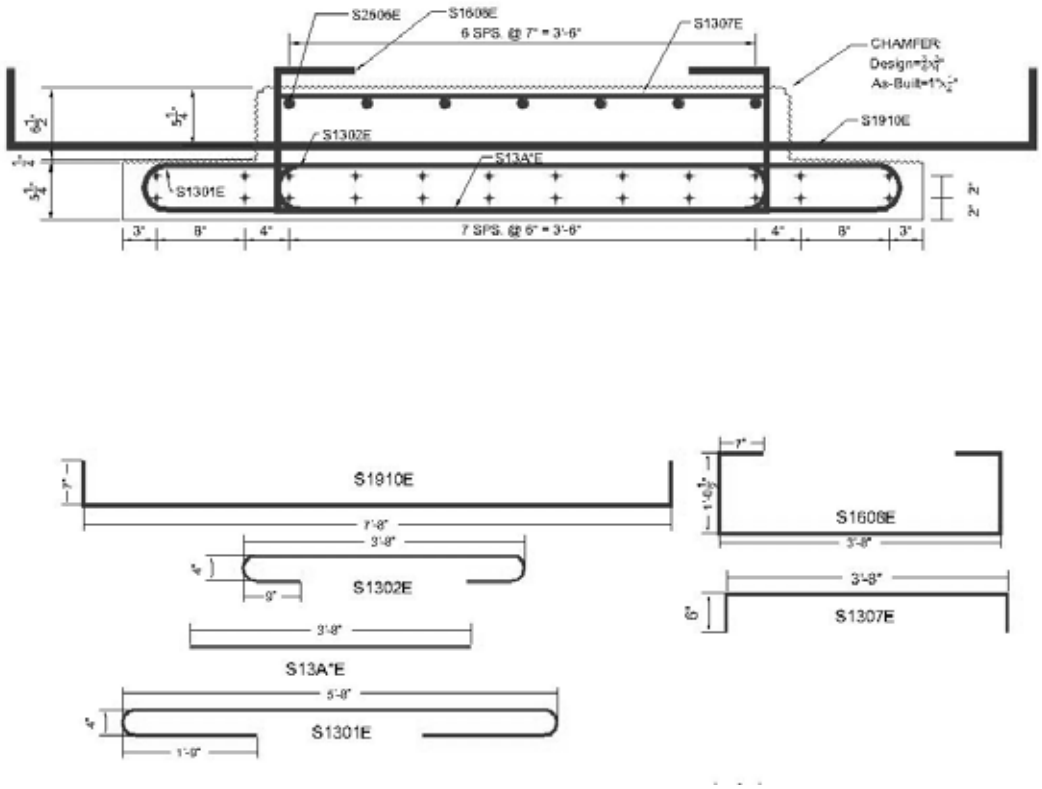

Figure 5.11: As-built cross section and reinforcement details for east end of Beam 2S

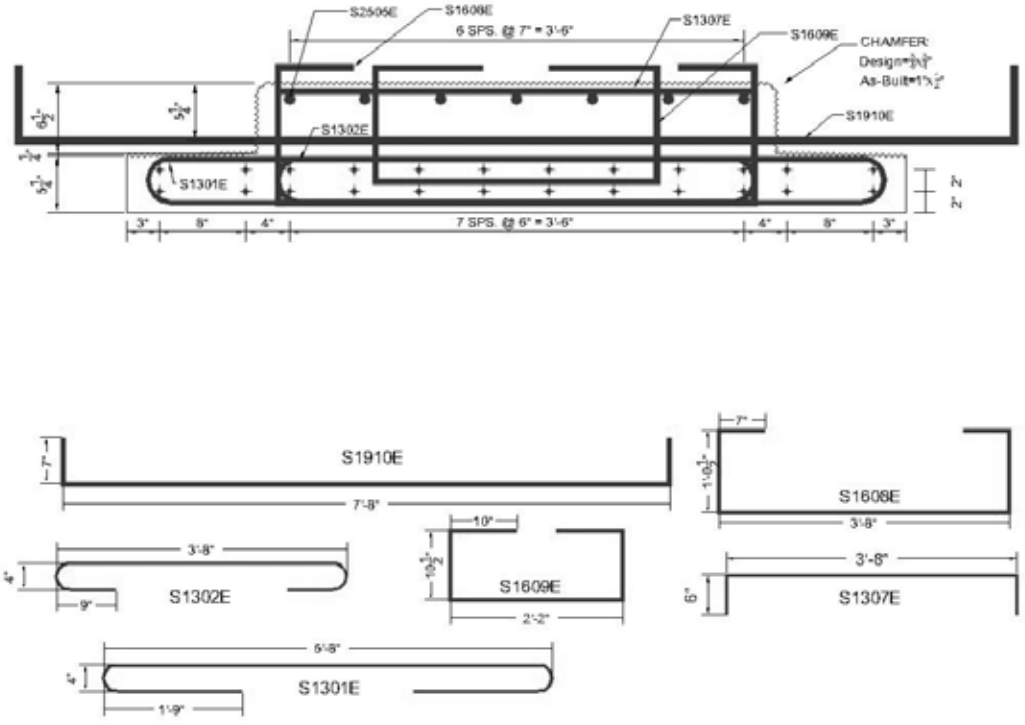

Figure 5 12: As-built cross section and reinforcement details for west end of Beam 2S

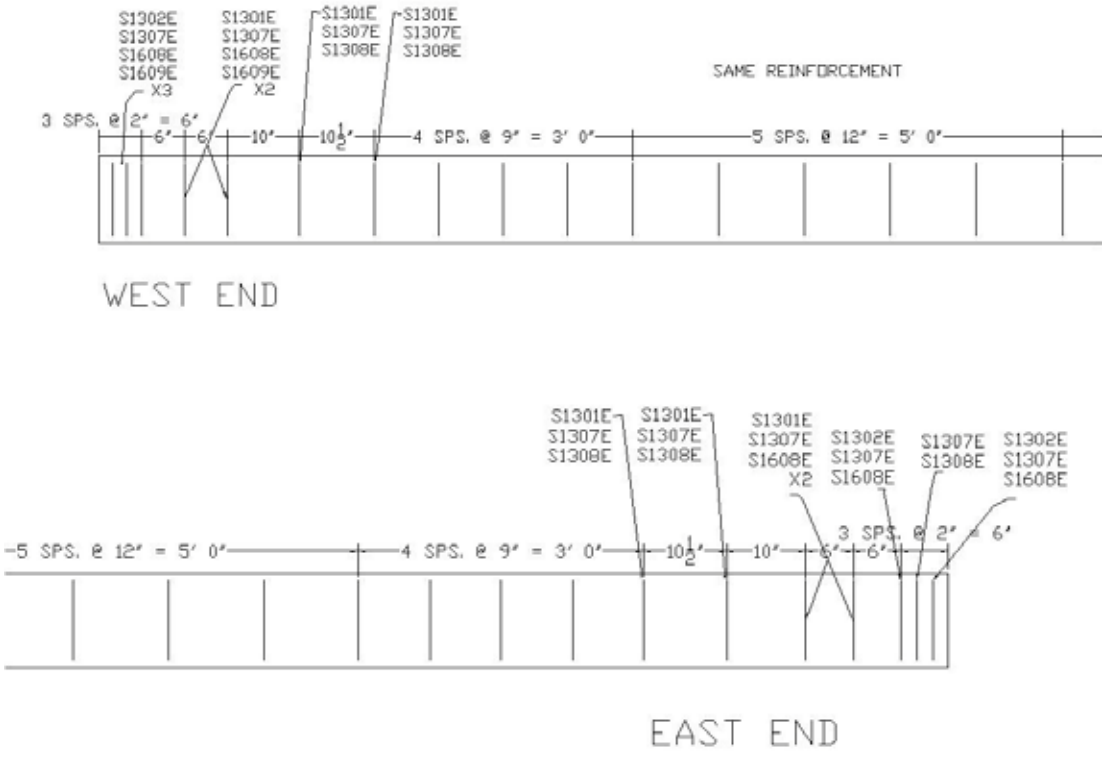

Figure 5.13: As-built reinforcement layout for Beam 2S (elevation view)

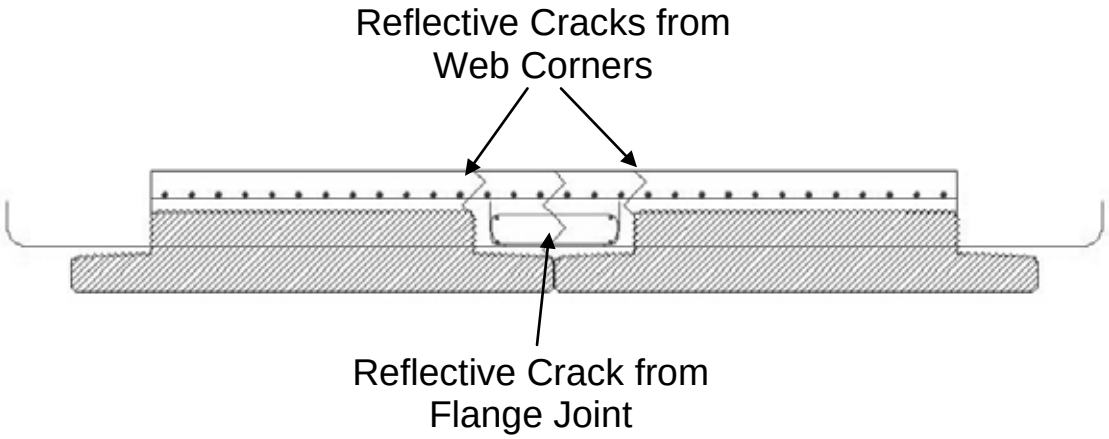

Figure 5.14: Predicted reflective cracking modes

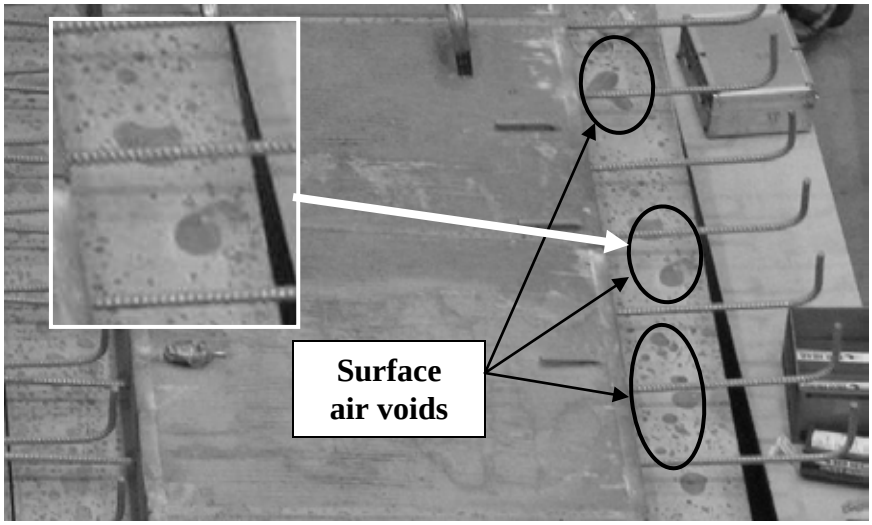

Figure 5.15: Unintentional roughness of flange surface due to shallow air voids

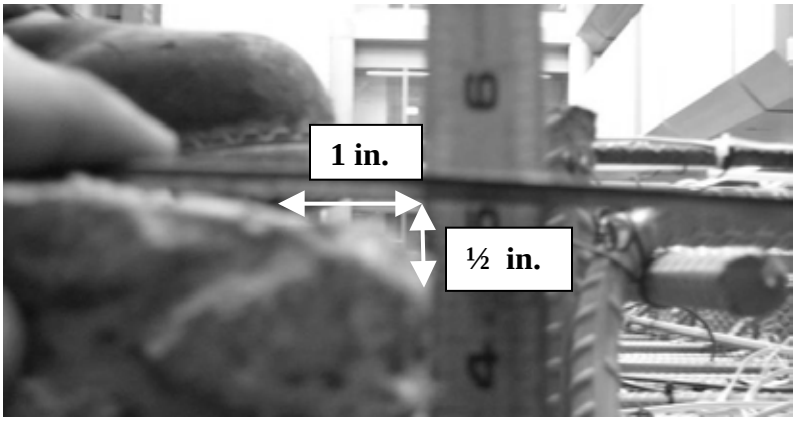

Figure 5.16: Chamfer fabricated in precast plant of 1 in. by ½ in.

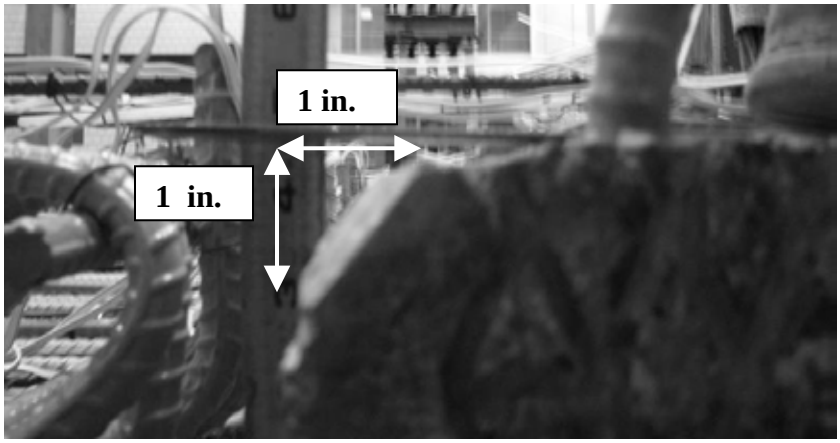

Figure 5.17: Modified 1 in. by 1 in. chamfer in north beams

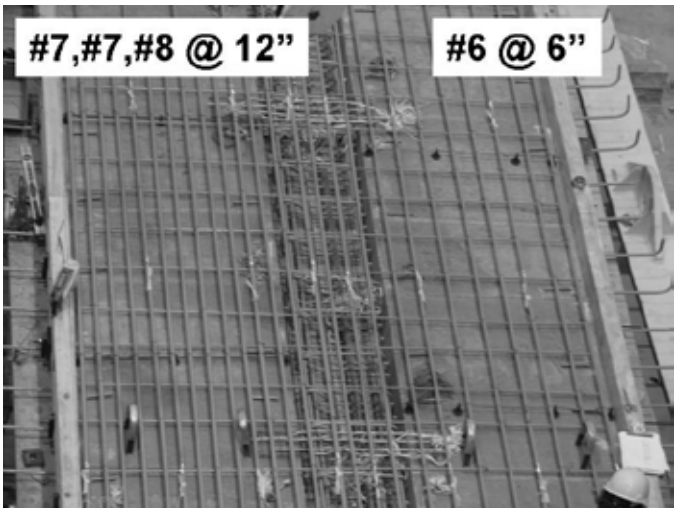

Figure 5.18: Longitudinal deck reinforcement in laboratory specimen (all longitudinal deck steel was continuous except for the #7 bars centered over the pier which were 26 ft. long)

Figure 5.19: Clear spacing under rebar hooks in Center City Bridge precast section

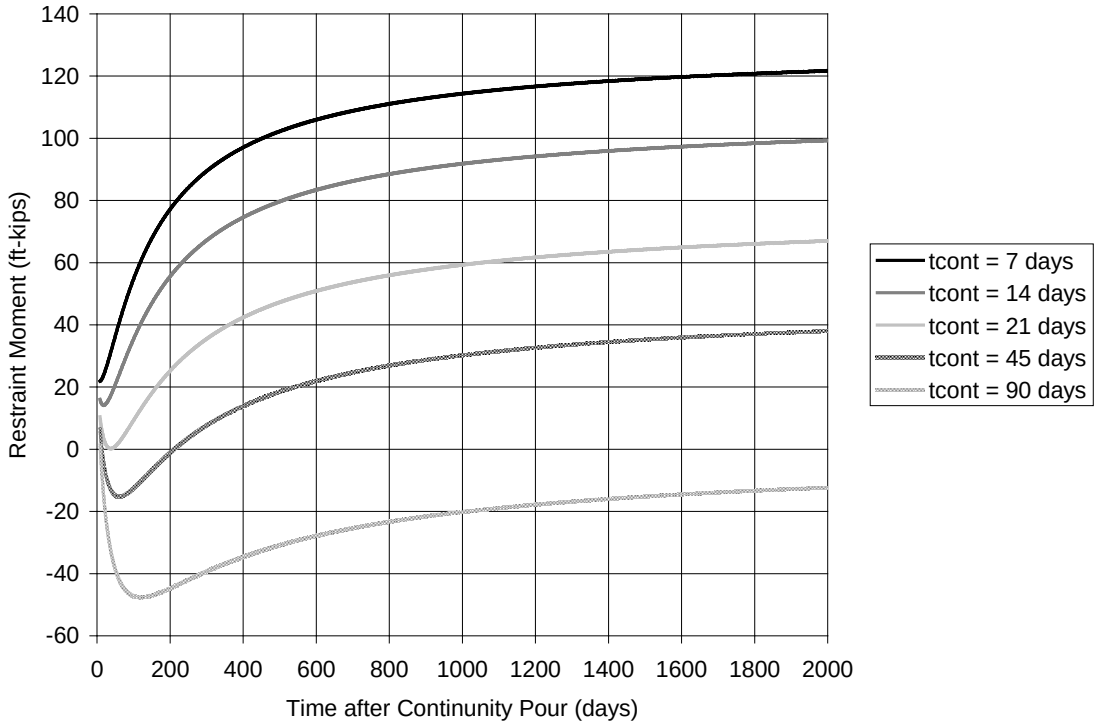

Figure 5.20: Restraint moment predictions for Center City Bridge with age of precast section at time of continuity varied

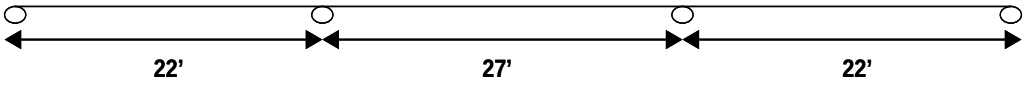

Figure 5.21: Center City Bridge modeling assumptions for PCA method

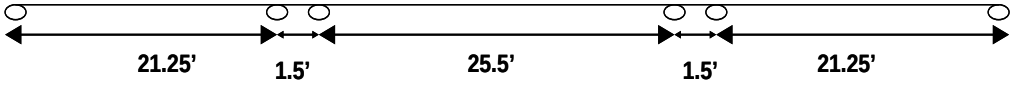

Figure 5.22: Center City Bridge modeling assumptions for P-method

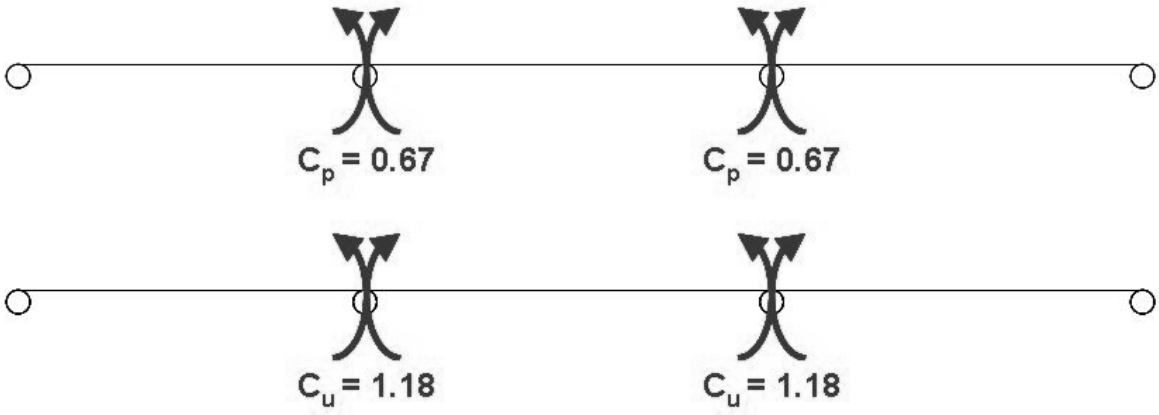

Figure 5.23: Moment coefficients for Center City Bridge using PCA method

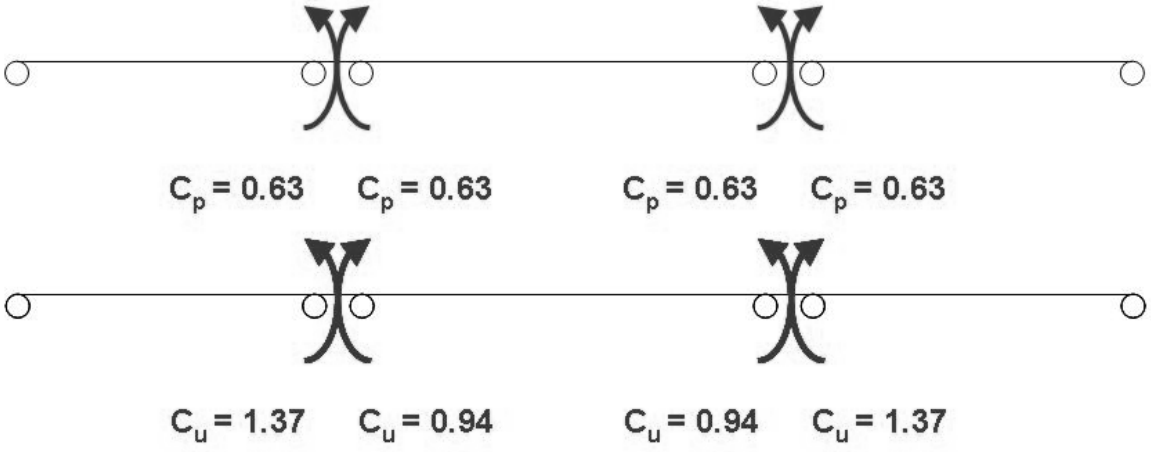

Figure 5.24: Moment coefficients for Center City Bridge using P-method

Figure 5.25: Rebar congestion at end of Center City Bridge precast section

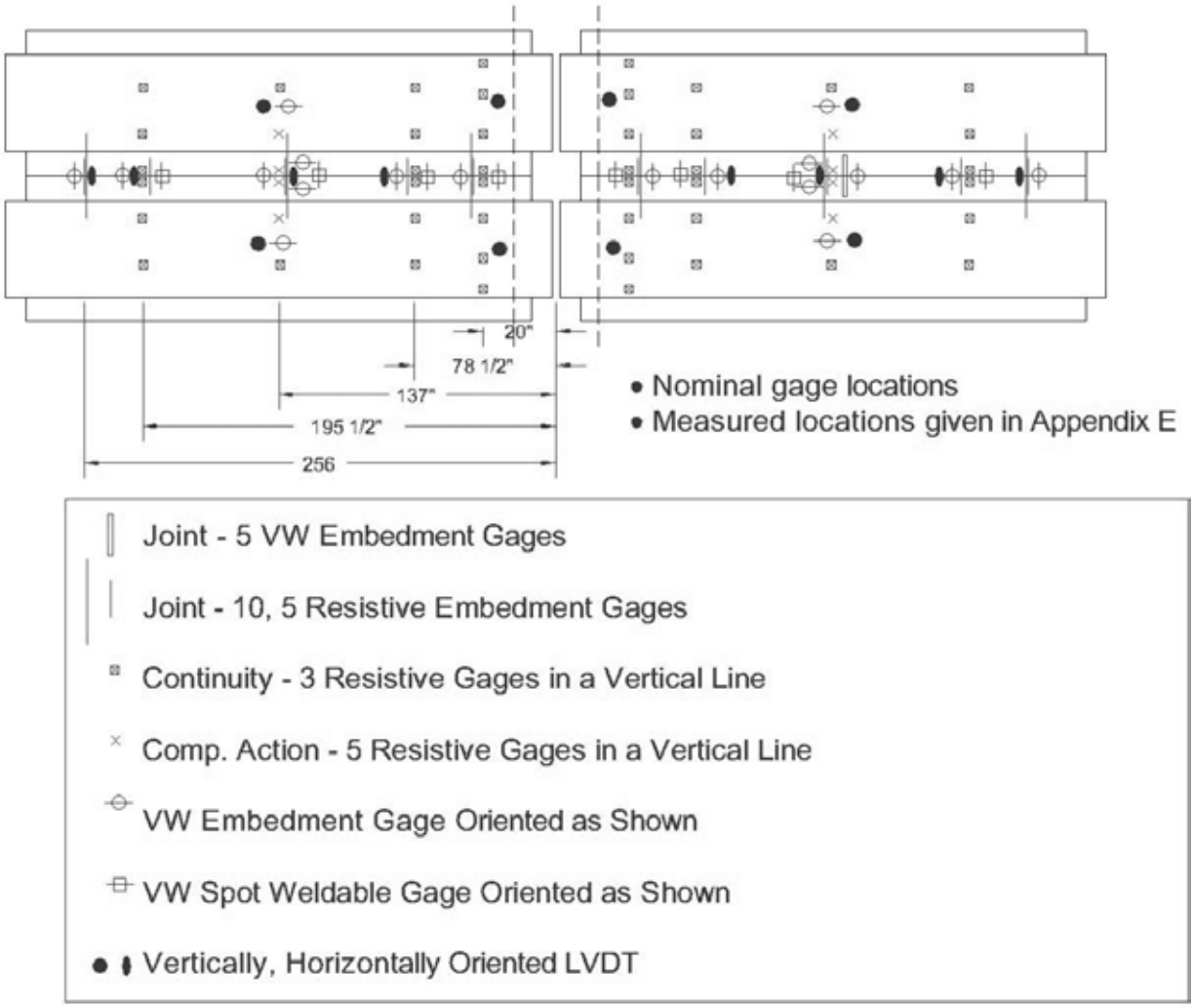

Figure 6.1: General layout of laboratory specimen instrumentation

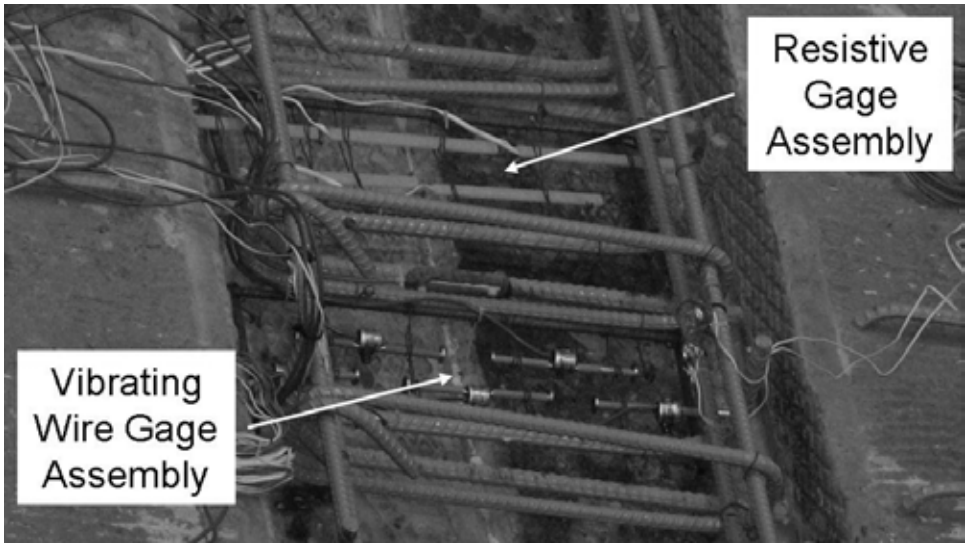

Figure 6.2: Five gage assemblies immediately above flange joint

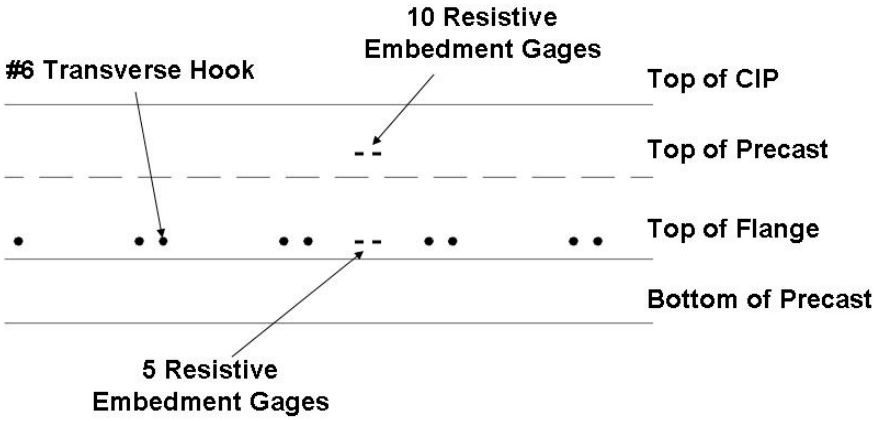

Figure 6.3: Elevation view of transverse instrumentation

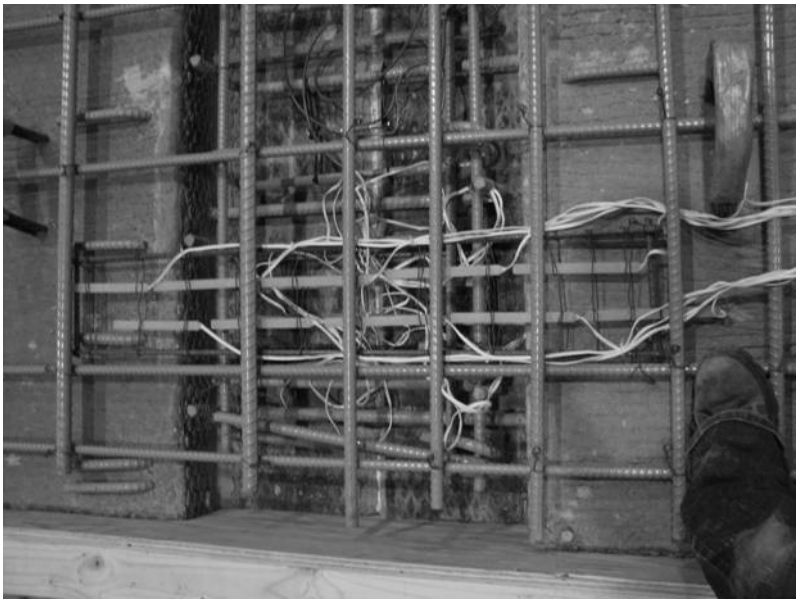

Figure 6.4: Ten gage resistive gage assemblies above web corners

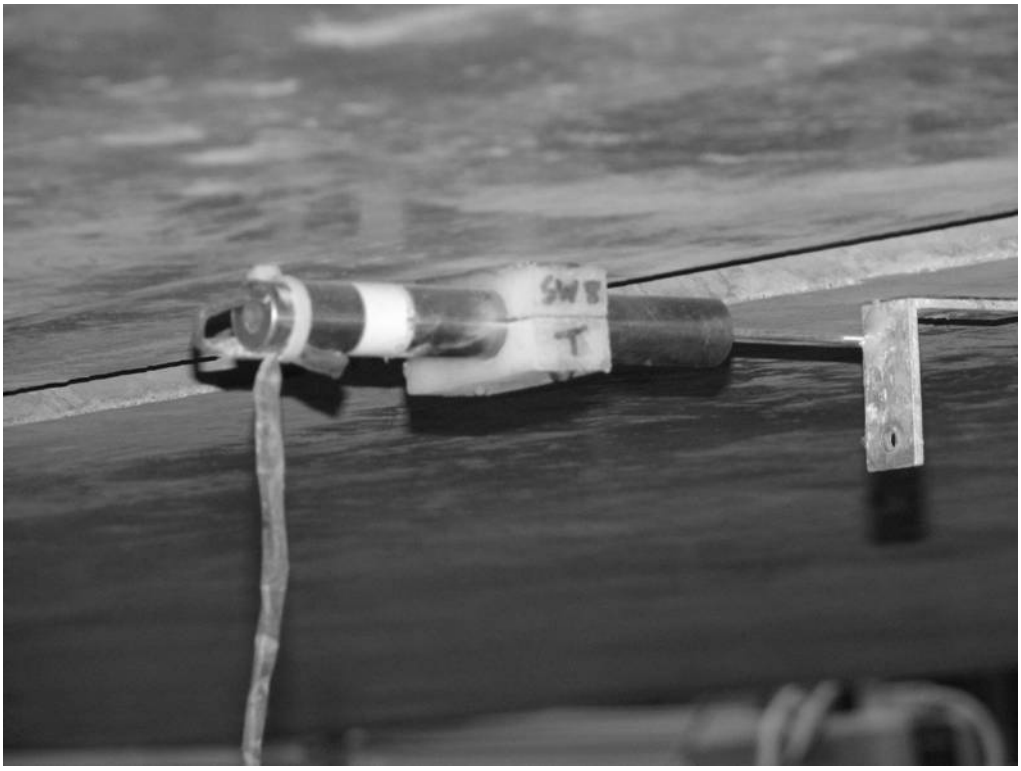

Figure 6.5: Transverse LVDT attachment to underside of laboratory specimen

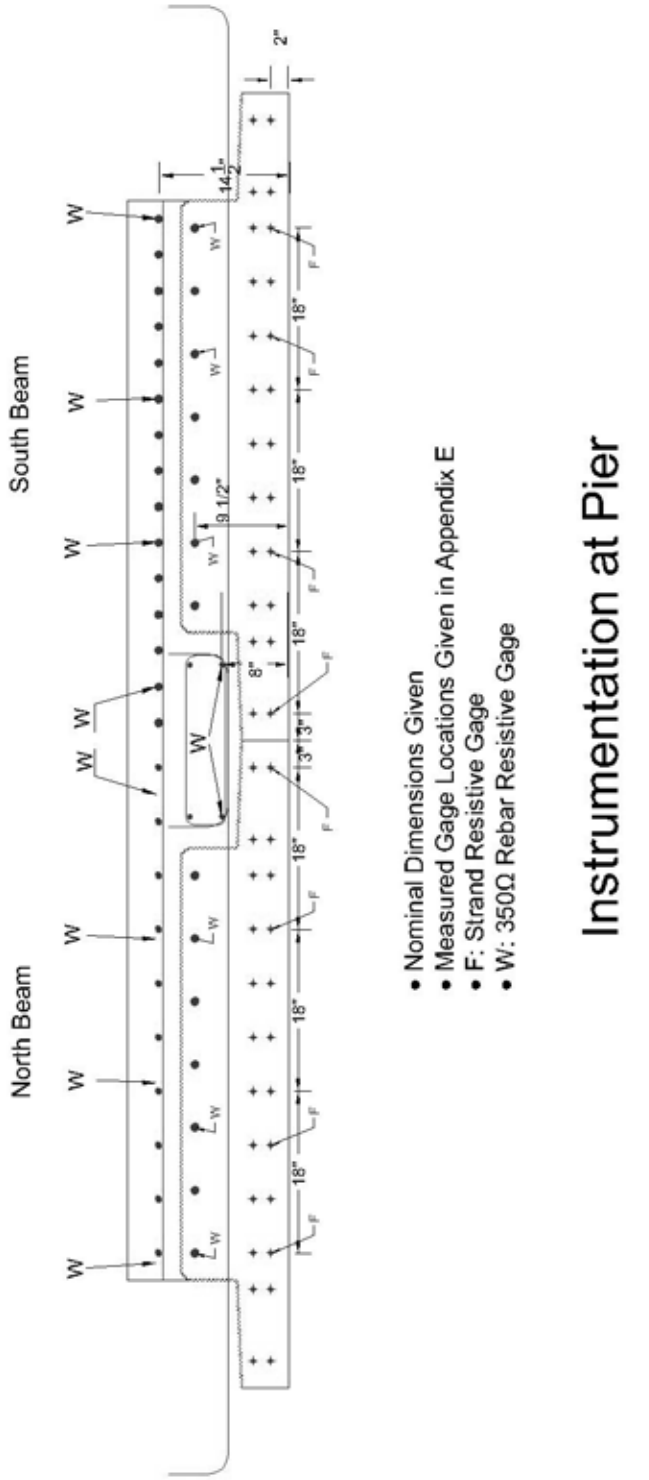

Figure 6.6: Longitudinal instrumentation layout within the cross section near the pier

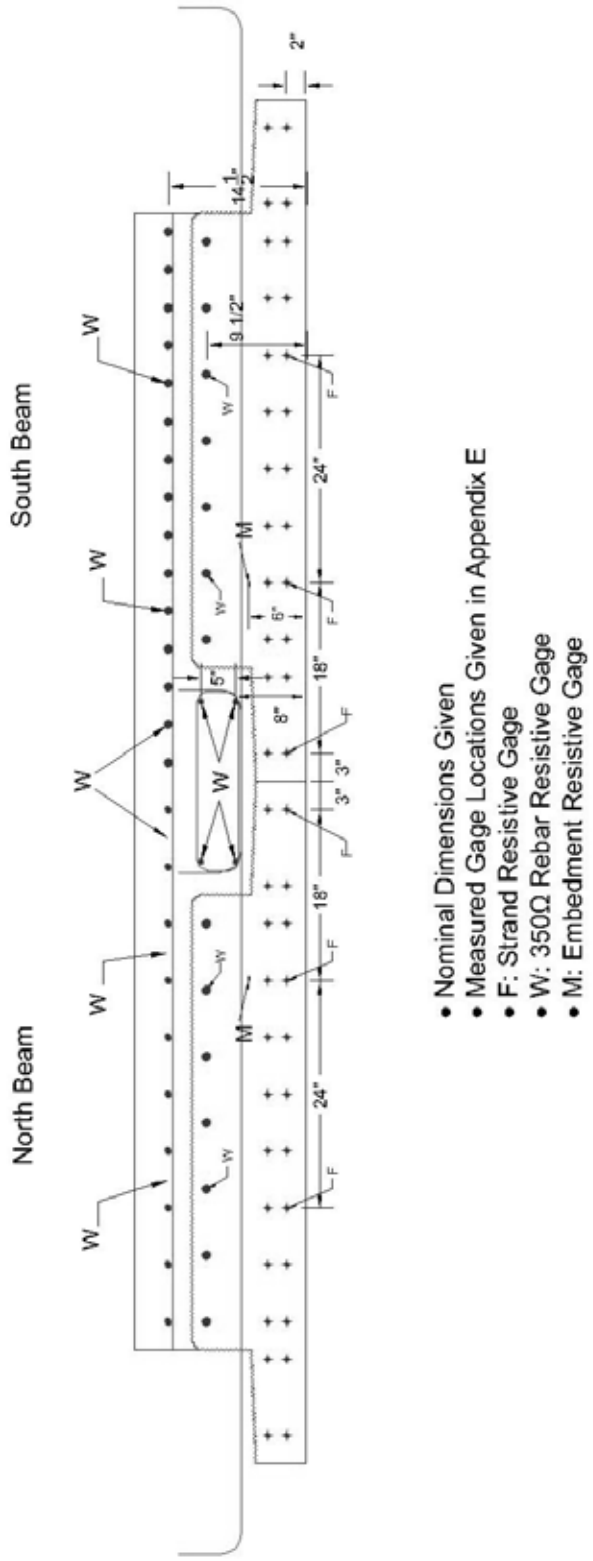

Figure 6.7: Longitudinal instrumentation layout within the cross section at midspan

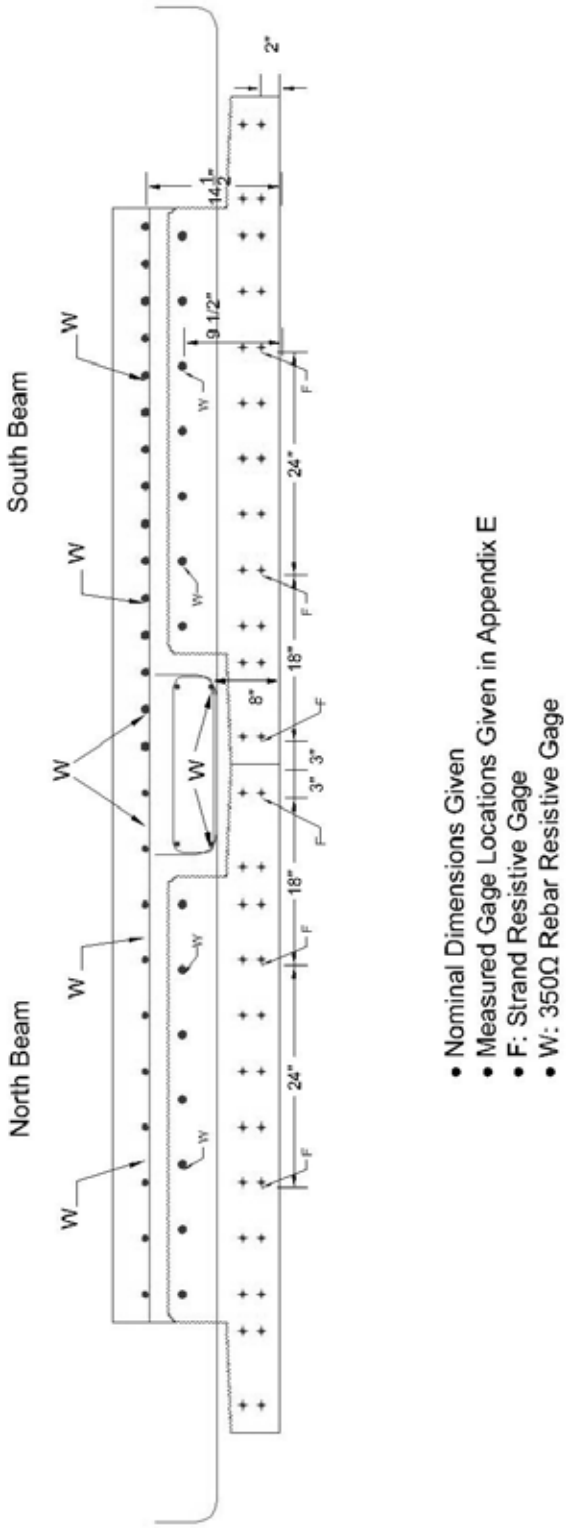

Figure 6.8: Longitudinal instrumentation layout within the cross section at quarter spans

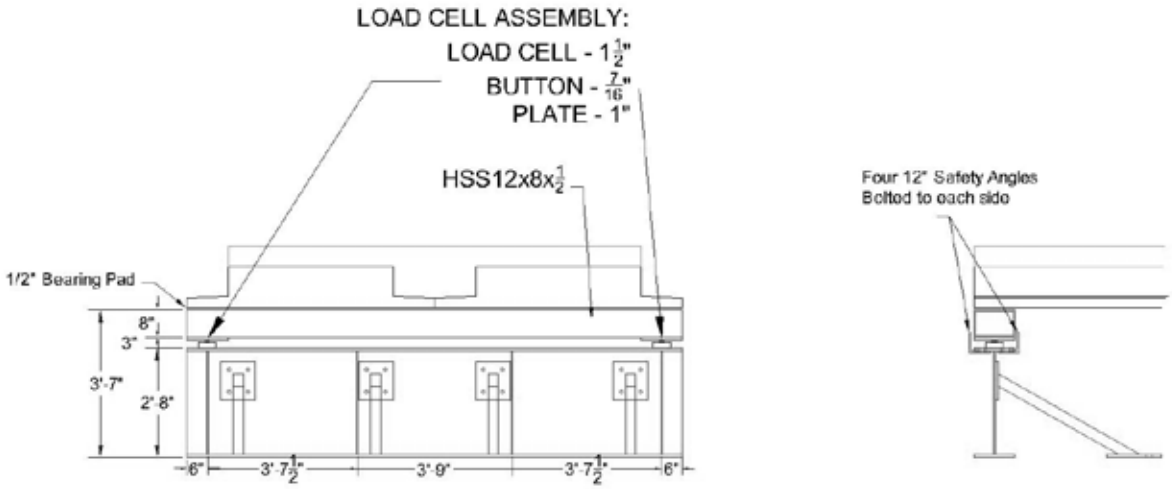

Figure 6.9: End reaction design with embedded load cells

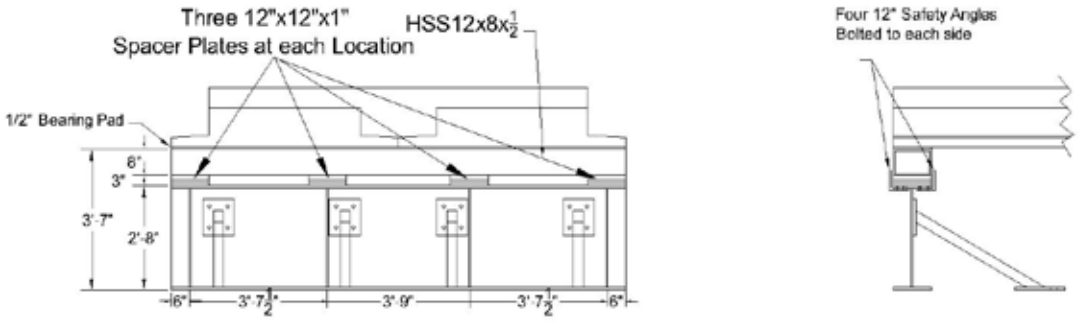

Figure 6.10: End reaction design with spacer plates

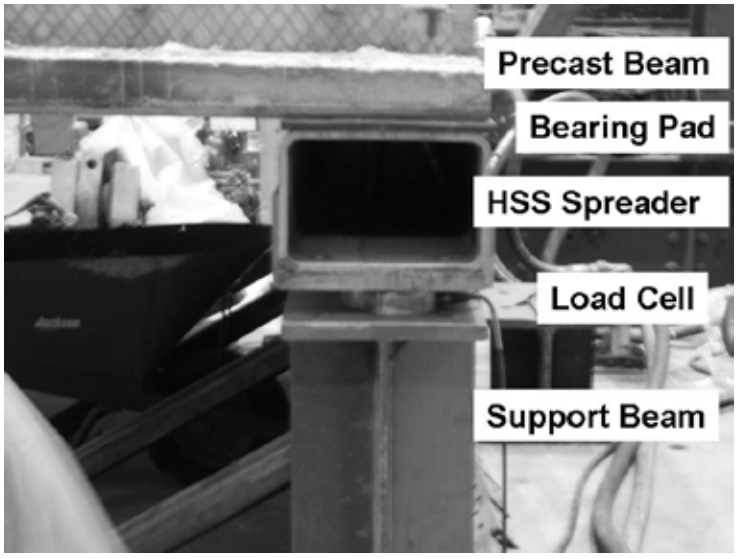

Figure 6.11: Picture of the end reaction with embedded load cell

Figure 6.12: Resistive strand gages for measurement of initial prestress force

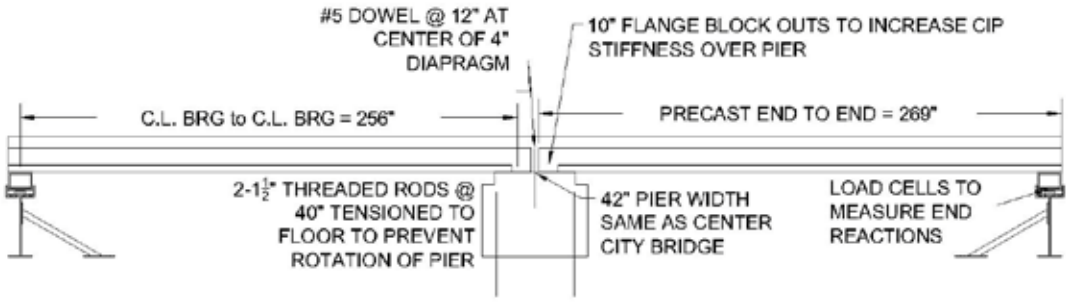

Figure 7.1: Elevation of laboratory bridge specimen

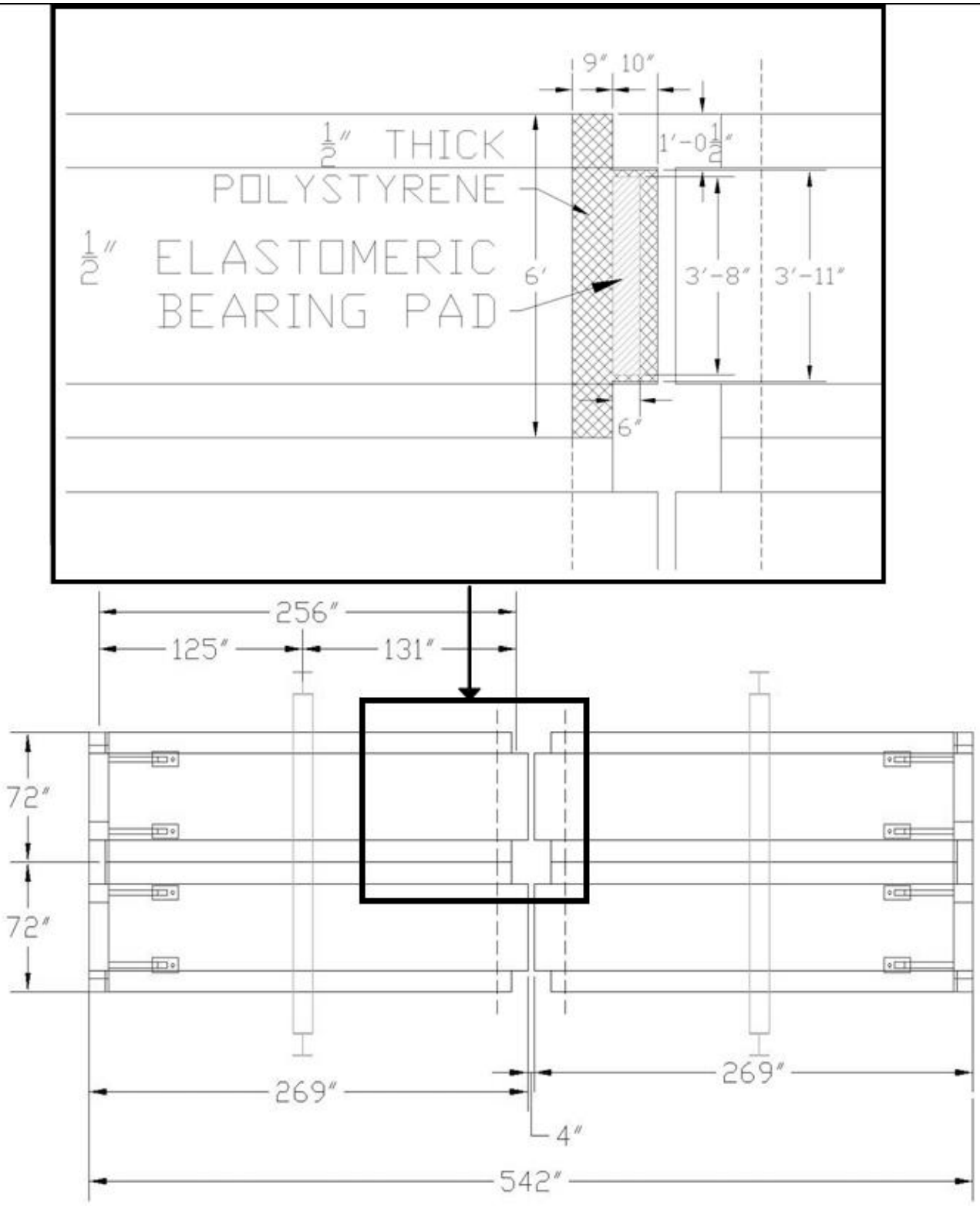

Figure 7.2: Plan layout of laboratory bridge specimen with enlargement of precast support at pier

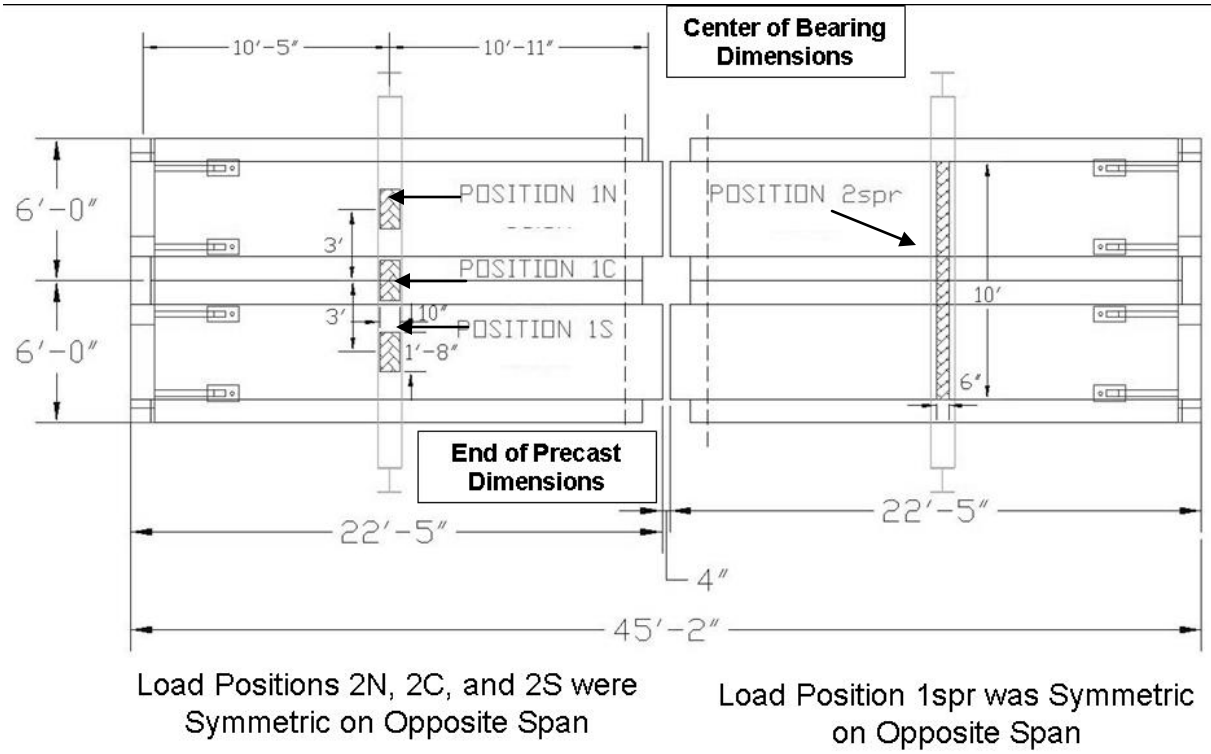

Figure 7.3: Test position layout for the laboratory bridge specimen

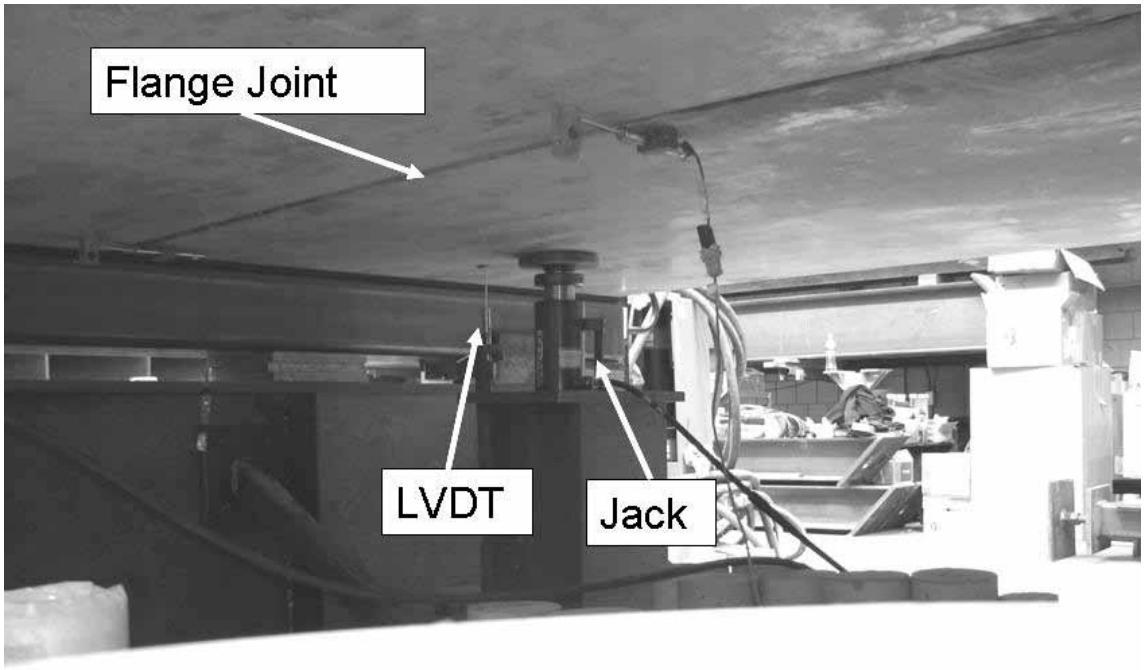

Figure 7.4: Position of jack during removal of load cells

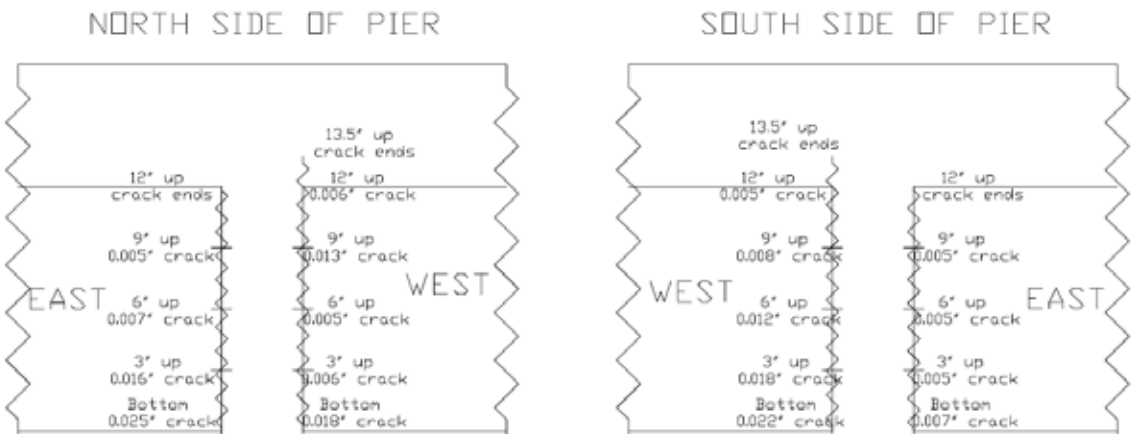

Figure 7.5: Cracking at pier observed during west load cell removal

Figure 7.6: Cracking at pier observed during east load cell removal

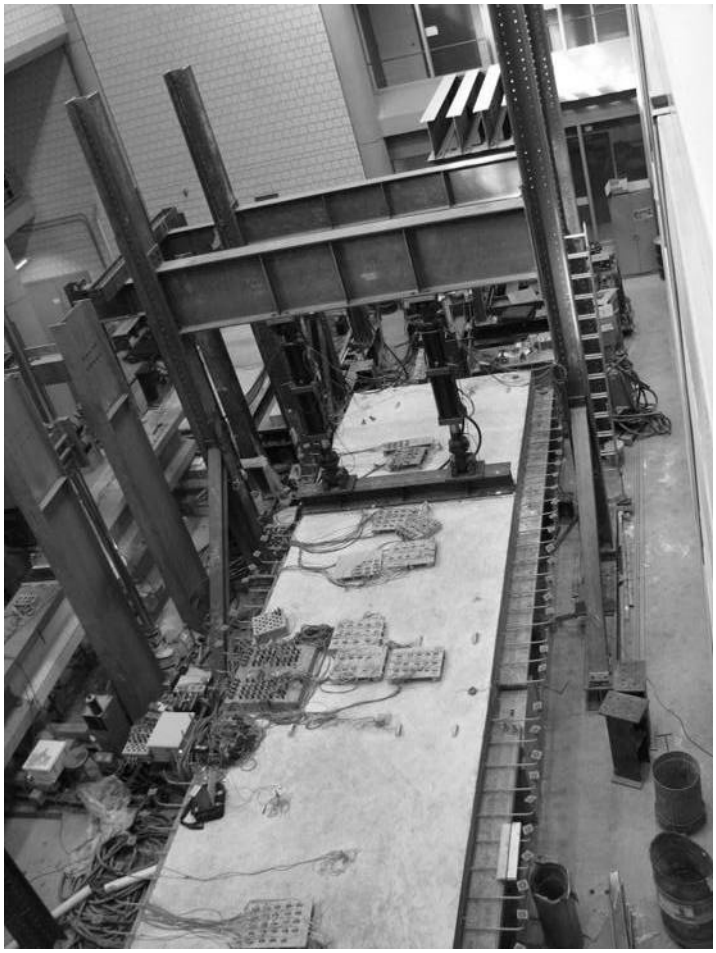

Figure 7.7: Laboratory bridge specimen during spreader beam test of Span 1

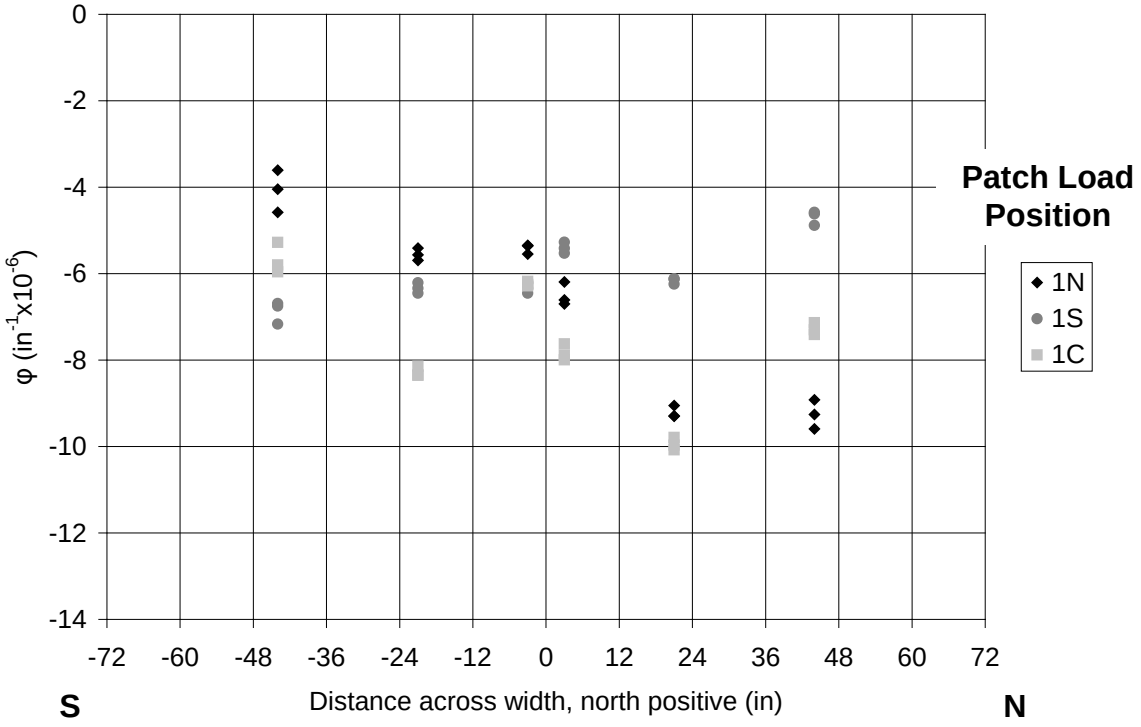

Figure 7.8: Curvatures across width at midspan of Span 1 under Span 1 patch loads

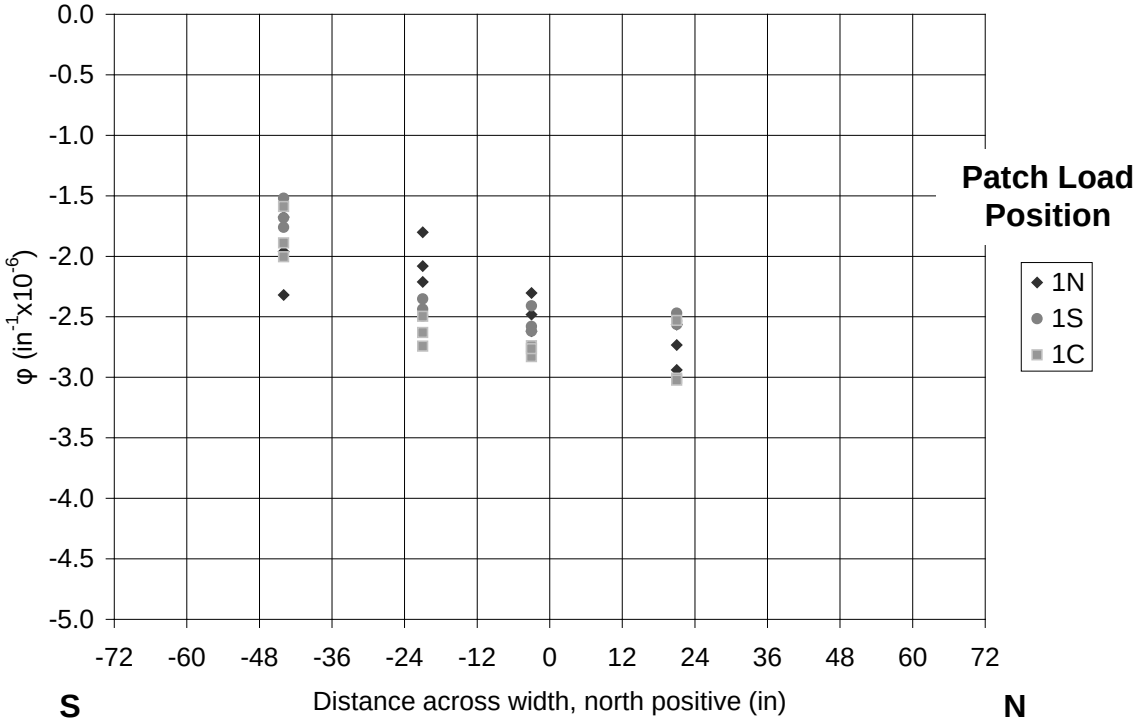

Figure 7.9: Curvatures across width at inner quarter span of Span 1 under Span 1 patch loads

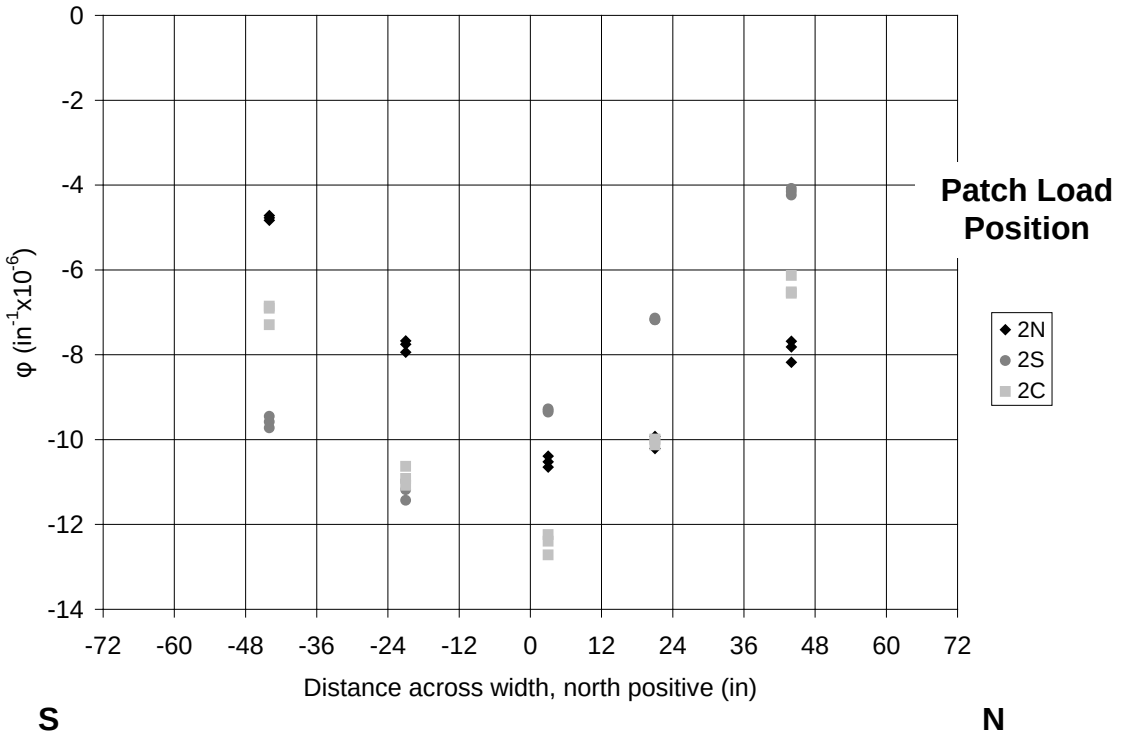

Figure 7.10: Curvatures across width at midspan of Span 2 under Span 2 patch loads

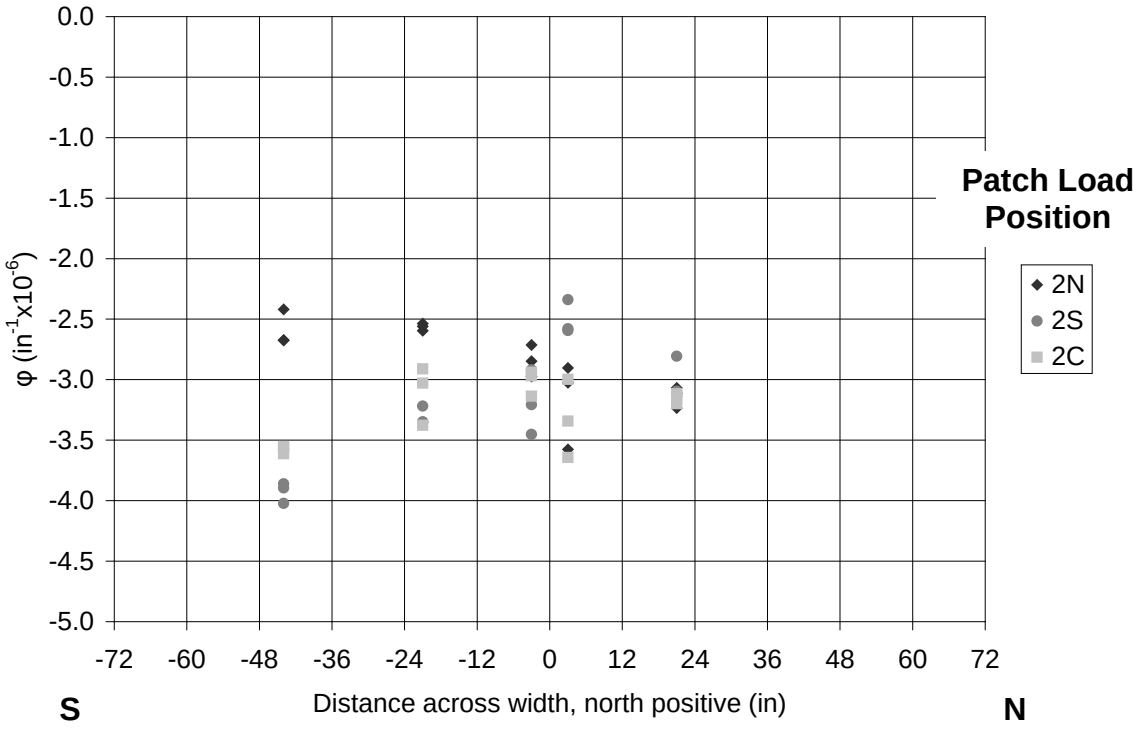

Figure 7.11: Curvatures across width at inner quarter span of Span 2 under Span 2 patch loads

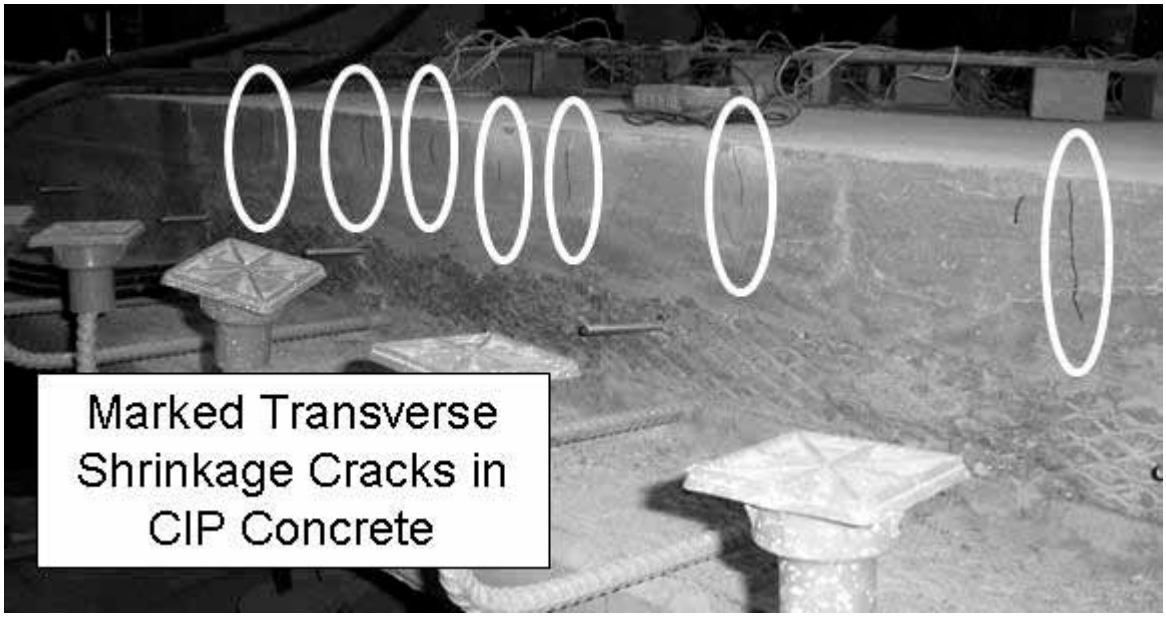

Figure 7.12: Photograph of marked shrinkage cracks in CIP of laboratory specimen

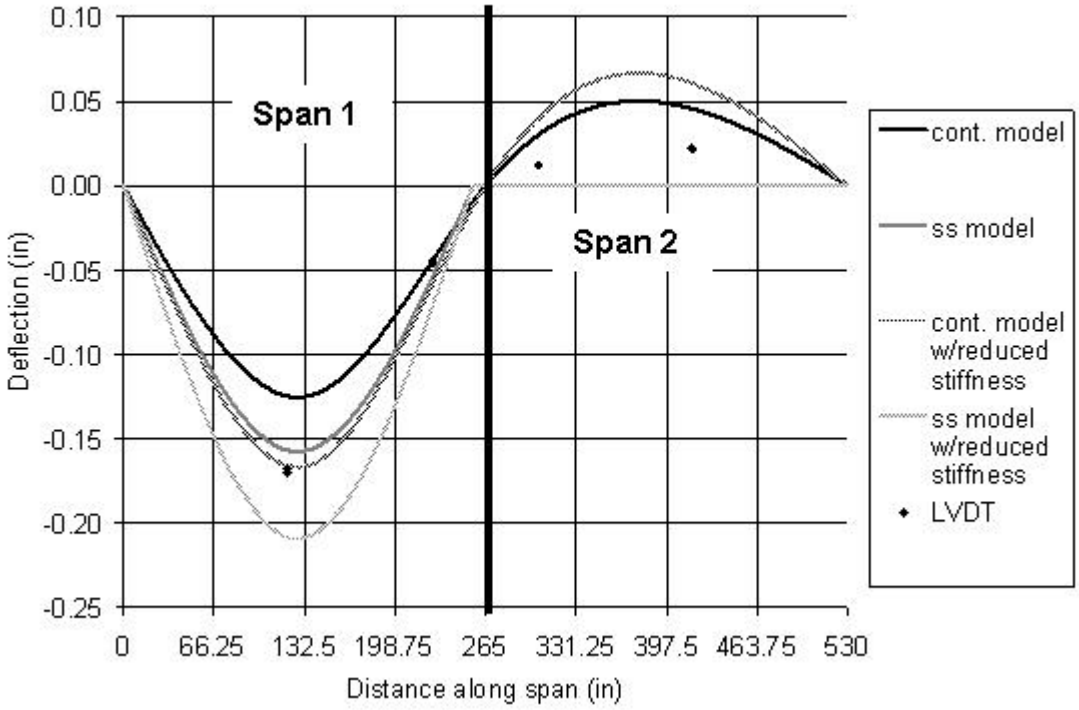

Figure 7.13: Deflections along bridge during spreader load at midspan of Span 1

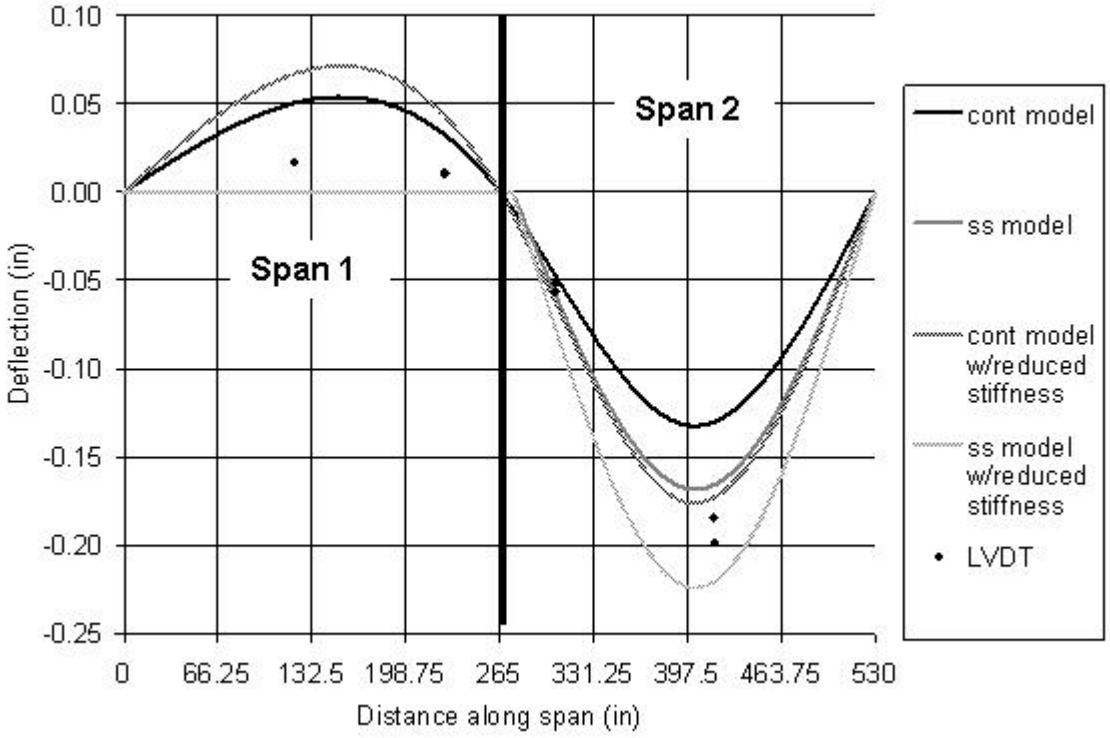

Figure 7.14: Deflections along bridge during spreader load at midspan of Span 2

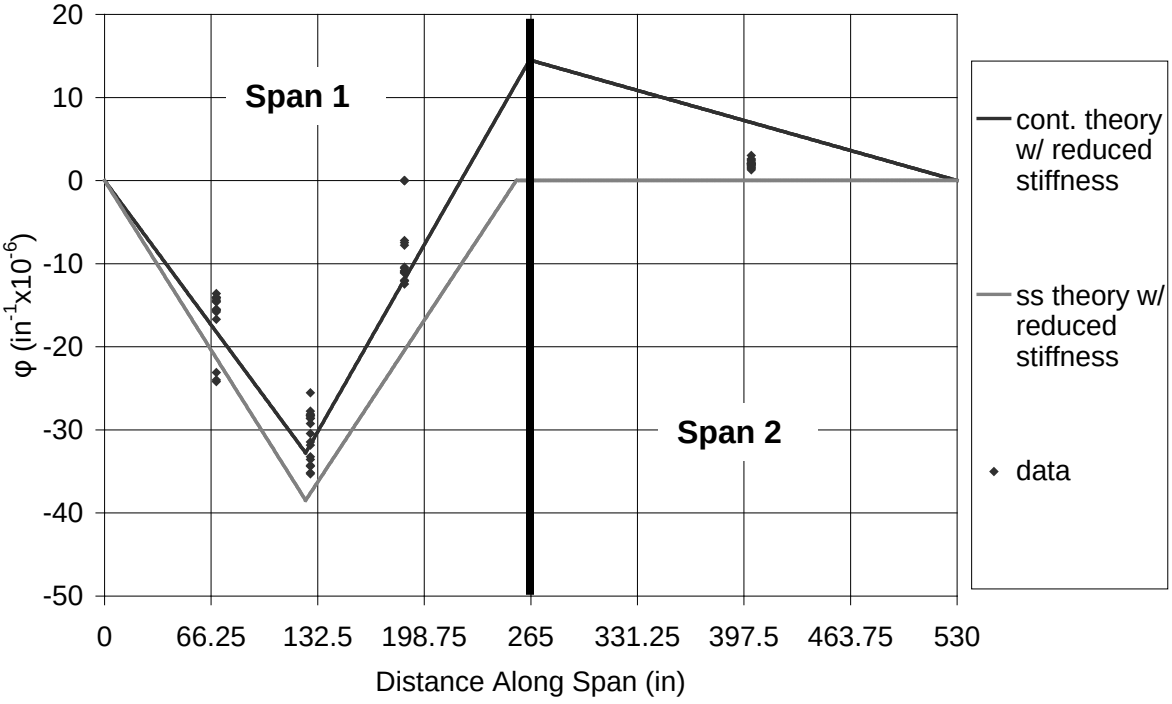

Figure 7.15: Curvatures along bridge during spreader load at midspan of Span 1

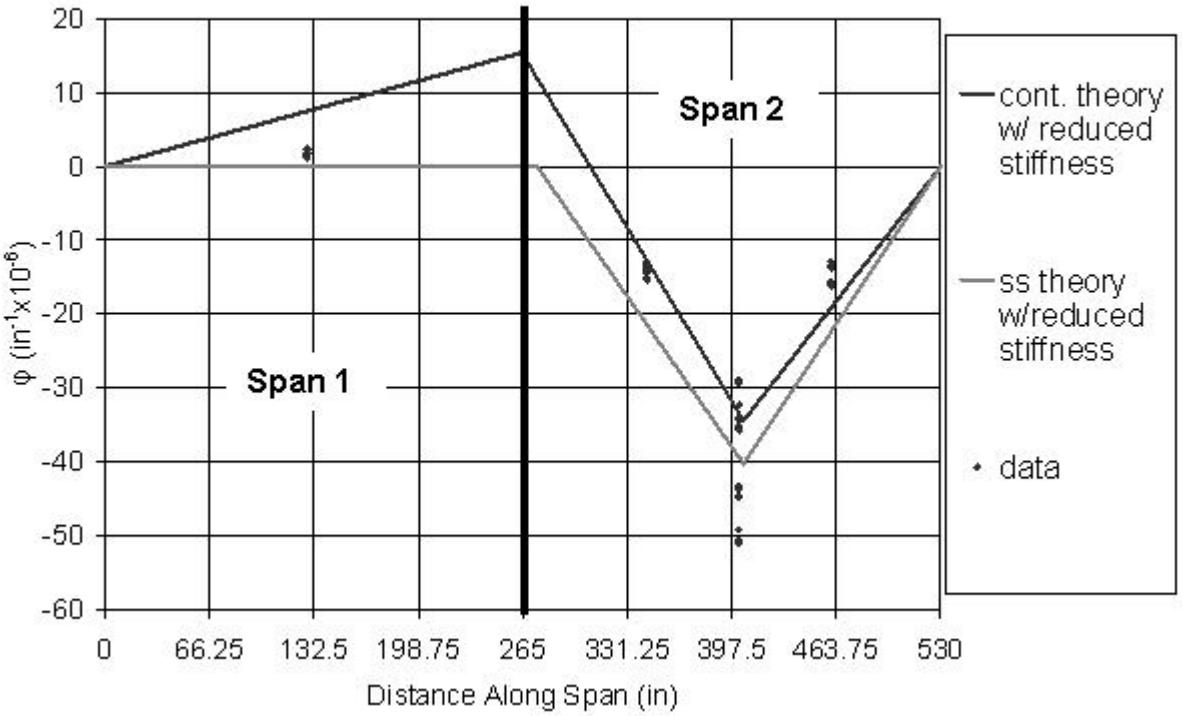

Figure 7.16: Curvatures along bridge during spreader load at midspan of Span 2

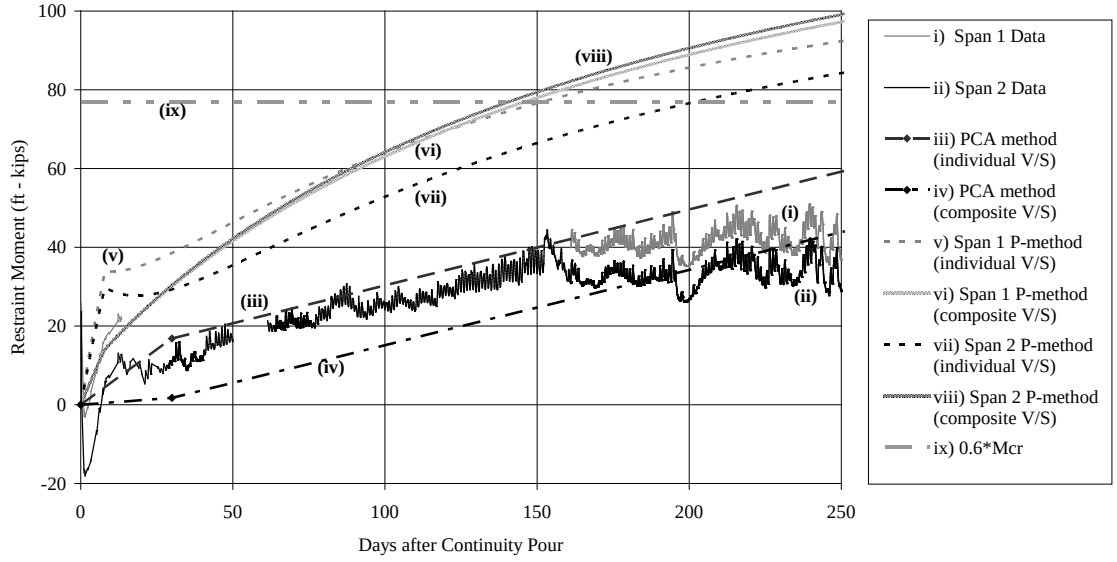

Figure 7.17: Predicted and measured restraint moments in laboratory bridge specimen and models using different assumed V/S ratios

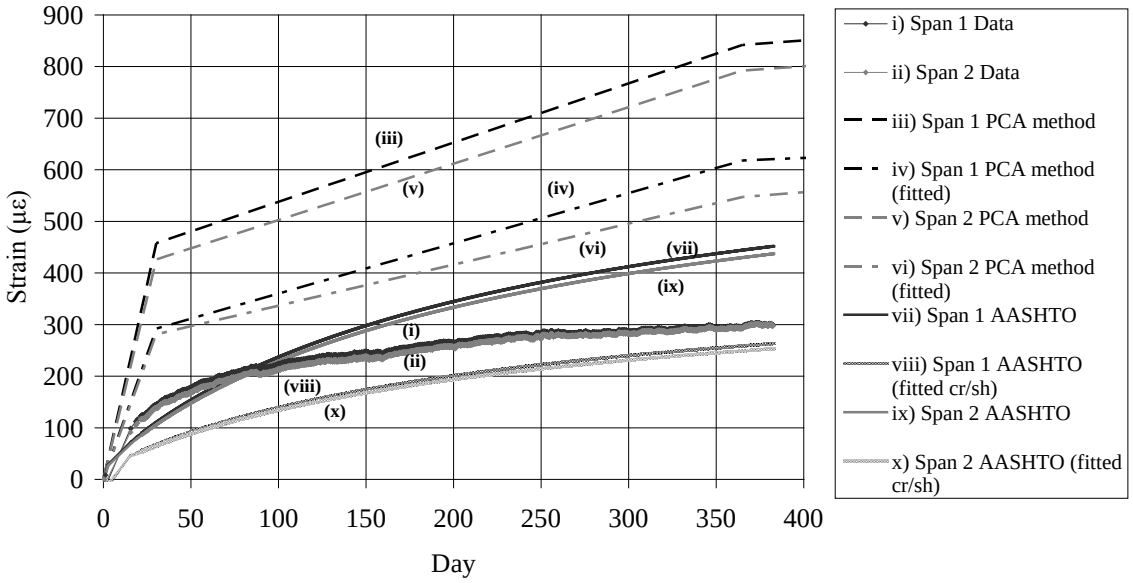

Figure 7.18: Combined creep and shrinkage strains at the center of gravity of strands

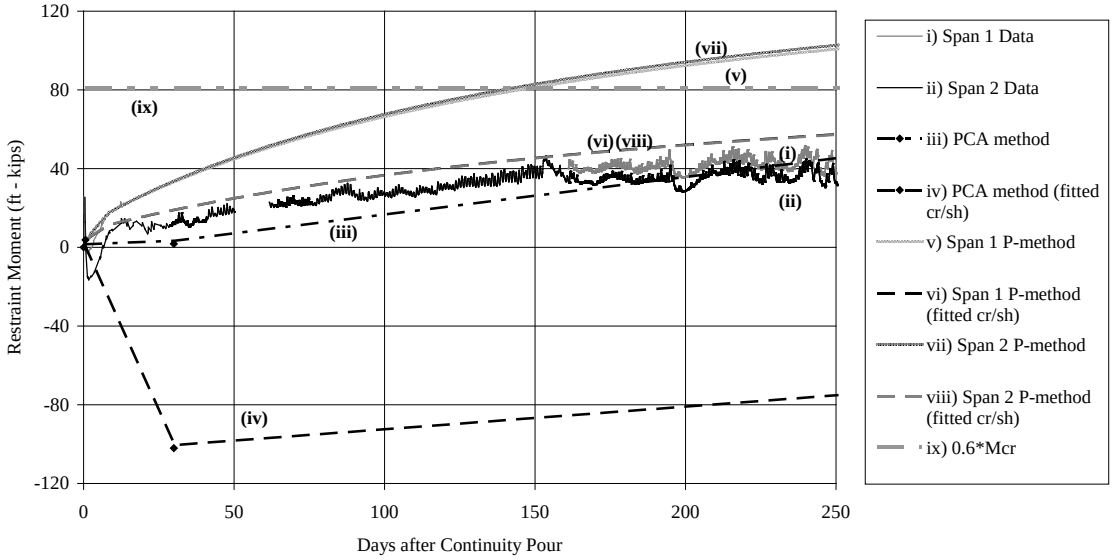

Figure 7.19: Restraint moments from laboratory bridge specimen and models fitted to creep and shrinkage data

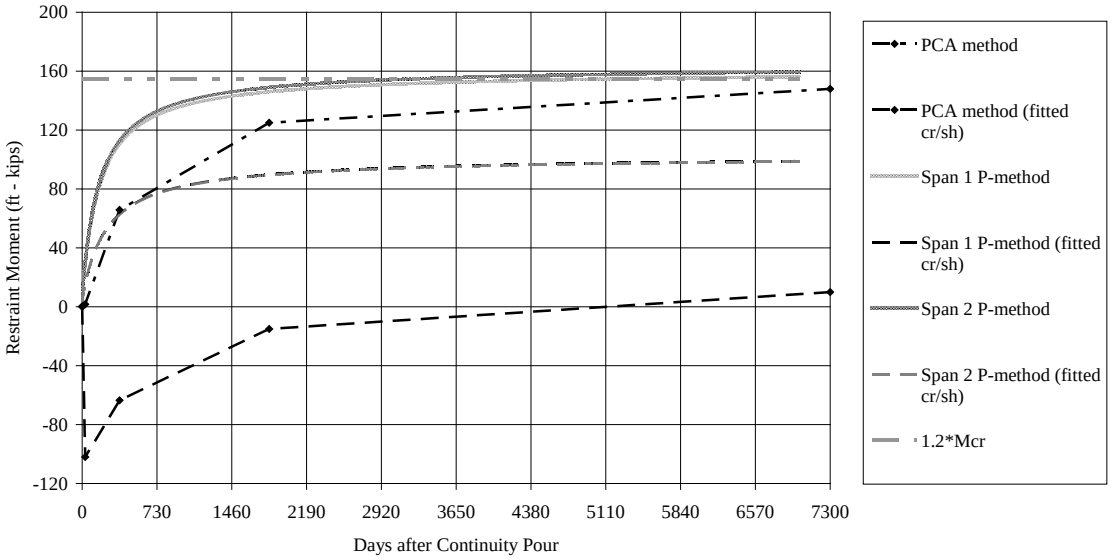

Figure 7.20: Laboratory bridge specimen restraint moment predictions carried out to 20 years

Appendix A: Modified Section Design Calculations

This section includes some of the calculations used to develop the design modifications for the Mn/DOT PCSSS. This includes calculations for the reductions in flange thickness, horizontal shear reinforcement, and bursting reinforcement.

A.1 Reduced Flange Thickness

The flange thickness was reduced from 5 ¼ in. to 3 in. at the tip and maintained the ¼ in. taper over the 12 in. flange. This was done to reduce the driving force that could cause reflective cracks. This reduction also required changing the reinforcement in the flange. The looped bar around the strands (S1301E in Bridge 13004) was reduced to a single #4 bar spaced no further than required for shrinkage and temperature according to AASHTO LRFD 2004 Section 5.10.8 (i.e. #4 @ 12 in.). The top layer of strands in the flange was eliminated (two in each flange). The following calculation was done to determine the robustness of the flange at the reduced thickness.

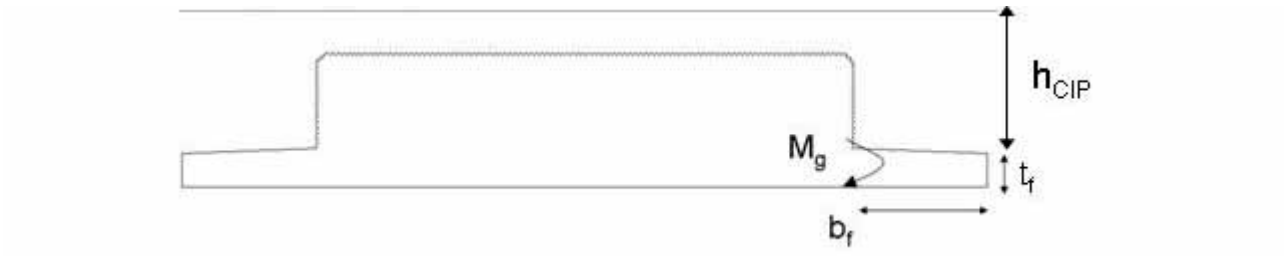

$$t_f = 3in \quad b_f = 12in \quad h_{CIP} = 22in \quad I = \frac{t_f^2}{12} \quad g_c = 155pcf \quad f'_c = 6.5ksi$$

$$M_{cr} = \frac{2 \times I \times 7.5\sqrt{f'_c}}{t_f} = 10.9\frac{in\text{-}k}{ft} \qquad M_g = \frac{g_c \times h_{CIP} \times b_f^2}{2} = 1.71\frac{in\text{-}k}{ft}$$

The cracking moment was more than five times the moment required to support the CIP during construction. Flange thicknesses smaller than 3 in. were believed to be prone to possible damage during handling.

The reduction in flange thickness also changed the strength of the positive moment connection at the pier. The calculations are shown below.

Center City Bridge (with 5-1/4 in. flange):

$d = 10in \quad A_s = 3.16in^2 \quad f'_c = 4ksi \quad f_y = 60ksi \quad b = 72in \quad h = 18in \quad \phi = 0.9$

$$M_{cr} = \frac{bh^2 7.5\sqrt{f'_c}}{6} = 154\,ft\text{-}k \qquad \phi M_n = \phi A_s f_y \left(d - \frac{A_s f_y}{1.7bf'_c}\right) = 137\,ft\text{-}k$$

Center City Bridge with reduced flange thickness (i.e., 3 in.):

$d = 12.25in \quad A_s = 3.16in^2 \quad f'_c = 4ksi \quad f_y = 60ksi \quad b = 72in \quad h = 18in \quad \phi = 0.9$

$$M_{cr} = \frac{bh^2 7.5\sqrt{f'_c}}{6} = 154\,ft\text{-}k \qquad \phi M_n = \phi A_s f_y \left(d - \frac{A_s f_y}{1.7bf'_c}\right) = 169\,ft\text{-}k$$

Beltrami County Bridge (with 5-1/4 in. flange):

$d = 14in \quad A_s = 3.16in^2 \quad f'_c = 4ksi \quad f_y = 60ksi \quad b = 72in \quad h = 22in \quad \phi = 0.9$

$$M_{cr} = \frac{bh^2 7.5\sqrt{f'_c}}{6} = 230\,ft\text{-}k \qquad \phi M_n = \phi A_s f_y \left(d - \frac{A_s f_y}{1.7bf'_c}\right) = 194\,ft\text{-}k$$

A.2 Horizontal Shear Reinforcement

Calculations were done to determine horizontal shear reinforcement requirements for both the Center City and Beltrami County bridges according to both AASHTO LRFD (2004) and ACI 318-02 requirements. For the ACI calculations, different values for ultimate shear were determined using the applicable load factors as they were different than the load factors used by Mn/DOT to calculate the ultimate shear using the AASHTO requirements. The shear loads were taken from the Mn/DOT design spreadsheets for the two bridges.

Notation for AASHTO C5.8.4.1

c = cohesion

μ = friction coefficient

φ_v = shear strength reduction factor

b_v = shear interface width

d_v = section depth considered for shear

s = spacing of horizontal shear reinforcement

A_{vf} = area of reinforcement crossing the shear plane per unit length

f_y = yield strength of reinforcement

V_u, V_h, V_n = factored shear, required horizontal shear, nominal shear resistance

Notation for ACI 17.5

φ_v = shear strength reduction factor

b_v = shear interface width

d_v = section depth considered for shear

V_u, V_n = factored shear, nominal horizontal shear resistance

Center City Bridge:

AASHTO 5.8.4.1

$$c = 0.1ksi \quad m = 1.0 \quad f_v = 0.9 \quad b_v = 48in \quad d_v = 13.7in \quad s = 24in \quad A_{vf} = \frac{2 \times 0.31in^2}{s}$$

$$V_u = 68.5kips \qquad V_h = \frac{V_u}{d_v} = 5.0\frac{kips}{in}$$

$$V_n = c \times b_v + m \times A_{vf} \times f_y = 6.35\frac{kips}{in} \qquad j_v V_n = 5.72\frac{kips}{in}$$

The 24 in. spacing provided exceeded the maximum spacing allowed by AASHTO LRFD (2004) horizontal shear reinforcement requirements. The requirements also stated that the reinforcement be developed to reach specified yield strength, which would not be achieved in the actual bridge design as this would have required the hooks in the slab to be anchored by longitudinal reinforcement or for the CIP deck to be thick enough to develop the reinforcement.

ACI 17.5

$$f_v = 0.75 \quad b_v = 48in \quad d_v = 13.7in \quad V_u = 68.5kips$$

Without minimum reinforcement: $V_n = 80psi \times b_v \times d_v = 52.6kips \qquad j_v V_n = 39.5kips$

With minimum reinforcement: $V_n = 260psi \times b_v \times d_v = 171kips \qquad j_v V_n = 128kips$

To meet the required horizontal shear resistance according to ACI 318-02, minimum reinforcement was required. Minimum reinforcement according to ACI 318-02 Section 11.5.5.3 Equation 11-13 required a #5 U-stirrup at 12 in. The horizontal shear reinforcement that was provided was a #5 U-stirrup at 24 in. which met the maximum spacing requirements for horizontal shear reinforcement as per ACI 17.6, however it exceed the minimum reinforcements. The rationale for providing a lower amount of reinforcement than that required stemmed from research results by Naito and Deschenes (2006) at Lehigh University which indicated current horizontal shear reinforcement requirements are overly conservative.

Beltrami County Bridge:

AASHTO C5.8.4.1

$c = 0.1ksi \quad m = 1.0 \quad f_v = 0.9 \quad b_v = 48in \quad d_v = 18.8in \quad s = 24in \quad A_{vf} = \frac{2 \times 0.31in^2}{s}$

$V_u = 95.1kips \qquad V_h = \frac{V_u}{d_v} = 5.1\frac{kips}{in}$

$V_n = c \times b_v + m \times A_{vf} \times f_y = 6.35\frac{kips}{in} \qquad \phi_v V_n = 5.72\frac{kips}{in}$

ACI 17.5

$f_v = 0.75 \quad b_v = 48in \quad d_v = 13.7in \quad V_u = 87.9kips$

Without minimum reinforcement: $V_n = 80psi \times b_v \times d_v = 72.1kips \quad \phi_v V_n = 54.0kips$

With minimum reinforcement: $V_n = 260psi \times b_v \times d_v = 234kips \quad \phi_v V_n = 176kips$

A.3 Bursting Resistance

Bursting resistance was calculated using both AASHTO LRFD Specifications (2004) 5.10.10.1 and a rational equation found in the literature (Marshall and Mattock 1962) that was believed to be the basis of the AASHTO requirement. The original Mn/DOT bursting design was developed for the Beltrami County Bridge which was near the maximum span length and prestress force envisioned for the Mn/DOT PCSSS. This same reinforcement

detail was used for the Center City Bridge even though the section had a shorter depth and one half the prestress force.

Original Design (AASHTO LRFD 5.10.10.1 for Beltrami County Bridge):

f_s = allowable service stress in mild reinforcement

P_j = prestress jacking force

P_r = required bursting resistance

$$f_s = 20ksi \quad P_j = 991kips$$

$$P_r = 0.04P_j \quad A_{s\_req} = \frac{P_r}{f_s} = 1.98in^2$$

Reinforcement for bursting must be within h/4 of end of beam.

$$h = 16in \quad \frac{h}{4} = 4in$$

Three double sets of #5 stirrups were provided at 2 in. increments to be conservative. This resulted in A_s=2.48in^2 to provide the required resistance.

AASHTO LRFD 5.10.10.1 for Center City Bridge:

$$f_s = 20ksi \quad P_j = 496kips$$

$$P_r = 0.04P_j \quad A_{s\_req} = \frac{P_r}{f_s} = 0.99in^2$$

Reinforcement for bursting must be within h/4 of end of beam.

$$h = 16in \quad \frac{h}{4} = 3in$$

Two #5 stirrups provided at 2 in. spacing would result in A_s=1.24in^2 to provide the required resistance. Three double sets of #5 stirrups were actually provided at 2 in. (consistent with the Beltrami County Bridge).

Minimum Reinforcement Design Using Equation from Marshall and Mattock (1962):

f_s = allowable service stress in mild reinforcement

P_j = prestress jacking force

P_r = required bursting resistance

h = depth of precast section

l_t = prestress transfer length (assumed to be $50d_{ps}$)

$$f_s = 20ksi \quad P_j = 496kips \quad h = 12in \quad l_t = 25in$$

$$P_r = 0.021\frac{P_j \times h}{l_t} \quad A_{s\_req} = \frac{P_r}{f_s} = 0.25in^2$$

There was no requirement for the proximity of the reinforcement to the face of the precast sections, so the same $h/4$ from the AASHTO requirement was used. Two configurations were considered to evaluate the necessity of the reinforcement to be as close as possible to the face of the precast section.

Configuration I: Used #3 stirrups at 2 in. and 4in. from the face of the precast section. This resulted in $A_s = 0.44in^2$

Configuration II: Used a #4 stirrup at 2 in. from the face of the precast section. This resulted in $A_s = 0.40in^2$

REFERENCES

Naito, C., Deschenes, D. 2006. Horizontal Shear Capacity of Composite Concrete Beams without Ties. *Proceedings, Prestressed/Precast Concrete Institute (PCI) National Bridge Conference*, Grapevine, TX.

Appendix B: Material Tests

B.1 Concrete Compressive Strength

The concrete compressive strength was measured as per ASTM C 39. The 4 by 8 in. cylinders were loaded at a rate of 450 lb/s in a Forney testing machine using displacement control. The displacement rate was manually adjusted during the test to maintain the required loading rate. The specimens were capped with Gilson Rediron High Strength Capping Compound. The capping compound had a specified strength of 8 ksi, but could reach higher strengths after a couple of days of curing. The sulfur capping compound worked well for all of the testing dates except for the precast cylinders at 415 days when only 1 of 15 samples failed properly. However, these samples were tested to correct an earlier problem with modulus of elasticity testing, and the concrete compressive strength was already expected to be well known. Concrete compressive strength tests were performed at ages of 7, 9, 28, 159, and 415 days for the precast concrete samples and ages of 5, 8, 28, 154, and 432 days for the CIP concrete samples. Two cylinders were also tested by the fabricator 18 hours after the beams were cast. The precast cylinders were stored with the precast sections at the precast facility until the beams were shipped to the Structures Laboratory, and all of the concrete samples were stored under the laboratory specimen after the continuity pour.

As expected, the results for the precast cylinders were consistent for the samples taken from each of the four precast sections, so the results were all averaged together. Due to the high strength of the precast concrete cylinders, some of the samples failed at lower than expected stresses, which was assumed to be due to failure of the capping compound as crushing was observed near one end of the cylinder in these cases. These results were discarded when computing the average compressive strength. For the CIP samples, the concrete for Span 2 was usually stronger than the concrete for Span 1, so the results are given separately. Tables B.1.1-B.1.3 summarize the concrete compressive strength results.

Table B.1.1 Measured Precast Concrete Compressive Strengths

Precast Samples			
Age (days)	Number of Specimens	Compressive Strength (ksi)	Coefficient of Variation (%)
1	2	7.41	2.9
7	7	10.5	4.9
9	8	11.4	7.6
28	11	12.9	5.3
159	13	12.9	5.3
415	1	12.7	--

Table B.1.2 Measured Span 1 CIP Concrete Compressive Strengths

Span 1 CIP Samples			
Age (days)	Number of Specimens	Compressive Strength (ksi)	Coefficient of Variation (%)
5	2	2.04	0.3
8	2	2.74	2.8
28	4	4.16	9.7
154	4	3.71	8.8
432	3	4.47	2.3

Table B.1.3 Measured Span 2 CIP Concrete Compressive Strengths

Span 2 CIP Samples			
Age (days)	Number of Specimens	Compressive Strength (ksi)	Coefficient of Variation (%)
5	2	2.74	11
8	2	3.21	3.8
28	4	4.59	1.8
154	4	4.19	14
432	2	4.55	9.4

B.2 Concrete Modulus of Elasticity

Modulus of elasticity for the concrete samples was measured as per ASTM C 469. The 4 by 8 in. cylinders were loaded and unloaded at a rate of 450 lb/s in the MTS test machine. The MTS test machine could be programmed to run a particular load program, such that the load process was computer controlled. The specimens were loaded to 40 % of the maximum measured concrete compressive strength. This process was repeated three times for each specimen to verify the consistency of the response and ensure the compressometer was properly seated. Displacements were measured by LVDT's attached to the compressometer, which were continuously read during testing. The modulus was found by fitting a line to the entire load profile up to 40% of the compressive strength rather than simply calculating the secant modulus from two points. This was done to average out the small amount of noise in the LVDT readings that could have caused a small amount of error if a secant modulus value was used. The modulus of elasticity was measured at 413 days for the precast samples and 427 days for the CIP samples. Modulus of elasticity was measured at an earlier age, but the results were affected by a problem with the compressometer and discarded.

The measured modulus of elasticity at 413 days of the precast samples was 6160 ksi with a coefficient of variation of 2.6%. The measured moduli of elasticity at 427 days of the CIP samples were 3540 ksi and 3780 ksi for Span 1 and Span 2, respectively, with coefficients of variation of 4.8% and 14%, respectively. Comparisons between the measurements of elasticity moduli to predicted models are given in the Table B.2.1. Both precast and CIP cylinders were compared to AASHTO LRFD Specification (2004) equations 5.4.2.4-1 and C5.4.2.4-1. The specific weight of the precast and CIP concrete were measured from the cylinders to use in equation 5.4.2.4-1. The specific weight of the precast concrete was measured as 154 pcf, and the specific weight of the CIP concrete was 136 pcf for Span 1 and 139 pcf for Span 2. The precast concrete elastic modulus was also estimated using equation 5-1 from ACI 363 (1992) for high strength concrete, which was the method used by Mn/DOT for design of the CIP.

Table B.2.1 Measured Modulus of Elasticity of Concrete

	Modulus of Elasticity		
	Precast	CIP Span 1	CIP Span 2
Measured	6160	3540	3780
AASHTO LRFD Eq. 5.4.2.4-1	7160	3380	3660
AASHTO LRFD Eq. C5.4.2.4-1	6540	3710	3900
ACI 363 Eq. 5-1	5540	--	--

B.3 Modulus of Rupture

Modulus of rupture for the concrete was measured as per ASTM C 78. The 6 by 6 by 24 in. beams were tested in four point bending in a Forney testing machine. A load rate of 30 lb/s was manually maintained. The modulus of rupture tests were performed when the samples were 28 days old for both the precast and CIP samples. The average modulus of rupture for the ten precast concrete samples was measured as 927 psi with a coefficient of variation of 9.3%. This was 8.7% higher than $7.5\sqrt{(f'_c)}$. The average modulus of rupture for the three CIP concrete samples from Span 1 was 528 psi with a coefficient of variation of 2.2%. This was 9.3% higher than $7.5\sqrt{(f'_c)}$. The average modulus of rupture for the three CIP concrete samples from Span 2 was 553 psi with a coefficient of variation of 6.4%. This was 8.7% higher than $7.5\sqrt{(f'_c)}$.

B.4 Split Cylinder Tensile Strength

Split cylinder tensile strength for the concrete was measured as per ASTM C 496. The 6 by 12 in. cylinders were tested in a Forney testing machine. A load rate of 300 lb/s was manually maintained. The split cylinder tests were performed when the samples were 28 days old for both the precast and CIP samples. The average tensile strength for the twelve precast concrete samples was 838 psi with a coefficient of variation of 11%. This was 23% higher than $6\sqrt{(f'_c)}$. The average tensile strength for the three CIP concrete samples from Span 1 was 411 psi with a coefficient of variation of 13%. This was 6.4% higher than

$6\sqrt{(f'_c)}$. The average tensile strength for the three CIP concrete samples from Span 2 was 457 psi with a coefficient of variation of 11%. This was 12% higher than $6\sqrt{(f'_c)}$.

B.5 Effective Modulus of Elasticity of Prestressing Strand

The resistive strain gages used to measure the initial prestress force and losses due to release were attached to and oriented with an individual wire of the prestressing strand. Thus the modulus of elasticity given by the manufacturer of the prestressing strand could not be used to relate the strains measured by the gages to the stresses in the strand. As a consequence, an "effective modulus of elasticity" was determined by testing two similarly instrumented strands to develop a stress-strain relationship. The two samples from the strand used in the precast sections were each instrumented with the same type of resistive gages on three of the seven wires of the strand. The strands were then loaded with axial tension at a rate of 0.05 kips/s or 0.33 ksi/s until the strands reached 75% of their ultimate strength of 270 ksi, which was the design level jacking prestress. During loading, the resistive strain gages were read at 1 Hz, and linear regression was applied to the stress-strain results using the loads and strains. The average effective modulus for the six gages was 30,108 ksi with a coefficient of variation of 2.7%. The average measured strand area from the precast fabricator was used, which was 0.153 $in.^2$.

B.6 Creep and Shrinkage Measurement

Creep and shrinkage cylinders were cast with the laboratory bridge specimen to compare the measured data to the material models used in the predictions of restraint moments and prestress losses. Creep and shrinkage samples were cast from the precast section concrete while only shrinkage samples were cast from the CIP deck concrete as there were no sustained loads (other than due to restraint) that would cause creep in the CIP deck of the laboratory specimen. The samples were cast in 4 in. diameter PVC pipe, cut to 11 in. long. The inside diameter of the 4 in. diameter schedule 40 PVC pipe was 3.998 in., which was nominally taken as 4.0 in. in all calculations. Three sets of two holes were drilled in the

PVC. Each set of two holes was evenly spaced at 120^{o} around the circumference. Longitudinally, the two holes in each set were spaced 8 in. apart and centered along the length of the cylinder. Brass inserts were held in place at the six locations by machine screws. Prior to casting the samples, the insides of the PVC were brushed with a formwork debonding agent to make extraction easier while paying special attention not to get any debonding agent on the brass inserts.

During casting of the precast sections, six samples were taken for each precast section, and during the casting of the CIP deck, three samples each were taken from the two concrete trucks used to fill the two spans. The cylinders were filled using ASTM Standard C 192 for 4 by 8 in. cylinders. Like the rest of the samples, the creep and shrinkage cylinders were removed from the forms as soon as possible after the formwork was removed from the corresponding laboratory bridge specimen. The samples were stored with the laboratory specimen so they would experience the same atmospheric conditions. More samples were cast than were required for measurement of creep and shrinkage to ensure that the samples used appeared to be free of voids, which can sometimes form around the brass insert. After the PVC was removed, one cylinder each from Beams 1N and 2N were designated as the creep cylinders as Beams 1N and 2N were the first and last precast sections cast during fabrication. Two cylinders from each of the four precast sections were brought to the creep room to serve as a shrinkage control for the creep cylinders. Two cylinders from each of the four precast sections were also left in the laboratory to determine precast shrinkage under laboratory conditions. For the CIP, two cylinders from each span were left in the laboratory to determine CIP shrinkage under laboratory conditions. To maintain the same volume-to-surface ratio as the creep specimens, all of the shrinkage cylinders were capped with epoxy to prevent moisture transport. Each of the brass inserts in the samples was fitted with a stainless steel contact seat. A picture of a completed sample is given in Figure B.1.

The two creep cylinders were loaded into a creep frame as shown in Figure B.2. The creep frame was loaded when the cylinders were 30 hours old, about 6 hours after the strands in the precast sections were released. The four threaded rods were instrumented with strain gages such that the strain indicator box gave the forces in the rods. The cylinders were capped with a sulfur capping compound and stacked on top of each other in the frame. The

top plate was then added, and the nuts of the threaded rod were brought to snug tight. A hand pump jack was then used to compress the cylinders to the desired load. The nuts were again tightened and the load in the bars was checked. This was repeated until the desired force was reached. The same process was used to maintain a constant stress on the cylinders throughout the testing period. The axial compression force used for the creep cylinders was 14.2 kips which corresponded to the calculated midspan bottom fiber compressive stress of 1.13 ksi due to the initial prestress force and self weight of the precast section . In March 2007, the strain indicator readings for two of the threaded rod forces became less reliable, so a load cell was embedded into the frame and used to measure the force in the cylinders. After the embedment of the load cell, the error of the threaded rod force measurements between the indicator box and load cell ranged from one to twelve percent. The estimated error before the embedment of the load cells, based on expecting the same average loss in the two threaded rods with reliable readings as in the two with unreliable readings, was in this range as well. The reason for the variation in this indicator box was unknown.

The length between the contact seats of each creep or shrinkage gage were measured with a digital Whittemore gage. Before the gages were measured, the gage was zeroed using an invar bar. Five readings were taken for each contact seat pair to a resolution of 0.00005 in. The creep gages were read before and after any adjustments to the axial force in the creep frame. After the precast section creep samples were installed in the creep frame, the creep frames were reloaded every day for the first eight days when the average load loss was 2% per day. All of the shrinkage cylinders were read every day as well. Over the next 52 days, this was extended to a one week reading frequency where the creep frame was reloaded if the force dropped more than 2% below the target. After 210 days the reading frequency was extended to two weeks.

The relative humidity in the creep room and the Structures Laboratory was measured with a sling psychrometer each time the creep and shrinkage cylinders were measured. The humidity readings are plotted in Figure B.3. The goal was to maintain the creep room humidity at 50% using humidifiers and dehumidifiers, but the humidity varied nearly as much in the creep room as in the Structures Laboratory. Over the 385 day monitoring period,

the average relative humidity was 41% in the Structures Laboratory and 49% in the creep room. These averages were calculated using the trapezoid rule.

Average readings for the creep strain are shown in Figure B.4. The strains were calculated by taking the average of the six creep gages and subtracting the average of the 24 shrinkage gages that were kept in the same room. The negative values were attributed to the variations between the creep and shrinkage strains due to human error introduced by the manual reading of the gages. It was not expected that the actual creep strain was negative at any time over the monitoring period. The measured creep strain was compared to two models, AASHTO LRFD Specification (2004) equation 5.4.2.3.2-1 and the charts from the paper outlining the PCA method for restraint moment prediction (Freyermuth 1969). Fitted lines were added to Figure B.3 to allow for more in depth comparison of the restraint moment models as done in Section 5.7. The fitted lines were created using a single, scalar coefficient to fit the models to the data. The coefficients were calculated by minimizing the square of the error between the data and the models. The fitted coefficients were found to be 0.54 for the AASHTO equation and 0.34 for the PCA charts. Both methods greatly over-predicted the creep strains in the precast samples. Because the loading stress was only 8.8% of the specimen's compressive strength, it was thought that the assumption of a linear relationship between stress and creep strain may not be valid at such a low stress.

The shrinkage strains for the precast cylinders kept in the creep room are given in Figure B.5, and the shrinkage strains for the samples stored in the Structures Laboratory are given for the precast and CIP in Figures B.6 and B.7, respectively. Erratic readings were removed from the plots as there was sufficient redundancy in the readings from having 24 precast shrinkage gages in each of the creep room and Structures Laboratory and 12 CIP shrinkage gages in the Structures Laboratory. Human error in the manual readings was the expected cause of the erratic readings. The measured shrinkage strains were also compared to two models, AASHTO LRFD Specification (2004) equation 5.4.2.3.3-1 and the charts from the paper outlining the PCA method for restraint moment prediction (Freyermuth 1969). As for the creep models, fitted lines were calculated for the shrinkage models. For the precast samples kept in the creep room, the coefficients were 0.58 and 0.98 for the AASHTO equation and PCA charts, respectively. For the precast samples kept in the

Structures Laboratory, the coefficients were 0.50 and 0.85 for the AASHTO equation and PCA charts, respectively. For the CIP samples kept in the Structures Laboratory, the coefficients were 0.68 and 0.97 for the AASHTO equation and PCA charts, respectively. For all three cases, the PCA Charts were far more accurate in predicting the shrinkage than the AASHTO equation.

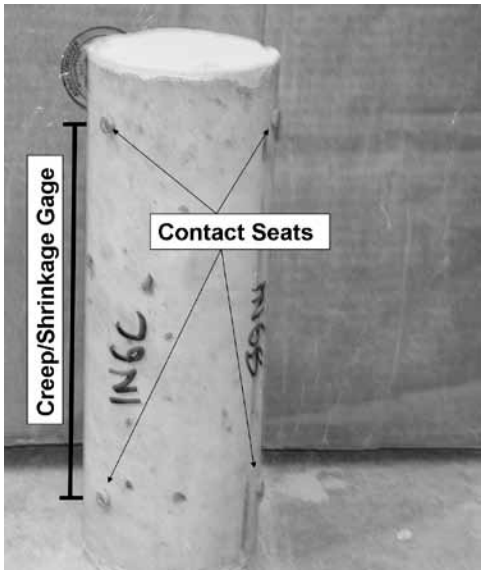

Figure B.1: Picture of prepared creep/shrinkage specimen

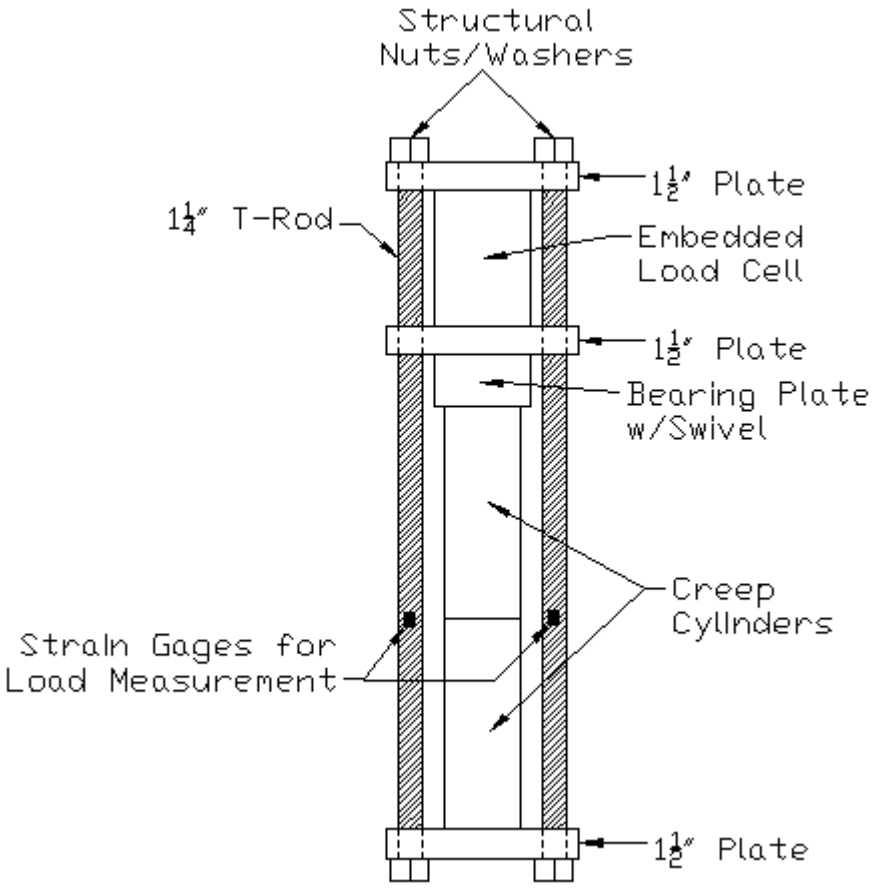

Figure B.2: Creep frame layout

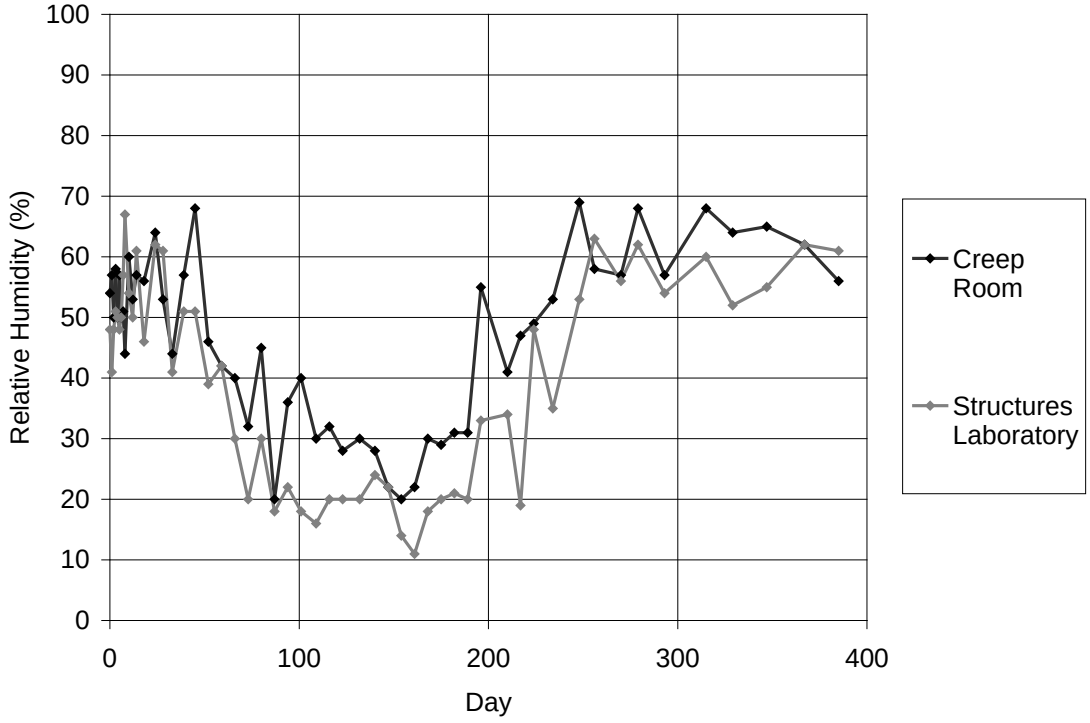

Figure B.3: Measured relative humidity in creep room and Structures Laboratory

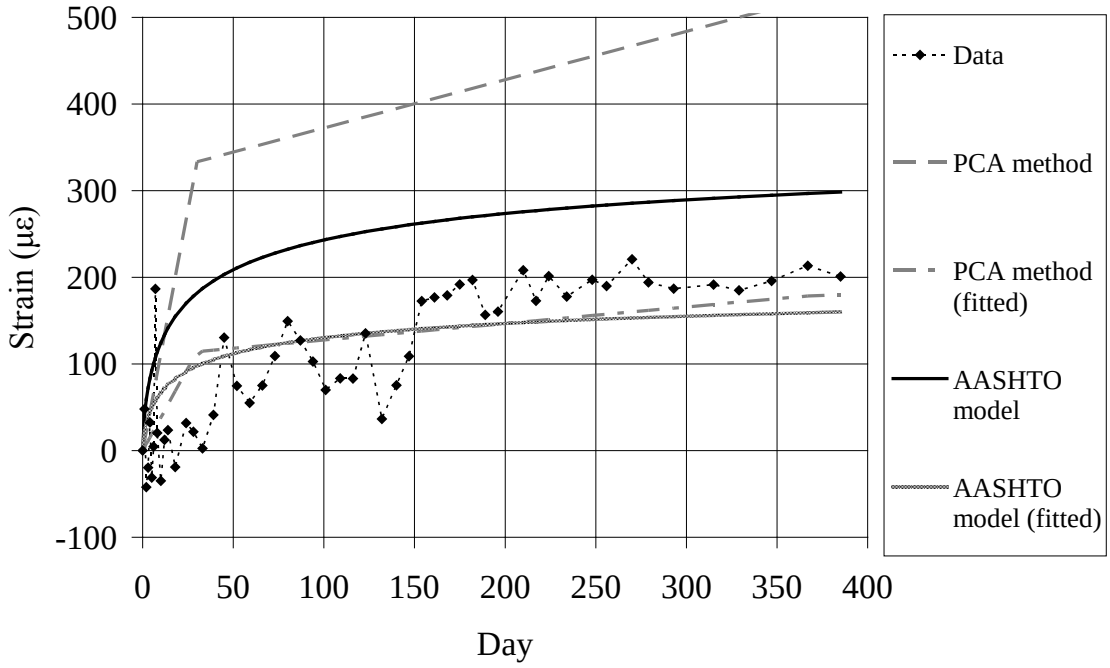

Figure B.4: Measured creep results

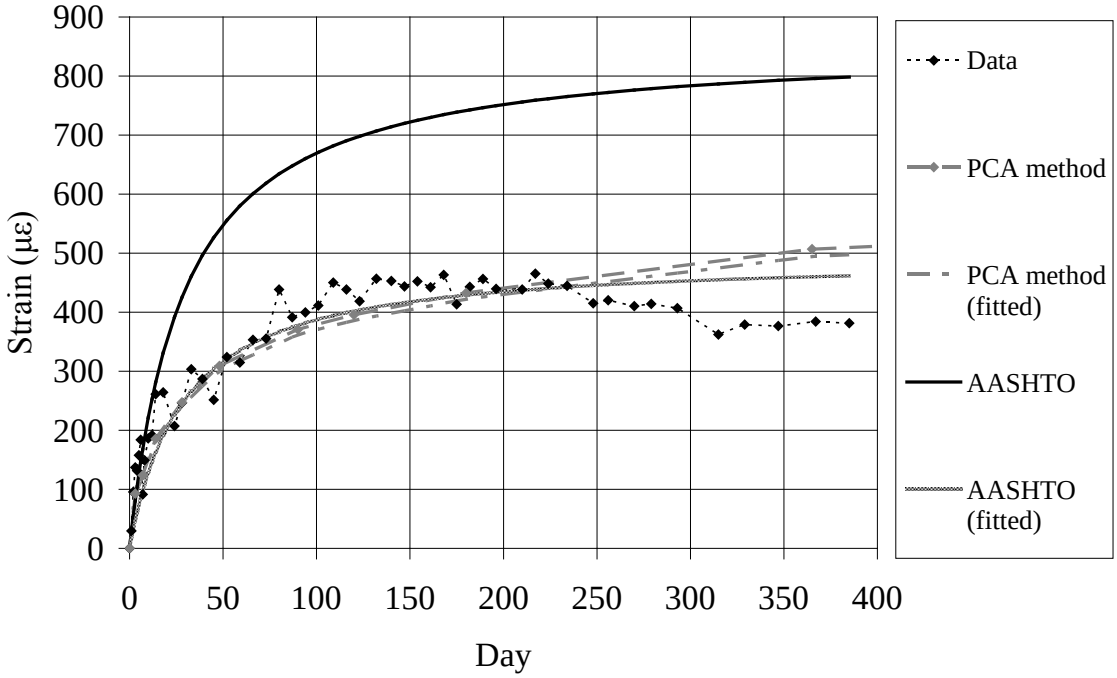

Figure B.5: Measured precast shrinkage results from creep room samples

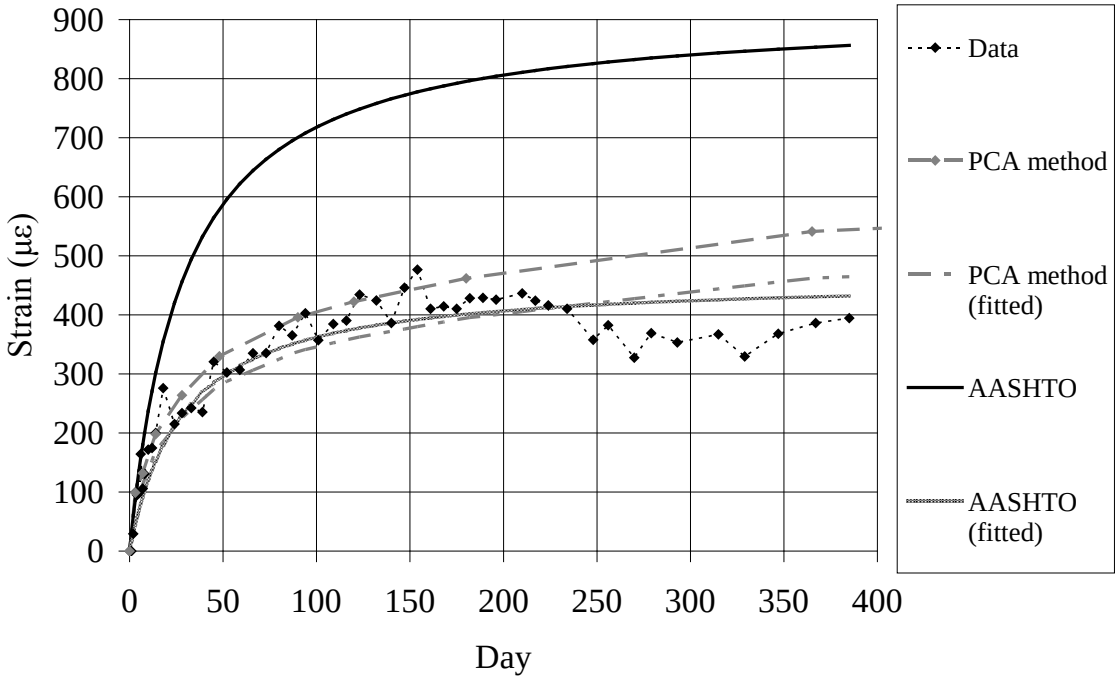

Figure B.6: Measured precast shrinkage results from Structures Laboratory

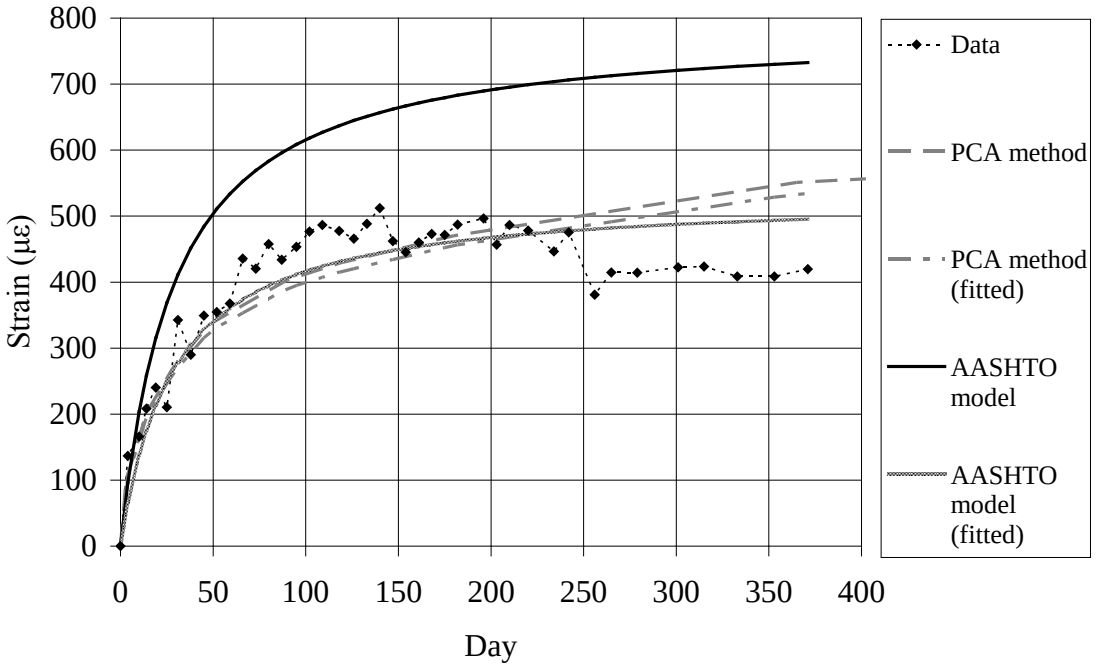

Figure B.7: Measured CIP shrinkage results from Structures Laboratory

Appendix C: Data Acquisition Set Up and Programs

This appendix contains overviews of the programs and procedures used to collect the data gathered for this research project. This includes the data acquisition for the vibrating wire strain gages read at the Center City Bridge, the resistive strain gages read at the precast facility, and the vibrating wire strain gages, resistive strain gages, LVDT's, and load cells read in the Structures Laboratory.

C.1 Center City Bridge Data Acquisition

The data acquisition set up was previously described in detail in the Mn/DOT 2006-37 Report (Bell 2006). The programs used to run the dataloggers were modified from those used for monitoring to include a switched voltage signal to serve as a data marker during the truck load tests. The program used for one of the two CR10X dataloggers is given below. The program for the other datalogger was similar with the appropriate changes for channel names.

```
;{CR10X}
;
*Table 1 Program
  01: 60       Execution Interval (seconds)

;Read voltage of switched battery which serves as a
;marker in the data file during truck test
1:  Volt (Diff) (P2)
 1: 1        Reps
 2: 25       2500 mV 60 Hz Rejection Range
 3: 6        DIFF Channel
 4: 98       Loc [ SWITCH1   ]
 5: 1.0      Multiplier
 6: 0.0      Offset


;Read Multiplexer 1

;Turn on Multiplexer 1 and reset connection to
;the first channel
2:  Do (P86)
 1: 41       Set Port 1 High

;Read Concrete Embedment Gages
```

```
;Begin loop
3:  Beginning of Loop (P87)
 1: 0000     Delay
 2: 6        Loop Count

;Switch between channels on multiplexer
    4:  Do (P86)
     1: 72       Pulse Port 2

;20ms Pause to allow contacts to settle

    5:  Excitation with Delay (P22)
     1: 1        Ex Channel
     2: 1        Delay W/Ex (0.01 sec units)
     3: 1        Delay After Ex (0.01 sec units)
     4: 0000     mV Excitation

;Read voltage of thermistor
    6:  Excite-Delay (SE) (P4)
     1: 1        Reps
     2: 15       2500 mV Fast Range
     3: 1        SE Channel
     4: 1        Excite all reps w/Exchan 1
     5: 1        Delay (0.01 sec units)
     6: 2500     mV Excitation
     7: 1     -- Loc [ TM1CE_1   ]
     8: .001     Multiplier
     9: 0.0      Offset

;Calculate temperature using voltage and
;given polynomial equation
    7:  Polynomial (P55)
     1: 1        Reps
     2: 1     -- X Loc [ TM1CE_1   ]
     3: 1     -- F(X) Loc [ TM1CE_1   ]
     4: -104.78  C0
     5: 378.11   C1
     6: -611.59  C2
     7: 544.27   C3
     8: -240.91  C4
     9: 43.089   C5

;Calculate strain.  Multiplier given by gage
;manufacturer
    8:  Vibrating Wire (SE) (P28)
     1: 1        Reps
     2: 5        SE Channel
     3: 1        Excite all reps w/Exchan 1
     4: 4        Starting Freq. (100 Hz units)
     5: 12       End Freq. (100 Hz units)
     6: 250      No. of Cycles
     7: 50       Rep Delay (0.01 sec units)
     8: 49    -- Loc [ M1CE_1    ]
     9: 3304     Multiplier
    10: 0.0      Offset

;End loop
9:  End (P95)

;Read Spot Weldable Gages
```

```
;Same commands as embedment gages but with
;a different multiplier for the vibrating
;wire reading

10:  Beginning of Loop (P87)
 1: 0000     Delay
 2: 10       Loop Count


    11:  Do (P86)
     1: 72       Pulse Port 2

    12:  Excitation with Delay (P22)
     1: 1        Ex Channel
     2: 1        Delay W/Ex (0.01 sec units)
     3: 1        Delay After Ex (0.01 sec units)
     4: 0000     mV Excitation

    13:  Excite-Delay (SE) (P4)
     1: 1        Reps
     2: 15       2500 mV Fast Range
     3: 1        SE Channel
     4: 1        Excite all reps w/Exchan 1
     5: 1        Delay (0.01 sec units)
     6: 2500     mV Excitation
     7: 7     -- Loc [ TM1SW_1   ]
     8: .001     Multiplier
     9: 0.0      Offset

    14:  Polynomial (P55)
     1: 1        Reps
     2: 7     -- X Loc [ TM1SW_1   ]
     3: 7     -- F(X) Loc [ TM1SW_1   ]
     4: -104.78  C0
     5: 378.11   C1
     6: -611.59  C2
     7: 544.27   C3
     8: -240.91  C4
     9: 43.089   C5

    15:  Vibrating Wire (SE) (P28)
     1: 1        Reps
     2: 5        SE Channel
     3: 1        Excite all reps w/Exchan 1
     4: 14       Starting Freq. (100 Hz units)
     5: 35       End Freq. (100 Hz units)
     6: 250      No. of Cycles
     7: 50       Rep Delay (0.01 sec units)
     8: 55    -- Loc [ M1SW_1    ]
     9: 391      Multiplier
    10: 0.0      Offset

16:  End (P95)

;Power down multiplexer
17:  Do (P86)
 1: 51       Set Port 1 Low

;Read Multiplexer 2

;Same as Multiplexer 1 but with
```

```
;different amounts of gages of the
;two types

18:  Do (P86)
 1: 43       Set Port 3 High

;Spot Weldable

19:  Beginning of Loop (P87)
 1: 0000     Delay
 2: 7        Loop Count

    20:  Do (P86)
     1: 74       Pulse Port 4

    21:  Excitation with Delay (P22)
     1: 1        Ex Channel
     2: 1        Delay W/Ex (0.01 sec units)
     3: 1        Delay After Ex (0.01 sec units)
     4: 0000     mV Excitation

    22:  Excite-Delay (SE) (P4)
     1: 1        Reps
     2: 15       2500 mV Fast Range
     3: 2        SE Channel
     4: 1        Excite all reps w/Exchan 1
     5: 1        Delay (0.01 sec units)
     6: 2500     mV Excitation
     7: 17    -- Loc [ TM2SW_1   ]
     8: .001     Multiplier
     9: 0.0      Offset

    23:  Polynomial (P55)
     1: 1        Reps
     2: 17    -- X Loc [ TM2SW_1   ]
     3: 17    -- F(X) Loc [ TM2SW_1   ]
     4: -104.78  C0
     5: 378.11   C1
     6: -611.59  C2
     7: 544.27   C3
     8: -240.91  C4
     9: 43.089   C5

    24:  Vibrating Wire (SE) (P28)
     1: 1        Reps
     2: 6        SE Channel
     3: 1        Excite all reps w/Exchan 1
     4: 14       Starting Freq. (100 Hz units)
     5: 35       End Freq. (100 Hz units)
     6: 250      No. of Cycles
     7: 50       Rep Delay (0.01 sec units)
     8: 65    -- Loc [ M2SW_1    ]
     9: 391      Multiplier
    10: 0.0      Offset

25:  End (P95)

;Embedment

26:  Beginning of Loop (P87)
 1: 0000     Delay
```

```
 2: 9        Loop Count

    27:  Do (P86)
     1: 74       Pulse Port 4

    28:  Excitation with Delay (P22)
     1: 1        Ex Channel
     2: 1        Delay W/Ex (0.01 sec units)
     3: 1        Delay After Ex (0.01 sec units)
     4: 0000     mV Excitation

    29:  Excite-Delay (SE) (P4)
     1: 1        Reps
     2: 15       2500 mV Fast Range
     3: 2        SE Channel
     4: 1        Excite all reps w/Exchan 1
     5: 1        Delay (0.01 sec units)
     6: 2500     mV Excitation
     7: 24    -- Loc [ TM2CE_1   ]
     8: .001     Multiplier
     9: 0.0      Offset

    30:  Polynomial (P55)
     1: 1        Reps
     2: 24    -- X Loc [ TM2CE_1   ]
     3: 24    -- F(X) Loc [ TM2CE_1   ]
     4: -104.78  C0
     5: 378.11   C1
     6: -611.59  C2
     7: 544.27   C3
     8: -240.91  C4
     9: 43.089   C5

    31:  Vibrating Wire (SE) (P28)
     1: 1        Reps
     2: 6        SE Channel
     3: 1        Excite all reps w/Exchan 1
     4: 4        Starting Freq. (100 Hz units)
     5: 12       End Freq. (100 Hz units)
     6: 250      No. of Cycles
     7: 50       Rep Delay (0.01 sec units)
     8: 72    -- Loc [ M2CE_1    ]
     9: 3304     Multiplier
    10: 0.0      Offset

32:  End (P95)

33:  Do (P86)
 1: 53       Set Port 3 Low

;Multiplexer 3

;Same as Multiplexer 1 but with
;different amounts of gages of the
;two types

34:  Do (P86)
 1: 45       Set Port 5 High

;Embedment
```

```
35:  Beginning of Loop (P87)
 1: 0000     Delay
 2: 6        Loop Count

    36:  Do (P86)
     1: 76       Pulse Port 6

    37:  Excitation with Delay (P22)
     1: 1        Ex Channel
     2: 1        Delay W/Ex (0.01 sec units)
     3: 1        Delay After Ex (0.01 sec units)
     4: 0000     mV Excitation

    38:  Excite-Delay (SE) (P4)
     1: 1        Reps
     2: 15       2500 mV Fast Range
     3: 3        SE Channel
     4: 1        Excite all reps w/Exchan 1
     5: 1        Delay (0.01 sec units)
     6: 2500     mV Excitation
     7: 33    -- Loc [ TM3CE_1   ]
     8: .001     Multiplier
     9: 0.0      Offset

    39:  Polynomial (P55)
     1: 1        Reps
     2: 33    -- X Loc [ TM3CE_1   ]
     3: 33    -- F(X) Loc [ TM3CE_1   ]
     4: -104.78  C0
     5: 378.11   C1
     6: -611.59  C2
     7: 544.27   C3
     8: -240.91  C4
     9: 43.089   C5

    40:  Vibrating Wire (SE) (P28)
     1: 1        Reps
     2: 7        SE Channel
     3: 1        Excite all reps w/Exchan 1
     4: 4        Starting Freq. (100 Hz units)
     5: 12       End Freq. (100 Hz units)
     6: 250      No. of Cycles
     7: 50       Rep Delay (0.01 sec units)
     8: 81    -- Loc [ M3CE_1    ]
     9: 3304     Multiplier
    10: 0.0      Offset

41:  End (P95)

;Spot Weldable

42:  Beginning of Loop (P87)
 1: 0000     Delay
 2: 10       Loop Count

    43:  Do (P86)
     1: 76       Pulse Port 6

    44:  Excitation with Delay (P22)
     1: 1        Ex Channel
     2: 1        Delay W/Ex (0.01 sec units)
```

```
   3: 1        Delay After Ex (0.01 sec units)
   4: 0000     mV Excitation

  45:  Excite-Delay (SE) (P4)
   1: 1        Reps
   2: 15       2500 mV Fast Range
   3: 3        SE Channel
   4: 1        Excite all reps w/Exchan 1
   5: 1        Delay (0.01 sec units)
   6: 2500     mV Excitation
   7: 39    -- Loc [ TM3SW_1   ]
   8: .001     Multiplier
   9: 0.0      Offset

  46:  Polynomial (P55)
   1: 1        Reps
   2: 39    -- X Loc [ TM3SW_1   ]
   3: 39    -- F(X) Loc [ TM3SW_1   ]
   4: -104.78  C0
   5: 378.11   C1
   6: -611.59  C2
   7: 544.27   C3
   8: -240.91  C4
   9: 43.089   C5

  47:  Vibrating Wire (SE) (P28)
   1: 1        Reps
   2: 7        SE Channel
   3: 1        Excite all reps w/Exchan 1
   4: 14       Starting Freq. (100 Hz units)
   5: 35       End Freq. (100 Hz units)
   6: 250      No. of Cycles
   7: 50       Rep Delay (0.01 sec units)
   8: 87    -- Loc [ M3SW_1    ]
   9: 391      Multiplier
  10: 0.0      Offset

48:  End (P95)

49:  Do (P86)
 1: 55       Set Port 5 Low

;Read Battery Voltage
50:  Batt Voltage (P10)
 1: 97       Loc [ Battery   ]

;Read voltage of switched battery which serves as a
;marker in the data file during truck test
51:  Volt (Diff) (P2)
 1: 1        Reps
 2: 25       2500 mV 60 Hz Rejection Range
 3: 6        DIFF Channel
 4: 99       Loc [ SWITCH2   ]
 5: 1.0      Multiplier
 6: 0.0      Offset

;Prepare datalogger to send output
52:  Do (P86)
 1: 10       Set Output Flag High (Flag 0)

;Set time stamp parameters
```

```
53:  Real Time (P77)^10788
 1: 110      Day,Hour/Minute (midnight = 0000)

;Set resolution of the results
54:  Resolution (P78)
 1: 1        High Resolution

;Copy data from input locations to output locations
55:  Sample (P70)^1767
 1: 99       Reps
 2: 1        Loc [ TM1CE_1   ]

;Send output to storage module
56:  Serial Out (P96)
 1: 71       Storage Module



*Table 2 Program
  02: 0.0000    Execution Interval (seconds)

*Table 3 Subroutines
```

End Program

C.2 Resistive Strain Gage Data Acquisition System used at Precast Facility

A schematic of the data acquisition system used at the precast facility is given in Figure C.2.1.

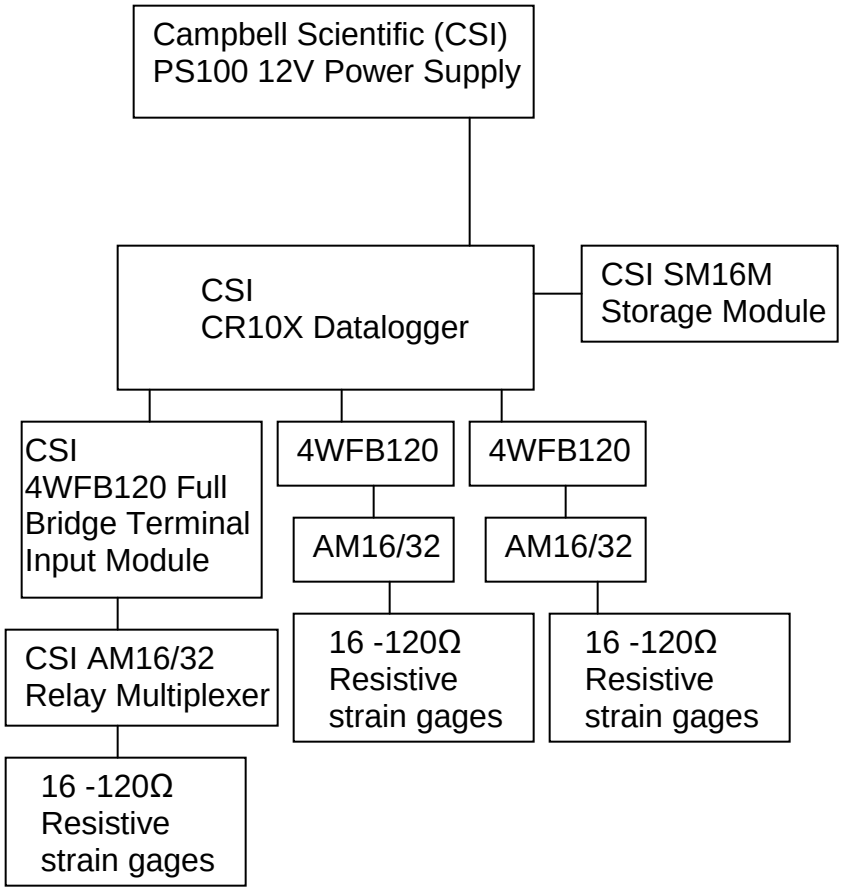

Figure C.2.1

The program used by one of the dataloggers to read the resistive strain gages during transfer is given below. The program for the other datalogger was the same except for the required modifications to the gage factor for different quantities of the gage types.

```
;{CR10X}
;
*Table 1 Program
  01: 60        Execution Interval (seconds)


;Read Multiplexer 1 gages

;Power up Multiplexer 1
1:  Do (P86)
 1: 41       Set Port 1 High
```

```
;Loop through gages
2:  Beginning of Loop (P87)
 1: 0000     Delay
 2: 16       Loop Count

;Switch to next channel on each pass through loop
    3:  Do (P86)
     1: 72       Pulse Port 2

;10ms pause to allow leads to settle
    4:  Excitation with Delay (P22)
     1: 1        Ex Channel
     2: 1        Delay W/Ex (0.01 sec units)
     3: 1        Delay After Ex (0.01 sec units)
     4: 0000     mV Excitation

;Full bridge resistive strain reading
;For this reading, the typical 2500mV excitation was
;reduced to 1800 so that the output voltage reading would be in
;the 7.5mV range.  This was required due to the high strains in the
;prestress strand during stressing.
    5:  Full Bridge (P6)
     1: 1        Reps
     2: 22       7.5 mV 60 Hz Rejection Range
     3: 1        DIFF Channel
     4: 1        Excite all reps w/Exchan 1
     5: 1800     mV Excitation
     6: 1        Loc [ Vr        ]
     7: 1.0      Multiplier
     8: 0.0      Offset

;Convert output voltage from full bridge to change
;in resisitance
    6:  Z=X*F (P37)
     1: 1        X Loc [ Vr        ]
     2: 0.001    F
     3: 1        Z Loc [ Vr        ]

    7:  Z=X*F (P37)
     1: 1        X Loc [ Vr        ]
     2: -2       F
     3: 2        Z Loc [ Vr2       ]

    8:  Z=Z+1 (P32)
     1: 2        Z Loc [ Vr2       ]

    9:  Z=X/Y (P38)
     1: 1        X Loc [ Vr        ]
     2: 2        Y Loc [ Vr2       ]
     3: 3        Z Loc [ Vr_Vr2    ]

    10:  Z=F x 10^n (P30)
     1: 4        F
     2: 6        n, Exponent of 10
     3: 5        Z Loc [ _4e6      ]

;Convert change in resistance to change in strain
;Input Gage factor for FLK type gage
    11:  Z=F x 10^n (P30)
     1: 2.11     F
```

```
   2: 00       n, Exponent of 10
   3: 6        Z Loc [ GF        ]

  12:  Z=X/Y (P38)
   1: 5        X Loc [ _4e6      ]
   2: 6        Y Loc [ GF        ]
   3: 4        Z Loc [ Mult      ]

  13:  Z=X*Y (P36)
   1: 3        X Loc [ Vr_Vr2    ]
   2: 4        Y Loc [ Mult      ]
   3: 7     -- Z Loc [ M1_1      ]

;End loop
14:  End (P95)

;Power down Multiplexer 1
15:  Do (P86)
 1: 51       Set Port 1 Low

;Read Multiplexer 2 Gages

;Same as Multiplexer 1 but with only 15 gages, and the
;gages have a different GF

16:  Do (P86)
 1: 43       Set Port 3 High

17:  Beginning of Loop (P87)
 1: 0000     Delay
 2: 15       Loop Count

  18:  Do (P86)
   1: 74       Pulse Port 4

  19:  Excitation with Delay (P22)
   1: 2        Ex Channel
   2: 1        Delay W/Ex (0.01 sec units)
   3: 1        Delay After Ex (0.01 sec units)
   4: 0000     mV Excitation

  20:  Full Bridge (P6)
   1: 1        Reps
   2: 22       7.5 mV 60 Hz Rejection Range
   3: 2        DIFF Channel
   4: 2        Excite all reps w/Exchan 2
   5: 2500     mV Excitation
   6: 1        Loc [ Vr          ]
   7: 1.0      Multiplier
   8: 0.0      Offset

  21:  Z=X*F (P37)
   1: 1        X Loc [ Vr        ]
   2: 0.001    F
   3: 1        Z Loc [ Vr        ]

  22:  Z=X*F (P37)
   1: 1        X Loc [ Vr        ]
   2: -2       F
   3: 2        Z Loc [ Vr2       ]
```

```
    23:  Z=Z+1 (P32)
     1: 2        Z Loc [ Vr2       ]

    24:  Z=X/Y (P38)
     1: 1        X Loc [ Vr        ]
     2: 2        Y Loc [ Vr2       ]
     3: 3        Z Loc [ Vr_Vr2    ]

    25:  Z=F x 10^n (P30)
     1: 4        F
     2: 6        n, Exponent of 10
     3: 5        Z Loc [ _4e6      ]


;Input gage factor for WFRA type gages
    26:  Z=F x 10^n (P30)
     1: 2.11     F
     2: 00       n, Exponent of 10
     3: 6        Z Loc [ GF        ]

    27:  Z=X/Y (P38)
     1: 5        X Loc [ _4e6      ]
     2: 6        Y Loc [ GF        ]
     3: 4        Z Loc [ Mult      ]

    28:  Z=X*Y (P36)
     1: 3        X Loc [ Vr_Vr2    ]
     2: 4        Y Loc [ Mult      ]
     3: 23    -- Z Loc [ M2_1      ]

29:  End (P95)

30:  Do (P86)
 1: 53       Set Port 3 Low

;Read Multiplexer 3 Gages

;Same as Multiplexer 1 but with two types of gages, so
;two loops are required for the varied GF's

31:  Do (P86)
 1: 45       Set Port 5 High

32:  Beginning of Loop (P87)
 1: 0000     Delay
 2: 5        Loop Count

    33:  Do (P86)
     1: 76       Pulse Port 6

    34:  Excitation with Delay (P22)
     1: 3        Ex Channel
     2: 1        Delay W/Ex (0.01 sec units)
     3: 1        Delay After Ex (0.01 sec units)
     4: 0000     mV Excitation

    35:  Full Bridge (P6)
     1: 1        Reps
     2: 22       7.5 mV 60 Hz Rejection Range
     3: 3        DIFF Channel
     4: 3        Excite all reps w/Exchan 3
```

```
   5: 2500     mV Excitation
   6: 1        Loc [ Vr       ]
   7: 1.0      Multiplier
   8: 0.0      Offset

  36:  Z=X*F (P37)
   1: 1        X Loc [ Vr       ]
   2: 0.001    F
   3: 1        Z Loc [ Vr       ]

  37:  Z=X*F (P37)
   1: 1        X Loc [ Vr       ]
   2: -2       F
   3: 2        Z Loc [ Vr2      ]

  38:  Z=Z+1 (P32)
   1: 2        Z Loc [ Vr2      ]

  39:  Z=X/Y (P38)
   1: 1        X Loc [ Vr       ]
   2: 2        Y Loc [ Vr2      ]
   3: 3        Z Loc [ Vr_Vr2   ]

  40:  Z=F x 10^n (P30)
   1: 4        F
   2: 6        n, Exponent of 10
   3: 5        Z Loc [ _4e6     ]

;Input gage factor for FLK type gages
  41:  Z=F x 10^n (P30)
   1: 2.11     F
   2: 00       n, Exponent of 10
   3: 6        Z Loc [ GF       ]

  42:  Z=X/Y (P38)
   1: 5        X Loc [ _4e6     ]
   2: 6        Y Loc [ GF       ]
   3: 4        Z Loc [ Mult     ]

  43:  Z=X*Y (P36)
   1: 3        X Loc [ Vr_Vr2   ]
   2: 4        Y Loc [ Mult     ]
   3: 38    -- Z Loc [ M3_1     ]

44:  End (P95)

45:  Beginning of Loop (P87)
 1: 0000     Delay
 2: 9        Loop Count

  46:  Do (P86)
   1: 76       Pulse Port 6

  47:  Excitation with Delay (P22)
   1: 3        Ex Channel
   2: 1        Delay W/Ex (0.01 sec units)
   3: 1        Delay After Ex (0.01 sec units)
   4: 0000     mV Excitation

  48:  Full Bridge (P6)
   1: 1        Reps
```

```
    2: 22       7.5 mV 60 Hz Rejection Range
    3: 3        DIFF Channel
    4: 3        Excite all reps w/Exchan 3
    5: 2500     mV Excitation
    6: 1        Loc [ Vr        ]
    7: 1.0      Multiplier
    8: 0.0      Offset

   49:  Z=X*F (P37)
    1: 1        X Loc [ Vr        ]
    2: 0.001    F
    3: 1        Z Loc [ Vr        ]

   50:  Z=X*F (P37)
    1: 1        X Loc [ Vr        ]
    2: -2       F
    3: 2        Z Loc [ Vr2       ]

   51:  Z=Z+1 (P32)
    1: 2        Z Loc [ Vr2       ]

   52:  Z=X/Y (P38)
    1: 1        X Loc [ Vr        ]
    2: 2        Y Loc [ Vr2       ]
    3: 3        Z Loc [ Vr_Vr2    ]

   53:  Z=F x 10^n (P30)
    1: 4        F
    2: 6        n, Exponent of 10
    3: 5        Z Loc [ _4e6      ]

;Input gage factor for WFLA type gages
   54:  Z=F x 10^n (P30)
    1: 2.13     F
    2: 00       n, Exponent of 10
    3: 6        Z Loc [ GF        ]

   55:  Z=X/Y (P38)
    1: 5        X Loc [ _4e6      ]
    2: 6        Y Loc [ GF        ]
    3: 4        Z Loc [ Mult      ]

   56:  Z=X*Y (P36)
    1: 3        X Loc [ Vr_Vr2    ]
    2: 4        Y Loc [ Mult      ]
    3: 43    -- Z Loc [ M3_6      ]

57:  End (P95)

58:  Do (P86)
 1: 55       Set Port 5 Low

;Read Battery Voltage
59:  Batt Voltage (P10)
 1: 52       Loc [ BATT      ]

;Prepare datalogger to send output
60:  Do (P86)
 1: 10       Set Output Flag High (Flag 0)

;Set time stamp parameters
```

```
61:  Real Time (P77)^29728
 1: 110      Day,Hour/Minute (midnight = 0000)

;Set resolution of the results
62:  Resolution (P78)
 1: 1        High Resolution

;Copy data from input locations to output locations
63:  Sample (P70)^30050
 1: 46       Reps
 2: 7        Loc [ M1_1      ]

;Send output to storage module
64:  Serial Out (P96)
 1: 71       Storage Module


*Table 2 Program
  02: 0.0000    Execution Interval (seconds)

*Table 3 Subroutines

End Program
```

C.3 Vibrating Wire Strain Gage Data Acquisition System used in Structures Laboratory

A schematic of the data acquisition system used for monitoring the vibrating wire gages in the Structures Laboratory is shown in Figure C.3.1.

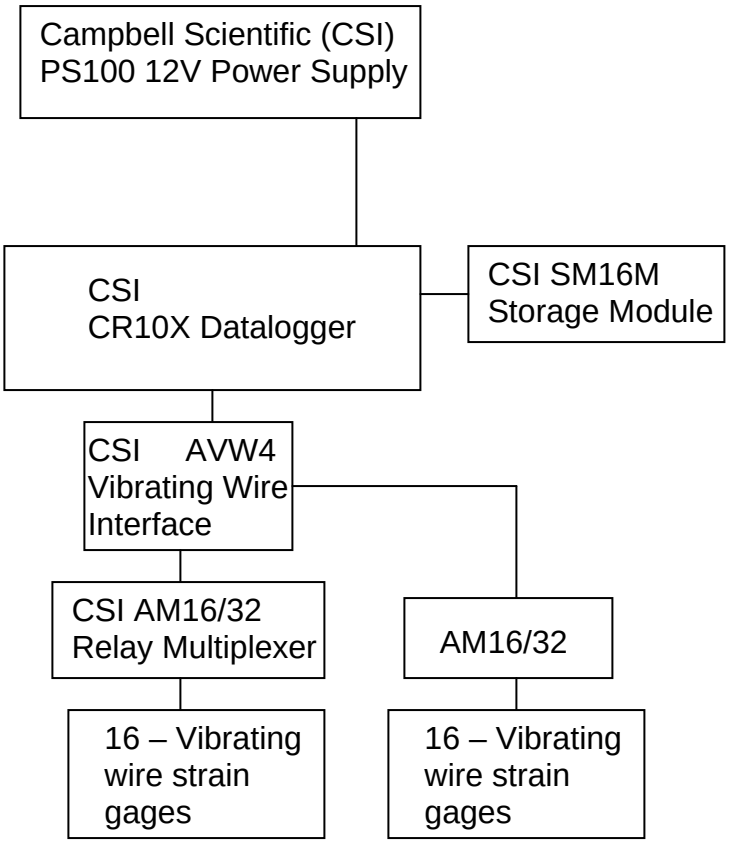

Figure C.3.1 Schematic of DAQ for Laboratory Specimen VW Gages

The program for monitoring vibrating wire strain gages in the structures laboratory over time and during testing was the same as that already shown for the live load truck test with modifications for the amounts of the two gage types and for having two rather than three multiplexers.

C.4 Load Cell Data Acquisition System used in Structures Laboratory

A schematic of the data acquisition system used for monitoring the load cells in the Structures Laboratory is shown in Figure C.4.1.

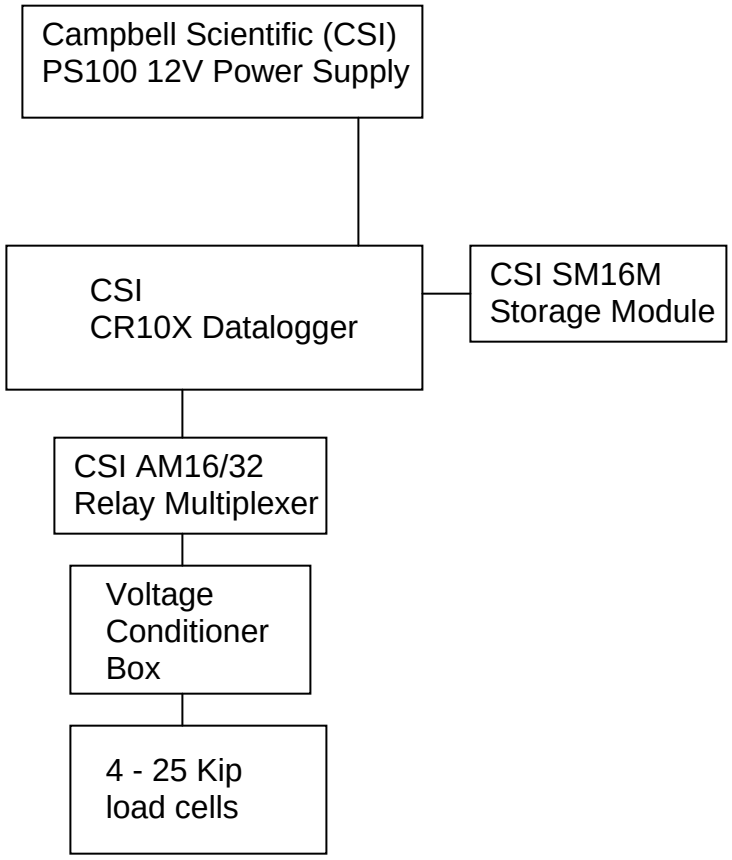

Figure C.4.1 Schematic of DAQ for Laboratory Specimen Load Cells

The program used by the datalogger to monitor end reaction load cells over time to determine restraint moments is given below. A simple differential voltage command was used to read the output from the voltage conditioner.

```
;{CR10X}
;
*Table 1 Program
  01: 900       Execution Interval (seconds)

;Turn on Multiplexer 1 and reset connection to the first channel
1:  Do (P86)
 1: 41       Set Port 1 High

;Begin loop
```

```
2:  Beginning of Loop (P87)
 1: 0000     Delay
 2: 4        Loop Count

;Switch to next channel on each pass through loop
     3:  Do (P86)
      1: 72       Pulse Port 2

;10ms pause to allow connection to settle
     4:  Excitation with Delay (P22)
      1: 1        Ex Channel
      2: 1        Delay W/Ex (0.01 sec units)
      3: 1        Delay After Ex (0.01 sec units)
      4: 0000     mV Excitation

;Differential voltage reading between the two leads from voltage conditioner
     5:  Volt (Diff) (P2)
      1: 1        Reps
      2: 25       2500 mV 60 Hz Rejection Range
      3: 1        DIFF Channel
      4: 1     -- Loc [ V1        ]
      5: 1.0      Multiplier
      6: 0.0      Offset

;end loop
6:  End (P95)

;Power down Multiplexer 1
7:  Do (P86)
 1: 51       Set Port 1 Low

;Read battery voltage
8:  Batt Voltage (P10)
 1: 5        Loc [ BATT      ]

;Prepare datalogger to send output
9:  Do (P86)
 1: 10       Set Output Flag High (Flag 0)

;Set time stamp parameters
10:  Real Time (P77)^15298
 1: 110      Day,Hour/Minute (midnight = 0000)

;Set resolution of the results
11:  Resolution (P78)
 1: 1        High Resolution

;Copy data from input locations to output locations
12:  Sample (P70)^20332
 1: 5        Reps
 2: 1        Loc [ V1        ]

;Send output to storage module
13:  Serial Out (P96)
 1: 71       Storage Module


*Table 2 Program
  02: 0.0000    Execution Interval (seconds)

*Table 3 Subroutines
```

End Program

C.4 Resistive Strain Gage and LVDT Data Acquisition Systems used in Structures Laboratory

Two data acquisition systems were used for monitoring the resistive strain gages in the Structures Laboratory during load testing. The first was the National Instruments (NI) SCXI-1000 data acquisition system which was used to measure strains from the 120Ω strain gages in the laboratory bridge specimen and the also displacements from the LVDT's. The second was the Campbell Scientific CR9000 data acquisition system used to measure strains from the 350Ω strain gages in the laboratory bridge specimen.

Appendix D: Restraint Moment Analysis Program

The following MATLAB M-file script was written to readily calculate the restraint moments using the P-method described in Sections 5.7, 6.7, and 7.7. Because the time dependent creep and shrinkage effects for the P-method were modeled using the AASHTO LRFD Specifications (2004) which gave equations as functions of time, the restraint moment could be calculated at any time. The PCA method, however, provided charts for creep and shrinkage values, so a similar procedure could only be performed if the charts were converted into equations, which was not done. The "%" symbols signify that the following text was notation, and not a functioning part of the script.

```
%Calculate Restraint Moment of laboratory specimen


%Section Properties of Beams in Span 1
%Area of Precast Section (in^2)
A_pc1=651;
%Overall Height and Width of Beam, Including Slab (in)
h=18;
b=72;
%Deck Thickness (in)
t_d=6;
%Deck Area (in^2)
A_cip1=466.5;
%Neutral axis height of transformed section and height of c.g.s. (in)
y_T=7.933;
y_ps=3;
%Distance from composite N.A. to c.g.s. (in)
d_1_1=y_T-y_ps;
%Distance from composite N.A. to center of deck (in)
d_2_1=h-t_d/2-y_T;


%Section Properties of Beams in Span 2
%Area of Precast Section (in^2)
A_pc2=705;
%Overall Height and Width of Beam, Including Slab (in)
h=18;
b=72;
%Deck Thickness (in)
t_d=6;
%Deck Area (in^2)
A_cip2=439.5;
%Neutral axis height of transformed section and height of c.g.s. (in)
y_T=7.865;
y_ps=3;
%Distance from composite N.A. to c.g.s. (in)
d_1_2=y_T-y_ps;
%Distance from composite N.A. to center of deck (in)
d_2_2=h-t_d/2-y_T;
```

```
%Strength Properties of Section 1
%Concrete Strengths: Precast Section 28 day, Precast Section initial,
Deck 28 day (ksi)
fc_pc1=12.9;
fci_pc1=7.5;
fc_cip1=4.155;

%Deck Mild Steel Elastic Modulus (ksi) and Area (in^2)
E_s1=29000;
A_s1=7.179;

%Concrete Elastic Modulus: Deck and Precast Section (ksi)
E_d1=33000*(.15-.005)^1.5*sqrt(fc_cip1);
E_b1=1265*sqrt(fc_pc1)+1000;

% Initial prestress force(k)
P_1_1=195*16*0.1527+20;

%Dead weight moment of Precast Section and Deck (in*k)
M_sw1=.155*A_pc1*256^2/(8*12^3);
M_cip1=.155*A_cip1*256^2/(8*12^3);


%Strength Properties of Section 2
%Concrete Strengths: Precast Section 28 day, Precast Section initial,
Deck 28 day (ksi)
fc_pc2=12.9;
fci_pc2=7.5;
fc_cip2=4.594;

%Deck Mild Steel Elastic Modulus (ksi) and Area (in^2)
E_s2=29000;
A_s2=7.179;

%Concrete Elastic Modulus: Deck and Precast Section (ksi)
E_d2=33000*(.15-.005)^1.5*sqrt(fc_cip2);
E_b2=1265*sqrt(fc_pc2)+1000;

%Initial prestress force (k)
P_1_2=195*16*0.1527+40;

%Dead weight moment of Precast Section and Deck (in*k)
M_sw2=.155*A_pc2*256^2/(8*12^3);
M_cip2=.155*A_cip2*256^2/(8*12^3);


%Relative Humidity (%) and Shrinkage Factor
RH1=50;
if RH1 < 80
    kh1=(140-RH1)/70;
else
    kh1=3*(100-RH1)/70;
end

RH2=50;
if RH2 < 80
    kh2=(140-RH2)/70;
else
    kh2=3*(100-RH2)/70;
end

%Creep Factor for Concrete Strength
kf1=1/(.67+fc_pc1/9);
```

```
kf2=1/(.67+fc_pc2/9);

% Volume to Surface ratio for Precast Section and Deck (in)
% before continuity (never used as rotations due to creep and
% shrinkage of precast sections before continuity was not restrained)
vs_pc11=3.89;
vs_pc21=4.21;
% after continuity
vs_pc12=6.78;
vs_cip1=7.07;
vs_pc22=7.34;
vs_cip2=6.66;

%Shrinkage Moment Reduction Factor due to restraint of deck steel and
%precast section
beta1=(1/(1+E_b1*A_pc1/(E_d1*A_cip1)))*(1/(1+E_s1*A_s1/(E_d1*A_cip1))
);
beta2=(1/(1+E_b2*A_pc2/(E_d2*A_cip2)))*(1/(1+E_s2*A_s2/(E_d2*A_cip2))
);

% Span 1 Times
%Time of Prestress Transfer (days)
ti1=1;
%Moist cure time of Precast Section (days)
td_pc1=1;

%Moist cure time of Deck (days) (All deck cast together)
td_cip=8;

% Span 2 Times
%Time of Prestress Transfer (days)
ti2=1;
%Moist cure time of Precast Section (days)
td_pc2=1;

%Time (days) that Span 2 is cast after Span 1
tD=0;

if td_cip < 5
    kd_cip=1.2;
else
    kd_cip=1;
end

if td_pc1 < 5
    kd_pc1=1.2;
else
    kd_pc1=1;
end

if td_pc2 < 5
    kd_pc2=1.2;
else
    kd_pc2=1;
end

% %For Steam Cured Beams (beams not steam cured)
% kd_pc1=1;
% kd_pc2=1;

%Time(s) at Continuity (days)
TC=[7];
```

```
%Time After Continuity (days)
% (The times for which the restraint moment will be predicted)
TA=[1:1:250]';
TB=[260:10:7000]';
TA=[TA;TB];

% Maximum values for upcoming indices
nc=length(TC);
n=length(TA);
% Empty matrices to store upcoming calcs
RM1=zeros(n,1);RM2=zeros(n,1);
Ms1=zeros(n,1);Ms2=zeros(n,1);
C1_1=zeros(n,1);C1_2=zeros(n,1);
C2_1=zeros(n,1);C2_2=zeros(n,1);
C3_1=zeros(n,1);C3_2=zeros(n,1);

vmax1=zeros(1,nc);
vmax2=zeros(1,nc);

% Prestress Moment Calcs
Mp1=P_1_1*d_1_1;
Mp2=P_1_2*d_1_2;

% Loop through time(s) of continuity
for j=1:nc

 tc1=TC(j);
    tc2=TC(j)-tD;

% Creep and shrinkage constants
    kc_cont1=(((tc1-ti1)/(26*exp(0.36*vs_pc12)+(tc1-ti1)))/((tc1-
ti1)/(45+(tc1-ti1))))*((1.80+1.77*exp(-0.54*vs_pc12))/2.587);
    ks_cont1=(((tc1-td_pc1)/(26*exp(0.36*vs_pc12)+(tc1-
td_pc1)))/((tc1-td_pc1)/(45+(tc1-td_pc1))))*((1064-94*vs_pc12)/923);

    kc_cont2=(((tc2-ti2)/(26*exp(0.36*vs_pc22)+(tc2-ti2)))/((tc2-
ti2)/(45+(tc2-ti2))))*((1.80+1.77*exp(-0.54*vs_pc22))/2.587);
    ks_cont2=(((tc2-td_pc2)/(26*exp(0.36*vs_pc22)+(tc2-
td_pc2)))/((tc2-td_pc2)/(45+(tc2-td_pc2))))*((1064-94*vs_pc22)/923);

    esh_cont1=kh1*ks_cont1*((tc1-td_pc1)/(35+(tc1-
td_pc1)))*kd_pc1*0.51e-3;
    v_cont1=3.5*kc_cont1*kf1*(1.58-RH1/120)*(ti1^-0.118)*((tc1-
ti1)^0.6)/(10+(tc1-ti1)^0.6);

    esh_cont2=kh2*ks_cont2*((tc2-td_pc2)/(35+(tc2-
td_pc2)))*kd_pc2*0.51e-3;
    v_cont2=3.5*kc_cont2*kf2*(1.58-RH2/120)*(ti2^-0.118)*((tc2-
ti2)^0.6)/(10+(tc2-ti2)^0.6);

% Loop through times for calculation
    for i=1:n

        t1=tc1+TA(i);
        t2=tc2+TA(i);

% Time dependant creep and shrinkage values
        kc1=(((t1-ti1)/(26*exp(0.36*vs_pc12)+(t1-ti1)))/((t1-
ti1)/(45+(t1-ti1))))*((1.80+1.77*exp(-0.54*vs_pc12))/2.587);

kc_after1=(((TA(i))/(26*exp(0.36*vs_pc12)+(TA(i))))/((TA(i))/(45+(TA(
i)))))*((1.80+1.77*exp(-0.54*vs_pc12))/2.587);
```

```
        ks_pc1=(((t1-td_pc1)/(26*exp(0.36*vs_pc12)+(t1-
td_pc1)))/((t1-td_pc1)/(45+(t1-td_pc1))))*((1064-94*vs_pc12)/923);
        esh_after1=kh1*ks_pc1*((t1-td_pc1)/(35+(t1-
td_pc1)))*kd_pc1*0.51e-3;


        kc2=(((t2-ti2)/(26*exp(0.36*vs_pc22)+(t2-ti2)))/((t2-
ti2)/(45+(t2-ti2))))*((1.80+1.77*exp(-0.54*vs_pc22))/2.587);

kc_after2=(((TA(i))/(26*exp(0.36*vs_pc22)+(TA(i))))/((TA(i))/(45+(TA(
i)))))*((1.80+1.77*exp(-0.54*vs_pc22))/2.587);
        ks_pc2=(((t2-td_pc2)/(26*exp(0.36*vs_pc22)+(t2-
td_pc2)))/((t2-td_pc2)/(45+(t2-td_pc2))))*((1064-94*vs_pc22)/923);
        esh_after2=kh2*ks_pc2*((t2-td_pc2)/(35+(t2-
td_pc2)))*kd_pc2*0.51e-3;

        if TA(i) <= td_cip
            ks_cip1=0;
            ks_cip2=0;
        else
            ks_cip1=(((TA(i)-td_cip)/(26*exp(0.36*vs_cip1)+(TA(i)-
td_cip)))/((TA(i)-td_cip)/(45+(TA(i)-td_cip))))*((1064-
94*vs_cip1)/923);
            ks_cip2=(((TA(i)-td_cip)/(26*exp(0.36*vs_cip2)+(TA(i)-
td_cip)))/((TA(i)-td_cip)/(45+(TA(i)-td_cip))))*((1064-
94*vs_cip2)/923);
        end

        esh_cip1=kh1*ks_cip1*((TA(i)-td_cip)/(35+(TA(i)-
td_cip)))*kd_cip*0.51e-3;
        esh_cip2=kh2*ks_cip2*((TA(i)-td_cip)/(35+(TA(i)-
td_cip)))*kd_cip*0.51e-3;


        es1=esh_cip1-(esh_after1-esh_cont1);
        es2=esh_cip2-(esh_after2-esh_cont2);


        v1=3.5*kc1*kf1*(1.58-RH1/120)*(ti1^-0.118)*((t1-
ti1)^0.6)/(10+(t1-ti1)^0.6);
        v2=3.5*kc2*kf2*(1.58-RH2/120)*(ti2^-0.118)*((t2-
ti2)^0.6)/(10+(t2-ti2)^0.6);

% Store max creep values
        if v1 > vmax1(1,j)
            vmax1(1,j)=v1;
        end

        if v2 > vmax2(1,j)
            vmax2(1,j)=v2;
        end


        v_after1=3.5*kc_after1*kf1*(1.58-RH1/120)*(tc1^-
0.118)*((TA(i))^0.6)/(10+(TA(i))^0.6);
        v_after2=3.5*kc_after2*kf2*(1.58-RH2/120)*(tc2^-
0.118)*((TA(i))^0.6)/(10+(TA(i))^0.6);


        Ms1(i,1)=es1*E_d1*A_cip1*d_2_1*beta1;
        Ms2(i,1)=es2*E_d2*A_cip2*d_2_2*beta2;
```

```
% Constants to evaluate contributions of various components to
restraint
% moment
        C1_1(i,1)=exp(-1*v_cont1)-exp(-1*v1);
        C1_2(i,1)=exp(-1*v_cont2)-exp(-1*v2);

        C2_1(i,1)=1-exp(-1*v_after1);
        C2_2(i,1)=1-exp(-1*v_after2);

        C3_1(i,1)=(1-exp(-1*v_after1))/v_after1;
        C3_2(i,1)=(1-exp(-1*v_after2))/v_after2;

        RM1_1=(1.403*d_1_1*P_1_1-0.935*M_sw1)*(exp(-1*v_cont1)-exp(-
1*v1))-0.935*M_cip1*(1-exp(-1*v_after1))-1.403*Ms1(i,j)*((1-exp(-
1*v_after1))/v_after1);
        RM1_2=(-0.046*d_1_2*P_1_2+0.031*M_sw2)*(exp(-1*v_cont2)-exp(-
1*v2))+0.031*M_cip2*(1-exp(-1*v_after2))+0.046*Ms2(i,j)*((1-exp(-
1*v_after2))/v_after2);

        RM2_1=(-0.046*d_1_1*P_1_1+0.031*M_sw1)*(exp(-1*v_cont1)-exp(-
1*v1))+0.031*M_cip1*(1-exp(-1*v_after1))+0.046*Ms1(i,j)*((1-exp(-
1*v_after1))/v_after1);
        RM2_2=(1.403*d_1_2*P_1_2-0.935*M_sw2)*(exp(-1*v_cont2)-exp(-
1*v2))-0.935*M_cip2*(1-exp(-1*v_after2))-1.403*Ms2(i,j)*((1-exp(-
1*v_after2))/v_after2);

        RM1(i,j)=RM1_1+RM1_2;
        RM2(i,j)=RM2_1+RM2_2;
 end
end

% Plot Results
figure(1)
hold off;plot(TA,RM1(:,1),'b');hold on;plot(TA,RM2(:,1),'r:');
title('\bf\fontsize{20}Restraint Moment vs. Time: TC=7
tD=0');ylabel('M_R (in*kips)');
xlabel('t (days)');legend('RM Span 1','RM Span 2');grid on;
axis([0 250 -Inf Inf]);
set(gca,'xtick',0:10:250);

figure(2)
hold off;plot(TA,Ms1,'b',TA,Ms2,'r:');
title('\bf\fontsize{20}Shrinkage Moment vs. Time: TC=7
tD=0');ylabel('M_S (in*kips)');
xlabel('t (days)');legend('Ms1','Ms2');grid on;
axis([0 250 -Inf Inf]);
set(gca,'xtick',0:10:250);

figure(3)
hold off;plot(TA,C1_1,'b',TA,C1_2,'r:');
title('\bf\fontsize{20}C1 vs. Time: TC=7 tD=0');ylabel('C_1
(in*kips)');
xlabel('t (days)');legend('C1_1','C1_2');grid on;
axis([0 250 -Inf Inf]);
set(gca,'xtick',0:10:250);

figure(4)
hold off;plot(TA,C2_1,'b',TA,C2_2,'r:');
title('\bf\fontsize{20}C2 vs. Time: TC=7 tD=0');ylabel('C_2
(in*kips)');
xlabel('t (days)');legend('C2_1','C2_2');grid on;
axis([0 250 -Inf Inf]);
set(gca,'xtick',0:10:250);
```

```
figure(5)
hold off;plot(TA,C3_1,'b',TA,C3_2,'r:');
title('\bf\fontsize{20}C3 vs. Time: TC=7 tD=0');ylabel('C_3
(in*kips)');
xlabel('t (days)');legend('C3_1','C3_2');grid on;
axis([0 250 -Inf Inf]);
set(gca,'xtick',0:10:250);

max1=zeros(2,nc);
tmax1=zeros(2,nc);
for i=1:nc
    [max1(1,i) j]=max(RM1(:,i));
    tmax1(1,i)=TA(j);
    [max1(2,i) j]=min(RM1(:,i));
    tmax1(2,i)=TA(j);
end

max2=zeros(2,nc);
tmax2=zeros(2,nc);
for i=1:nc
    [max2(1,i) j]=max(RM2(:,i));
    tmax2(1,i)=TA(j);
    [max2(2,i) j]=min(RM2(:,i));
    tmax2(2,i)=TA(j);
end
```

Appendix E: Laboratory Specimen Instrumentation Designation and Measured Locations

E.1 Laboratory Specimen Instrumentation Designation

The instrumentation for the laboratory specimen was labeled as follows. An example designation is given in Figure E.1.1.

1. The first character indicated the type of gage.
   - C = VW concrete embedment gage
   - F = Strand resistive gage
   - M = Polyester Mold concrete resistive gage
   - P = Polyester Wire surface resistive gage
   - S = VW spot-weldable gage
   - V = 120Ω waterproof resistive gage
   - W = 350Ω waterproof resistive gage

2. The second character indicated the span in which the gages were located.
   - 1 = West span
   - 2 = East span
   - D = CL Pier

3. The third character indicated the precast section within the span in which the gages were located.
   - N = North precast section
   - S = South precast section
   - J = Joint

There was a hyphen after the third character.

4. The fourth character indicated the position of the gages along the precast section.
   - 1 = Pinned end of the beam
   - 2 = Outer quarter point
   - 3 = Midspan
   - 4 = Inner quarter point
   - 5 = Continuous end of the beam

5. The fifth character indicated where the gage was located in the depth of the cross section.

Curvature Gages:

Flange Region
   - 1 = Gage on strand

- 2 = Gage at bottom of R/F cage
- 3 = Gage on deck steel

Web Region
- 1 = Gage on strand
- 2 = Gage on mild R/F in beam
- 3 = Gage on deck steel

Composite Action Gages (Additional to those used for long. curvature):

Flange Region
- 5 = Gage at top of R/F cage

Web Region
- 4 = Gage half-way between strand and mild R/F

Prestress Loss Gages:
- 1 = Center of Gravity of Strands

Transverse Gages:
- 1 = Gage over flange
- 2 = Gage over web corner

Bursting Gages:
- M = Mid-height of web

6. The sixth character indicated the orientation of the gage.
- L = Longitudinal
- T = Transverse
- V = Vertical

There was a hyphen after the sixth character.

7. The seventh character indicated the number of the gage at that position. For transverse gages, the numbering increased from south to north. For longitudinal gages, the numbering increased from the outside of the specimen to the middle of the specimen. For bursting rebar gages, the numbering increased from the stirrup closest to the face of the beam toward the center of the precast section.

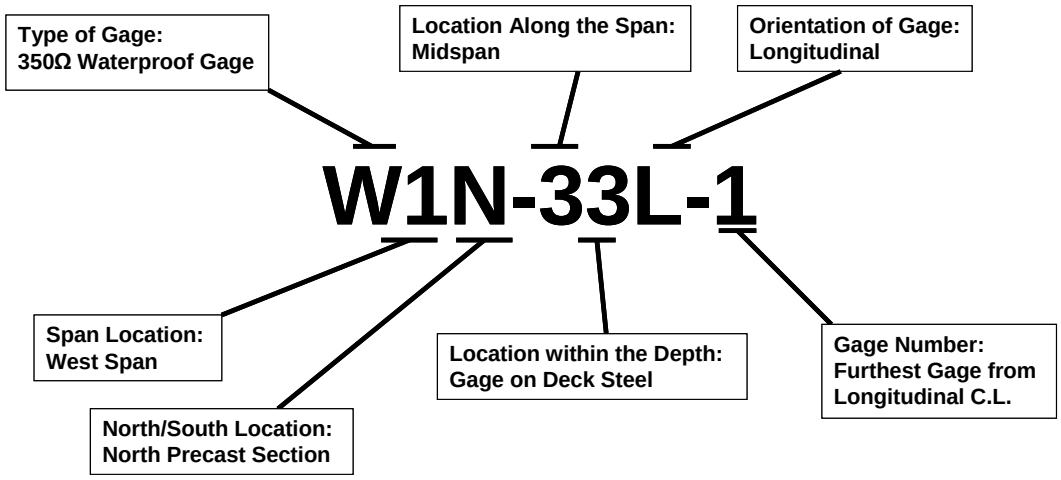

Figure E.1.1: Laboratory specimen strain gage designation example

Gages used solely for the measurement of the prestressing force were labeled as follows, and an example is given in Figure E.1.2.

1. The first character indicated the type of gage: F for strand gage

2. The next two characters designated the strand on which the gage was placed. Looking from the live end, the top row of strands was designated 01-08 left to right and the bottom row was 09-16 left to right. The partially stressed strands in the flanges were not counted in the numbering scheme, and the gages on these strands were given an "X".

There was a hyphen after the first three characters.

3. Next there was a character to designate where along the bed the gage was located.
- 1 = Free strand at live end
- 2 = In first beam (beam 1) closest to live end
- 3 = Free strand between beams 1 and 2
- 4 = In second beam
- 5 = Free strand between beams 2 and 3
- 6 = In third beam
- 7 = Free strand between beams 3 and 4
- 8 = In fourth beam (closest to dead end)
- 9 = Free strand at dead end

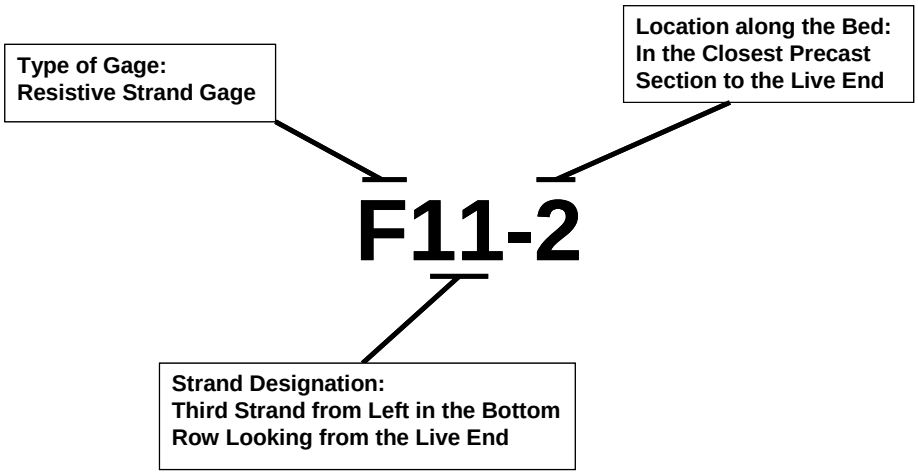

Figure E.1.2: Prestress measurement strain gage designation example

E.2 Measured Locations of Laboratory Specimen Instrumentation

All of the instrumentation in the laboratory specimen was measured to the nearest ¼ in. The sign convention of the gage ordinates is shown in Figure E.2.1. The X axis was measured in the E-W direction from the centerline of the pier (E positive); Y was measured in the N-S direction from the joint (N positive); the Z axis was measured in the vertical direction from the bottom of the precast sections (upward positive). The measurements are given in Table E.2.1.

The strain gages only used in the precast facility are given in Table E.2.2. Here the measurements of the gages are relative to the precast section they are in where X and Y are measured longitudinally and transversely, respectively, from the corner that would be placed on the interior over the pier.

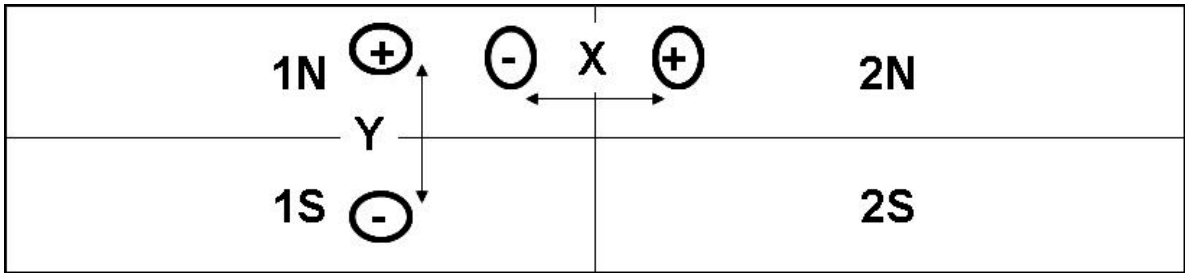

Figure E.2.1: Sign convention for the strain gage location measurements

Table E.2.1: Global Gage Locations for Instruments in Laboratory Bridge Specimen

X from CL pier (E+);Y from joint (N+); Z from bottom of section			
Gage	X	Y	Z
M1J-11T-1	-255	-7	6
M1J-11T-2	-257.5	-4.5	6
M1J-11T-3	-255	0	6
M1J-11T-4	-257.5	4.5	6
M1J-11T-5	-255	7	6
M1J-12T-1	-253.5	-18.5	14.25
M1J-12T-2	-251	-14.5	14.25
M1J-12T-3	-253.5	-10.5	14.25
M1J-12T-4	-251	-6.5	14.25
M1J-12T-5	-253.5	-2.5	14.25
M1J-12T-6	-251	2.5	14.25
M1J-12T-7	-253.5	6.5	14.25
M1J-12T-8	-251	10.5	14.25
M1J-12T-9	-253.5	14.5	14.25
M1J-12T-10	-251	18.5	14.25
M1J-21T-1	-194.5	-7	7
M1J-21T-2	-197.5	-4.5	7
M1J-21T-3	-194.5	0	7
M1J-21T-4	-197.5	4.5	7
M1J-21T-5	-194.5	7	7
M1J-31T-1	-134	-7	6
M1J-31T-2	-136.5	-4	6

X from CL pier (E+);Y from joint (N+); Z from bottom of section			
Gage	X	Y	Z
M1J-31T-3	-134	0	3
M1J-31T-4	-136.5	4.5	6
M1J-31T-5	-134	7	6
M1J-32T-1	-134.5	-18.5	14
M1J-32T-2	-132	-14.5	14
M1J-32T-3	-134.5	-10.5	14
M1J-32T-4	-132	-6.5	14
M1J-32T-5	-134.5	-2.5	14
M1J-32T-6	-132	2.5	14
M1J-32T-7	-134.5	6.5	14
M1J-32T-8	-132	10.5	14
M1J-32T-9	-134.5	14.5	14
M1J-32T-10	-132	18.5	14
M1J-41T-1	-74	-7	6
M1J-41T-2	-76.5	-4.5	6
M1J-41T-3	-74	0	6
M1J-41T-4	-76.5	4.5	6
M1J-41T-5	-74	7	6
M1J-51T-1	-26	-7	6
M1J-51T-2	-29	-4.5	6
M1J-51T-3	-26	0	6
M1J-51T-4	-29	4.5	6

X from CL pier (E+);Y from joint (N+); Z from bottom of section			
Gage	X	Y	Z
M1J-51T-5	-26	7	6
M1J-52T-1	-27.5	-18.5	14
M1J-52T-2	-25	-14.5	14
M1J-52T-3	-27.5	-10.5	14
M1J-52T-4	-25	-6.5	14
M1J-52T-5	-27.5	-2.5	14
M1J-52T-6	-25	2.5	14
M1J-52T-7	-27.5	6.5	14
M1J-52T-8	-25	10.5	14
M1J-52T-9	-27.5	14.5	14
M1J-52T-10	-25	18.5	14
M2J-11T-1	257.75	-7	7.25
M2J-11T-2	255	-4.5	7.25
M2J-11T-3	257.75	0	7.25
M2J-11T-4	255	4.5	7.25
M2J-11T-5	257.75	7	7.25
M2J-12T-1	255	-18.5	13.75
M2J-12T-2	257.5	-14.5	13.75
M2J-12T-3	255	-10.5	13.75
M2J-12T-4	257.5	-6.5	13.75
M2J-12T-5	255	-2.5	13.75
M2J-12T-6	257.5	2.5	13.75

X from CL pier (E+);Y from joint (N+); Z from bottom of section			
Gage	X	Y	Z
M2J-12T-7	255	6.5	13.75
M2J-12T-8	257.5	10.5	13.75
M2J-12T-9	255	14.5	13.75
M2J-12T-10	257.5	18.5	13.75
M2J-21T-1	198	-7	6.5
M2J-21T-2	195.5	-4.5	6.5
M2J-21T-3	198	0	6.5
M2J-21T-4	195.5	4.5	6.5
M2J-21T-5	198	7	6.5
M2J-31T-1	147.5	-7	7.25
M2J-31T-2	145	-4.5	7.25
M2J-31T-3	147.5	0	7.25
M2J-31T-4	145	4.5	7.25
M2J-31T-5	147.5	7	7.25
M2J-32T-1	134	-18.5	13.5
M2J-32T-2	136.5	-14.5	13.5
M2J-32T-3	134	-10.5	13.5
M2J-32T-4	136.5	-6.5	13.5
M2J-32T-5	134	-2.5	13.5
M2J-32T-6	136.5	2.5	13.5
M2J-32T-7	134	6.5	13.5
M2J-32T-8	136.5	10.5	13.5

X from CL pier (E+);Y from joint (N+); Z from bottom of section			
Gage	X	Y	Z
F1N-21L-1	-76.5	44.25	1.75
F1N-21L-2	-76.5	20.25	1.75
F1N-21L-3	-78.5	2.25	1.75
F1N-31L-1	-135.75	56.5	2
F1N-31L-2	-136.5	45	2
F1N-31L-3	-136.75	21	1.75
F1N-41L-1	-194.5	44.25	1.75
F1N-41L-2	-195.5	20.25	1.75
F1N-41L-3	-194.5	2.25	1.75
F1N-51L-1	-22.5	44.25	1.75
F1N-51L-2	-21	20.25	1.75
F1N-51L-3	-22.5	2.25	1.75
F1N-51L-4	-15.5	3	1.75
M1N-52L-1	-22.5	52.5	9.5
M1N-52L-2	-22	32.5	9.25
M1N-52L-3	-23.5	18	9.25

X from CL pier (E+);Y from joint (N+); Z from bottom of section			
Gage	X	Y	Z
F2N-21L-1	198	44	1.75
F2N-21L-2	199	21	1.75
F2N-21L-3	198	3.5	2
F2N-31L-1	136.75	45	1.75
F2N-31L-2	136.5	21	1.75
F2N-31L-3	136.5	3.75	2
F2N-41L-1	79.5	44.25	2
F2N-41L-2	80	21.25	1.75
F2N-41L-3	78.5	3.75	2
F2N-51L-1	21	57	2.25
F2N-51L-2	19.5	39	2
F2N-51L-3	20.25	21	2
F2N-51L-4	20.75	3.5	2
M2N-52-1	22	53	8.5
M2N-52-2	22.5	39.5	9
M2N-52-3	22.5	17.75	9.25

X from CL pier (E+);Y from joint (N+); Z from bottom of section			
Gage	X	Y	Z
M1N-34L-2	-136	22	6.25
C1N-31L-1	-137.5	36	2.5
C1N-31L-2	-134	7	1.5
F1N-1MV-1a	-269.5	58.25	6.75
F1N-1MV-2a	-267.5	58.25	6.75
W1N-5MV-1b	-4.75	57.5	6.5
W1N-22L-1	-197	42.5	9.5
W1N-22L-2	-197	21.5	9.5
W1N-32L-1	-137	43	9
W1N-32L-2	-136	22	9.25
W1N-42L-1	-80	42.5	9.25
W1N-42L-2	-80	21.5	9.5
W1N-52L-1	-22.5	55	9.5
W1N-52L-2	-21.5	36	9.5
W1N-52L-3	-23	22	9.25

X from CL pier (E+);Y from joint (N+); Z from bottom of section			
Gage	X	Y	Z
W2N-22L-1	198	43	10
W2N-22L-2	198	22	10
W2N-32L-1	135.5	43	9.5
W2N-32L-2	135.75	21.5	9.5
W2N-42L-1	80	41.75	9.5
W2N-42L-2	79.5	21.25	9.5
W2N-52L-1	21.5	55.5	9.5
W2N-52L-2	22.75	35.25	9.5
W2N-52L-3	24	20.5	9.5
M2N-34L-2	136.5	21.5	6
W2N-5MV-1a	3.5	58	5.5
W2N-5MV-2a	7.5	58	5.5
W2N-1MV-1b	269.5	58	6
C2N-31L-1	136.75	36.5	2.75
C2N-31L-2	136.75	7	2.75

X from CL pier (E+);Y from joint (N+); Z from bottom of section			
Gage	X	Y	Z
C1J-11T-1	-243.5	0	6
C1J-21T-1	-183.5	0	6.5
C1J-31T-1	-123.5	0	6
C1J-41T-1	-64.5	0	6
C1J-51T-1	-15	0	6.5
C2J-11T-1	244.5	0	7.25
C2J-21T-1	207.5	0	7.25
C2J-31T-1	134.5	-8.5	7
C2J-31T-2	136.5	-5.5	7
C2J-31T-3	134.5	0	7
C2J-31T-4	136.5	5.5	7
C2J-31T-5	134.5	8.5	7
C2J-41T-1	87.5	0	7.25
C2J-51T-1	16.5	0	7.25
S1J-21T-1	-192	0	6.5
S1J-31T-1	-132.5	0	5.75
S1J-41T-1	-72.5	0	6.75
S1J-51T-1	-24	0	6.5
S2J-21T-1	202	0	7
S2J-31T-1	141.5	0	7
S2J-41T-1	81.5	0	7

X from CL pier (E+);Y from joint (N+); Z from bottom of section			
Gage	X	Y	Z
M2J-32T-9	134	14.5	13.5
M2J-32T-10	136.5	18.5	13.5
M2J-41T-1	77.75	-7	7.5
M2J-41T-2	75	-4.5	7.5
M2J-41T-3	77.75	0	7.5
M2J-41T-4	75	4.5	7.5
M2J-41T-5	77.75	7	7.5
M2J-51T-1	30	-7	6.75
M2J-51T-2	27	-4.5	6.75
M2J-51T-3	30	0	6.75
M2J-51T-4	27	4.5	6.75
M2J-51T-5	30	7	6.75
M2J-52T-1	25	-18.5	13.75
M2J-52T-2	27.5	-14.5	13.75
M2J-52T-3	25	-10.5	13.75
M2J-52T-4	27.5	-6.5	13.75
M2J-52T-5	25	-2.5	13.75
M2J-52T-6	27.5	2.5	13.75
M2J-52T-7	25	6.5	13.75
M2J-52T-8	27.5	10.5	13.75
M2J-52T-9	25	14.5	13.75
M2J-52T-10	27.5	18.5	13.75

X from CL pier (E+);Y from joint (N+); Z from bottom of section			
Gage	X	Y	Z
F1S-21L-1	-196.5	-44	1.75
F1S-21L-2	-197	-21	1.75
F1S-21L-3	-196.5	-3	2
F1S-31L-1	-138.5	-44.5	1.75
F1S-31L-2	-138	-21	1.75
F1S-31L-3	-138	-3	2
F1S-41L-1	-78.5	-39.25	1.75
F1S-41L-2	-79.5	-21	1.75
F1S-41L-3	-79	-3	2
F1S-51L-1	-21	-57	2.25
F1S-51L-2	-20	-38.5	2
F1S-51L-3	-21	-21	1.75
F1S-51L-4	-19	-3	2
W1S-1MV-1c	-269	-49.5	7.5
W1S-1MV-1d	-269.25	-58	5.5
W1S-1MV-2c	-267	-49.5	7.5
W1S-1MV-2d	-267.25	-58	5.5
W1S-5MV-1a	-4.75	-58	5.75
W1S-5MV-2a	-6	-58	5.75

X from CL pier (E+);Y from joint (N+); Z from bottom of section			
Gage	X	Y	Z
F2S-21L-1	197.5	-45	1.75
F2S-21L-2	198.5	-21	1.75
F2S-21L-3	199	-3.5	2
F2S-31L-1	139.5	-45	2
F2S-31L-2	140	-21	1.75
F2S-31L-3	141.5	-3.25	2
F2S-41L-1	79	-44.75	1.75
F2S-41L-2	79.5	-21	1.75
F2S-41L-3	79.5	-3	2
F2S-51L-1	23	-57	2
F2S-51L-2	22.5	-45.25	2
F2S-51L-3	22.5	-21.25	1.75
F2S-51L-4	22.5	-3	2
W2S-22L-1	198	-43	9
W2S-22L-2	197.75	-22	9.25
W2S-32L-1	138.5	-42.25	9.25
W2S-32L-2	139.5	-21.5	9.25
W2S-42L-1	19	-42	9.25
W2S-42L-2	79.5	-21.25	9.5
W2S-52L-1	23.5	-56	9.25
W2S-52L-2	23.5	-36	9.5
W2S-52L-3	23.5	-21.5	9.5

X from CL pier (E+);Y from joint (N+); Z from bottom of section			
Gage	X	Y	Z
W1N-22L-3	-196.5	8	8
W1N-23L-1	-196	45.5	14.5
W1N-23L-2	-195	20.5	14.5
W1N-23L-3	-195	3.75	15
W1N-32L-3	-137.5	8	8
W1N-33L-1	-138	45.25	14.5
W1N-33L-2	-137	20.5	14.25
W1N-33L-3	-137	4	14.75
W1N-42L-3	-77.5	8	7.5
W1N-43L-1	-79	44.75	14.5
W1N-43L-2	-78	19.75	14.25
W1N-43L-3	-78	3.5	14.75
W1N-52L-4	-20.5	3.25	5
W1N-53L-1	-20.5	57	14.25
W1N-53L-2	-20.5	39.75	14.25
W1N-53L-3	-20.5	20	14.5
W1N-53L-4	-20.5	3.24	15
W1S-22L-3	-196.5	-8	8
W1S-23L-1	-196	-42.5	14.5
W1S-23L-2	-196	-18.5	14.5
W1S-23L-3	-195	-4.5	15
W1S-32L-3	-137.5	-8.5	8

X from CL pier (E+);Y from joint (N+); Z from bottom of section			
Gage	X	Y	Z
W2N-43L-2	79	20.5	14.25
W2N-43L-3	79	2.75	14
W2N-52L-4	19	3	8.25
W2N-53L-1	20	56.75	14
W2N-53L-2	19	39	14.25
W2N-53L-3	21	19.5	14.5
W2N-53L-4	21	2.75	14.5
W2S-22L-3	197.5	-6.5	8.75
W2S-23L-1	196	-42.5	14.5
W2S-23L-2	195	-18.5	14.75
W2S-23L-3	195	-5	14.5
W2S-32L-3	137.5	-8	9
W2S-33L-1	137	-42	14.5
W2S-33L-2	137	-18	14.5
W2S-33L-3	137	-5	14
W2S-42L-3	77.5	-7.5	8.25
W2S-43L-1	78	-41.5	14.5
W2S-43L-2	78	-17.5	14.5
W2S-43L-3	79	-4.5	14.25
W2S-52L-4	19	-2.5	8.25
W2S-53L-1	22	-58.25	14.5
W2S-53L-2	22	-37.5	14.25

X from CL pier (E+);Y from joint (N+); Z from bottom of section			
Gage	X	Y	Z
W1S-22L-1	-197	-42.25	9
W1S-22L-2	-197	-21.5	9.25
W1S-32L-1	-139	-42.5	8.75
W1S-32L-2	-137.5	-21.5	9.25
W1S-42L-1	-78.75	-43	8.75
W1S-42L-2	-79.75	-21.5	9.5
W1S-52L-1	-20	-55.5	9
W1S-52L-2	-19.5	-36	9.25
W1S-52L-3	-18.5	-21.5	9.5
M1S-34L-2	-137.5	-21	7
C1S-31L-1	-139	-36	2.75
C1S-31L-2	-143	-6.75	1.75
M1S-52L-1	-20.5	-52.5	9
M1S-52L-2	-20.5	-39.5	9.25
M1S-52L-3	-18.5	-19	9.25

X from CL pier (E+);Y from joint (N+); Z from bottom of section			
Gage	X	Y	Z
M2S-34L-2	138.5	-21.5	5.5
C2S-31L-1	140.5	-36	2.75
C2S-31L-2	141	-7	2.5
W2S-1MV-1a	168.5	-58	6
W2S-1MV-2a	266.5	-58	6.25
W2S-5MV-1c	5.25	-49	7
W2S-5MV-1d	5.5	-58	7.25
W2S-5MV-2c	7.5	-49	7
W2S-5MV-2d	7.5	-58	7.25
M2S-52L-1	20	-53.5	9.25
M2S-52L-2	20	-39.5	9.5
M2s-52L-3	20	-18.5	9.5

X from CL pier (E+);Y from joint (N+); Z from bottom of section			
Gage	X	Y	Z
W1S-33L-1	-138	-42.75	14.25
W1S-33L-2	-138	-18.5	14.25
W1S-33L-3	-138	-4.5	14.75
W1S-42L-3	-77.5	-8	7
W1S-43L-1	-79	-42.5	14.5
W1S-43L-2	-79	-19	14.25
W1S-43L-3	-78	-4.5	14.5
W1S-52L-4	-20.5	-2.25	7.75
W1S-53L-1	-17	-58.25	14.25
W1S-53L-2	-17	-38	14.25
W1S-53L-3	-17	-22	14.25
W1S-53L-4	-19	-4.5	15
W2N-22L-3	197.5	8.75	9
W2N-23L-1	196	44.5	14.5
W2N-23L-2	196	20	14.5
W2N-23L-3	196	2.25	14.25
W2N-32L-3	137.5	-9	9
W2N-33L-1	137	45	14.5
W2N-33L-2	138	20	14
W2N-33L-3	138	2.5	14
W2N-42L-3	77.5	8	8.75
W2N-43L-1	79	45	14.5

X from CL pier (E+);Y from joint (N+); Z from bottom of section			
Gage	X	Y	Z
W2S-53L-3	24	-21.5	14.25
W2S-53L-4	19	-4	14.75
W1N-35L-3	-137.5	8	15.25
W1S-35L-3	-137.5	-8.5	15.25
W2N-35L-3	137.5	-9	15.25
W2N-35L-3	137.5	8.5	11.75
CDN-51L-1	0	6.5	2.625
CDS-51L-1	0	-6.75	2.5

X from pier end of beam;Y from joint side of beam; Z from bottom of beam			
Gage	X	Y	Z
R1N-11L-1	266.25	60	7
R1N-11V-1	266.25	60	7
R1N-11S-1	266.25	60	7
R1N-51L-1	2.75	60	6.5
R1N-51V-1	2.75	60	6.5
R1N-51S-1	2.75	60	6.5
R1S-11L-1	266.75	60	6.25
R1S-11V-1	266.75	60	6.25
R1S-11S-1	266.75	60	6.25
R1S-51L-1	3.25	60	6.25
R1S-51V-1	3.25	60	6.25
R1S-51S-1	3.25	60	6.25
R2N-51L-1	2.5	60	7.5
R2N-51V-1	2.5	60	7.5
R2N-51S-1	2.5	60	7.5
R2N-11L-1	267.5	60	7
R2N-11V-1	267.5	60	7
R2N-11S-1	267.5	60	7
R2S-11L-1	265	60	7
R2S-11V-1	265	60	7
R2S-11S-1	265	60	7
R2S-51L-1	2.75	60	7.25
R2S-51V-1	2.75	60	7.25
R2S-51S-1	2.75	60	7.25

Table E.2.2: Locations of Gages Used Only at Precast Facility

X from pier end of beam;Y from joint side of beam; Z from bottom of beam			
Gage	X	Y	Z
F01-2	19.5	57	3.25
F02-2	19.5	51	3.5
F03-2	18	45	3.75
F04-2	18.5	39	3.75
F05-2	19	33	3.75
F06-2	19	27	3.75
F07-2	20	21	3.75
F08-2	20	15	3.25
F10-2	19	51	1.75
F11-2	18.5	45	2
F13-2	19.5	33	2
F14-2	19.5	27	1.75
F16-2	19	15	2.25
FX1-2	12.5	11	1.75
FX2-2	12.5	3	3.75

X from pier end of beam;Y from joint side of beam; Z from bottom of beam			
Gage	X	Y	Z
F01-8	22	57	3.75
F02-8	22	51	3.75
F03-8	22	45	3.75
F04-8	21.5	39	4
F05-8	21.5	33	4
F06-8	21	27	4
F07-8	21	21	3.75
F08-8	20	15	3.75
F10-8	22	51	1.75
F11-8	22	39	1.75
F13-8	21.5	33	2
F14-8	20.5	21	1.75
F16-8	20.5	15	2.25

Appendix F: Center City Bridge Instrumentation Designation and Measured Locations

The instrumentation in the Center City Bridge was documented in Mn/DOT Report 2006-37 (Bell 2006). However, the instrument locations given were nominal, and the measured instrument locations are given in Table F.1. The measurements that differed from the Mn/DOT report are highlighted, italicized, and bold. The instrument designation convention is given in Figure F.1. The origin and sign convention of the strain gage measurements is given in Figure F.2. Web #1 was located between Joints #1 and 2, and Web #2 was located between Joints #2 and 3. The center of Joints 1, 2, and 3 are located at 128.5, 200.5 and 272.2 in., respectively from the parapet (i.e., measured distance "Y" in Figure F.1).

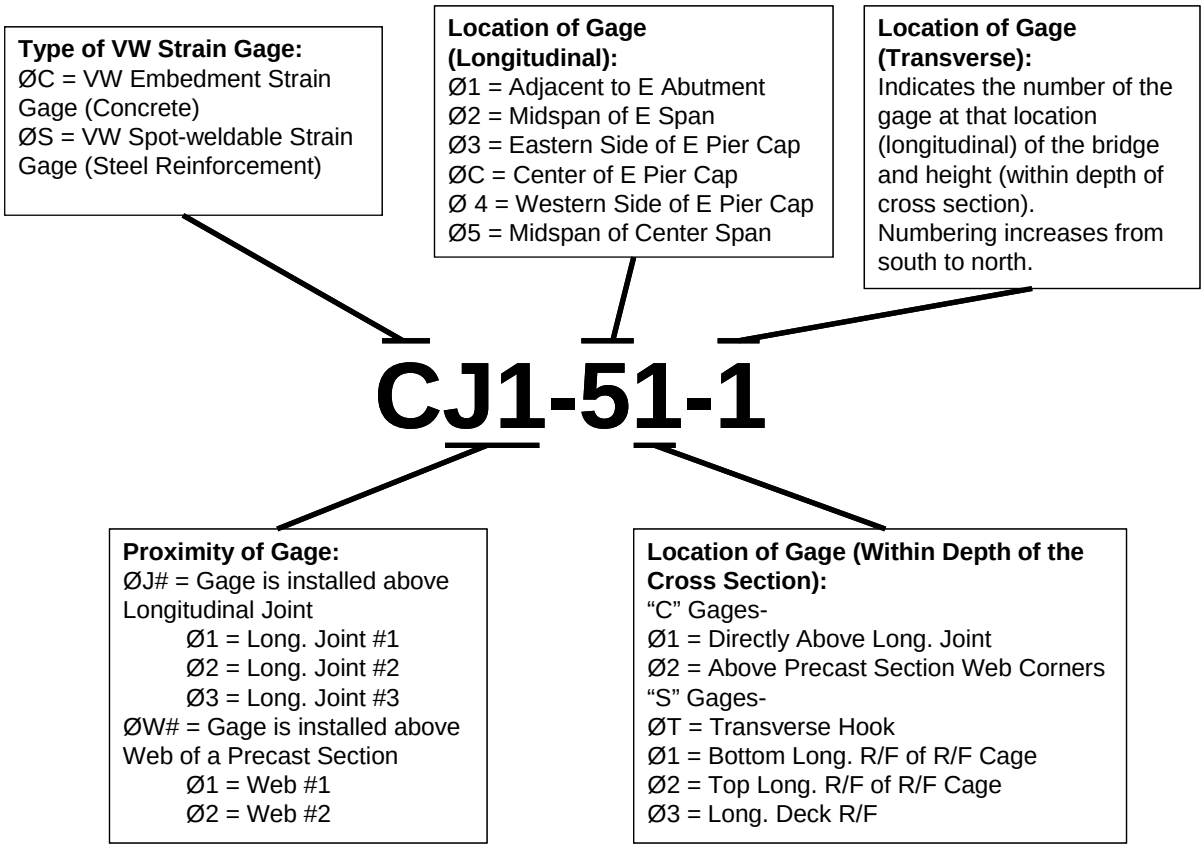

Figure F.1: Center City Bridge Instrumentation Designation

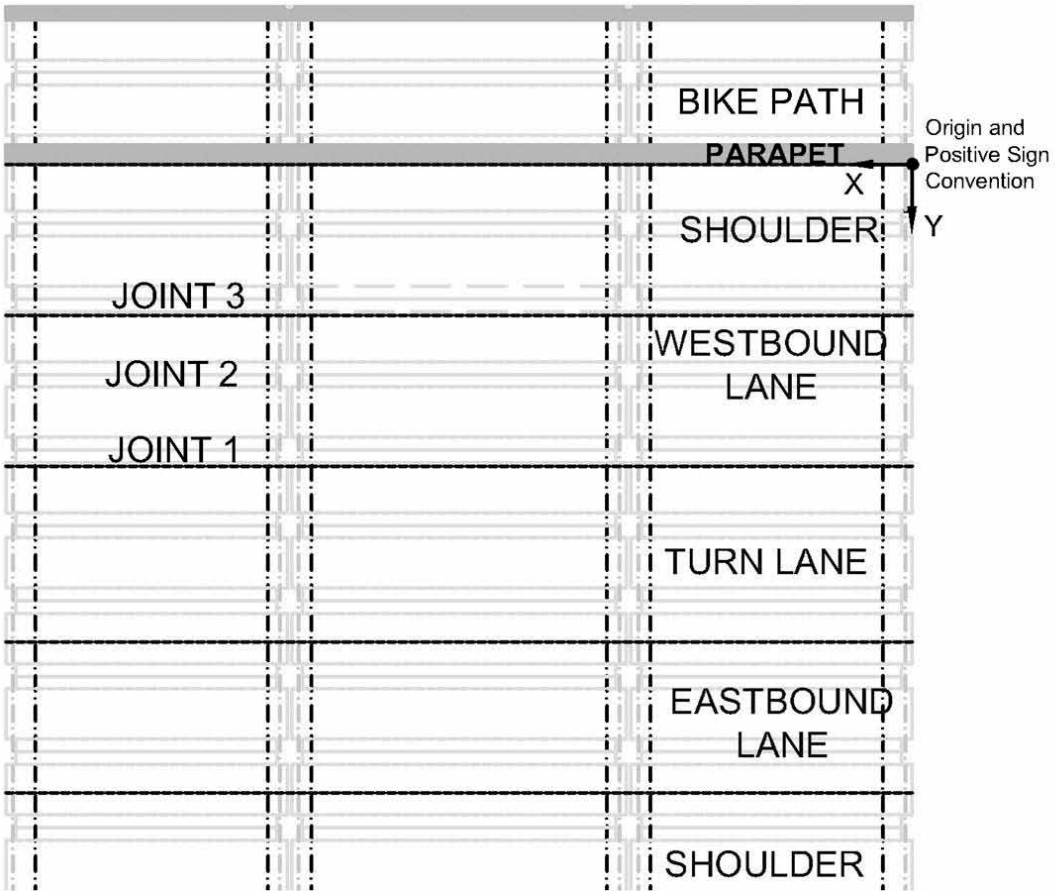

Figure F.2: Center City Bridge Measurement Origin and Sign Convention

Table F.1: Nominal and measured locations of longitudinal spot-weldable strain gages in the Center City Bridge

	Nominal (Mn/DOT 2006-37)			Measured		
Instrument	**X**	**Y**	**Z**	**X**	**Y**	**Z**
SJ1-51-1	429	264	9	429.00	***263.25***	***8.75***
SJ1-52-1	429	264	12.5	429.00	***263.25***	***12.00***
SJ1-53-1	427.5	276.5	15.5	427.50	***276.25***	***15.00***
SJ1-53-2	427.5	263.5	15.5	427.50	***264.50***	***15.00***
SJ1-41-1	290	268.5	9	290.00	***268.75***	9.00
SJ1-43-1	290	280	15.5	290.00	280.00	***15.00***
SJ1-43-2	290	268.5	15.5	290.00	268.50	***15.00***
SJ1-C1-1	271	268.5	9	271.00	***269.50***	9.00
SJ1-C3-1	271	268.5	15.5	271.00	268.50	***14.00***
SJ1-C3-2	271	296	15.5	271.00	296.00	***14.00***
SJ1-31-1	252	268.5	9	252.00	268.50	9.00
SJ1-33-1	251	280	15.5	***250.00***	280.00	***15.00***
SJ1-33-2	250	269.5	15.5	***249.00***	269.50	***15.00***
SJ1-21-1	128.5	264	9	128.50	264.00	9.00
SJ1-22-1	128.5	264	12.5	128.50	264.00	***13.00***
SJ1-23-1	130	261.5	15.5	130.00	261.50	15.50
SJ1-11-1	22	264	9	22.00	***264.25***	9.00
SJ1-12-1	22	264	12.5	22.00	***264.25***	***13.00***
SJ1-13-1	21	261.5	15.5	21.00	261.50	15.50
SJ2-51-1	427.5	192	9	427.50	***191.50***	9.00
SJ2-52-1	427.5	192	12.5	427.50	***191.50***	12.50
SJ2-53-1	426.5	193.5	15.5	426.50	193.50	***14.75***
SJ2-41-1	289.5	198	9	289.50	***198.25***	9.00
SJ2-43-1	291.5	197	15.5	291.50	197.00	***15.25***
SJ3-41-1	287	124.5	9	***287.50***	124.50	9.00
SJ3-43-1	286	124	15.5	***285.00***	124.00	***15.00***
SW1-43-1	292.5	249.5	15.5	292.50	249.50	***14.50***
SW1-43-2	292.5	236	15.5	292.50	236.00	***14.50***
SW1-43-3	292.5	225	15.5	***292.00***	225.00	***14.50***
SW2-43-1	291	177.5	15.5	***291.50***	***177.75***	***14.50***
SW2-43-2	291	165.5	15.5	291.00	165.50	***14.50***
SW2-43-3	291	154.5	15.5	291.00	***154.25***	***14.50***

Table F.2: Nominal and measured locations of transverse spot-weldable strain gages in the Center City Bridge

	Nominal (Mn/DOT 2006-37)			Measured		
Instrument	**X**	**Y**	**Z**	**X**	**Y**	**Z**
SJ1-5T-1	434	278.5	7	434.00	278.50	7.00
SJ1-5T-2	432.5	276.5	7	***432.25***	276.50	7.00
SJ1-5T-3	434	274.5	7	434.00	274.50	7.00
SJ1-5T-4	432.5	272.5	7	***432.25***	272.50	7.00
SJ1-5T-5	434	270.5	7	434.00	270.50	7.00
SJ1-5T-6	432.5	268.5	7	***432.25***	268.50	7.00
SJ1-5T-7	434	266.5	7	434.00	266.50	7.00
SJ2-5T-1	434	206.5	7	434.00	206.50	7.00
SJ2-5T-2	432.5	204.5	7	***433.00***	204.50	7.00
SJ2-5T-3	434	202.5	7	434.00	202.50	7.00
SJ2-5T-4	432.5	200.5	7	***433.00***	200.50	7.00
SJ2-5T-5	434	198.5	7	434.00	198.50	7.00
SJ2-5T-6	432.5	196.5	7	***433.00***	196.50	7.00
SJ2-5T-7	434	194.5	7	434.00	194.50	7.00
SJ3-5T-1	434	134.5	7	434.00	134.50	7.00
SJ3-5T-2	432.5	132.5	7	432.50	132.50	7.00
SJ3-5T-3	434	130.5	7	434.00	130.50	7.00
SJ3-5T-4	432.5	128.5	7	432.50	128.50	7.00
SJ3-5T-5	434	126.5	7	434.00	126.50	7.00
SJ3-5T-6	432.5	124.5	7	432.50	124.50	7.00
SJ3-5T-7	434	122.5	7	434.00	122.50	7.00

Table F.3: Nominal and measured locations of transverse concrete embedment strain gages in the Center City Bridge

	Nominal (Mn/DOT 2006-37)			Measured		
Instrument	X	Y	Z	X	Y	Z
CJ1-51-1	438	278.5	8.5	438.00	278.50	***8.25***
CJ1-51-2	438	275.5	8.5	438.00	275.50	***8.25***
CJ1-51-3	438	272.5	8.5	438.00	272.50	***8.25***
CJ1-51-4	438	269.5	8.5	438.00	269.50	***8.25***
CJ1-51-5	438	266.5	8.5	438.00	266.50	***8.25***
CJ2-51-1	438	206.5	8.5	***439.00***	206.50	***8.25***
CJ2-51-2	438	203.5	8.5	***439.00***	203.50	***8.25***
CJ2-51-3	438	200.5	8.5	***439.00***	200.50	***8.25***
CJ2-51-4	438	197.5	8.5	***439.00***	197.50	***8.25***
CJ2-51-5	438	194.5	8.5	***439.00***	194.50	***8.25***
CJ3-51-1	438	134.5	8.5	***438.50***	134.50	***8.25***
CJ3-51-2	438	131.5	8.5	***438.50***	131.50	***8.25***
CJ3-51-3	438	128.5	8.5	***438.50***	128.50	***8.25***
CJ3-51-4	438	125.5	8.5	***438.50***	125.50	***8.25***
CJ3-53-5	438	122.5	8.5	***438.50***	122.50	***8.25***
CJ1-53-1	438	293	13.5	***437.00***	293.00	13.50
CJ1-53-2	438	288.5	13.5	***437.00***	288.50	13.50
CJ1-53-3	438	284	13.5	***437.00***	284.00	13.50
CJ1-53-4	438	279.5	13.5	***437.00***	279.50	13.50
CJ1-53-5	438	275	13.5	***437.00***	275.00	13.50
CJ1-53-6	438	270.5	13.5	***437.00***	270.50	13.50
CJ1-53-7	438	266	13.5	***437.00***	266.00	13.50
CJ1-53-8	438	261.5	13.5	***437.00***	261.50	13.50
CJ1-53-9	438	257	13.5	***437.00***	257.00	13.50
CJ1-53-10	438	252.5	13.5	***437.00***	252.50	13.50
CJ2-53-1	438	221	13.5	438.00	221.00	13.50
CJ2-53-2	438	216.5	13.5	438.00	216.50	13.50
CJ2-53-3	438	212	13.5	438.00	212.00	13.50
CJ2-53-4	438	207.5	13.5	438.00	207.50	13.50
CJ2-53-5	438	203	13.5	438.00	203.00	13.50
CJ2-53-6	438	198.5	13.5	438.00	198.50	13.50
CJ2-53-7	438	194	13.5	438.00	194.00	13.50
CJ2-53-8	438	189.5	13.5	438.00	189.50	13.50
CJ2-53-9	438	185	13.5	438.00	185.00	13.50
CJ2-53-10	438	180.5	13.5	438.00	180.50	13.50
CJ3-53-1	438	149	13.5	***439.00***	149.00	13.50
CJ3-53-2	438	144.5	13.5	***439.00***	144.50	13.50
CJ3-53-3	438	140	13.5	***439.00***	140.00	13.50
CJ3-53-4	438	135.5	13.5	***439.00***	135.50	13.50
CJ3-53-5	438	131	13.5	***439.00***	131.00	13.50
CJ3-53-6	438	126.5	13.5	***439.00***	126.50	13.50
CJ3-53-7	438	122	13.5	***439.00***	122.00	13.50
CJ3-53-8	438	117.5	13.5	***439.00***	117.50	13.50
CJ3-53-9	438	113	13.5	***439.00***	113.00	13.50
CJ3-53-10	438	108.5	13.5	***439.00***	108.50	13.50

Appendix G: Complete Plotted Strain Measurements from Center City Bridge over 24-Month Monitoring Period

The following plots provide all of the measured strains for the 24 month monitoring period of the Center City Bridge as described in Chapter 3. Measured location and instrument designation are given in Appendix F. The strain gages were zeroed at 10:00am on October 1, 2005 when the lowest thermal gradient was observed through the depth of the cross section on the first day the readings were automatically taken at two hour intervals. For all of the strain values presented, mechanical strains are given that were obtained by subtracting the thermal strains from the total strains using the coefficient of thermal expansion discussed in Appendix H.

The data for gage SJ1-C3-2 in Figure G.17 is missing for the last three months of the monitoring period as the gage stopped reading for an unknown reason. It is not believed that the cracking at this location caused the error.

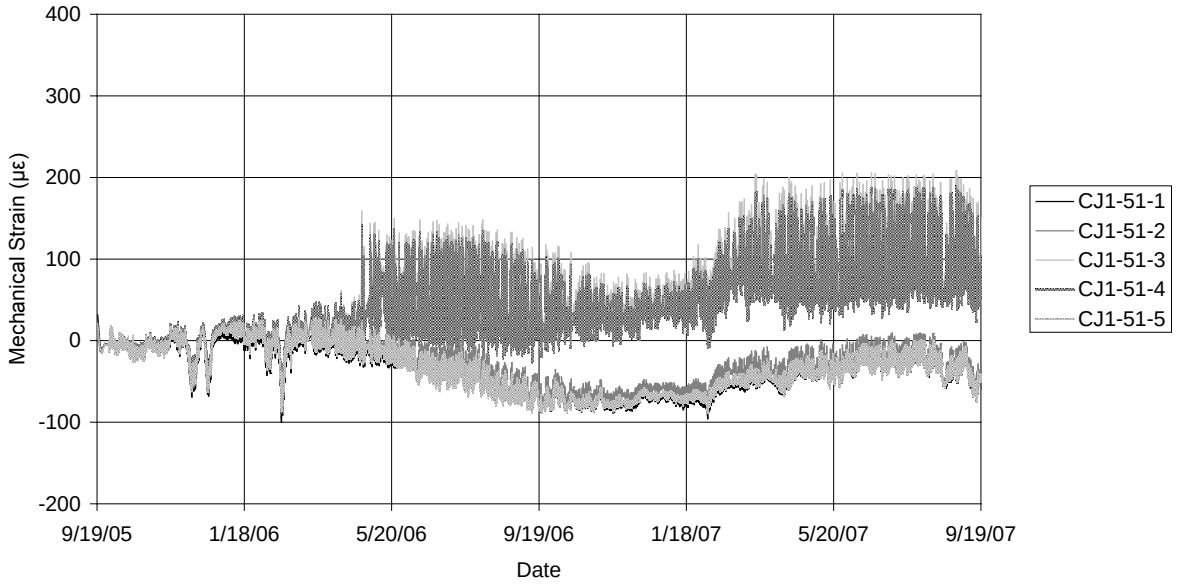

Figure G.1: Mechanical strains for transverse concrete embedment strain gages immediately over Joint 1

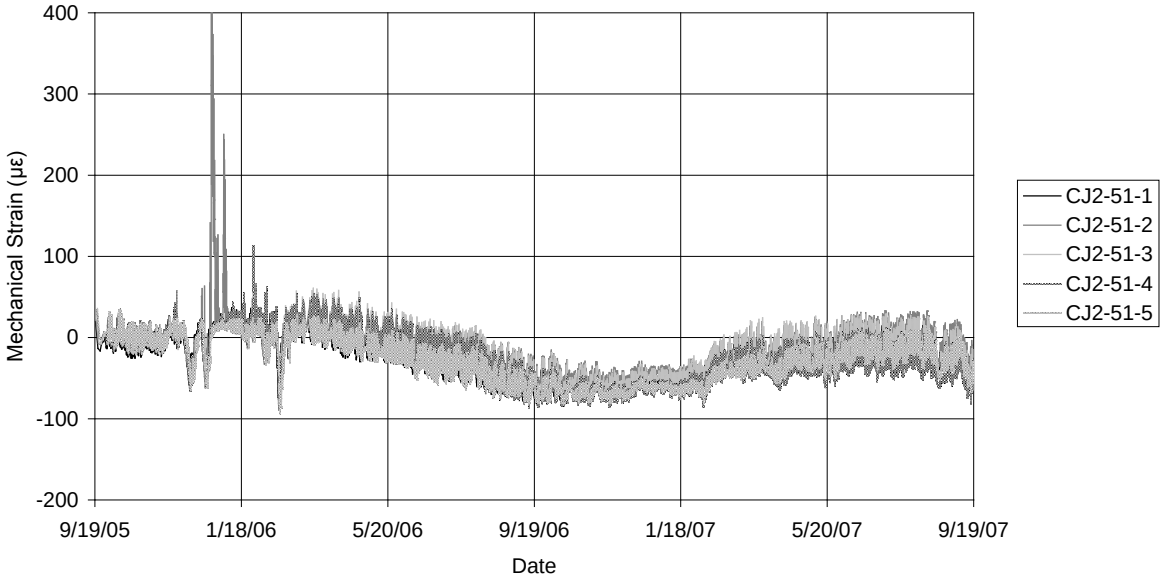

Figure G.2: Mechanical strains for transverse concrete embedment strain gages immediately over Joint 2

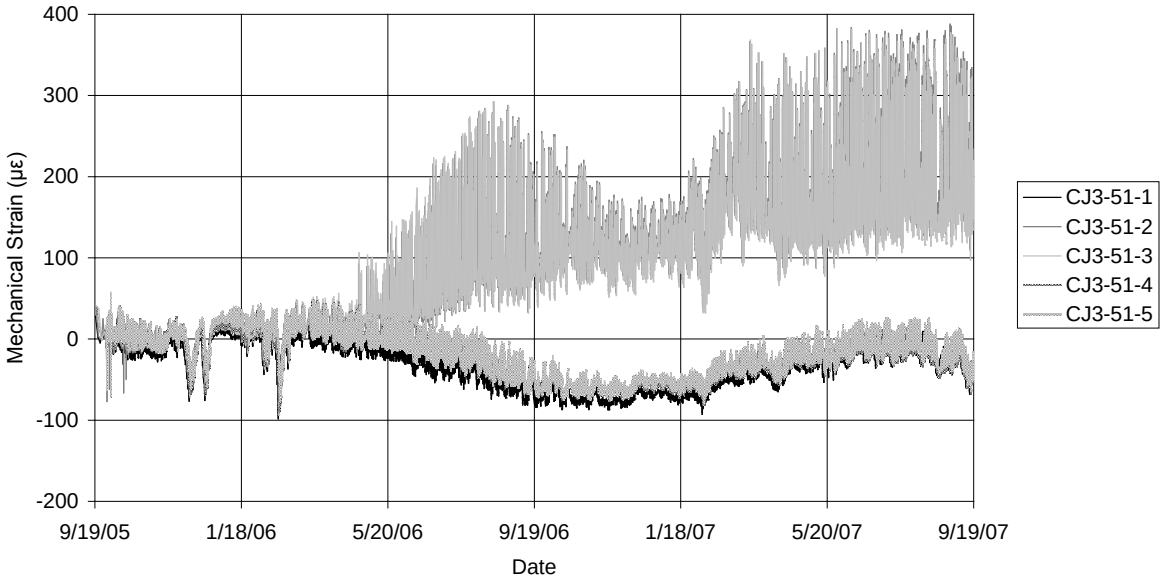

Figure G.3: Mechanical strains for transverse concrete embedment strain gages immediately over Joint 3

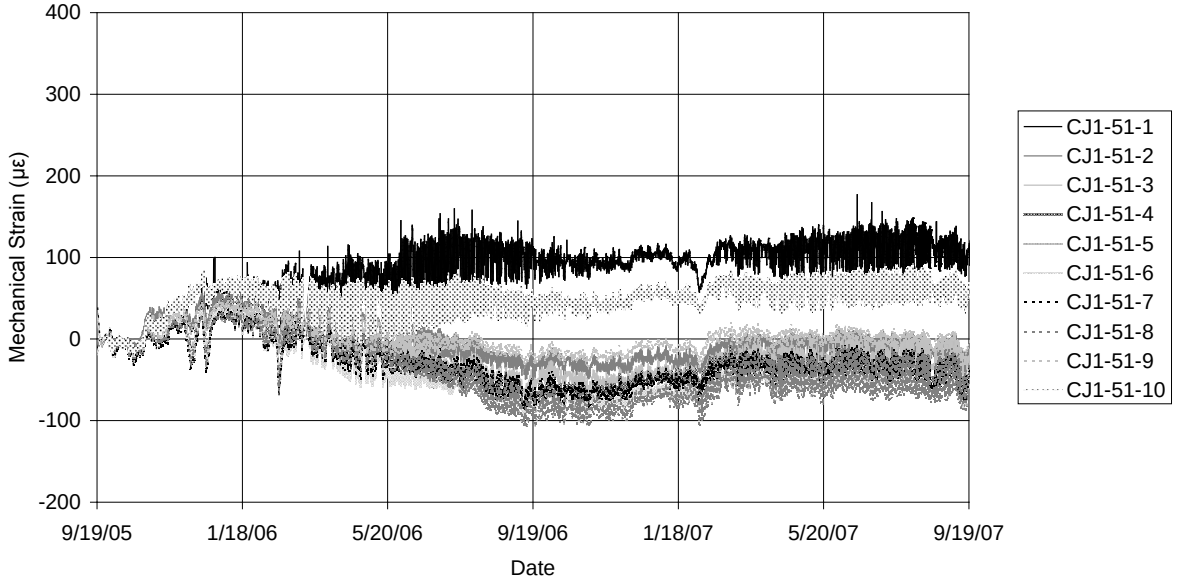

Figure G.4: Mechanical strains for transverse concrete embedment strain gages above the precast webs at Joint 1

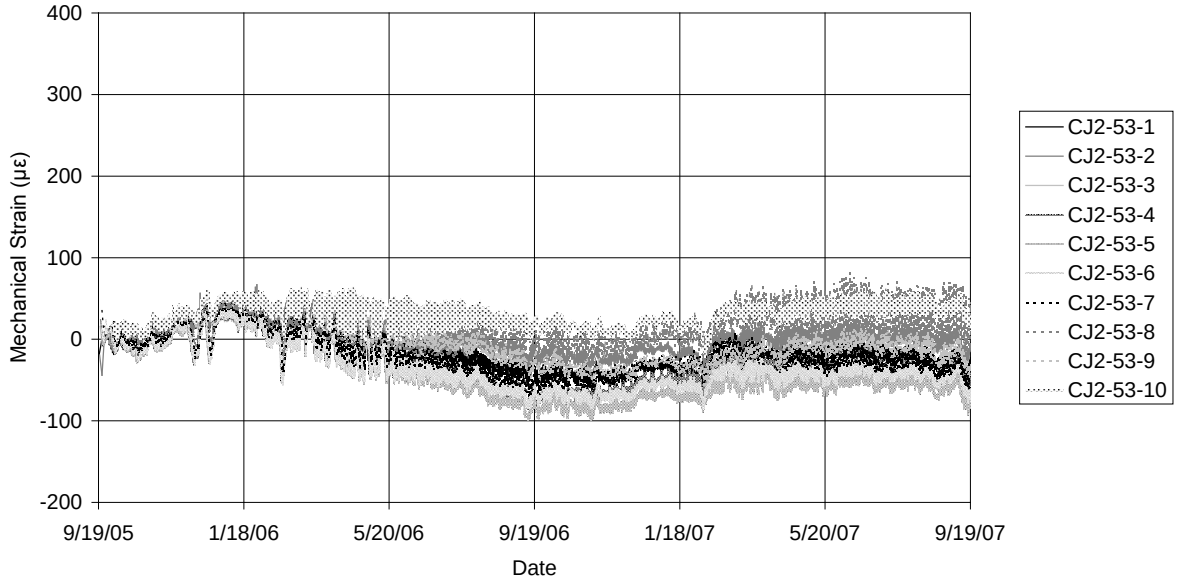

Figure G.5: Mechanical strains for transverse concrete embedment strain gages above the precast webs at Joint 2

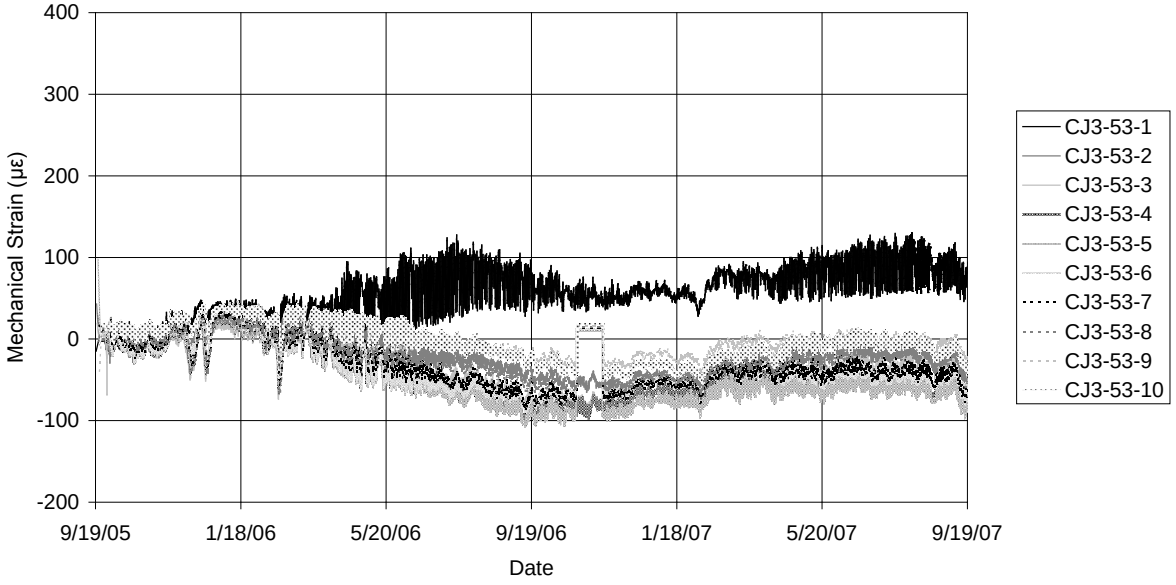

Figure G.6: Mechanical strains for transverse concrete embedment strain gages above the precast webs at Joint 3

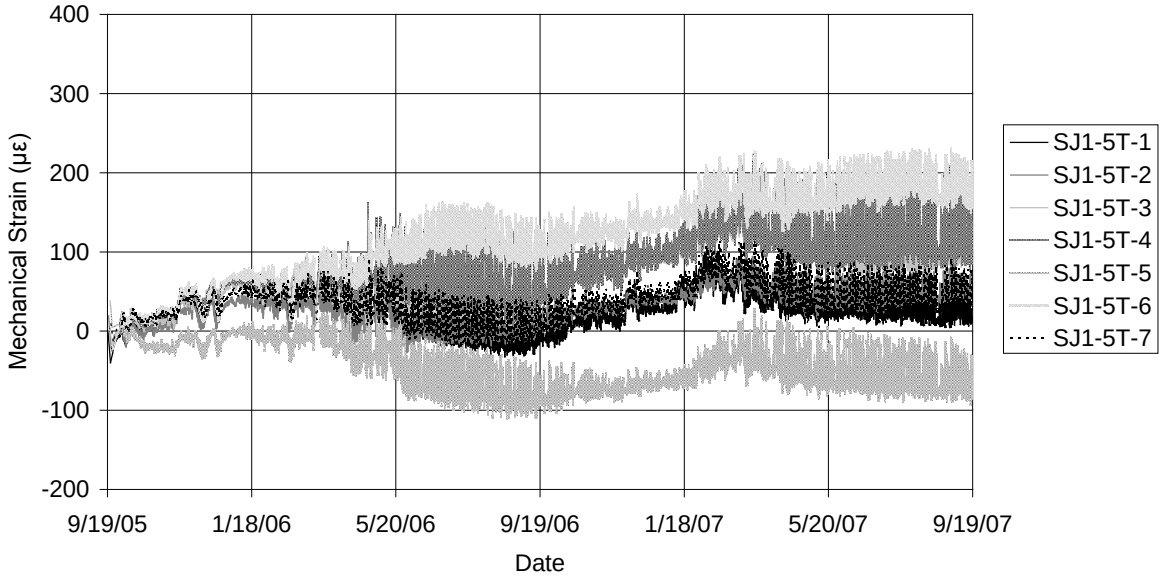

Figure G.7: Mechanical strains for the spot-weldable strain gages on the transverse hooks at Joint 1

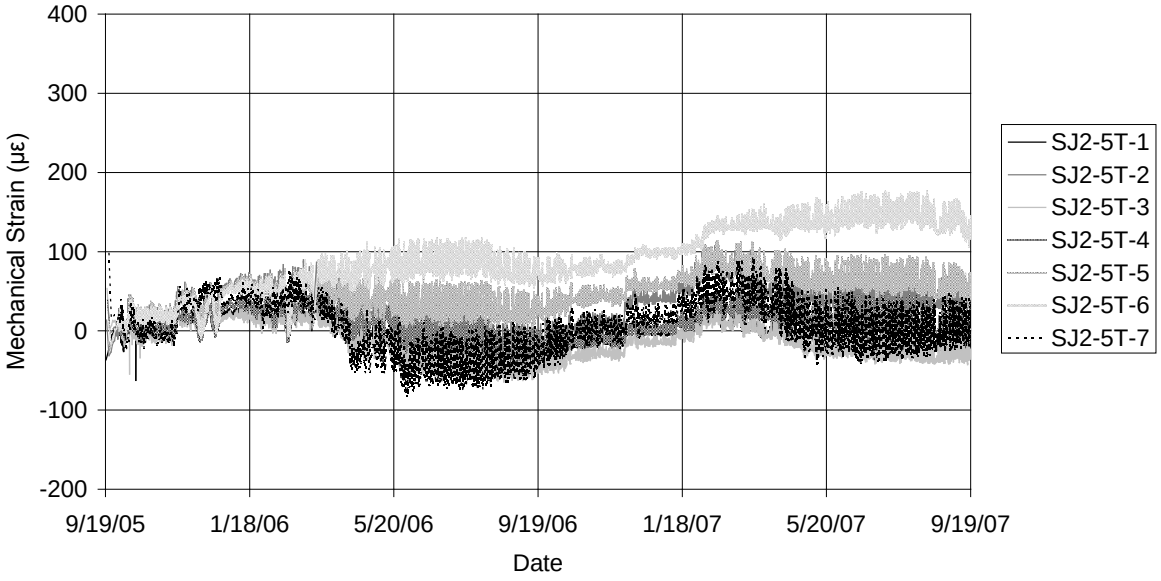

Figure G.8: Mechanical strains for the spot-weldable strain gages on the transverse hooks at Joint 2

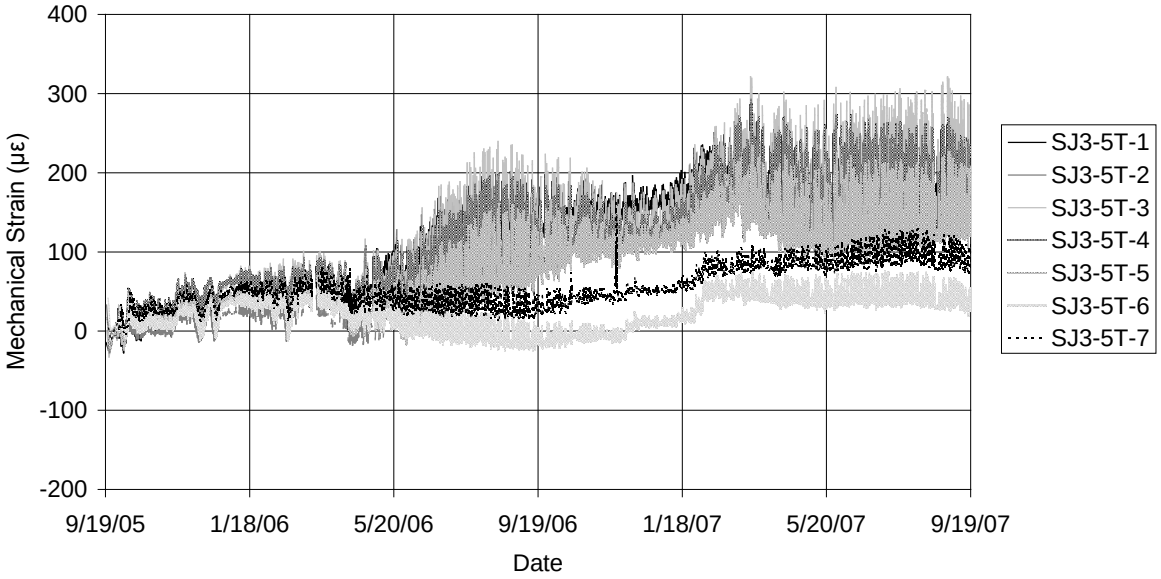

Figure G.9: Mechanical strains for the spot-weldable strain gages on the transverse hooks at Joint 3

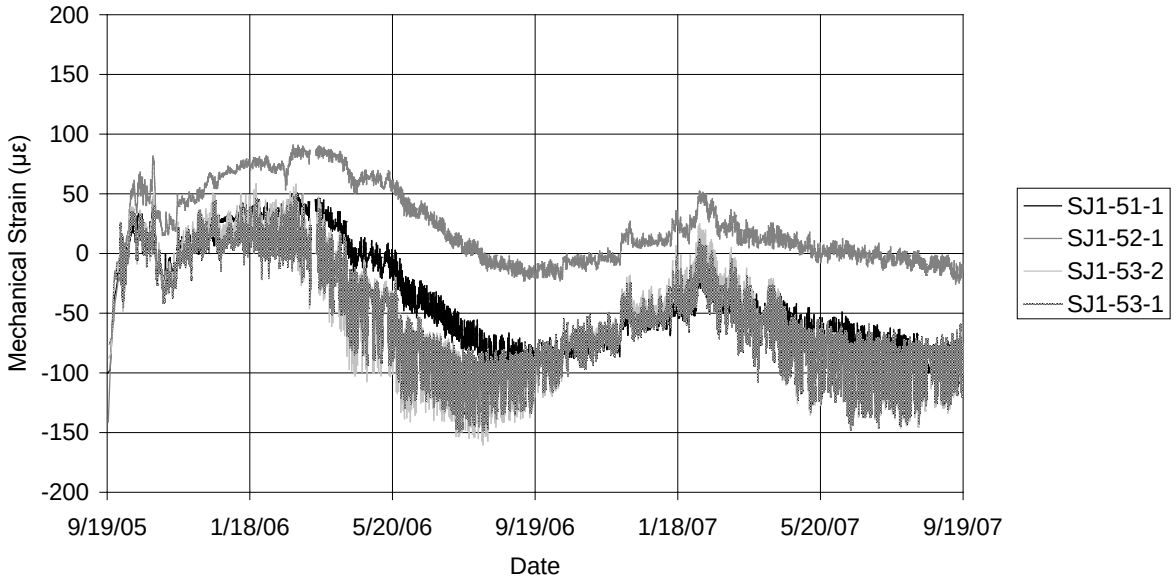

Figure G.10: Mechanical strains for the longitudinal gages at midspan of the center span in Joint 1

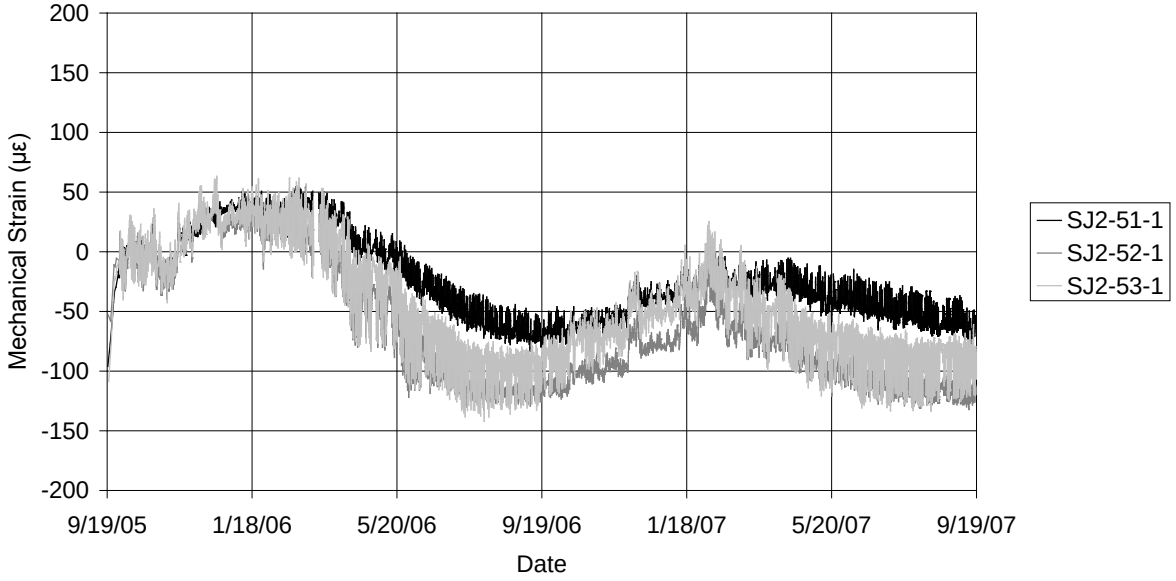

Figure G.11: Mechanical strains for the longitudinal gages at midspan of the center span in Joint 2

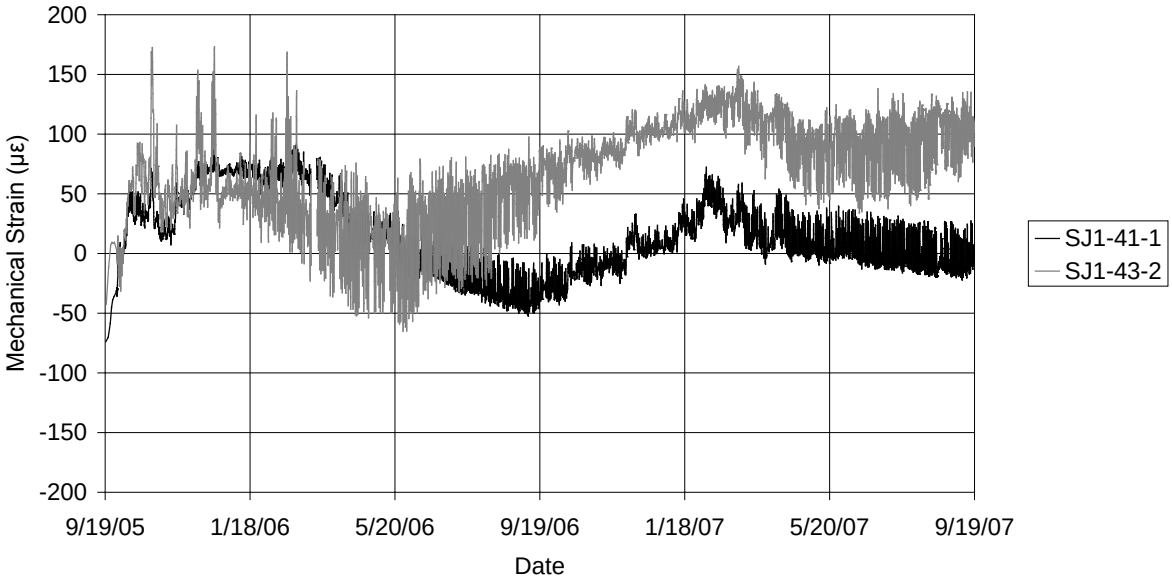

Figure G.12: Mechanical strains for the longitudinal gages near the east pier in the center span in Joint 1

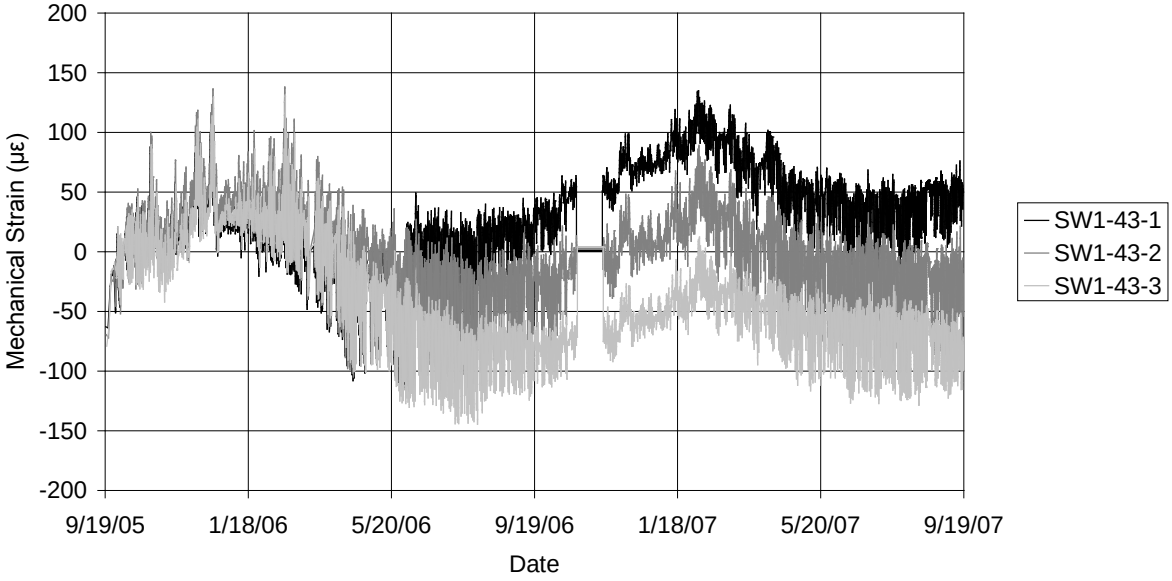

Figure G.13: Mechanical strains for the longitudinal gages near the east pier in the center span over the precast section between Joints 1 and 2

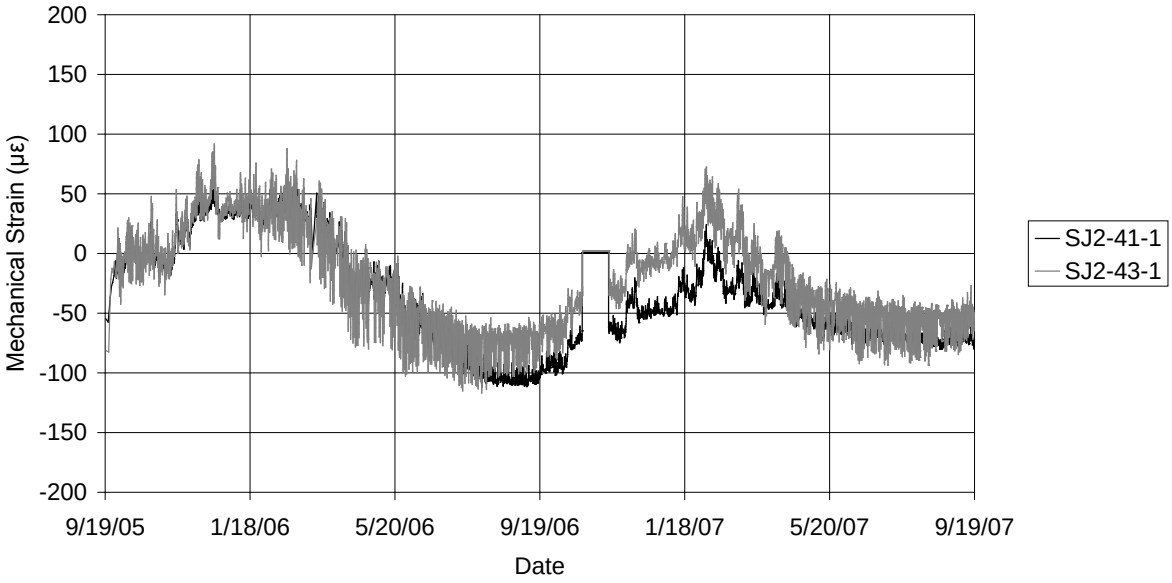

Figure G.14: Mechanical strains for the longitudinal gages near the east pier in the center span in Joint 2

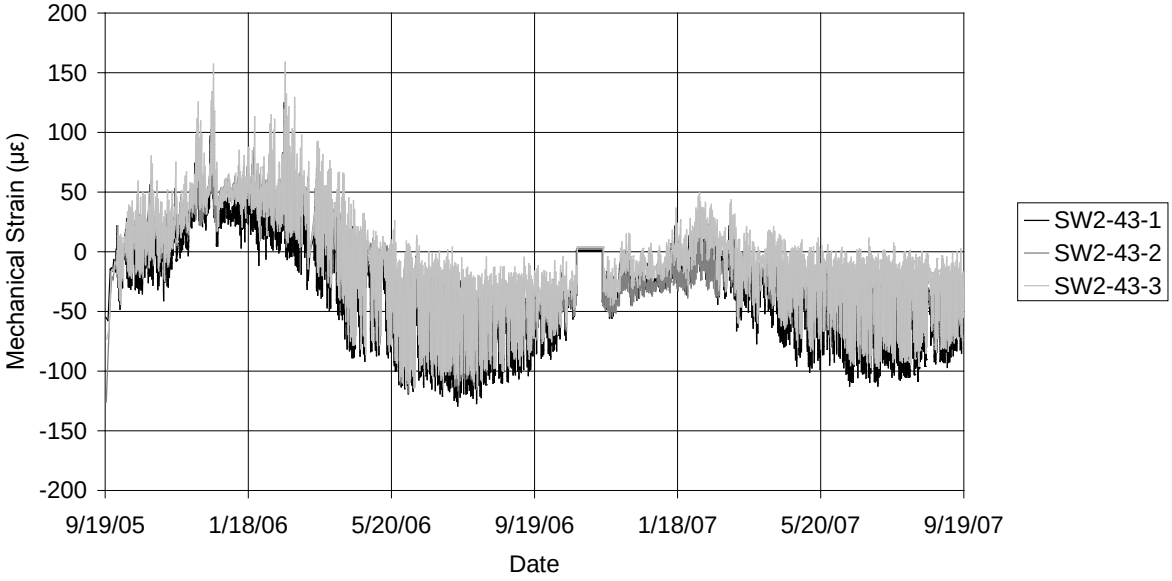

Figure G.15: Mechanical strains for the longitudinal gages near the east pier in the center span over the precast section between Joints 2 and 3

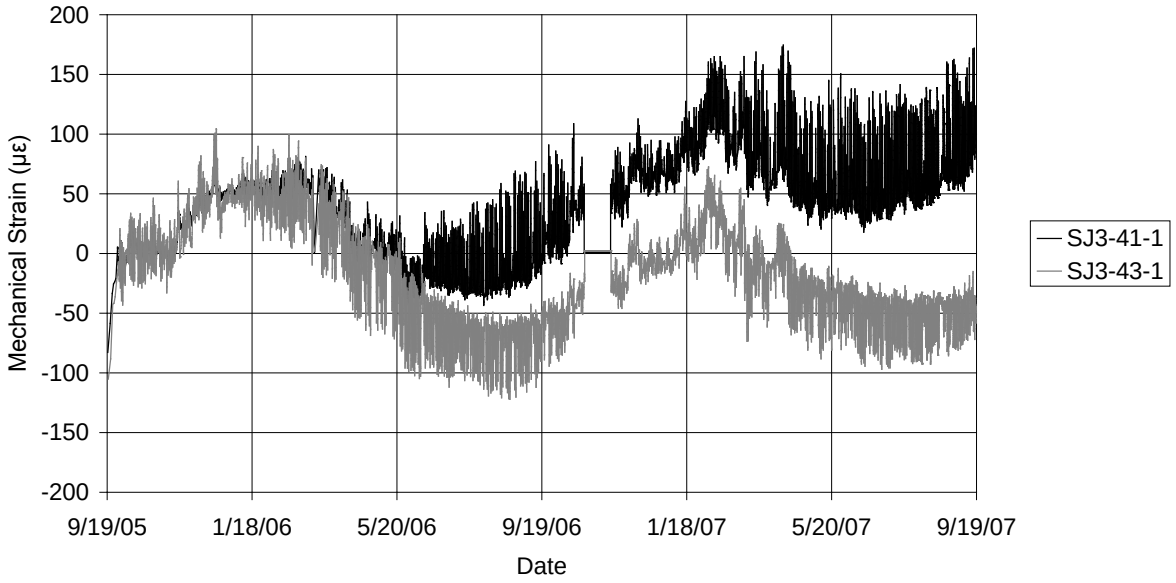

Figure G.16: Mechanical strains for the longitudinal gages near the east pier in the center span in Joint 3

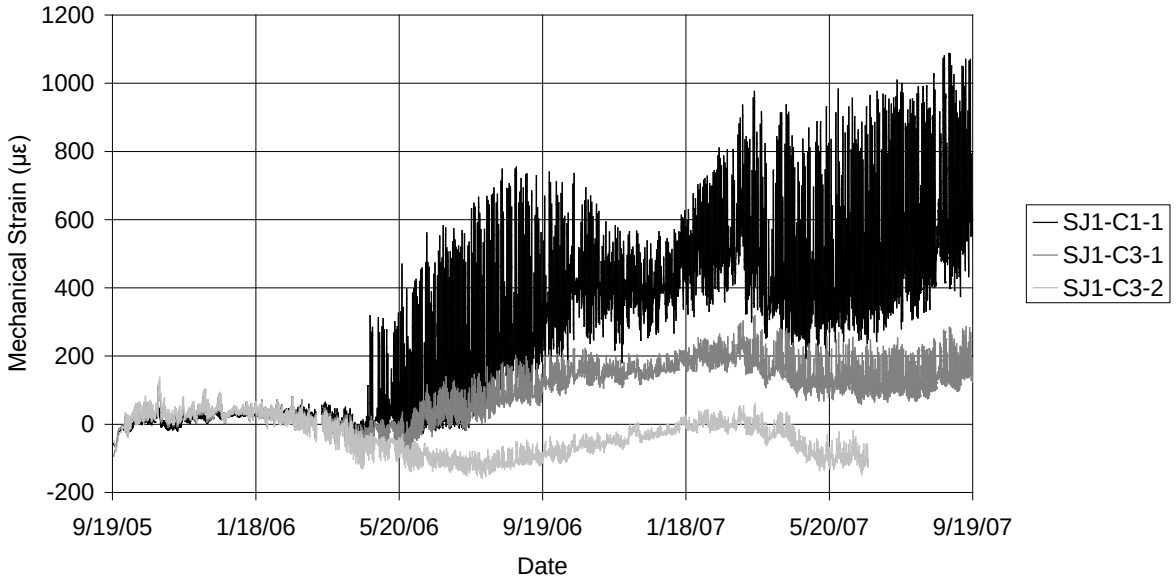

Figure G.17: Mechanical strains for the longitudinal gages at the center of the east pier in Joint 1

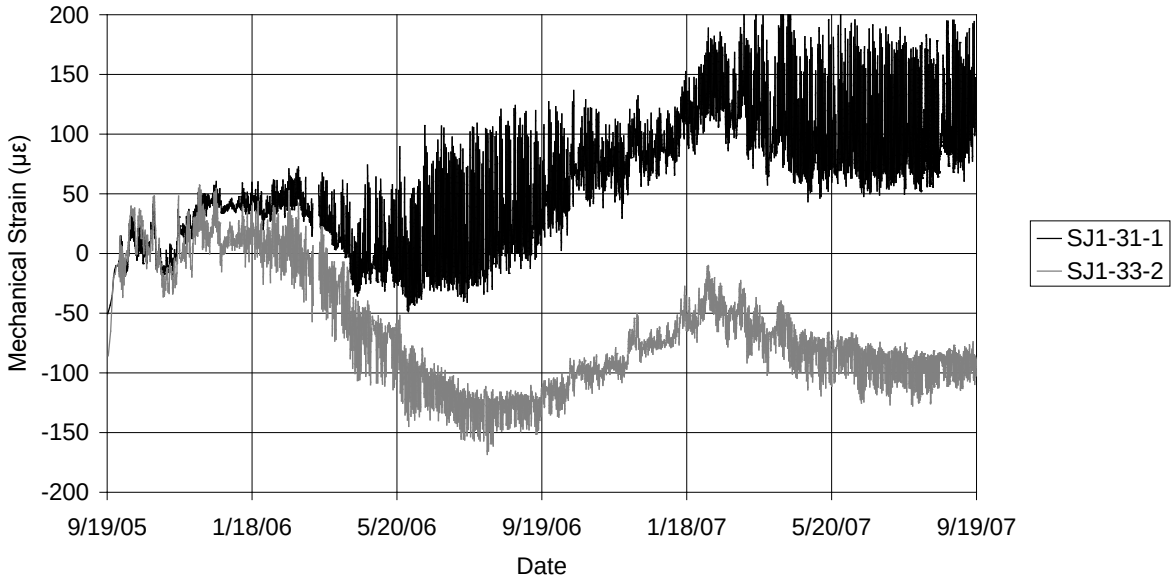

Figure G.18: Mechanical strains for the longitudinal gages near the east pier in the east span in Joint 1

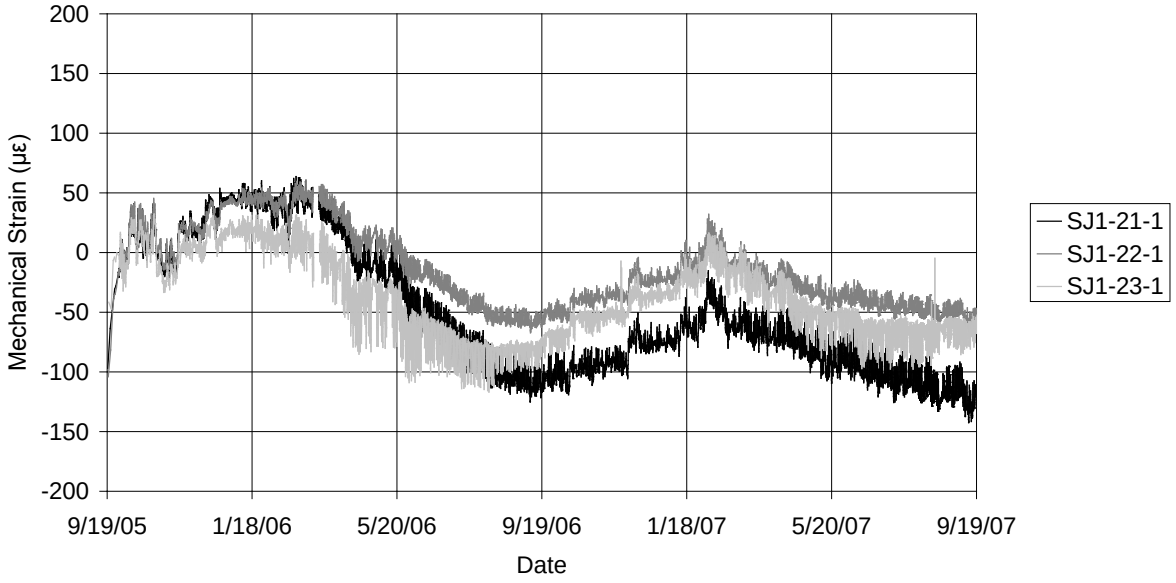

Figure G.19: Mechanical strains for the longitudinal gages at midspan in the east span in Joint 1

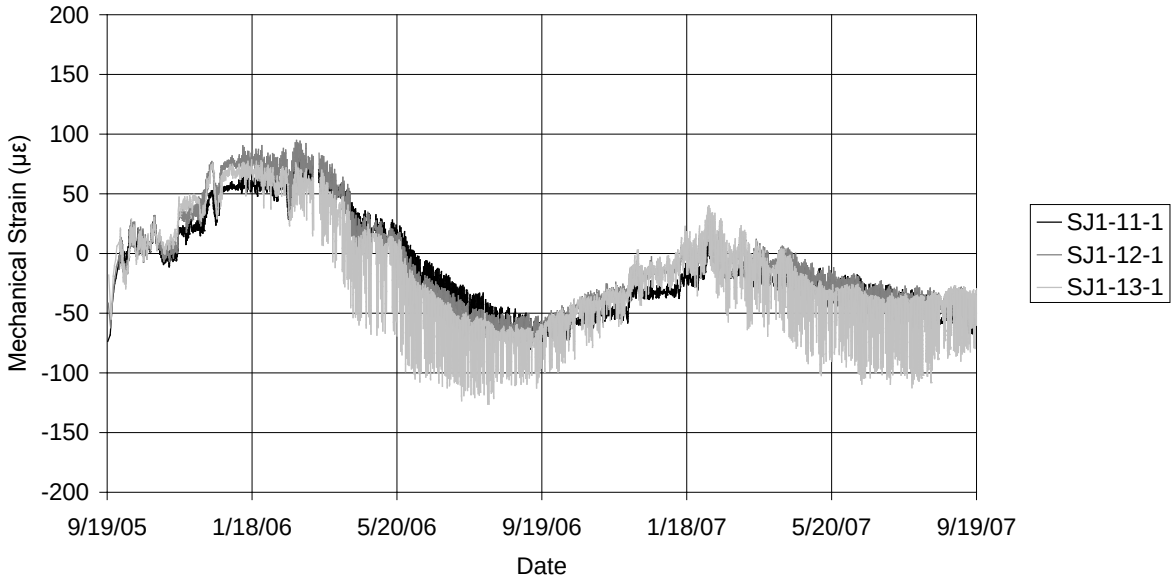

Figure G.20: Mechanical strains for the longitudinal gages near the east abutment in the east span in Joint 1

Appendix H: Determination of Concrete Coefficient of Thermal Expansion for the Center City Bridge

The value of the coefficient of thermal expansion of concrete (α_c) for the CIP deck was calculated using the data obtained during field monitoring. The CIP deck was subjected to a complicated stress state due to the restraint of thermal effects, especially on days with high solar radiation which created large temperature gradients in the bridge superstructure. To minimize the effects of the temperature gradients, α_c was computed using readings from December 1, 2006 to February 28, 2007 when solar radiation was the lowest and temperatures through the depth of the section were relatively uniform. Creep and shrinkage were not considered as the CIP was not under continuous load and most of the shrinkage should have already occurred. Also, the daily temperature changes during this period were largely cyclic whereas any shrinkage would have been monotonic with time. The data was also filtered such that only readings where the temperature gradient was less than 0.2 ^{o}C/in at midspan of the center span were used. Only gages at midspan were included in the calculations as less constraint was expected to exist farther from the piers. Data was included from gages oriented longitudinally as well as transversely. This resulted in 52 data points over the three month period for each gage.

Even with such low temperature gradients, there were consistent variations among gages at various locations in the cross section. The transverse concrete embedment gages immediately above the web gave an α_c value of 5.89 $\mu\varepsilon/^{o}$F compared to 5.67 $\mu\varepsilon/^{o}$F from the transverse concrete embedment gages high above the flange. Using the spot-weldable gages on the longitudinal reinforcement, α_c was calculated to be 6.00 $\mu\varepsilon/^{o}$F . It was thought that this was caused by more interaction due to the closer proximity to the precast sections that would interact with the CIP in such a manner if the precast sections had a higher α_c than the CIP. It was assumed that the transverse gages high above the flange would have the least effect of restraint, so the α_c value of 5.67 $\mu\varepsilon/^{o}$F was used in the calculation of mechanical strains for the concrete embedment strain gages. This was near the typical value of 6.00 $\mu\varepsilon/^{o}$F and well within the given range of 3 to 8 $\mu\varepsilon/^{o}$F given by the AASHTO LRFD Specification (2004) 5.4.2.2. The same analysis was performed for the data from December

1, 2005 to February 28, 2006 which resulted in an α_c value of 6.44 με/^{o}F. This change from the first to second winter was unexpected as α_c generally decreases with age (Neville 1981).

Longitudinal instrumentation at midspan gave similar results where gages in the trough area between adjacent webs had a higher apparent α_c values than gages located above the webs. It is recommended that for future research where thermal properties of concrete are required, that at least one block of concrete be cast from each batch used for both the precast sections and the CIP, and for the blocks to be instrumented with concrete embedment gages and left at the field site so that an accurate calculation of α_c can be obtained.

Appendix I: Complete Tabulated Strain Results from Truck Test

The following tables provide all of the measured, mechanical strains for the truck test of the Center City Bridge as described in Chapter 4. Measured locations and instrument designations are given in Appendix F. All of the strain values represent the average of the three readings recorded as the truck was stationed at a position. Each of the configurations was utilized one to three times as designated by the decimal after the character representing the test. For example 4.1 and 4.2 are the two repeats of truck test configuration 4. All of the strain values for the concrete embedment gages have been corrected for temperature (with respect to the VW gage itself) using the coefficient of thermal expansion discussed in Appendix H.

Table I.1: Complete Mechanical Strain Data for Longitudinal Gages

Test	SJ1-51-1	SJ1-52-1	SJ1-53-2	SJ1-53-1	SJ1-21-1	SJ1-22-1	SJ1-23-1	SJ1-11-1	SJ1-12-1	SJ1-13-1	SJ2-51-1	SJ2-52-1
1.1	-0.4	-3.6	-5.3	-5.2	0.1	0.2	1.0	0.1	0.0	0.8	-1.3	-6.4
1.2	0.0	-3.7	-6.1	-5.8	0.3	0.6	0.9	0.2	0.2	0.2	-1.0	-6.3
2.1	-0.9	-4.6	-7.4	-7.4	0.2	0.4	1.1	0.0	0.1	0.9	-0.4	-6.2
2.2	-0.7	-4.9	-7.9	-7.7	0.3	0.7	1.2	0.2	0.4	0.5	-0.2	-6.3
3.1	-2.1	-5.4	-9.1	-8.8	0.3	0.6	1.1	0.1	0.2	0.8	-1.3	-5.6
3.2	-1.7	-5.7	-9.5	-9.3	0.3	0.9	1.4	0.3	0.5	0.8	-1.3	-5.5
4.1	-1.4	-5.5	-10.2	-10.2	0.4	0.6	0.9	0.2	0.2	0.5	-0.3	-4.1
4.2	-1.2	-5.6	-9.8	-10.0	0.3	0.9	1.5	0.2	0.4	0.6	-0.4	-4.0
6.1	0.1	0.5	0.7	0.9	-1.6	-5.4	-9.2	-0.2	2.0	3.6	0.1	0.6
6.2	0.3	0.5	1.0	1.0	-2.0	-5.4	-8.7	-0.9	0.7	1.8	-0.1	0.3
A.1	0.0	-2.4	-3.9	-4.0	-0.1	0.5	1.0	0.0	0.2	0.6	0.0	-5.4
B.1	-0.1	-1.4	-2.5	-2.5	-0.2	0.4	0.9	-0.1	0.1	0.3	0.0	-3.6
8.1	0.3	0.8	1.2	1.1	-3.3	-10.5	-17.0	-0.7	1.2	2.6	0.0	0.7
8.2	0.3	0.6	1.1	1.1	-3.2	-10.5	-17.1	-0.7	1.2	2.5	0.0	0.7
8.3	0.3	0.6	1.1	1.3	-3.2	-10.5	-17.4	-0.7	1.4	2.5	0.0	0.7
9.1	-1.1	-5.2	-8.0	-9.0	0.5	0.9	1.2	0.0	0.3	0.5	0.0	-4.0
9.2	-0.9	-4.9	-7.3	-8.1	0.6	1.1	1.6	0.2	0.4	0.5	-0.1	-3.8
9.3	-1.1	-5.4	-7.9	-8.6	0.6	1.2	1.7	0.1	0.3	0.5	-0.2	-4.5
10.1	-1.9	-8.8	-16.3	-17.2	0.7	1.0	1.3	0.2	0.2	0.2	-0.6	-8.2
10.2	-1.7	-8.7	-16.6	-17.2	0.8	1.2	1.5	0.3	0.3	0.2	-0.4	-8.7
10.3	-1.9	-8.8	-16.4	-17.1	0.7	1.3	1.7	0.2	0.2	0.3	-0.7	-8.5
11.1	-1.0	-4.3	-6.2	-6.7	0.4	0.8	1.1	0.1	0.2	0.3	-0.8	-3.8
11.2	-1.1	-3.8	-5.6	-5.8	0.4	0.7	1.1	0.1	0.1	0.2	-0.7	-3.5
11.3	-1.4	-4.5	-7.0	-6.9	0.3	0.7	0.8	0.0	0.2	0.3	-0.8	-4.2
E.1	-1.5	-8.1	-15.1	-15.1	0.6	1.1	1.6	0.2	0.3	0.4	-0.7	-11.0
E.2	-1.3	-7.8	-14.0	-14.2	0.5	1.0	1.3	0.2	0.3	0.3	0.0	-9.3
E.3	-1.9	-7.4	-12.2	-12.6	0.5	0.9	1.1	0.2	0.2	0.2	0.2	-6.6

Test	SJ2-53-1	SJ1-41-1	SJ1-43-2	SJ1-C3-1	SJ1-C1-1	SJ1-31-1	SJ1-33-2	SJ1-C3-2	SJ3-41-1	SJ3-43-1	SW2-43-1	SW2-43-2
1.1	-9.2	-1.5	2.0	-2.9	-21.2	-3.1	1.0	-0.3	-0.1	4.1	4.6	4.0
1.2	-9.7	-1.3	1.6	-1.0	-17.4	-2.5	1.2	0.8	0.5	4.5	4.0	3.9
2.1	-9.2	-1.6	3.5	-1.7	-22.9	-2.8	1.7	0.7	-0.2	3.1	4.6	3.8
2.2	-10.0	-1.4	3.2	-0.6	-21.3	-3.1	2.0	1.6	0.6	3.3	4.0	3.7
3.1	-8.1	-1.4	4.9	-0.7	-24.3	-2.0	2.4	1.7	0.2	1.8	3.9	3.0
3.2	-8.9	-1.2	4.8	0.1	-24.1	-2.9	2.6	2.3	0.5	1.9	3.3	2.9
4.1	-6.6	-1.1	5.2	-0.3	-24.9	-1.6	2.6	2.1	0.2	0.9	2.5	1.9
4.2	-6.8	-0.8	5.1	0.2	-24.5	-2.7	2.6	2.5	0.2	1.0	2.2	2.0
6.1	0.6	-0.3	3.2	-1.1	-24.2	-1.8	-0.7	2.2	-1.3	0.4	1.9	1.4
6.2	0.6	-0.4	3.2	-1.3	-25.8	-3.3	-1.0	2.6	-1.6	0.5	1.8	1.4
A.1	-8.6	-1.1	0.6	-2.0	-16.1	-3.1	0.8	0.0	-1.0	5.1	3.5	3.5
B.1	-5.9	-0.8	-0.2	-1.7	-12.1	-2.6	0.4	-0.6	-2.1	4.9	1.9	2.3
8.1	1.2	-0.8	4.7	0.0	-42.1	-4.3	-2.4	6.5	-2.1	1.9	3.3	2.8
8.2	1.0	-0.8	4.0	0.6	-42.2	-4.3	-2.1	7.2	-2.2	1.9	3.3	2.8
8.3	0.9	-0.8	4.4	2.1	-41.0	-4.3	-2.2	8.5	-2.0	1.7	3.2	2.7
9.1	-6.7	-1.8	3.2	-0.9	-39.4	-4.0	2.6	5.4	1.3	0.7	1.9	1.2
9.2	-6.2	-1.7	2.9	2.5	-33.5	-2.4	2.5	6.8	1.3	1.0	1.6	1.2
9.3	-7.5	-1.7	3.3	3.1	-34.8	-2.4	2.5	7.4	1.4	0.9	2.3	1.6
10.1	-12.8	-1.3	6.7	0.5	-45.4	-4.3	2.7	6.5	1.0	2.4	4.4	3.3
10.2	-13.7	-1.3	6.8	2.9	-43.3	-3.4	2.7	7.8	0.9	2.5	4.6	3.6
10.3	-13.4	-1.2	6.6	3.9	-42.3	-3.2	2.8	8.4	1.2	2.2	4.3	3.3
11.1	-5.4	-0.4	2.0	1.8	-19.5	-1.2	1.8	3.9	0.8	1.8	1.7	1.4
11.2	-5.5	-0.5	1.1	2.2	-21.0	-1.2	1.7	4.7	0.8	1.4	1.1	-0.1
11.3	-6.4	-0.7	2.7	2.2	-19.1	-1.3	1.4	4.7	0.7	1.7	2.0	1.1
E.1	-16.5	-1.9	5.3	2.7	-40.3	-3.2	2.4	8.0	0.9	5.4	6.1	5.2
E.2	-14.4	-1.7	4.9	2.7	-38.9	-3.3	2.1	7.6	0.3	5.1	4.7	4.1
E.3	-10.7	-1.3	4.0	1.8	-35.5	-3.1	1.6	5.8	-0.7	4.4	3.1	2.8

Test	SW2-43-3	SJ2-41-1	SJ2-43-1	SW1-43-1	SW1-43-2	SW1-43-3
1.1	4.8	-1.4	3.0	3.1	3.7	4.4
1.2	4.9	-1.0	3.0	2.9	3.3	4.1
2.1	4.1	-1.6	3.0	4.7	4.9	5.0
2.2	4.3	-1.4	3.0	4.4	4.7	5.0
3.1	3.0	-1.9	2.6	5.4	5.5	5.0
3.2	3.2	-1.7	2.4	5.2	5.2	5.1
4.1	1.7	-1.7	1.6	5.0	4.8	4.0
4.2	2.1	-1.6	1.6	5.0	4.7	4.2
6.1	1.0	-0.5	1.6	3.7	3.5	3.1
6.2	1.3	-0.7	1.6	4.0	3.6	3.2
A.1	4.4	-0.4	2.4	1.5	2.0	2.8
B.1	3.2	0.0	1.4	0.4	0.7	1.4
8.1	2.7	-1.2	2.4	5.4	5.5	4.8
8.2	3.0	-1.0	2.5	5.2	5.1	4.7
8.3	2.8	-1.1	2.6	5.4	5.0	5.0
9.1	0.9	-2.7	0.8	4.0	3.3	3.2
9.2	0.7	-2.3	0.5	3.3	2.4	2.5
9.3	1.5	-2.3	1.2	3.8	3.3	2.9
10.1	3.4	-2.5	2.8	6.7	7.0	6.1
10.2	3.8	-2.2	3.1	6.9	6.7	6.1
10.3	3.8	-2.2	3.0	6.6	6.2	5.9
11.1	1.2	-0.9	1.2	2.1	2.3	2.7
11.2	-0.1	-0.9	1.0	2.3	1.4	1.8
11.3	1.6	-0.9	1.5	2.5	2.4	2.6
E.1	6.4	-1.7	4.6	6.3	6.5	7.0
E.2	5.4	-1.5	3.5	5.6	5.5	5.8
E.3	3.9	-1.1	2.1	4.2	3.9	3.6

Table I.2: Complete Mechanical Strain Data for Transverse Gages

Test	CJ1-51-1	CJ1-51-2	CJ1-51-3	CJ1-51-4	CJ1-51-5	CJ1-53-1	CJ1-53-2	CJ1-53-3	CJ1-53-4	CJ1-53-5	CJ1-53-6	CJ1-53-7
1.1	-1.1	-0.4	-2.4	-1.9	-0.1	-0.3	0.6	0.0	0.1	-0.5	-0.7	0.0
1.2	-0.8	-1.3	-1.8	-1.1	-0.2	1.9	0.7	0.7	0.2	-0.1	-0.5	-0.1
2.1	-0.2	1.6	5.4	5.2	2.0	-1.0	-0.3	-0.5	-0.6	-1.4	-1.5	-0.2
2.2	0.4	0.5	5.2	5.6	1.1	1.1	0.1	0.1	-0.6	-1.2	-2.1	-0.3
3.1	2.6	4.5	19.0	17.5	4.1	-2.1	-3.5	-2.8	-2.9	-3.4	-4.0	-1.3
3.2	2.6	4.6	19.3	17.0	3.6	-2.7	-3.6	-2.2	-2.7	-3.1	-4.6	-1.4
4.1	2.8	3.5	14.1	12.8	3.1	-5.2	-4.8	-3.1	-2.3	-2.3	-2.9	-0.8
4.2	1.8	4.5	14.5	12.6	2.8	-4.8	-4.0	-1.9	-1.8	-1.8	-2.5	-0.2
6.1	0.1	-0.1	-0.2	-0.5	-0.1	0.4	0.1	-0.2	-0.1	0.0	0.0	0.0
6.2	0.1	-0.4	-0.7	-1.0	0.0	-0.1	0.5	0.4	0.2	0.2	0.2	0.1
A.1	-1.2	-1.5	-4.2	-3.7	-0.2	1.7	1.7	1.2	1.1	1.0	0.6	0.5
B.1	-1.0	-1.2	-4.2	-3.7	-0.4	1.6	1.3	1.0	0.9	0.9	0.7	0.5
8.1	-0.1	-0.1	-0.2	-0.1	-0.1	-0.2	-0.1	0.0	0.1	-0.1	0.3	0.2
8.2	0.5	-0.3	0.3	0.3	-0.1	-0.1	0.1	0.0	0.0	-0.1	-0.2	0.1
8.3	-0.2	0.0	-0.1	-0.1	-0.1	-0.1	0.0	0.2	0.0	0.0	0.1	0.0
9.1	1.7	2.2	9.1	8.4	2.0	-4.4	-3.6	-2.7	-2.1	-2.5	-1.5	-1.4
9.2	1.0	1.9	8.9	8.1	2.5	-3.5	-3.5	-2.9	-2.7	-2.5	-3.7	-1.3
9.3	1.4	2.0	9.6	8.5	2.7	-3.0	-3.9	-3.5	-2.0	-2.4	-2.1	-1.2
10.1	2.2	3.5	15.3	14.2	2.3	-4.3	-4.2	-2.9	-2.7	-3.0	-2.7	-1.2
10.2	1.4	3.2	15.2	13.4	2.8	-6.1	-5.1	-4.0	-3.2	-3.3	-3.8	-1.5
10.3	1.8	3.1	15.1	13.8	3.2	-4.9	-4.6	-4.2	-2.7	-3.3	-3.7	-1.2
11.1	1.3	2.1	9.4	8.5	2.5	-3.5	-3.4	-2.8	-2.5	-1.7	-2.2	-1.2
11.2	1.1	1.8	9.3	7.9	2.7	-4.2	-3.5	-3.4	-1.8	-2.8	-2.8	-1.1
11.3	0.8	2.5	9.5	8.3	2.8	-4.5	-3.0	-2.4	-2.7	-2.6	-2.4	-1.0
E.1	1.0	2.1	9.9	8.6	2.8	-4.5	-4.0	-2.4	-2.2	-1.4	-1.9	-0.4
E.2	0.2	1.8	7.8	7.5	2.5	-2.6	-1.9	-1.3	-1.7	-1.9	-1.6	0.1
E.3	0.2	2.1	11.6	10.4	3.0	-2.5	-1.8	-1.6	-2.0	-2.4	-2.3	-0.7

Test	CJ1-53-8	CJ1-53-9	CJ1-53-10	SJ1-5T-1	SJ1-5T-2	SJ1-5T-3	SJ1-5T-4	SJ1-5T-5	SJ1-5T-6	SJ1-5T-7	CJ2-51-1	CJ2-51-2
1.1	-0.6	0.1	0.4	-2.6	-1.2	-2.0	-1.6	-1.3	-0.7	-1.2	5.2	6.5
1.2	-0.8	-0.7	-2.3	-2.4	-1.1	-1.3	-0.9	-0.8	-0.4	-1.0	5.1	6.1
2.1	-0.8	-2.1	-3.9	-0.2	0.9	2.4	5.2	3.6	3.4	2.2	4.1	5.2
2.2	-1.1	-3.3	-5.2	-0.3	1.0	2.5	5.2	4.1	3.5	2.2	4.1	3.9
3.1	-1.0	-2.2	-2.6	5.3	5.6	9.5	15.7	10.4	8.4	7.6	4.7	5.9
3.2	-1.0	-2.6	-4.0	6.5	5.8	10.4	15.8	11.3	8.0	7.3	4.9	4.6
4.1	-0.5	-1.8	-2.6	5.8	4.5	8.5	12.3	8.7	6.0	5.5	3.3	2.1
4.2	0.1	-0.8	-4.8	5.8	4.7	8.1	12.2	9.0	6.0	5.7	1.9	1.9
6.1	-0.4	-0.1	-0.3	-0.2	-0.2	-0.1	-0.2	-0.3	-0.3	-0.1	-0.4	0.0
6.2	0.2	0.3	-0.4	-0.3	-0.4	-0.4	-0.8	-0.5	-0.4	-1.0	-0.4	-0.7
A.1	-0.1	0.5	0.7	-2.8	-1.9	-2.4	-3.4	-2.4	-1.6	-2.7	0.4	1.4
B.1	0.2	0.5	-0.1	-2.4	-1.7	-2.2	-3.5	-2.6	-1.7	-2.5	-1.4	-1.3
8.1	0.0	0.0	0.1	-0.1	-0.1	-0.2	-0.3	-0.2	-0.1	-0.2	-0.2	-0.3
8.2	0.1	-0.2	-0.1	-0.1	-0.1	0.0	0.2	0.5	0.8	0.7	-0.2	-0.2
8.3	0.1	0.4	0.3	0.0	-0.1	-0.1	-0.1	-0.2	-0.1	0.0	0.0	0.0
9.1	-1.4	-2.5	-3.4	4.3	3.4	5.6	8.3	6.8	4.1	4.0	1.3	1.1
9.2	-1.4	-1.5	-2.7	4.4	3.2	5.5	7.8	6.2	4.1	3.6	1.8	2.5
9.3	-1.7	-3.0	-3.6	4.1	3.4	6.4	9.0	7.4	5.4	4.3	2.7	3.1
10.1	-0.4	-2.7	-5.9	5.4	4.8	8.8	13.6	10.2	7.4	6.2	1.2	1.5
10.2	-1.7	-2.2	-5.5	6.0	4.7	8.7	13.1	9.8	6.8	5.7	2.1	3.0
10.3	-1.4	-2.9	-5.9	5.5	4.7	8.8	13.5	10.5	7.6	6.4	2.7	3.2
11.1	-0.3	-1.2	-4.2	4.1	3.2	5.3	8.2	6.7	4.4	3.6	1.6	2.0
11.2	-1.5	-3.2	-2.9	3.8	3.0	5.2	7.7	6.1	4.6	3.6	2.3	3.1
11.3	-1.3	-0.5	-4.3	3.8	3.2	5.9	8.5	6.2	4.6	3.6	2.8	2.9
E.1	-1.0	-0.7	-4.8	4.1	3.3	6.5	9.0	7.0	5.0	3.4	4.2	4.0
E.2	-0.6	-0.7	-4.8	2.4	2.4	5.2	7.5	5.6	4.4	3.0	2.5	2.6
E.3	-0.9	-0.3	-3.7	2.9	3.1	6.2	9.5	6.8	5.1	4.2	-0.6	-1.0

Test	CJ2-51-3	CJ2-51-4	CJ2-51-5	CJ2-53-1	CJ2-53-2	CJ2-53-3	CJ2-53-4	CJ2-53-5	CJ2-53-6	CJ2-53-7	CJ2-53-8	CJ2-53-9
1.1	8.0	6.7	3.2	-1.9	-2.4	-2.6	-3.0	-3.5	-3.9	-2.2	-0.2	-0.8
1.2	8.0	7.0	3.9	-2.9	-3.4	-2.7	-3.7	-3.8	-4.1	-2.2	-0.2	-1.2
2.1	4.9	4.5	2.4	-3.7	-3.1	-2.3	-3.3	-2.7	-1.8	-1.0	0.2	-0.9
2.2	5.0	4.5	2.2	-3.9	-3.6	-2.5	-3.0	-2.8	-1.7	-1.3	0.0	-1.2
3.1	5.9	5.1	2.7	-2.9	-3.1	-2.9	-4.2	-3.5	-2.6	-1.6	-0.1	-0.4
3.2	6.1	4.7	2.0	-3.2	-3.5	-3.0	-3.7	-3.3	-2.2	-2.0	-0.5	-0.3
4.1	2.4	1.3	-0.2	-3.3	-2.6	-1.2	-2.0	-0.6	-0.3	-1.0	0.0	0.5
4.2	2.2	1.2	-0.1	-2.9	-2.1	-2.8	-1.6	-0.7	0.1	-0.3	0.0	0.6
6.1	0.0	-0.3	0.0	-0.1	-0.1	-0.2	0.0	-0.2	-0.1	0.0	-0.1	-0.3
6.2	0.0	0.0	-0.6	0.2	0.1	0.1	0.1	0.3	-0.1	0.3	0.0	0.0
A.1	2.5	2.4	1.9	0.9	0.1	-0.1	-0.8	-0.6	0.0	0.6	0.4	-1.0
B.1	-1.2	-0.5	-1.1	1.4	1.3	1.5	1.1	1.2	0.6	0.4	0.1	-0.2
8.1	-0.1	-0.1	0.1	-0.2	0.0	0.1	0.1	0.2	0.2	0.2	-0.2	-0.1
8.2	-0.3	-0.3	0.0	0.1	0.0	-0.1	0.2	0.2	0.0	0.1	0.2	0.2
8.3	-0.3	-0.1	0.0	0.0	-0.1	0.0	0.0	0.0	0.1	0.1	0.0	-0.1
9.1	2.2	1.4	0.5	-2.8	-2.5	-1.7	-2.3	-1.3	-2.1	-1.9	-0.7	-0.7
9.2	1.1	1.2	0.1	-2.2	-2.1	-2.6	-1.9	-2.7	-2.3	-1.0	-0.6	-1.0
9.3	1.0	2.0	0.1	-2.7	-2.4	-3.0	-3.1	-2.4	-1.5	-1.3	-0.5	-0.5
10.1	2.8	2.1	0.7	-2.0	-2.4	-2.2	-2.7	-2.1	-2.4	-2.3	-0.5	-0.7
10.2	1.5	1.6	0.1	-2.2	-1.8	-2.3	-2.3	-2.8	-2.7	-1.0	-1.4	-0.7
10.3	1.4	2.4	0.1	-2.0	-2.4	-3.0	-3.3	-2.5	-1.9	-1.7	-0.4	-0.4
11.1	1.8	1.3	0.4	-2.1	-2.8	-3.1	-2.2	-2.8	-1.4	-1.4	-0.4	-0.8
11.2	1.0	1.5	0.0	-2.4	-1.6	-2.0	-2.4	-1.9	-1.7	-0.8	-2.0	-0.9
11.3	1.9	2.3	0.0	-2.3	-2.7	-2.3	-2.2	-1.4	-2.2	-1.4	-0.4	-1.0
E.1	3.9	4.1	0.7	-3.8	-3.3	-3.6	-4.3	-3.1	-3.0	-1.5	0.2	-0.6
E.2	1.3	1.9	0.1	-1.8	-1.8	-1.4	-1.4	-0.7	-1.3	-0.5	0.2	-0.1
E.3	-2.7	-1.4	-1.2	0.6	0.2	0.0	0.1	0.0	0.5	-0.7	-0.3	-0.1

Test	CJ2-53-10	SJ2-5T-1	SJ2-5T-2	SJ2-5T-3	SJ2-5T-4	SJ2-5T-5	SJ2-5T-6	SJ2-5T-7	CJ3-51-1	CJ3-51-2	CJ3-51-3	CJ3-51-4
1.1	-2.6	2.3	5.6	5.4	6.5	6.5	6.1	8.1	3.1	30.1	31.0	2.6
1.2	-2.2	2.8	5.8	5.4	6.6	5.8	5.7	8.1	3.5	29.1	30.0	2.8
2.1	-2.6	1.7	4.3	4.0	4.9	4.6	4.3	6.4	0.9	10.2	10.4	0.2
2.2	-2.6	2.0	4.1	3.8	4.6	4.0	4.2	6.8	1.1	9.5	9.3	0.6
3.1	-1.5	1.9	4.8	4.4	5.4	4.7	4.5	5.8	-1.0	-3.2	-3.6	-1.0
3.2	-1.6	2.4	4.6	4.1	5.1	4.1	4.4	5.2	-1.4	-5.2	-5.6	-1.8
4.1	0.6	0.8	2.2	1.5	1.9	1.0	1.0	0.6	-0.9	-5.4	-5.6	-0.9
4.2	0.6	1.1	1.8	1.3	1.6	1.2	1.1	0.3	-1.7	-6.9	-7.5	-1.6
6.1	-0.2	-0.1	-0.1	-0.1	-0.1	-0.1	-0.2	-0.1	0.0	-0.3	0.1	0.0
6.2	-0.1	-0.1	-0.2	0.0	-0.1	-0.1	-0.1	-0.1	-0.1	-1.4	-1.1	-0.3
A.1	-3.3	0.6	0.8	1.4	1.6	2.4	2.3	5.3	3.7	26.0	27.0	3.0
B.1	-0.5	-0.9	-1.0	-0.7	-0.9	-0.6	-0.6	0.3	4.7	32.3	34.2	4.0
8.1	0.0	0.0	-0.1	-0.1	-0.1	-0.1	-0.1	-0.2	-0.1	-0.3	-0.4	0.1
8.2	0.0	-0.1	-0.2	-0.1	-0.2	-0.2	-0.2	-0.1	0.1	0.1	0.6	0.0
8.3	-0.1	-0.1	-0.1	-0.1	-0.1	-0.1	-0.1	0.0	0.0	-0.3	-0.1	0.0
9.1	-1.4	1.2	1.8	1.9	2.2	2.0	2.0	2.4	-0.4	-1.6	-1.9	-0.4
9.2	-1.2	1.1	1.8	1.7	1.9	1.7	1.8	2.9	-0.5	-0.4	-0.7	-0.5
9.3	-1.6	1.2	2.1	2.0	2.2	2.1	2.2	3.5	-1.1	-1.2	-1.1	-0.9
10.1	-2.5	0.9	2.2	2.4	2.8	2.8	2.8	4.9	-1.0	-3.6	-4.7	-1.5
10.2	-2.0	1.0	2.3	2.1	2.5	2.5	2.6	4.9	-1.0	-1.0	-1.4	-1.6
10.3	-2.2	1.0	2.3	2.1	2.5	2.5	2.8	5.0	-1.8	-3.2	-3.5	-2.0
11.1	-2.2	1.2	2.1	1.7	2.1	2.1	2.2	2.9	-0.1	1.4	1.3	-0.4
11.2	-1.6	1.1	1.9	1.4	1.7	1.7	1.9	2.4	0.3	2.3	2.2	-0.3
11.3	-1.5	1.1	2.2	1.5	2.0	2.0	2.3	2.9	0.2	1.9	2.0	-0.4
E.1	-3.4	2.5	4.3	3.9	4.7	4.9	5.0	8.8	1.8	19.1	19.7	1.5
E.2	-1.3	0.6	1.7	1.5	1.8	1.8	1.9	4.5	2.0	22.0	22.4	1.5
E.3	0.5	-1.4	-1.9	-1.4	-1.8	-1.7	-1.6	-1.9	2.4	24.5	25.5	2.2

Test	CJ3-51-5	CJ3-53-1	CJ3-53-2	CJ3-53-3	CJ3-53-4	CJ3-53-5	CJ3-53-6	CJ3-53-7	CJ3-53-8	CJ3-53-9	CJ3-53-10	SJ3-5T-1
1.1	2.1	-4.8	-3.0	-3.5	-3.3	-3.7	-3.2	-3.2	-2.4	-2.1	-1.7	10.1
1.2	2.3	-5.4	-4.0	-2.3	-3.5	-3.8	-3.5	-3.1	-2.7	-1.8	-1.7	10.7
2.1	-0.7	-4.1	-2.4	-2.0	-1.5	-1.1	0.1	-0.4	0.1	-0.2	0.1	4.5
2.2	-0.3	-3.7	-3.1	-0.9	-1.2	-1.1	-0.7	-0.1	0.0	0.1	0.4	3.5
3.1	-1.3	-1.5	-0.9	0.4	-0.3	0.2	1.0	0.9	0.6	0.7	1.0	-1.4
3.2	-1.0	-0.3	-0.1	0.3	-0.7	0.2	0.6	0.4	-0.3	0.7	1.0	-1.2
4.1	-1.9	0.5	0.6	0.4	0.6	0.9	1.5	1.2	1.3	1.1	1.2	-2.0
4.2	-0.8	0.9	0.7	1.5	-0.6	0.6	1.3	0.8	0.3	0.3	1.2	-1.9
6.1	0.1	0.2	0.1	-0.1	0.0	0.0	-0.1	-0.1	0.0	0.0	0.0	-0.1
6.2	0.1	0.7	0.2	0.3	0.1	-0.1	0.6	0.2	0.3	-1.1	0.0	-0.2
A.1	2.9	-4.4	-2.7	-2.4	-2.3	-3.4	-3.9	-3.1	-2.6	-3.2	-3.6	8.6
B.1	3.4	-3.0	-1.8	-2.8	-2.5	-4.6	-5.2	-4.3	-3.3	-3.5	-3.3	10.1
8.1	-0.1	-0.1	0.0	-0.1	0.1	0.0	0.0	0.1	0.0	0.0	0.0	-0.1
8.2	0.0	0.0	0.1	0.1	0.0	0.1	0.0	0.0	0.1	0.0	0.0	-0.1
8.3	0.0	0.1	0.1	0.0	0.1	0.1	0.2	0.1	0.1	0.1	0.0	-0.1
9.1	0.0	-1.2	-0.2	-0.6	-0.5	0.0	0.6	0.3	0.5	0.2	0.7	-0.9
9.2	-0.3	-1.7	-0.6	-0.9	-0.4	-0.3	0.1	0.2	0.1	0.2	0.6	-0.1
9.3	-0.8	-1.4	-0.8	-1.0	-0.4	-0.2	0.4	0.3	0.7	0.2	0.8	-0.3
10.1	-0.6	-0.9	-0.1	0.1	0.2	0.7	1.1	1.3	0.6	1.6	1.6	-1.6
10.2	-1.4	-2.2	-0.8	-1.6	0.0	0.4	1.3	1.4	2.6	1.0	1.8	-0.1
10.3	-1.9	-1.2	-0.5	-0.2	-1.2	0.3	1.2	1.4	1.0	1.5	1.9	-1.0
11.1	-0.1	-1.7	-0.5	0.1	-1.4	-0.6	-0.1	0.2	0.1	0.6	0.4	0.8
11.2	-0.3	-2.7	-1.5	-2.4	-0.6	-0.7	-0.6	-0.3	0.0	0.2	0.2	1.0
11.3	-0.6	-1.9	-1.2	-0.1	-1.3	-0.7	-0.5	0.1	0.4	0.5	0.4	0.9
E.1	0.7	-4.8	-2.9	-3.4	-2.1	-3.2	-3.2	-2.9	-3.0	-2.6	-2.8	6.6
E.2	0.7	-6.3	-3.7	-3.6	-2.6	-3.3	-2.8	-2.3	-1.0	-1.8	-2.0	8.2
E.3	1.9	-2.7	-1.9	-1.1	-3.0	-4.5	-4.2	-3.8	-2.7	-2.4	-2.3	8.6

Test	SJ3-5T-3	SJ3-5T-4	SJ3-5T-5	SJ3-5T-6	SJ3-5T-7
1.1	23.9	14.3	11.9	4.3	4.0
1.2	23.3	12.9	11.1	4.3	3.8
2.1	9.0	4.8	4.2	0.8	0.6
2.2	9.4	4.6	3.8	1.2	0.7
3.1	-2.9	-1.9	-1.6	-1.2	-1.0
3.2	-3.1	-3.6	-2.4	-1.3	-0.9
4.1	-4.9	-3.4	-2.4	-1.5	-1.2
4.2	-4.3	-4.6	-3.2	-1.4	-1.0
6.1	-0.1	-0.1	-0.1	0.1	0.0
6.2	0.1	-0.9	-0.3	0.0	0.0
A.1	21.2	10.7	9.8	4.4	3.7
B.1	24.5	14.1	12.5	5.4	4.6
8.1	-0.3	-0.2	0.0	0.0	0.0
8.2	-0.5	0.2	-0.1	0.1	0.0
8.3	-0.1	0.0	-0.1	0.0	0.1
9.1	-1.9	-1.9	-1.3	-0.9	-0.6
9.2	-1.4	-0.7	-0.6	-0.7	-0.5
9.3	-1.2	-0.6	-1.0	-0.9	-0.6
10.1	-3.4	-2.7	-2.3	-1.5	-1.3
10.2	-1.3	-0.9	-1.0	-1.1	-0.9
10.3	-1.4	-1.4	-1.7	-1.3	-1.1
11.1	1.5	0.9	0.5	0.0	-0.1
11.2	3.0	1.1	1.0	0.3	0.1
11.3	2.7	0.9	0.8	0.2	0.1
E.1	15.2	8.3	7.8	2.6	2.6
E.2	17.9	9.6	9.0	2.9	2.8
E.3	18.8	10.6	10.1	3.9	3.6